# POLYESTER BASED 'NANOSPONGES' AS A DELIVERY PLATFORM FOR DIVERSE THERAPEUTICS TO ADVANCE THE TREATMENT OF A BROAD RANGE OF DISEASES

By

Alice E. van der Ende

Dissertation

Submitted to the Faculty of the

Graduate School of Vanderbilt University

in partial fulfillment of the requirements

for the degree of

DOCTOR OF PHILOSOPHY

in

Chemistry

August, 2010

Nashville, Tennessee

Approved:

Dr. Eva M. Harth

Dr. Timothy P. Hanusa

Dr. Charles M. Lukehart

Dr. Frederick R. Haselton

To my family

# ACKNOWLEDGEMENTS

This thesis arose in part out of years of research that has been done since I came to the Harth group at Vanderbilt. During that time, I have worked with a great number of people whose contribution, in assorted ways, to the research and the making of this thesis deserve special mention. It is a pleasure to convey my gratitude to them all through this acknowledgment.

Foremost, I would like to acknowledge my gratitude to Dr. Eva Harth for her supervision, advice, and guidance throughout my research as well as giving me extraordinary experiences. Above all, she has provided me unflinching encouragement and support in various ways. Her truly chemist intuition has made her a constant oasis of ideas and passion in science, which has inspired and enriched my growth as a student, a researcher, and a chemist. I am indebted to her more than she knows!

Along with my advisor, I would like to thank my dissertation committee members, Dr. Hanusa, Dr. Lukehart, and Dr. Haselton. I have appreciated all of the constructive discussions during my committee meetings, which has aided in the development of both my project and me as a chemist.

The members of the Harth group, past and present, have contributed immensely to my personal and professional time at Vanderbilt. The group has been a source of friendships as well as good advice and collaboration. These friends have been my family and my support network throughout the years. Without their continuous love and support, I would not be where I am today. My enormous debt of gratitude can hardly be repaid.

Moreover, I would like to thank my family for all their love and encouragement. My parents have raised me with a love of science and supported me in all my pursuits. I also want to show gratitude to my entire extended family for providing a loving environment for me. My brothers, my sisters, my mother-in-law and father-in-law, my brothers-in-law, and my sister-in-law have been so supportive. And most of all, I am grateful for my loving, supportive, encouraging, and patient husband Eric whose faithful support during the stages of this Ph.D. has been so greatly appreciated.

Lastly, I offer my regards and blessings to all of those who supported me in any respect during the completion of my research.

Thank you!

# ABSTRACT

While traditional polyesters, such as poly(lactic acid) and poly(glycolic acid), have long been of interest for the development of nanoparticles as effective drug delivery devices, they are restricted in their utility due to several major drawbacks. To circumvent these limitations, a practical approach has been developed for the formation of discrete functionalized polyester particles, which have been termed as 'nanosponges', with amorphous and semicrystalline morphologies in selected nanoscale size dimensions via a controlled intermolecular chain cross-linking process. This technique involves the coupling of epoxide functionalized polyesters with diamine to give well-defined multifunctional nanoparticles. The synthesis of discrete polyester nanoparticles using the intermolecular chain cross-linking process has also been successfully facilitated via click chemistry approaches, employing alkyne-azide click chemistry and the more recently developed thiol-ene reaction.

The formation of functionalized polyester nanoparticles containing amine, keto, and allyl groups has allowed for the tailoring of the particles towards the conjugation of bioactive building blocks, such as a dendritic molecular transporter and peptides. Synthetic strategies that enable efficient chemistries to conjugate targeting units and molecular transporter entities to the functionalized polyester particles have been developed to form potent carrier systems for targeted drug delivery and transport across biological barriers.

The versatile nature of the nanoparticle platform has allowed for the tailoring of the particles to meet the needs of specific drug delivery applications. The cross-linked

supramolecular structure of the prepared polyester based nanoparticle has enabled the increased and efficient encapsulation of drug molecules and the post-modification with targeting peptides. These drug loaded particles, or nanosponges, have been shown to maintain a linear therapeutic release profile which can be tuned to the demands of a disease as a result of the adjustable supramolecular architecture. The ability to incorporate all of these properties into a single nanoparticle carrier system has demonstrated that the particles have been efficiently optimized for numerous therapeutic applications, such as the treatment of cancer and glaucoma, and the encapsulation of macromolecular therapeutics.

TABLE OF CONTENTS

LIST OF TABLES

LIST OF FIGURES

LIST OF SCHEMES

# LIST OF ABBREVIATIONS

| | |
|---|---|
| 3-D | three dimenional |
| ° | degrees |
| °C | degrees celsius |
| °C/min | degrees celsius per minute |
| Å | angstrom |
| AF | Alexa Fluor® |
| AIBN | azobisisobutyronitrile |
| AMD | age-related macular degeneration |
| $Ar_{(g)}$ | argon gas |
| avl | α-allyl-δ-valerolactone |
| Boc | *tert*-butoxycarbonyl |
| $^{13}C$ NMR | carbon-13 nuclear magnetic resonance |
| CP | chemoattractant peptide |
| Da | Dalton |
| DCC | *N*,*N*'-dicyclohexylcarboiimide |
| d | doublet |
| dd | doublet of doublets |
| DDS | drug delivery system |
| $D_H$ | diameter of hydration |
| DIC | differential interference contrast |
| DIPEA | *N*,*N*-diisopropylethylamine |

| | |
|---|---|
| DLS | dynamic light scattering |
| DMF | dimethylformamide |
| DMSO | dimethyl sulfoxide |
| DSC | differential scanning calorimetry |
| DTT | dithiothreitol |
| EDC | *N*-(3-dimethylaminopropyl)-*N'*-ethylcarbodiimide |
| ERRβ | estrogen related receptor beta |
| EtOH | ethanol |
| evl | epoxide-valerolactone |
| FDA | Food and Drug Administration |
| Fmoc | Fluorenylmethyloxycarbonyl |
| FRI | free-radical-induced |
| g | gram |
| GFP | green fluorescent protein |
| gl | glycidol |
| GPC | gel-permeation chromatography |
| $\Delta H_m$ | melting enthalpy |
| h | hour |
| $^1$H NMR | proton nuclear magnetic resonance |
| HCl | hydrochloric acid |
| HBTU | O-benzotriazole-*N*,*N*,*N*',*N*'-tetramethyl-uronium-hexafluoro-phosphate |
| HBSS | Hank's buffered saline solution |

| | |
|---|---|
| HMPA | hexamethylphosphoramide |
| HOBt | *N*-hydroxybenzotriazole |
| HPLC | high performance liquid chromatography |
| Hz | hertz |
| IOP | intraocular pressure |
| J/g | joules per gram |
| kV | kilovolt |
| M | molar |
| m | multiplet |
| MALDI | Matrix-Assisted Laser Desorption/Ionization |
| m-CPBA | meta-chloroperbenzoic acid |
| MDR | multidrug resistance |
| MeOH | methanol |
| $MeSi_4$ | tetramethylsilane |
| mg | milligram |
| mg/mL | milligram per milliliter |
| MHz | megahertz |
| min | minute |
| mL | milliliter |
| mL/min | milliliter per minute |
| mm | millimeter |
| mmol | millimole |
| mol | mole |

| | |
|---|---|
| $M_w$ | weight-average molecular weight |
| MWCO | molecular weight cut-off |
| $M_n$ | number-average molecular weight |
| mRNA | messenger ribonucleic acid |
| MT | molecular transporter |
| MTT | 3-(4,5-Dimethylthiazol-2-yl)-2,5-diphenyltetrazolium bromide |
| *m/z* | mass-to-charge ratio |
| NBED | *N*-(boc) ethylene diamine |
| NHS | *N*-hydroxysuccinimidyl |
| NIR | near-infrared |
| nm | nanometer |
| NP | nanoparticle |
| NMR | nuclear magnetic resonance |
| ODmab | α-4-{N-[1-(4,4-dimethyl-2,6-dioxocyclohexylidene)-3-methylbutyl]-amino} benzyl ester |
| opd | 2-oxepane-1,5-dione |
| P | peptide |
| PBS | phosphate buffered saline |
| PCL | poly(ε-caprolactone) |
| PDI | polydispersity index |
| PEG | poly(ethylene glycol) |
| PGA | poly(glycolic acid) |
| PLGA | poly(lactic-co-glycolic acid) |

| | |
|---|---|
| PLLA | poly(L-lactic acid) |
| ppm | parts per million |
| pvl | α-propargyl-δ-valerolactone |
| q | quartet |
| RGC | retinal ganglion cell |
| RI | refractive index |
| ROP | ring-opening polymerization |
| siRNA | small interfering ribonucleic acid |
| SLK | shell cross-linked micelles |
| SLS | static light scattering |
| $Sn(Oct)_2$ | tin(II) 2-ethylhexanoate |
| SVEC | succinimidyl 2-(vinyl sulfonyl) ethyl carbonate |
| sxt | sextet |
| T | temperature |
| t | triplet |
| *t*-BuOH | *tert*-butanol |
| $TC_{50}$ | concentration causing a 50% cytotoxic effect |
| TEM | transmission electron microscopy |
| TFA | trifluoroacetic acid |
| $T_g$ | glass transition temperature |
| THF | tetrahydrofuran |
| $T_m$ | melting temperature |
| TMS | trimethylsilane |

| | |
|---|---|
| $t_{reac}$ | reaction time |
| TUNEL | terminal deoxynucleotidyl transferase dUTP nick end labeling |
| µL | microliter |
| µM | micromolar |
| µm | micrometer |
| µmol | micromole |
| vitamin E TPGS | $_{D}$-α-tocopherol polyethylene glycol 1000 succinate |
| vl | δ-valerolactone |
| W/g | watts per gram |
| wt% | weight percent |
| XRT | x-ray treated |

# CHAPTER I

## INTRODUCTION

The development of a wide spectrum of nanoscale technologies is beginning to change the foundations of disease diagnosis, treatment and prevention.[1] Various nano-devices have had a significant impact on medical technology, greatly enhancing the efficacy of many existing drugs and enabling the construction of entirely new therapeutic modalities.[2] In recent years, significant efforts have been devoted to use the potentials of nanotechnology in drug delivery to develop a suitable means of site-specific and/or time-controlled delivery of small or large molecular weight drugs and other bioactive cargo.[3] Research into the delivery and targeting of pharmaceutical and therapeutic agents with nanosized particles is at the forefront of projects in nanomedicine. Nanoparticles show tremendous promise for drug delivery, while exhibiting structural properties that are not feasible for single molecules.[4] Polymeric nanoparticles, in particular, are the most widely researched therapeutic carriers due to their unique flexibility with respect to fabrication techniques.

Biodegradable polymers have long been of interest for the development of nanoparticles as effective drug delivery devices.[5] The most widely used and studied class of biodegradable polymers is the polyesters, including poly(lactic acid), poly(glycolic acid), poly(ε-caprolactone) (Figure I-1), and their copolymers.[6] The low immunogenicity and toxicity of these traditional polyesters offers a biocompatible vehicle for drug delivery.[7] However, the majority of these polyesters are restricted in their utility as

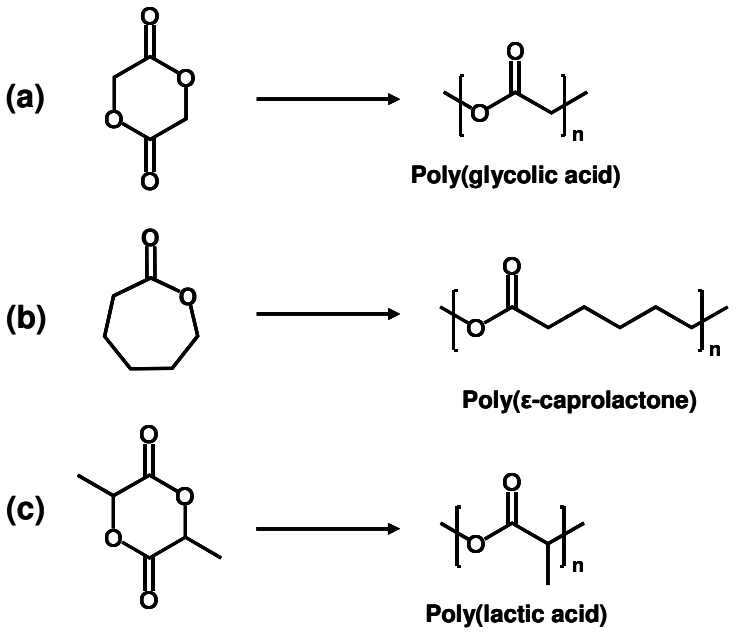


**Figure I-1.** Ring-opening polymerization of **(a)** glycolide to give poly(glycolic acid), **(b)** ε-caprolactone to afford poly(ε-caprolactone), and **(c)** lactide to give poly(lactic acid).

effective drug delivery systems due to several major drawbacks. First of all, nanoparticle formation employing these traditional polyesters encounters difficulty in providing particles with well-defined monodisperse sizes and well-characterized surface properties[8] and results in the creation of hydrophobic crystalline particles. Secondly, the lack of suitable functionalities on these polyesters limits the investigation of more efficient and orthogonal modification strategies that would enable the attachment of targeting and molecular building blocks to tailor the system for specific delivery applications. Finally, these traditional drug delivery systems suffer from a low drug payload and a burst release of therapeutics that leads to a decrease in treatment efficacy as drug is lost in an uncontrolled and unpredictable pattern, [9, 10] which can contribute to the development of multidrug resistance (MDR).[11]

Nanoparticle size influences almost every aspect of particle function including degradation, flow properties, clearance and uptake mechanisms.[12] The control over particle size has been recognized to be crucial to predict the interaction[13] with cells[14] and other biological barriers[8, 15, 16] Inconsistencies, however, in size distributions and shape, caused by the lack of reproducibility of common methodologies, such as the emulsion technique[17] and suspension polymerization,[18] have lead to difficulties in interpreting and controlling biological responses.

Particle diameter has been typically controlled through the physical properties of the materials, such as polymer and surfactant concentration,[17] or through the experimental parameters of the fabrication method, mixing method and speed, and, therefore, has been limited to only a range of specific nanoparticle size dimensions.[19-22] In the effort to achieve the necessary narrow nanoparticle dispersities, many of these methods require centrifugation steps to yield particles with size standard deviations that do not exceed 20%.[23] An ideal methodology, however, would provide a practical formation of functionalized monodisperse amorphous particles with a variety of distinct size dimensions and would address these aforementioned challenges.

Along with the ability to form well-defined nanoparticles with control over size, hydrophilicity and the integration of functionalities will also be key factors to utilize polyester materials in the increasingly specified drug delivery applications. The majority of the traditional polyesters are highly crystalline and hydrophobic, which makes them generally brittle and hard in physiologic environments.[24, 25] Drug delivery, however, requires the use of soft materials that can withstand dynamic conditions and exhibit linear degradation and therapeutic release profiles over time. The crystalline, hydrophobic

materials based on these traditional polyesters cannot tolerate such circumstances and, therefore, have a nonlinear biodegradation profile due to poor water permeability and poor solubility in aqueous systems. Consequently, these types of properties limit their utility for drug delivery purposes. Increasing the amorphous nature or limiting the crystallinity of the system can greatly improve the property control and tailor the material towards individual biological environments to advance the treatment of a broad range of disease requiring targeted or non-targeted sustained delivery systems.[24-26] Nevertheless, traditional aliphatic polyesters suffer from the lack of functional groups[27] and cannot easily be modified to enhance their physicochemical and mechanical properties. Therefore, the precedent developments support the efforts to enhance properties by tuning polyesters into refined polymers through the incorporation of functionalities that can influence hydrophilicity, biorecognition and bioadhesion.[28-30]

Biodegradability makes the traditional aliphatic polyesters valuable candidates for biomaterials. However, the lack of reactive sites along the polymeric backbone is a severe limitation when specific molecules, such as targeting moieties or bioadhesion promoters, need to be attached to the polymer chains. At best, these polyesters can be capped with a functional group at one or both chain ends, depending on the polymerization technique. However, since the content of end groups is directly dependent on the molecular weight, the number of functionalities is usually insignificant to be of any benefit for drug delivery applications.[31]

While functionalized linear polyester polymers have been subject of several post-modification strategies, the translation to 3-D functionalized polyester structures that are pertinent in the delivery and controlled release of drug molecules is only

beginning to be exploited. The systemic delivery of many therapeutics suffers from several major hindrances, such as rapid clearance, low targeting efficiency, and difficulty in crossing biological barriers.[1] Therefore, the development of nanoparticle delivery systems that are capable of molecular targeting and rapid entry into infected tissues are highly desirable. However, the absence of suitable functionalities limits the investigation of more efficient attachment strategies for the conjugation of targeting moities and other molecular building blocks and, consquently, impedes the cultivation of efficient targeted drug delivery systems. Using traditional conjugation strategies, such as 1-Ethyl-3-(3-dimethylaminopropyl)carbodiimide hydrochloride (EDC) coupling, can be expensive and time consuming since the conditions require a large excess of reagents and need to be optimized for each polymer-ligand combination.[32] Moreover, the introduction of multiple ligands using traditional conjugation approaches can often require tedious and inefficient sequential syntheses and purification steps. Therefore, the tailoring of complex macromolecular architectures with specific properties by straightforward, effective and selective chemical reactions remains a challenge.[33]

Solubility is an essential factor for drug effectiveness, independent of administration route. It also poses a major challenge for pharmaceutical companies developing new pharmaceutical products, since nearly half the active substances are either insoluble or poorly soluble in water.[34, 35] To alleviate the hindrance of delivering insoluble therapeutics, significant interest has been focused on the development of nanoparticle delivery systems that can enhance therapeutic solubility, bioavailability, and

permeability, release the drug in sustained manner, preferentially localize the therapeutic to the site of action and overall enhance therapeutic efficacy.[5]

Traditional polyester nanoparticle delivery systems are commonly self-assembled from linear polyesters chains driven by the polarity of the solvent, emulsion composition and addition techniques.[9, 19, 36] These procedures, however, result in low drug loading during nanoparticle formation and limit post-modification chemistries.[37] Furthermore, the result of this self-assembly can negatively affect the morphology and degradation properties of the release systems. Typical release kinetics exhibit an initial drug burst upon immersion in release medium either *in vitro* or *in vivo* (Figure I-2). The loss over

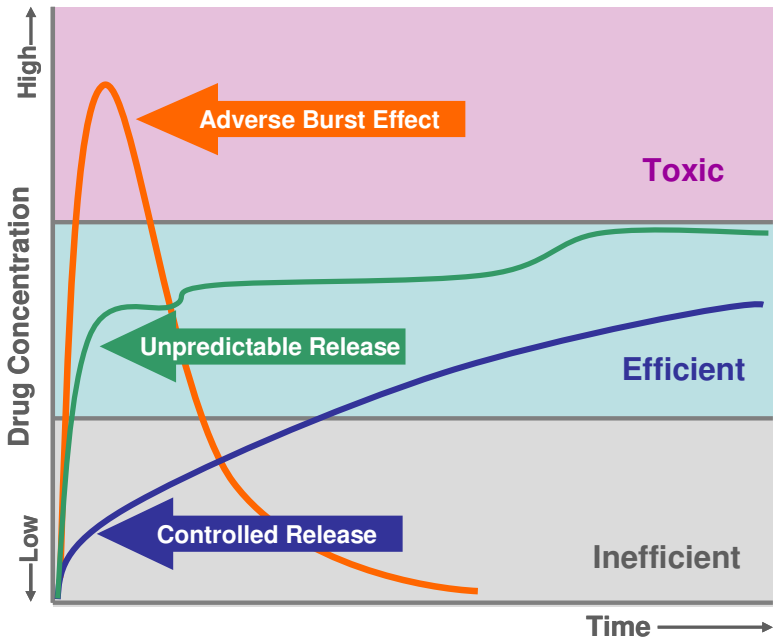


**Figure I-2.** Drug concentration profiles showing an adverse burst effect, an unpredictable release, and a controlled release.

the initial 24 h can be greater than 60% of the total loaded drug.[9, 10] This phenomenon is referred to as a 'burst effect', which leads to a loss in treatment efficiency, as drug is lost in an uncontrolled and unpredictable pattern (Figure I-2). These release profiles prevent

the establishment of reliable dosages, lead to drug concentrations near or above the toxic level *in vivo* (Figure I-2),[38] and contribute to developing multidrug resistance (MDR),[11] often times the result of non-optimized drug concentrations. Therefore, there still remains a need for the development of delivery systems which allow for the controlled linear release of therapeutics and overcome the additional challenges of traditional drug delivery systems.

**Dissertation Overview**

To circumvent the limitations of traditional polyesters and their associated nanoparticle drug delivery systems, a practical approach has been developed for the formation of discrete functionalized polyester particles with amorphous and semicrystalline morphologies in selected nanoscale size dimensions via a controlled intermolecular chain cross-linking process (Chapter II). The novel technique involves the controlled coupling of epoxide functionalized polyesters with diamine to give well-defined nanoparticles with narrow size distribution, and with incorporated functionalities, such as amines, keto groups, and alkynes, for post-modification reactions.

Along with the epoxide amine cross-linking reaction, efficient reactions, such as the alkyne-azide and thiol-ene click chemistries, were employed for particle formation. Degradable nanoparticles in a variety of distinct nanoscopic size dimensions were synthesized using the traditional alkyne-azide click chemistry and the more recently developed thiol-ene click reaction by covalently cross-linking alkyne or allyl functionalized linear polyesters with bisazides or dithiols, respectively (Chapter III).

The formation of polyester nanoparticles containing amine, keto, and allyl

groups has allowed for the tailoring of the particles towards the conjugation of bioactive building blocks, such as a dendritic molecular transporter and peptides. Several efficient post-modification strategies have been developed using mild conjugation chemistries, reductive amination and thiol-ene chemistry, to form polyester bioconjugates with specific functionalities to serve as a platform for an array of therapeutic applications (Chapter IV).

The versatile nature of the nanoparticle platform has allowed for the tailoring of the particles to meet the needs of specific drug delivery applications (Chapter V). The cross-linked supramolecular structure of the prepared polyester based nanoparticle, which has been termed a 'nanosponge', has enabled the increased and efficient encapsulation of small drug molecules and the post-modification with targeting peptides. These drug loaded particles, or nanosponges, have been shown to maintain a linear therapeutic release profile which can be tuned to the demands of a disease as a result of the adjustable supramolecular architecture. The ability to incorporate all of these properties into a single nanoparticle carrier system demonstrates that the particles have been efficiently optimized for numerous therapeutic applications, such as the treatment of cancer and glaucoma, and the encapsulation of macromolecular therapeutics.

References

1. Doshi, N.; Mitragotri, S., Designer Biomaterials for Nanomedicine. *Advanced Functional Materials* **2009,** *19* (24), 3843-3854.

2. Moghimi, S. M.; Hunter, A. C.; Murray, J. C., Nanomedicine: current status and future prospects. *Faseb Journal* **2005,** *19* (3), 311-330.

3. Hamidi, M.; Azadi, A.; Rafiei, P., Hydrogel nanoparticles in drug delivery. *Advanced Drug Delivery Reviews* **2008,** *60* (15), 1638-1649.

4. Sajja, H. K.; East, M. P.; Mao, H.; Wang, Y. A.; Nie, S.; Yang, L., Development of multifunctional nanoparticles for targeted drug delivery and noninvasive imaging of therapeutic effect. *Current Drug Discovery Technologies* **2009,** *6* (1), 43-51.

5. Kumari, A.; Yadav, S. K.; Yadav, S. C., Biodegradable polymeric nanoparticles based drug delivery systems. *Colloids and Surfaces, B Biointerfaces 75* (1), 1-18.

6. Brannonpeppas, L., Recent Advances on the Use of Biodegradable Microparticles and Nanoparticles in Controlled Drug-Delivery. *International Journal of Pharmaceutics* **1995,** *116* (1), 1-9.

7. Mohamed, F.; van der Walle, C. F., Engineering biodegradable polyester particles with specific drug targeting and drug release properties. *Journal of Pharmaceutical Sciences* **2008,** *97* (1), 71-87.

8. Delie, F., Evaluation of nano- and microparticle uptake by the gastrointestinal tract. *Advanced Drug Delivery Reviews* **1998,** *34* (2-3), 221-233.

9. Chan, J. M.; Zhang, L. F.; Yuet, K. P.; Liao, G.; Rhee, J. W.; Langer, R.; Farokhzad, O. C., PLGA-lecithin-PEG core-shell nanoparticles for controlled drug delivery. *Biomaterials* **2009,** *30* (8), 1627-1634.

10. Feng, S. S.; Zhao, L. Y.; Zhang, Z. P.; Bhakta, G.; Win, K. Y.; Dong, Y. C.; Chien, S., Chemotherapeutic engineering: Vitamin E TPGS-emulsified nanoparticles of biodegradable polymers realized sustainable paclitaxel chemotherapy for 168 h in vivo. *Chemical Engineering Science* **2007,** *62* (23), 6641-6648.

11. Harasym, T. O.; Liboiron, B. D.; Mayer, L. D., Drug ratio-dependent antagonism: a new category of multidrug resistance and strategies for its circumvention. *Methods in Molecular Biology* **2010,** *596*, 291-323.

12. Champion, J. A.; Katare, Y. K.; Mitragotri, S., Particle shape: A new design parameter for micro- and nanoscale drug delivery carriers. *Journal of Controlled Release* **2007,** *121* (1-2), 3-9.

13. Maassen, S.; Fattal, E.; Mueller, R. H.; Couvreur, P., Cell cultures for the assessment of toxicity and uptake of polymeric particulate drug carriers. *S.T.P. Pharma Sciences* **1993,** *3* (1), 11-22.

14. Dong, Y. C.; Feng, S. S., Poly(D,L-lactide-co-glycolide)/montmorillonite nanoparticles for oral delivery of anticancer drugs. *Biomaterials* **2005,** *26* (30), 6068-6076.

15. Durrer, C.; Irache, J. M.; Duchene, D.; Ponchel, G., Study of the interactions between nanoparticles and intestinal mucosa. *Progress in Colloid & Polymer Science* **1994,** *97*, 275-80.

16. Jani, P.; Halbert, G. W.; Langridge, J.; Florence, A. T., Nanoparticle uptake by the rat gastrointestinal mucosa: quantitation and particle size dependency. *The Journal of pharmacy and pharmacology* **1990,** *42* (12), 821-6.

17. Musyanovych, A.; Schmitz-Wienke, J.; Mailander, V.; Walther, P.; Landfester, K., Preparation of biodegradable polymer nanoparticles by miniemulsion technique and their cell interactions. *Macromolecular Bioscience* **2008,** *8* (2), 127-139.

18. Ma, G., Control of polymer particle size using porous glass membrane emulsification: A review. *China Particuology* **2003,** *1* (3), 105-114.

19. Kumar, M. N. V. R.; Bakowsky, U.; Lehr, C. M., Preparation and characterization of cationic PLGA nanospheres as DNA carriers. *Biomaterials* **2004,** *25* (10), 1771-1777.

20. Zweers, M. L. T.; Grijpma, D. W.; Engbers, G. H. M.; Feijen, J., The preparation of monodisperse biodegradable polyester nanoparticles with a controlled size. *Journal of Biomedical Materials Research Part B-Applied Biomaterials* **2003,** *66B* (2), 559-566.

21. Oster, C. G.; Wittmar, M.; Bakowsky, U.; Kissel, T., DNA nano-carriers from biodegradable cationic branched polyesters are formed by a modified solvent displacement method. *Journal of Controlled Release* **2006,** *111* (3), 371-381.

22. Muller, K.; Klapper, M.; Mullen, K., Polyester nanoparticles by non-aqueous emulsion polycondensation. *Journal of Polymer Science Part a-Polymer Chemistry* **2007,** *45* (6), 1101-1108.

23. Gaumet, M.; Gurny, R.; Delie, F., Fluorescent biodegradable PLGA particles with narrow size distributions: Preparation by means of selective centrifugation. *International Journal of Pharmaceutics* **2007,** *342* (1-2), 222-230.

24. Amsden, B. G.; Misra, G.; Gu, F.; Younes, H. M., Synthesis and characterization of a photo-cross-linked biodegradable elastomer. *Biomacromolecules* **2004,** *5* (6), 2479-2486.

25. Brown, A. H.; Sheares, V. V., Amorphous unsaturated aliphatic polyesters derived from dicarboxylic monomers synthesized by Diels-Alder chemistry. *Macromolecules* **2007,** *40* (14), 4848-4853.

26. Olson, D. A.; Sheares, V. V., Preparation of unsaturated linear aliphatic polyesters using condensation polymerization. *Macromolecules* **2006,** *39* (8), 2808-2814.

27. Sasatsu, M.; Onishi, H.; Machida, Y., In vitro and in vivo characterization of nanoparticles made of MeO-PEG amine/PLA block copolymer and PLA. *International Journal of Pharmaceutics* **2006,** *317* (2), 167-174.

28. Riva, R.; Lenoir, S.; Jerome, R.; Lecomte, P., Functionalization of poly(epsilon-caprolactone) by pendant hydroxyl, carboxylic acid and epoxide groups by atom transfer radical addition. *Polymer* **2005,** *46* (19), 8511-8518.

29. Parrish, B.; Breitenkamp, R. B.; Emrick, T., PEG- and peptide-grafted aliphatic polyesters by click chemistry. *Journal of the American Chemical Society* **2005,** *127* (20), 7404-7410.

30. Galindo-Rodriguez, S.; Allemann, E.; Fessi, H.; Doelker, E., Physicochemical parameters associated with nanoparticle formation in the salting-out, emulsification-diffusion, and nanoprecipitation methods. *Pharmaceutical Research* **2004,** *21* (8), 1428-1439.

31. Gautier, S.; D'Aloia, V.; Halleux, O.; Mazza, M.; Lecomte, P.; Jerome, R., Amphiphilic copolymers of epsilon-caprolactone and gamma-substituted epsilon-caprolactone. Synthesis and functionalization of poly(D,L-lactide) nanoparticles. *Journal of Biomaterials Science-Polymer Edition* **2003,** *14* (1), 63-85.

32. Patil, Y. B.; Toti, U. S.; Khdair, A.; Ma, L.; Panyam, J., Single-step surface functionalization of polymeric nanoparticles for targeted drug delivery. *Biomaterials* **2009,** *30* (5), 859-866.

33. Lecomte, P.; Riva, R.; Jerome, C.; Jerome, R., Macromolecular engineering of biodegradable polyesters by ring-opening polymerization and 'Click' chemistry. *Macromolecular Rapid Communications* **2008,** *29* (12-13), 982-997.

34. Kocbek, P.; Baumgartner, S.; Kristl, J., Preparation and evaluation of nanosuspensions for enhancing the dissolution of poorly soluble drugs. *International Journal of Pharmaceutics* **2006,** *312* (1-2), 179-186.

35. Merisko-Liversidge, E. M.; Liversidge, G. G., Drug nanoparticles: formulating poorly water-soluble compounds. *Toxicologic Pathology* **2008,** *36* (1), 43-48.

36. Uhrich, K. E.; Cannizzaro, S. M.; Langer, R. S.; Shakesheff, K. M., Polymeric systems for controlled drug release. *Chemical Reviews* **1999,** *99* (11), 3181-3198.

37. Cheng, J.; Teply, B. A.; Sherifi, I.; Sung, J.; Luther, G.; Gu, F. X.; Levy-Nissenbaum, E.; Radovic-Moreno, A. F.; Langer, R.; Farokhzad, O. C., Formulation of functionalized PLGA-PEG nanoparticles for in vivo targeted drug delivery. *Biomaterials* **2007,** *28* (5), 869-876.

38. Huang, X.; Brazel, C. S., On the importance and mechanisms of burst release in matrix-controlled drug delivery systems. *Journal of Controlled Release* **2001,** *73* (2-3), 121-136.

# CHAPTER II

# MULTIFUNCTIONAL POLYESTER PARTICLES IN CONTROLLED NANOSCOPIC SIZE DIMENSIONS

## Introduction

Degradable aliphatic polyester materials, such as poly(L-lactic acid) (PLLA), poly(glycolic acid) (PGA), poly(ε-caprolactone) (PCL), and their copolymers, have received considerable attention in the medical and pharmaceutical fields finding applications as drug delivery systems,[1-6] implant materials[7-12] and diagnostic systems.[13-15] For many of these applications, in particular for drug delivery purposes, the polyester materials are administered in form of nanoparticles as they are able to cross physiological epithelial barriers and give means to controlled release profiles. However, the majority of these polyesters are restricted in their utility due to their crystalline and hydrophobic properties,[16-18] which influence their physico-chemical properties, together with challenges to provide particles in well-defined sizes and well-characterized surface properties.[19]

The control over particle size has been recognized to be crucial to predict the interaction[20] with cells[21] and other biological barriers,[19, 22, 23] but discrepancies in size distributions and shape, caused by the lack of reproducibility of common methodologies, have lead to difficulties in interpreting and controlling biological responses. Current techniques are profoundly influenced by the selection of stabilizer and solvent and, therefore, are limited to only a range of specific nanoparticle size dimensions.[24] For example, solvent displacement, emulsion-diffusion-evaporation, and salting-out methods can only produce particles with size dimensions greater than 100 nm,[24-26] whereas other

approaches utilizing non-aqueous emulsion polymerization lead to a polyester nanoparticle size from 38-60 nm.[27] In the effort to achieve the necessary narrow nanoparticle dispersities, many of these methods require centrifugation steps to yield particles with size standard deviations that do not exceed 20%.[28] In these purification steps not only particles, but also drug molecules, that are typically encapsulated during nanoparticle formation, are lost. Furthermore, a low drug load during nanoparticle formation is required (1-5%) to prevent high polydispersities of the resulting particles.[6] An ideal methodology, however, would provide a practical formation of functionalized monodisperse amorphous particles with a variety of distinct size dimensions and would address the aforementioned challenges.

In addition to the demand for well-defined nanoparticles with control over size and a wide range of different nanoparticle dimensions, hydrophilicity and the integration of functionalities will be key factors to utilize polyester materials in the increasing specified applications in the biomedical arena. Recent reports have described efforts to predict and increase the mechanical and degradation properties by reacting diols with diacids to create poly(ester ether) via polycondensation reactions.[18] Other approaches have attached short polyethyleneglycol units onto functional groups in linear polyesters prepared from δ-valerolactones in ring-opening polymerization procedures.[16, 18] These examples document that the amorphous nature or limited crystallinity can greatly improve the property control and tailor the material towards individual biological environments.[18, 29, 30] In this vein, a variety of new lactone polymerization catalysts[31-38] have accelerated the investigations of ring-opening polymerizations involving substituted lactones that prove to be a valuable asset to introduce pendant functionalities along the

linear polyester backbones. Monomers, such as δ-valerolactone and α-propargyl-δ-valerolactone, have been copolymerized and investigated in post-modification strategies[39] to form bioconjugates containing peptidic targeting units and other bioactive compounds utilizing the integrated pendant functionality.[40] Traditional aliphatic polyesters, however, suffer from the lack of functional groups[41, 42] and those precedent developments support the efforts to foster properties that tune polyesters into refined polymers by incorporating functionalities that influence hydrophilicity, biorecognition and bioadhesion.[43-45]

A practical approach, therefore, has been developed for the formation of polyester particles with amorphous and semicrystalline morphologies in a variety of distinct nanoscopic ranges through a controlled cross-linking strategy that allows the preparation of 3-D polyester architectures that not only inherit the solubility of their linear polymer precursors, but also contain a variety of functionalities as a result of the cross-linking process with one type of linear polyester or a mixture of different linear chains. The presented technique bears opportunities that will further advance the application potential of polyester based materials in the biomedical field.

## Results and Discussion

For the formation of functionalized and amorphous polyester nanoparticles, the use of a controlled cross-linking method was investigated rather than employing salting-out strategies,[45, 46] solvent displacement techniques,[47] emulsion polymerization,[27, 48] or emulsion diffusion methods[24, 41] that require salts or surfactants, which are difficult to remove sufficiently after particle formation.[49] It was found that reacting epoxide groups with diamines to form alkane-OH groups could provide clean and non-toxic cross-

linking. While this cross-linking technique has been employed to form acrylate based microparticles[50] and hydrogels,[51] it has never been investigated in the formation of degradable nanoparticles due to the lack of suitable linear precursors.

**Synthesis of Multifunctional Linear Polyester Precursors with Epoxide Moieties**

The epoxide entity, for the formation of discrete cross-linked nanoparticles, was integrated by first polymerizing a low molecular weight linear copolymer, $\mathbf{Ab_1}$, with pendant allyl groups. Pendant allyl groups represent valuable intermediates to many functional groups and, therefore, were incorporated into the polymer backbone by copolymerizing α-allyl-δ-valerolactone, (b), and commercially available δ-valerolactone, (A), via ring-opening polymerization (ROP) using the catalyst tin 2-ethylhexanoate ($Sn(Oct)_2$), as reported.[52] Upon copolymerization, the pendant allyl groups of $\mathbf{Ab_1}$ were oxidized with meta-chloroperbenzoic acid (m-CPBA)[53] under mild conditions to convert the double bonds to epoxide rings to give $\mathbf{AB_1}$ (Table II-1) that contained, thereby, the crucial functionality for nanoparticle formation via controlled cross-linking.

**Table II-1.** Multifunctional linear polyester precursors with epoxide cross-linking units.

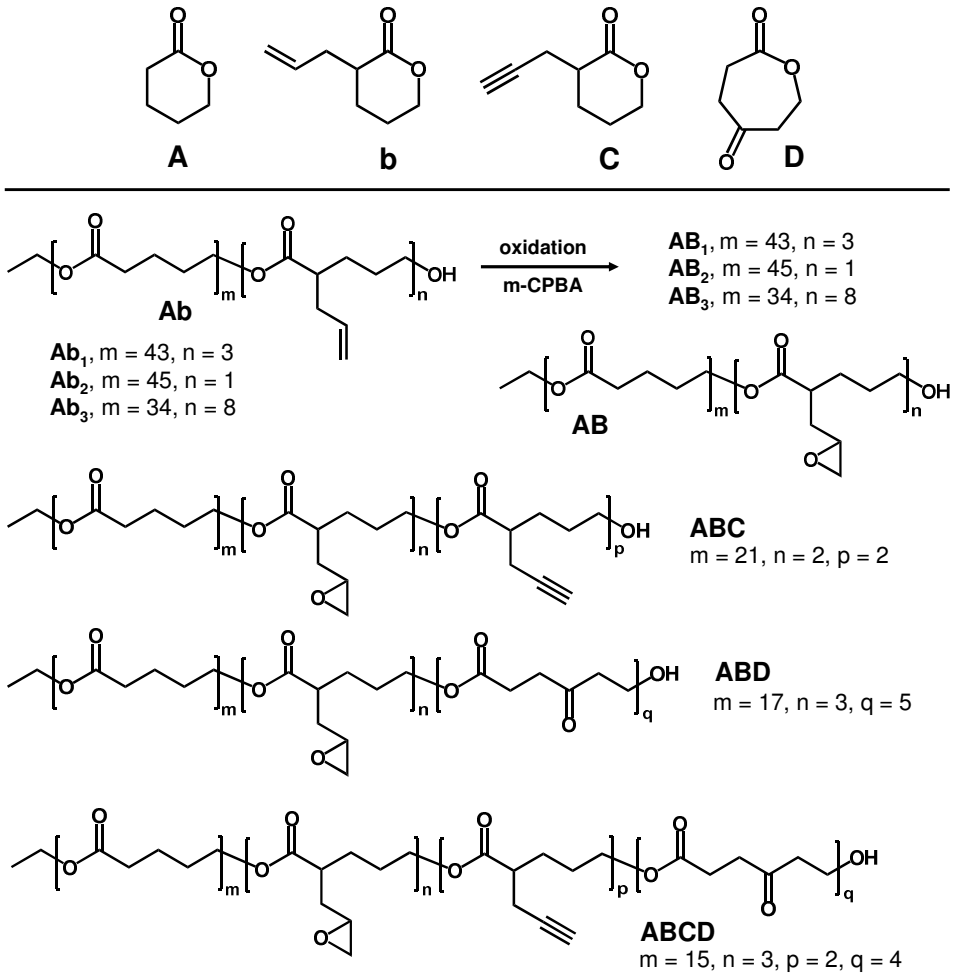


In order to introduce various functionalities into the resulting particles, additional monomers were synthesized, α-propargyl-δ-valerolactone,[44] (C), and 2-oxepane-1,5-dione,[54] (D), according to the literature. These monomers were then individually copolymerized with α-allyl-δ-valerolactone (b) and δ-valerolactone, (A), in a similar manner as **Ab1**, to give rise to novel polyesters with acetylene or keto functionalities respectively. In addition to these copolymers, polymer **AbCD** was synthesized, which further increased the number of functional groups. These functionalities are anticipated to enrich the nanoparticle utilization and to govern orthogonal conjugation strategies for

targeting units, dyes and a dendritic molecular transporter.[55] After polymerizing each of the aforementioned copolymers, the formation of the epoxide groups was achieved by oxidizing the pendant allyl functionalities with m-CPBA (Table II-1). The modified copolymers were obtained in molecular weight ranges of 3400-4800 Da with narrow polydispersities of 1.16-1.27.

**Nanoparticle Formation using Amine-Epoxide Intermolecular Cross-linking**

The formation of nanoparticles in controlled size dimensions progressed from covalently cross-linking the epoxide functionalized linear polymers with 2,2'-(ethylenedioxy)bis(ethylamine) (Scheme II-1). In order to study the particle formation

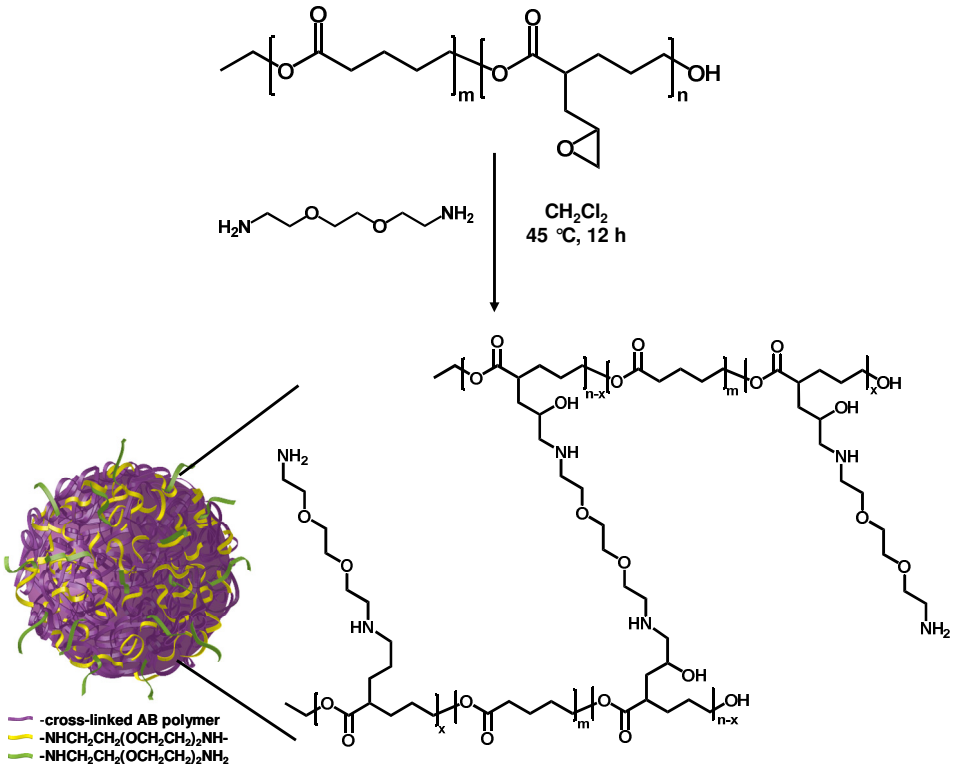


**Scheme II-1.** Nanoparticle formation by covalent cross-linking polymer **AB** with 2,2'-(ethylenedioxy)bis(ethylamine).

under controlled conditions, a set of experiments was first performed with linear polymer **$AB_1$**, in which a solution of **$AB_1$** in dichloromethane of known concentration was added dropwise (13 mL/min) to a refluxing solution of 2,2'-(ethylenedioxy)bis(ethylamine) in dichloromethane. The diamine cross-linking reagent, 2,2-(ethylenedioxy)bis(ethylamine), was specifically chosen to enhance the hydrophilic, and amorphous properties of the resulting particle.

For the first set of experiments, polymer solutions with concentrations varying from 0.1 M to 0.7 M were prepared and each was dropped into its respective refluxing solution of dichloromethane containing 1 or 2 equivalents of amine per pendant epoxide cross-linking entity in the linear polymer. While each of these reactions was successful in producing small quantities of nanoparticles after refluxing for 4 h, as evidenced by dynamic light scattering (DLS), there was still a considerable amount of remnant starting **$AB_1$** polymer. Therefore, in order to drive the cross-linking to completion, the refluxing time was increased from 4 h to 12 h, which significantly improved the yield of particles. It was observed that during particle formation the linear precursor and the formed particles were both soluble in dichloromethane and the reaction mixture remained clear for the duration of the cross-linking reaction. Due to their low cross-linking density, the nanoparticles retain the physico-chemical behavior of the linear polymer precursors as it was also observed in nanoparticle structures from the intramolecular chain collapse processes introduced by Hawker and coworkers,[56] as well as in shell cross-linked micelles (SLK) pioneered by Wooley and coworkers.[57]

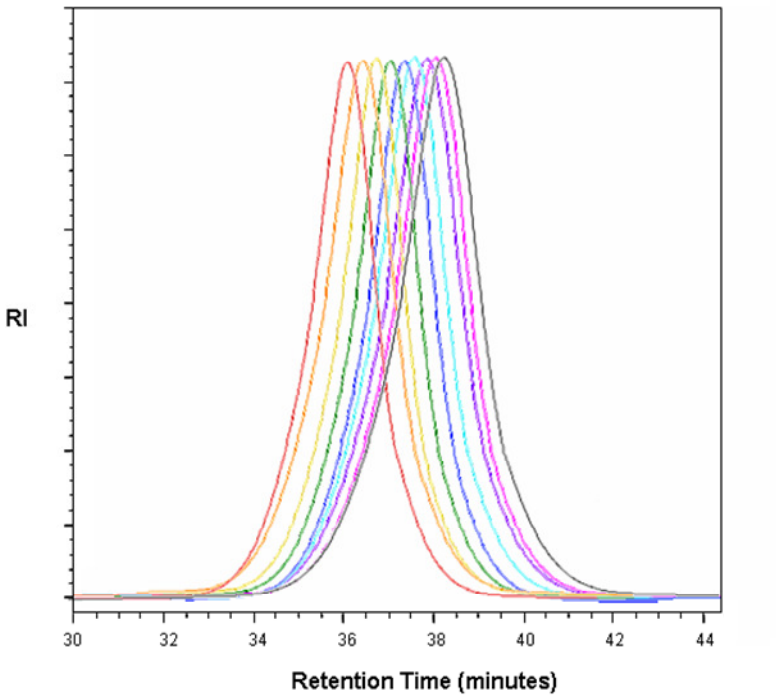


**(—)AB; (—) I; (—) II; (—) III; (—) IV; (—) V; (—) VI; (—) VII; (—) VIII**

| Entry | Amine/ 1 Epoxide | Diameter (nm) **$AB_1$** nanoparticles[a] | $M_{w,\ RI}$ (g/mol)[b] | PDI[c] | $M_w$ (kg/mol)[d] |
|---|---|---|---|---|---|
| I | 1 | 30.7 ± 2.2 | 3403 | 1.16 | 60.5 |
| II | 2 | 58.1 ± 6.2 | 3445 | 1.16 | 81.5 |
| III | 3 | 82.6 ± 5.7 | 3544 | 1.17 | 96.1 |
| IV | 4 | 115.6 ± 12.5 | 3860 | 1.18 | 112 |
| V | 5 | 255.7 ± 26.9 | 4005 | 1.18 | 187 |
| VI | 6 | 342.2 ± 42.2 | 4267 | 1.21 | 222 |
| VII | 8 | 425.1 ± 44.6 | 4470 | 1.21 | 328 |
| VIII | 10 | 725.1 ± 94.3 | 4887 | 1.22 | 525 |

**Figure II-1**. **Top:** Overlay of GPC traces for **AB** the linear polyester precursor, $M_w$= 3400, PDI=1.16; and nanoparticles **$AB_1$** (I-VIII) derived from controlled cross-linking with increasing equivalents (1-10) of amine per epoxide group; **Bottom:** [a]Hydrodynamic diameter of **$AB_1$** nanoparticle series measured by dynamic light scattering (DLS), [b]gel permeation chromatography (GPC) data of the cross-linked nanoparticle **$AB_1$** series relative to polystyrene standards; weight-average molecular weight ($M_w$) after dialysis; and [c]polydispersity (PDI=$M_w/M_n$), measured by GPC; [d]weight-average molecular weight, measured by static light scattering (SLS).

With the goal to form monodisperse particles with controlled nanoscopic size dimensions, the effect of varying the amount of diamine available for cross-linking was assessed in a second series of experiments. For these reactions, the equivalents of

diamine cross-linker were increased from 1 to 10 amines per epoxide group in **$AB_1$** while using a polymer solution of 0.5 M, which were found to be the optimum conditions to observe distinguishable changes in particle sizes. The precision of nanoparticle formation was examined in detail using the resulting **$AB_1$** particles and it was shown that the controlled cross-linking is a facile process that gives well-defined nanoparticles with a polynominal increase in molecular weight and hydrodynamic diameter. As seen in Figure II-1, the gel permeation chromatography (GPC) traces shift to higher hydrodynamic diameters when the equivalents of diamine crosslinker per epoxide groups of the linear precursor chain systematically increase. One of the pertinent features of the GPC traces is their symmetrical nature accompanied by narrow polydispersities and the lack of any high-molecular weight shoulders. In each case, the nanoparticles exhibited lower molecular weights as determined from GPC analysis and, therefore, the particles' actual molecular weights were obtained with static light scattering (SLS). For example, the **$AB_1$** linear polymer with an initial $M_w$ of 3400 Da, when reacted with four equivalents of amine per epoxide, gave a particle with a molecular weight of 3860 Da and a polydispersity of 1.18. However, the actual molecular weight of this particle was found to be 112 000 Da by SLS, which demonstrates that there was a significant increase in molecular weight during the cross-linking process, but with no significant increase of the polydispersity as compared to the starting material.

The unique feature of being able to accurately control the nanoparticle sizes was also apparent through DLS measurements which showed a polynominal increase in nanoscopic diameter (Figure II-1 and Figure II-7) with only 10% standard deviation, which improves the typical 20% standard deviation accepted for particles formed through

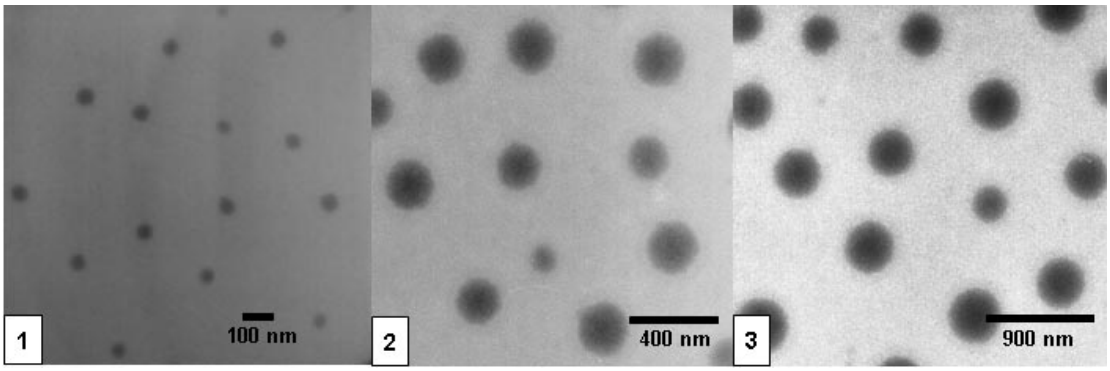


**Figure II-2.** TEM images of $\mathbf{AB_1}$ nanoparticles: (1) 2 equivalents of amine; (2) 5 equivalents of amine, and (3) 8 equivalents of amine.

micellization or standard techniques only after thorough centrifugation.[28] Along with DLS, transmission electron microscopy (TEM) images from three selected particles of the $\mathbf{AB_1}$ series, shown in Figure II-2, underline the versatility of the novel approach to prepare spherical nanoparticles in narrow nanoscopic size dimensions, controlled by the equivalents of diamine.

The ability to control the size of the nanoparticles was examined in further detail using three different linear **AB** polymers with varying levels of epoxide incorporation: 2% $\mathbf{AB_2}$, 7% $\mathbf{AB_1}$, and 19% $\mathbf{AB_3}$. The conversion of the **AB** series into nanoparticles was found to be a facile process at all percentages of epoxide units studied. For example, 85 nm particles were obtained when using eight amines per epoxide whereas five amines per epoxide were necessary to achieve a 33 nm size dimension for polymer precursor $\mathbf{AB_2}$. In addition, a comparable particle size of approximately 85 nm was attained either with

**Table II-2.** Sizes of **AB** particles with varying percents of epoxide groups.

| Amine/ 1 Epoxide | Diameter (nm) **$AB_2$** nanoparticles 2% epoxide | Diameter (nm) **$AB_1$** nanoparticles 7% epoxide | Diameter (nm) **$AB_3$** nanoparticles 19% epoxide |
|---|---|---|---|
| 3 | 8.0 ± 0.6 | 82.6 ± 5.7 | 179.9 ± 18.0 |
| 4 | 19.0 ± 1.3 | 115.6 ± 12.5 | 225.6 ± 22.5 |
| 5 | 33.6 ± 1.9 | 255.7 ± 26.9 | 299.0 ± 31.2 |
| 6 | 48.7 ± 3.2 | 342.2 ± 42.2 | 409.1 ± 42.7 |
| 8 | 84.9 ± 10.5 | 425.1 ± 44.6 | 843.3 ± 88.0 |

eight or three equivalents of amine with precursor **$AB_2$** or **$AB_1$** respectively (Table II-2). From these results, it can be concluded that a systematic increase in the nanoparticle size dimensions was also observed with an increase in the number of the epoxide groups in the linear precursor polymers, which is consistent with a rise in the level of intermolecular chain coupling in the presence of increased amounts of diamine cross-linker (Figure II-3).

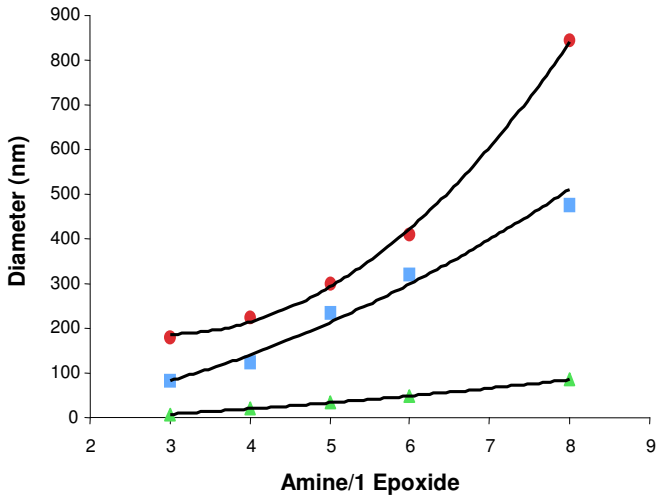


**Figure II-3.** Variation in nanoparticle sizes for differing percents of oxirane in the starting linear **AB**: (▲) **$AB_2$** nanoparticles with 2% epoxy groups; (■) **$AB_1$** nanoparticles with 7% epoxy groups, and; (●) **$AB_3$** nanoparticles with 19% epoxy groups.

Further characterization of the particles with $^{1}$H NMR also confirmed nanoparticle formation since the diamine's methylene protons adjacent to the amine functionalities experienced a shift in resonance from 2.86 to 2.89 ppm due to the transformation of the primary amine to a secondary amine after successful cross-linking with the polymer. In addition, $^{1}$H MNR was able to indicate an increase in particle size, since the signals at 3.63, 3.54 and 2.89 ppm corresponding to the methylene protons neighboring the secondary amines of the ethylene dioxide linker intensified as the particles became larger in size (Figure II-4).

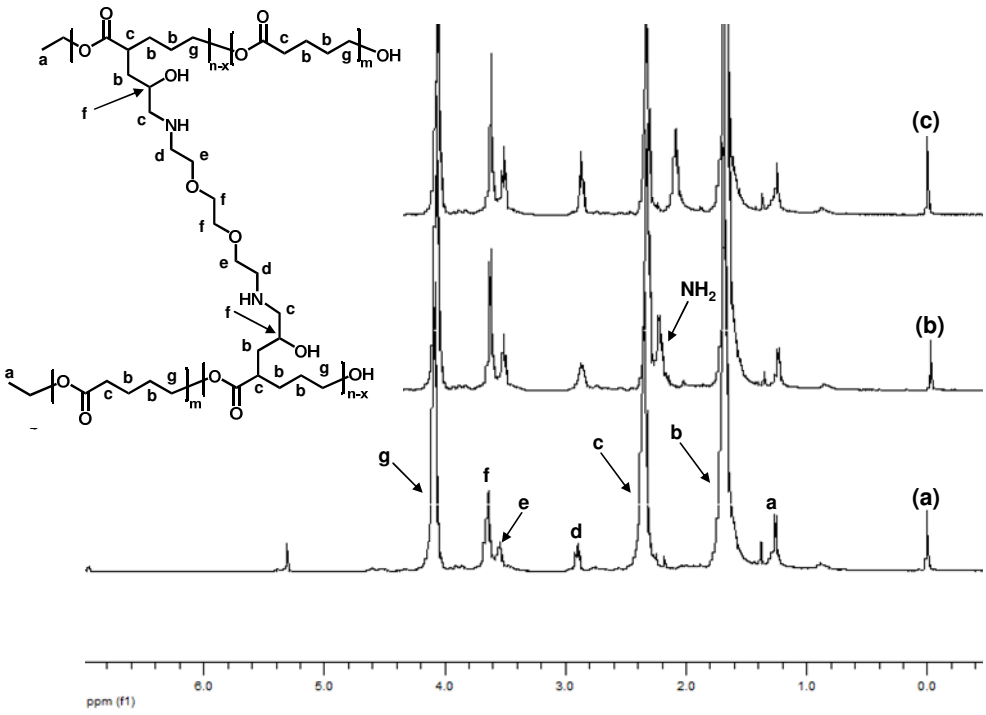


**Figure II-4.** $^{1}$H NMR spectra of **AB$_1$** nanoparticles with increasing cross-linking: **(a)** 6 amines/1 epoxide; **(b)** 8 amines/1 epoxide, and; **(c)** 10 amines/1 epoxide. The chemical structure of the cross-linked particle and appropriate proton resonance assignments are shown.

In conjunction with 2,2'-(ethylenedioxy)bis(ethylamine) as the diamine cross-linker, longer pegylated diamines, such as Jeffamines® ED-600, D-4000 and ED-2003, have been investigated for the preparation of **AB** particles (Figure II-5). By increasing the cross-linker length, particles with enhanced hydrophilicity and wider network architectures could be made. Cross-linking Jeffamine® ED-600, with a molecular weight of 600 Da, with linear polymer $\mathbf{AB_1}$ at 1 amine per epoxide group in the polymer resulted in 163.5 nm particles, which is five times larger in size than the 30.7 nm particles obtained from cross-linking $\mathbf{AB_1}$ with 2,2'-(ethylenedioxy)bis(ethylamine) (Figure II-1 and Table II-4). With Jeffamine® D-4000, which has a molecular weight of 4000 Da, as

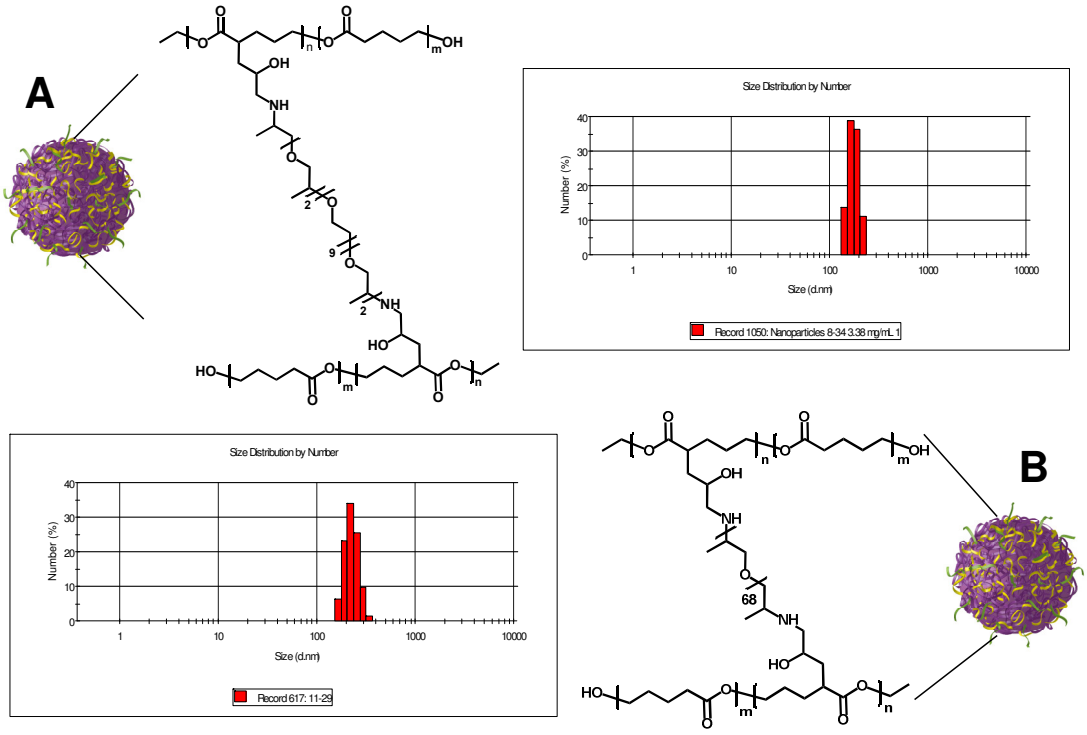


**Figure II-5.** Nanoparticle formation by covalent cross-linking polymer **AB** with Jeffamine® cross-linkers **(A)** 164 nm particles formed from coupling polymer **AB** with Jeffamine® ED-600; **(B)** 241 nm particles obtained from cross-linking precursor **AB** with Jeffamine® D-4000.

the cross-linker, particles of 240.8 nm with increased hydrophilicity can be achieved with only 0.25 equivalents of amine per epoxide in the linear polymer $\mathbf{AB_1}$. Based on these results, the particle size can be tailored not only by the equivalents of diamine linker, but also by the length of the pegylated diamine. With these adjustable properties, the particles can be effectively tailored for specific biomedical applications.

**Thermal Properties of Nanoparticles**

Important information regarding the morphology of the nanoparticles was inferred from their thermal properties gathered through differential scanning calorimetry (DSC). Several $\mathbf{AB_1}$ nanoparticle samples, 30.7 ± 2.2 nm, 115.6 ± 12.5 nm, and 725.1 ± 94.3 nm, were analyzed by DSC to learn how the increased ratios of 2,2'-(ethylenedioxy)bis(ethylamine) accompanied by the increased nanoscopic size affected the melting transitions of the particles (Figure II-6). As a comparison, particles that were formed from the $\mathbf{AB_2}$ and $\mathbf{AB_3}$ series were also investigated in order to evaluate the influence of lower (2%) and higher (19%) percentages of epoxides incorporated into the linear precursors which led to lower and higher cross-linking densities of the respective nanoparticles.

From the DSC results, it was evident the particles from the $\mathbf{AB_1}$ series were amorphous at the intended temperature of use, at 37 °C, with glass transition temperatures reaching from –25.4 to -33.2 °C. In this series, the crystallinity ranged from 19.9% to 21.3% with the highest value corresponding to the smallest particle, 30.7 ± 2.2 nm. As the crystallinity decreased with increasing diameter of the nanoparticle, a shift of the melting temperature from 44.6 °C to 40.3 °C was observed. In comparison, the

nanoparticle from the **AB$_2$** series showed an expected higher crystallinity of 29% that led to a higher melting temperature, which is in agreement with the trend observed for the **AB$_1$** series as a result of the lower density of cross-linking units in the linear precursor chain (2%) that led to fewer cross-linking events. At higher densities of cross-linking, as experienced with higher percentages of epoxide groups along the linear precursor backbone (19%), the resulting particle from the **AB$_3$** series was fully amorphous since a glass transition temperature, at –24.9 °C, and no melting transition, was observed.

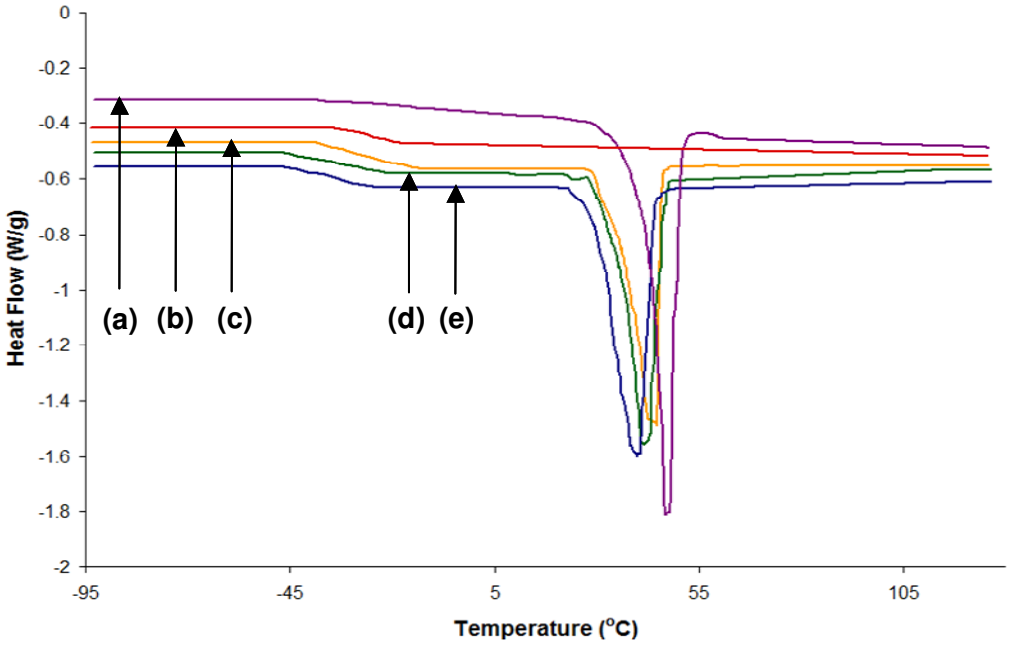


| Entry | Nanoparticle | Diameter (nm) | $T_g$ (°C)[a] | $T_m$ (°C)[a] | $\Delta H_m$ (J/g)[a] | Crystallinity (%)[b] |
|---|---|---|---|---|---|---|
| **a** | **AB$_2$** | 84.9 ± 10.5 | — | 46.7 | 85.44 | 29.0 |
| **b** | **AB$_3$** | 179.9 ± 18.0 | -24.9 | — | — | — |
| **c** | **AB$_1$** | 30.7 ± 2.2 | -25.4 | 44.6 | 62.95 | 21.3 |
| **d** | **AB$_1$** | 115.6 ± 12.5 | -31.6 | 42.9 | 60.82 | 20.6 |
| **e** | **AB$_1$** | 725.1 ± 94.3 | -33.2 | 40.3 | 58.63 | 19.9 |

**Figure II-6.** DSC trace overlay of 84.89 ± 10.47 nm **AB$_2$** nanoparticles, **(a)**, 179.9 ± 18.0 nm **AB$_3$** nanoparticles, **(b)**, and 30.7 ± 2.2 nm **AB$_1$** nanoparticles, **(c)**, 115 ± 12.5 nm **AB$_1$** nanoparticles, **(d)** and 725.1 ± 94.3 nm **AB$_1$** nanoparticles **(e)** in the glass and melting transition regions. [a] determined by DSC. [b] determined by taking the ratios of $\Delta H_m$ of the samples to the $\Delta H_m$ of a 100% crystalline polyester.

Therefore, it was concluded that the particles can be tuned to give either completely amorphous particles or particles with amorphous behavior at the intended temperature of use[30, 58] with a limiting percentage of crystallinity, approximately 20%, as seen by controlling the degree of cross-linking.

**Quantification of Nanoparticle Amine Groups**

The continuous increase in 2,2'-(ethylenedioxy)bis(ethylamine) cross-linker equivalents not only extends the particle size and maintains the increased hydrophilic behavior, but it also introduces additional amine functionalities that are created during the cross-linking event. The intermolecular cross-linking mechanism induces these valuable functionalities due to unreacted free amine units of the diamine cross-linking unit with the oxirane of the polyester backbone. In view of the further utilization of the amine groups in the final particle, it was important to quantify and determine the weight percent of the primary and secondary amines groups using a non-aqueous salicylaldehyde

**Table II-3.** Nonaqueous titration of amines for several $\mathbf{AB_1}$ nanoparticle samples.

| $\mathbf{AB_1}$ nanoparticle size (nm) | Primary amine wt % | Secondary amine wt % |
|---|---|---|
| 58.1± 6.2 | 0.008 ± 0.001 | 0.031 ± 0.001 |
| 255.7 ± 26.9 | 0.025 ± 0.001 | 0.100 ± 0.002 |
| 425.1 ± 44.6 | 0.055 ± 0.002 | 0.200 ± 0.002 |

titration as reported in the literature.[59] The titration was completed by first reacting the primary amines with salicylaldehyde to form a salicylaldehyde-imine for each of the $\mathbf{AB_1}$ particle samples. The unreacted secondary amines were then titrated with standardardized perchloric acid in glacial acetic acid using bromocresol green indicator. After neutralization of the secondary amines, the salicylaldehyde-imines, therefore the primary

amines, were titrated with the standardized perchloric acid using congo red indicator. The results of the titrations (Table II-3) showed a consistent increase in the weight percents of both the primary and the secondary amines as the particle sizes increased, which is indicative of a controlled cross-linking process that leads to functionalized, well-defined and amorphous particles.

**Formation of Multifunctional Nanoparticles**

In addition to amine functionalities, acetylene and keto groups have been successfully incorporated into the nanoparticles since the goal was to extend the availability of functional groups to provide the opportunity to tailor the physical and chemical properties of the particles. Utilizing the experimental conditions established for the **AB** linear precursors, as previously discussed, linear copolymers **ABC**, **ABD**, and **ABCD** were effectively transformed into nanoparticles via the facile cross-linking technique. With each copolymer, a series of nanoparticles was prepared in which the equivalents of amine were varied from 1 to 10 amines/epoxide entity within the polymer

**Table II-4.** Nanoparticle size dimensions in relation to varying amine ratios.

| Amine/ 1 Epoxide | Diameter (nm) **$AB_1$** nanoparticles | Diameter (nm) **ABD** nanoparticles | Diameter (nm) **ABC** nanoparticles | Diameter (nm) **ABCD** nanoparticles |
|---|---|---|---|---|
| 1 | 30.7 ± 2.2 | 34.3 ± 3.2 | 21.4 ± 2.9 | 19.0 ± 1.8 |
| 2 | 58.1 ± 6.2 | 63.5 ± 7.7 | 41.7 ± 5.4 | 36.7 ± 2.2 |
| 3 | 82.6 ± 5.7 | 118.3 ± 13.6 | 114.9 ± 8.9 | 73.4 ± 5.3 |
| 4 | 115.6 ± 12.5 | 164.9 ± 17.2 | 148.3 ± 15.3 | 114.8 ± 9.2 |
| 5 | 255.7 ± 26.9 | 292.7 ± 32.2 | 186.1 ± 18.5 | 168.2 ± 16.5 |
| 6 | 342.2 ± 42.2 | 341.0 ± 32.4 | 253.9 ± 25.9 | 247.2 ± 14.5 |
| 8 | 425.1 ± 44.6 | 525.0 ± 55.4 | 472.1 ± 43.8 | 451.1 ± 20.4 |
| 10 | 725.1 ± 94.3 | 800.0 ± 135.0 | 675.0 ± 95.4 | 614.1 ± 56.2 |

backbone, in line with the experiments conducted with polymer **AB$_1$**. All three copolymers were found to respond in the same fashion as **AB$_1$** to the controlled chain cross-linking conditions to form distinct monodisperse nanoparticles as determined by DLS (Table II-4).

Parallel to the formation of the **AB$_1$** nanoparticles, a polynomial increase in the sizes of the **ABC**, **ABD**, and **ABCD** nanoparticles was observed as the amounts of diamine were increased (Figure II-7). It was concluded that the incorporated

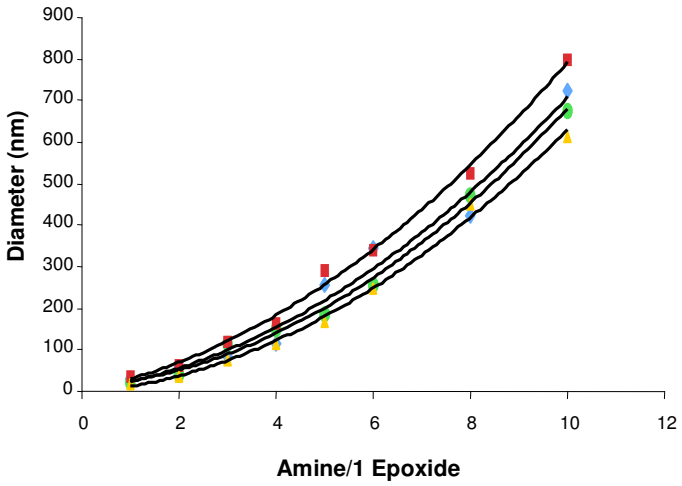


**Figure II-7.** Polynomial increase in nanoparticle size with increasing equivalents of amine cross-linker: (■) **ABD** nanoparticles; (♦) **AB$_1$** nanoparticles; (●) **ABC** nanoparticles; and (▲) **ABCD** nanoparticles.

functionalities did not affect the particle formation and participate in the cross-linking event, except for the designated oxirane unit. These results also demonstrated that the formation of the particle was adaptable for a range of functionalized polyesters and was established by the amount of both of the adjustable cross-linking partners, the epoxide and the diamine respectively.

In order to advance the availability of functional groups, methods were sought after to manipulate the quantities of each functional group incorporated into the particles. Therefore, the effect of cross-linking together two linear polymers was considered, such as specific amounts of **ABC** and **ABD**, but with comparable epoxide percentages, to integrate particular selected quantities of acetylene and keto groups. The process began by cross-linking **ABC** with **ABD** in a 7/3 ratio with 4 equivalents of amine, which resulted in the formation of nanoparticles with a size dimension of 124.7 ± 6.7 nm, as observed by DLS. The size of these nanoparticles correlated to the sizes observed from cross-linking **ABC**, **ABD**, and **ABCD** independently with similar equivalents of amine, 164.9 ± 17.2, 148.3 ± 15.3, and 114.8 ± 9.2 nm respectively (Table II-4). Characterization of the **ABC**-co-**ABD** particles by $^{1}$H NMR confirmed the incorporation of both **ABC** and **ABD** in the nanoparticle in a ratio of 7/3, which further proves that the particles were formed by a controlled intermolecular cross-linking mechanism and provides yet another avenue for controlling the integration of functional groups in the nanoparticle. With the presence of amine, acetylene and keto functionalities in the nanoparticles, a wealth of chemical and physical modifications can be accomplished.

**One-Pot Method for Controlled Nanoparticle Formation**

In view of future applications, it was intended to simplify the nanoparticle formation and make it even more attractive for commercial synthesis processes. Therefore, a one-pot method was developed in which the polymer solution is added to the diamine solution before heating to 45 ºC, thus eliminating the approximately 10 minute dropwise addition of the polymer at the beginning of the 12 hour heating

period as done with the previous method. Using this technique, the **AB** polymer was dissolved in $CH_2Cl_2$, combined with the diamine solution and then heated to reflux for 12 hours. It was found that the one-pot technique, with the polymer and diamine present in the reaction mixture at once, gave particles equivalent to the previously reported drop-in method according to investigations with TEM, DLS, and nuclear magnetic resonance spectroscopy (NMR), (Scheme II-2). The one-pot technique had also no influence on the observed solubility in common organic solvents in

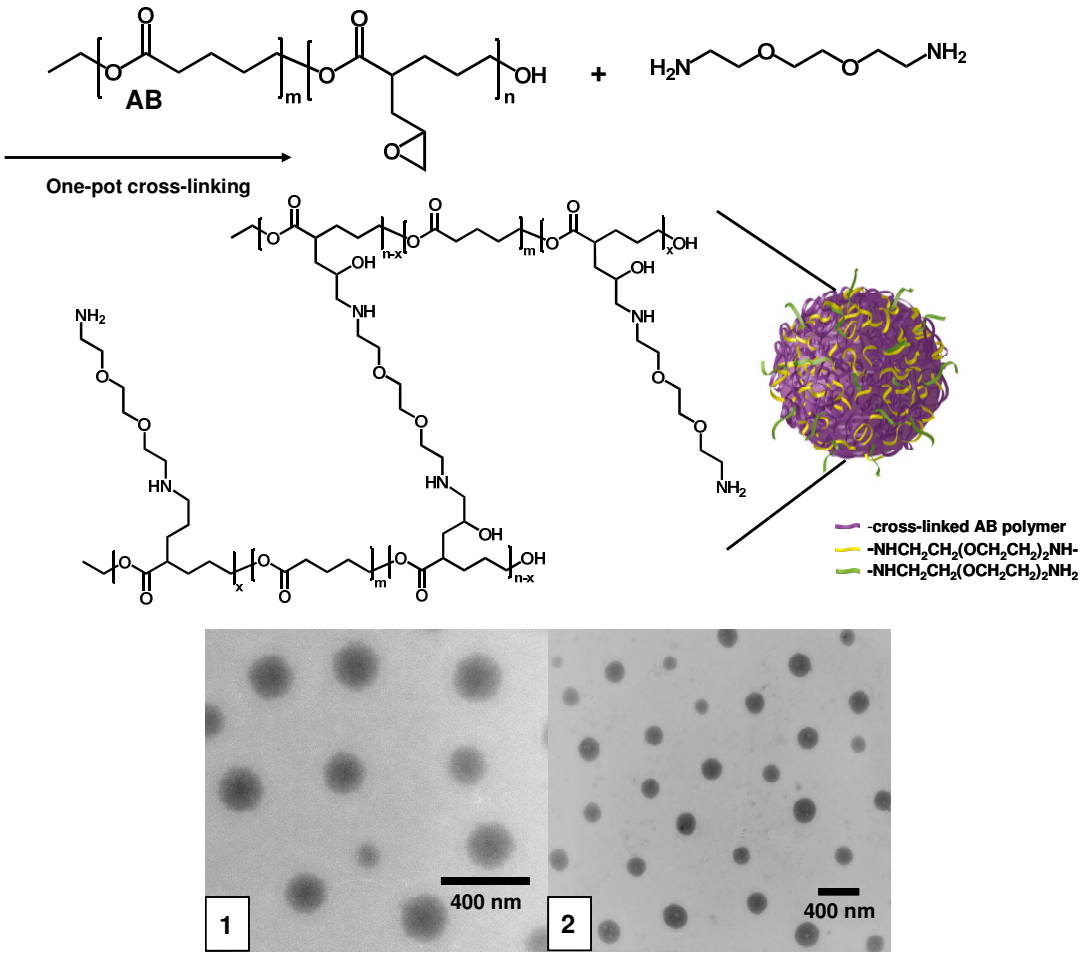


**Scheme II-2. Top:** One-pot polyester nanoparticle formation via controlled cross-linking of selected equivalencies of diamine and linear polymer precursor containing epoxide units as cross-linking partners showed with the **AB** polymer as linear precursor. **Bottom**: Comparison of TEM images of **AB** particles, 256 nm formed via the drop-in method with 5 equivalents of amine (**1**), and 272 nm prepared via the one-pot technique with 5 equivalents of amine (**2**).

comparison to the reported nanoparticles prepared with the drop-in method[60] as the result of the low cross-linking density of the final nanoparticles. Therefore, it was concluded that a drop-wise addition of polymer solution is not critical for the process of nanoparticle formation and control over nanoscopic dimensions, rather it is the equivalencies of the two cross-linking components, the epoxide and the diamine, respectively (Scheme II-1). With this, the optimized technique achieved an equivalent control of nanoparticle formation and nanoscopic size dimensions as it was observed with the previously developed drop-in technique.

## Conclusion

A new direct method to provide distinct, functionalized polyester nanoparticles in any selected nanoscopic dimension from 8 nm-700 nm has been developed. Ring-opening polymerization procedures provided linear copolymers of δ-valerolactone with α-allyl-δ-valerolactone, α -propargyl-δ-valerolactone and 2-oxepane-1,5-dione. The allyl functionality was transformed into epoxide units as one of the critical cross-linking entities to facilitate the nanoparticle formation. The reaction of the epoxide units with diamine 2,2'-(ethylenedioxy)bis(ethylamine) led to the controlled preparation of nanoparticles, in which the size dimension depended on the amount of diamine present during the cross-linking process. Additionally, it was shown that the nanoscopic dimensions could be controlled by the adjustment of incorporated epoxide groups per linear precursor. A higher percentage of epoxide gave larger particles with the same equivalents of amines present than with lower percentages of epoxide.

With the incorporation of additional functionalities in the linear polymer, the cross-linking procedure was not influenced by other functionalities present in the linear polymers, which demonstrated the universal nature of the developed procedure to gain access to functionalized polyester nanoparticles. With this said, not only identical, homogenous linear polyesters can form nanoparticles with fixed amounts of functional units, but also the amount of functionalities, such as keto-, alkyne and amine groups, per particle could be adjusted by mixing different linear polyesters with comparable epoxide percentages. In this way, a plethora of well-defined functionalized polyester nanoparticles could be prepared in different sizes and functionalities that are completely amorphous at the intended temperature of use. Using an optimized one-pot synthesis approach, functionalized polyester particles were prepared which further demonstrates the control over the individual nanoscale dimensions by the equivalents of the diamine cross-linker and the percentages of epoxides incorporated in the polyester backbone and proves that nanoparticle formation is independent of a drop-in process.

## Experimental

**Characterization.** Nuclear magnetic resonance (NMR) was performed on a Bruker DPX-300 or a Bruker AV-I 400 MHz spectrometers. Chemical shifts are reported in ppm and referenced to the corresponding residual nuclei in deuterated solvents. Gel-permeation chromatography (GPC) was carried out with a Waters chromatograph system equipped with a Waters 2414 refractive index detector, a Waters 2481 dual λ absorbance detector, a Waters 1525 binary HPLC pump, and four 5 mm Waters columns (300 mm x 7.7 mm), connected in series with increasing pore size (100, 1000, 100,000 and 1,000,000

Å respectively). All runs were performed with tetrahydrofuran (THF) as the eluent at a flow rate of 1 mL/min. For dynamic light scattering (DLS), a Malvern Nano ZS system by Malvern Instruments (Malvern Zetasizer Nanoseries, Malvern, UK) was employed at a fixed angle of 90º at 25 ºC, taking the average of three measurements. The particles were diluted with toluene to a concentration which gave the desired number of counts in order to obtain a good signal-to-noise ratio. Static light scattering (SLS) was also performed on the Malvern Nano ZS to obtain the absolute weight average molecular weights of the nanoparticles. Different sample concentrations (0.25-0.67 mg/mL) were prepared by dilution of a high concentration stock solution in toluene (1 mg/mL) to obtain the weight average molecular weight. Samples for transmission electron microscopy (TEM) imaging were prepared by dissolving 0.5 mg nanoparticles in 1 mL isopropanol, 0.3 mL acetonitrile and 0.2 mL toluene. The samples were sonicated for 5 min and were stained with 3 drops of 3% phosphotungstic acid. The carbon grids were prepared by slowly dipping an Ultrathin Carbon Type-A 400 Mesh Copper Grid (Ted Pella, Inc., Redding, CA) into the particle solutions three times and drying the grid at ambient temperature. A Philips CM20T transmission electron microscope operating at 200 kV in bright-field mode was used to obtain TEM micrographs of the polymeric nanoparticles. Differential scanning calorimetry (DSC) was performed under nitrogen atmosphere using 40 μL aluminum pans on a TA Instruments 2920 MDSC with a heating rate of 10 °C/min from -100 °C to 125 °C and a cooling rate of 10 °C/min. Three complete cycles were recorded. Glass transitions were determined at the inflection point of the endotherm, and melting points were determined at the peak of the endotherm. The degree of crystallinity was determined by quantifying the enthalpy associated with the

melting temperature of the nanoparticles. The enthalpies were used to calculate the % crystallinity by ratioing against the heat of fusion for a 100% crystalline sample (290 J/g).

**Materials.** Reagent chemicals were purchased from Aldrich (St. Louis, MO), and Acros (Morris Plains, NJ) and used as received, unless otherwise stated. Spectra/Por® Dialysis membrane and SnakeSkin® Pleated Dialysis Tubing, regenerated cellulose, were purchased from Spectrum Laboratories Inc. and Pierce Biotechnology, respectively. Analytical TLC was performed on commercial Merck plates coated with silica gel 60 $F_{254}$. Silica gel for column chromatography was Sorbent Technologies 60 Å (40-63 μm, technical grade).

**Synthesis of α-allyl-δ-valerolactone (avl) (b).** A two-necked 500 mL round bottom flask, equipped with stir bar, was sealed with a septum, purged with nitrogen and cooled in a dry ice/acetone bath. To the flask, tetrahydrofuran (156 mL), and diisopropylamine (3.30 mL, 23.4 mmol) were added. A solution of butyllithium (2.5 M in hexanes, 9.35 mL, 23.4 mmol) was added dropwise to the round bottom flask. A nitrogen purged solution of δ-valerolactone (1.97 mL, 21.3 mmol) in THF (60 mL) was added dropwise *via* syringe over 30 min. After an additional 30 min of stirring, a solution of allyl bromide (2.21 mL, 25.5 mmol) in hexamethylphosphoramide (HMPA) (4.43 mL, 25.5 mmol) was added dropwise *via* syringe over 15 min. The reaction mixture was warmed up to -40 °C and stirred for 3 h. The reaction was quenched with excess $NH_4Cl$ solution and warmed to room temperature. The crude product was washed twice with brine, dried with

anhydrous magnesium sulfate and concentrated with silica gel *via* rotary evaporator. Column chromatography with 15% EtOAc in hexanes as eluent gave a yellow product (3.43 g, 41%). $^{1}$H NMR (300 MHz, $CDCl_3$/ $Me_4Si$): δ 5.7 (m, 1H, $H_2C$=C*H*-), 5.08 (m, 2H, *H*$_2$C=CH-), 4.28 (m, 2H, -C(O)OC*H*$_2$-), 2.53-2.58 (m, 2H, $H_2C$=CHC*H*$_2$-), 2.27 (m, 1H, $H_2C$=CHCH$_2$C*H*-), 2.06 (m, 1H, $H_2C$=CHCH$_2$CHC*H*$_2$-), 1.89 (m, 2H, C(O)OCH$_2$C*H*$_2$-), 1.55 (m, 1H, $H_2C$=CHCH$_2$CHC*H*$_2$-). $^{13}$C NMR (400 MHz, $CDCl_3$): δ 173.8 (-*C*(O)O-), 135.0 ($H_2C$=*C*H-), 117.4 ($H_2C$=CH-), 68.4 (-C(O)O*C*H$_2$-), 39.2 ($H_2C$=CHCH$_2$*C*H-), 35.4 ($H_2C$=CH*C*H$_2$-), 24.0 (-*C*H$_2$CH$_2$CH$_2$-), 21.9 (-CH$_2$*C*H$_2$CH$_2$-).

**Synthesis of copolymer poly(vl-avl) (Ab).** A 50 mL 3-necked round bottom flask, equipped with stir bar, was sealed with two septa and a gas inlet. The flask was evacuated and refilled with $Ar_{(g)}$ three times. Stock solutions of 1.7 M ethanol (EtOH) in THF and $3.7x10^{-2}$ M tin(II) 2-ethylhexanoate ($Sn(Oct)_2$) in THF were made in sealed $Ar_{(g)}$ purged flasks. Solutions of EtOH (0.32 mL, $5.41x10^{-1}$ mmol) and $Sn(Oct)_2$ (0.30 mL, $1.12x10^{-2}$ mmol) were combined in the nitrogen purged 50 mL flask. After stirring the mixture for 30 min, α-allyl-δ-valerolactone (1.16 g, 8.32 mmol) and δ-valerolactone (vl, 2.50 g, 24.97 mmol) were added. The reaction vessel stirred at 105 °C for 48 h. Residual monomer and catalyst were removed by dialyzing with Spectra/Por® dialysis membrane (MWCO = 1000) against $CH_2Cl_2$ to give a golden brown polymer, **Ab** (3.24 g, 88%). $M_w$ = 3400 Da, PDI = 1.16. $^{1}$H NMR (300 MHz, $CDCl_3$/$Me_4Si$) : δ 5.7 (m, $H_2C$=C*H*-), 5.09 (m, *H*$_2$C=CH-), 4.09 (m,-C*H*$_2$-O-), 3.65 (m, CH$_3$C*H*$_2$O-), 2.35 (m, vl -CH$_2$C*H*$_2$C(O)O-, avl $H_2C$=CHCH$_2$C*H*-, $H_2C$=CHC*H*$_2$CH-), 1.68 (m, avl & vl -CHC*H*$_2$C*H*$_2$-), 1.25 (t,

C*H*$_3$CH$_2$O-); $^{13}$C NMR (400 MHz, $CDCl_3$): δ 174.6 (avl -*C*(O)-), 172.7 (vl -*C*(O)-), 134.6 ($H_2C$=*C*H-), 116.4 ($H_2$*C*=CH-), 63.3, 44.3, 35.9, 33.1, 27.5, 25.9, 23.6, 20.9.

**Synthesis of α-propargyl-δ-valerolactone (pvl) (C).** A two-necked 500 mL round bottom flask, equipped with stir bar, was sealed with a septum, purged with nitrogen and cooled in a dry ice/acetone bath (-78 °C). To the flask, tetrahydrofuran (THF) (156 mL) and diisopropylamine (3.30 mL, 23.4 mmol) were added. Slowly butyllithium (2.5 M in hexanes, 9.35 mL, 23.4 mmol) was added *via* syringe and the reaction mixture stirred for 20 min. A nitrogen purged solution of δ-valerolactone (1.97 mL, 21.3 mmol) in THF (56 mL) was added dropwise *via* syringe over 30 min. After an additional 30 min of stirring, a solution of propargyl bromide (2.85 mL, 25.5 mmol) in HMPA (4.43 mL, 25.5 mmol) was added dropwise *via* syringe. The reaction mixture was warmed up to -40 °C and stirred for 3 h. The reaction was quenched with excess $NH_4Cl$ solution and warmed to room temperature. The crude product was washed twice with brine, dried with anhydrous magnesium sulfate and concentrated with silica gel *via* rotary evaporator. Column chromatography with 20% ethyl acetate in hexanes as the eluent gave a yellow viscous product (1.9 g, 69%). $^1$H NMR (300 MHz, $CDCl_3$/$Me_4Si$): δ 4.36 (m, 2H, -C(O)OC*H*$_2$-), 2.69 (m, 2H, HC≡CC*H*$_2$C*H*-), 2.53 (m, 1H, HC≡CC*H*$_2$CH-), 2.29 (s, J = 6.3 Hz, 1H, HC≡CCH$_2$CHC*H*$_2$-), 2.09 (t, J = 2.5 Hz, 1H, *H*C≡C-), 1.96 (q, J = 6.5 Hz, 2H, HC≡CCH$_2$CHCH$_2$C*H*$_2$-), 1.75 (m, 1H, HC≡CCH$_2$CHC*H*$_2$-); $^{13}$C NMR (400 MHz, $CDCl_3$): δ 172.9 (-*C*(O)O-), 82.1 (HC≡*C*-), 70.6 (-H$_2$*C*O-), 68.4 (H*C*≡C-), 38.5 (-*C*HCH$_2$CH$_2$-), 23.8 (-CH*C*H$_2$CH$_2$-), 21.7 (-CHCH$_2$*C*H$_2$-), 20.4 (-*C*H$_2$C≡CH).

**Synthesis of copolymer poly (vl-avl-pvl) (AbC).** A 50 mL 3-necked round bottom flask, equipped with stir bar, was sealed with two septa and a gas inlet. The flask was evacuated and refilled with $Ar_{(g)}$ three times. Stock solutions of 1.7 M ethanol in THF and $3.7x10^{-2}$ M $Sn(Oct)_2$ in THF were made in sealed $Ar_{(g)}$ purged flasks. Solutions of ethanol (0.21 mL, $3.69x10^{-1}$ mmol) and $Sn(Oct)_2$ (0.20 mL, $5.41x10^{-3}$ mmol) were combined in the nitrogen purged 50 mL flask. After stirring the mixture for 30 min, α-allyl-δ-valerolactone (0.8 g, 5.7 mmol), δ-valerolactone (1.26 g, 12.6 mmol) and α-propargyl-δ-valerolactone (0.63 g, 4.6 mmol) were added. The reaction vessel stirred at 105 °C for 48 h. Residual monomer and catalyst were removed by dialyzing with Spectra/Por® dialysis membrane (MWCO = 1000) against $CH_2Cl_2$ to give a golden brown polymer (2.25 g, 84%). $M_w$ = 3500 Da, PDI = 1.26. $^1$H NMR (300 MHz, $CDCl_3/Me_4Si$): δ 5.71 (m, $H_2C$=C*H*-), 5.03 (m, *H*$_2$C=CH-), 4.08 (m, -C*H*$_2$O-), 3.65 (m, $CH_3$C*H*$_2$O-), 2.55 (m, pvl, -C(O)C*H*-, -CHC*H*$_2$C≡CH), 2.45 (m, -C*H*$_2$C≡CH), 2.34 (m, vl, -$CH_2$C*H*$_2$C(O)O-, avl, $H_2C$=CHC$H_2$C*H*-, $H_2C$=CHC*H*$_2$CH-), 2.02 (m, pvl, -C≡C*H*), 1.68 (m, pvl, avl & vl, -CHC*H*$_2$C*H*$_2$-), 1.25 (m, C*H*$_3$CH$_2$O-); $^{13}$C NMR (400 MHz, $CDCl_3$): δ 174.6, 172.7, 133.6, 117.2, 80.7, 69.9, 63.3, 44.3, 35.9, 33.1, 27.5, 25.9, 23.6, 20.9.

**Synthesis of 2-oxepane-1,5-dione (opd) (D).** A 100 mL round bottom flask, equipped with stir bar, was charged with 1,4-cyclohexanedione (2.0 g, 17.84 mmol) and meta-chloroperbenzoic acid (4.5 g, 26.08 mmol). Dichloromethane (22 mL) was added and the reaction mixture stirred and refluxed for 3 h at 40 °C. The reaction mixture was cooled to room temperature and the solvent was removed *via* rotary evaporation. The crude product was washed three times with cold diethyl ether (100 mL for each wash) and dried *in*

*vacuo* at room temperature to yield a white solid (1.48 g, 64.7%). $^{1}$H NMR (300 MHz, $CDCl_3/Me_4Si$): δ 4.4 (t, J = 5.2 Hz, 2H, -C(O)OC*H*$_2$CH$_2$C(O)-), 2.84 (m, 4H, -C*H*$_2$C(O)C*H*$_2$-), 2.72 (m, 2H, -C*H*$_2$C(O)O-); $^{13}$C NMR (400 MHz, $CDCl_3$): δ 204.9 (-*C*(O)-), 173.3 (-*C*(O)O-), 63.3 (-*C*H$_2$O-), 44.7 (-OCH$_2$*C*H$_2$C(O)-), 38.6 (-C(O)CH$_2$*C*H$_2$C(O)-), 27.9 (-*C*H$_2$C(O)O-).

**Synthesis of copolymer poly(vl-avl-opd) (AbD).** To a 50 mL 3-necked round bottom flask, equipped with stir bar, condenser, gas inlet and 2 rubber septa, 2-oxepane-1,5-dione (0.70 g, 5.45 mmol) was added. The round bottom flask was purged with argon for 10 min and then dry toluene (4 mL) was added. The mixture stirred in an oil bath at 70 °C to dissolve the monomer. Upon dissolving, δ-valerolactone (1.5 g, 14.98 mmol), α-allyl-δ-valerolactone (0.95 g, 6.81 mmol), absolute ethanol (0.0205 g, 4.4 x$10^{-1}$ mmol) and Sn(Oct)$_2$ (11.9 mg, 2.73x$10^{-2}$ mmol) were then added to the reactor and the mixture was heated for 48 h at 105 °C. Residual monomer and catalyst were removed by dialyzing with Spectra/Por® dialysis membrane (MWCO = 1000) against $CH_2Cl_2$ to give a golden brown polymer (2.70 g, 85%). $M_w$ = 4858 Da, PDI = 1.27. $^{1}$H NMR (300 MHz, $CDCl_3/Me_4Si$): δ 5.72 (m, H$_2$C=C*H*-), 5.06 (m, *H*$_2$C=CH-), 4.34 (m, -CH$_2$CH$_2$C(O)CH$_2$C*H*$_2$O-), 4.08 (m, -C*H*$_2$O-), 3.67 (m, -OC*H*$_2$CH$_3$), 2.78 (m, opd, -OC(O)CH$_2$C*H*$_2$C(O)CH$_2$-), 2.58 (m, opd, -OC(O)CH$_2$CH$_2$C(O)C*H*$_2$-), 2.34 (m, vl, -CH$_2$C*H*$_2$C(O)O-, avl, H$_2$C=CHCH$_2$C*H*-, H$_2$C=CHC*H*$_2$CH-), 1.66 (m, avl & vl, -CHC*H*$_2$C*H*$_2$-), 1.25 (t, -CH$_2$C*H*$_3$); $^{13}$C NMR (400 MHz, $CDCl_3$): δ 204.9, 175.2, 173.7, 173.2, 135.0, 117.0, 63.9, 44.8, 36.4, 33.6, 28.0, 26.3, 21.3.

**Synthesis of copolymer poly(vl-avl-pvl-opd) (AbCD).** To a 25 mL 3-necked round bottom flask, equipped with stir bar, 2-oxepane-1,5-dione (0.26 g, 2.05 mmol) was added and the flask was sealed with two septa and a gas inlet. The flask was evacuated and refilled with $Ar_{(g)}$ three times. Dry toluene (1.25 mL) was added and the mixture stirred in an oil bath at 70 °C to dissolve the monomer. Upon dissolving, $Sn(Oct)_2$ (1.8 g, $4.41x10^{-3}$ mmol in 0.15 mL dry toluene), absolute ethanol (12.8 μL, $2.22x10^{-1}$ mmol), δ-valerolactone (0.62 g, 6.2 mmol), α-allyl-δ-valerolactone (0.38 g, 2.69 mmol), and α-propargyl-δ-valerolactone (0.38 g, 2.73 mmol) were added. The temperature of the oil bath was increased to 105 °C and the mixture stirred for 50 h. Residual monomer and catalyst were removed by dialyzing with Spectra/Por® dialysis membrane (MWCO = 1000) against $CH_2Cl_2$ to give a golden brown polymer (1.31 g, 80%). $M_w$ = 3525 Da, PDI = 1.27. $^1$H NMR (300 MHz, $CDCl_3$/$Me_4Si$): δ 5.86 (m, $H_2C$=C*H*-), 5.09 (m, *H*$_2$C =CH-), 4.34 (m, opd, -$CH_2CH_2C(O)CH_2CH_2O$-), 4.08 (m, avl, pvl & vl, -C*H*$_2$O-), 3.65 (m, -OC*H*$_2$$CH_3$), 2.74 (m, opd, -OC(O)C*H*$_2$C*H*$_2$C(O)-), 2.60 (m, opd, -$CH_2CH_2C(O)CH_2CH_2$-pvl, -OC(O)C*H*-, -CHC*H*$_2$C≡CH), 2.50 (m, CHC*H*$_2$C≡CH), 2.34 (m, vl, -$CH_2CH_2C(O)O$-avl, $H_2C$=$CHCH_2CH$-, $H_2C$=$CHCH_2CH$-), 2.02 (m, *H*C≡C-), 1.68 (m, pvl, avl & vl, -CHC*H*$_2$C*H*$_2$-), 1.25 (m, -$CH_2CH_3$); $^{13}$C NMR (400 MHz, $CDCl_3$): δ 204.9, 175.2, 173.7, 172.8, 133.7 117.2, 80.6, 70.1, 63.9, 44.8, 36.4, 33.6, 28.0, 26.3, 23.7, 21.3.

**General procedure for oxidation of copolymers.** In a 200 mL round bottom flask, equipped with stir bar, poly(vl-avl), **Ab**, (2.74 g, 6.12 mmol) was dissolved in 37 mL of $CH_2Cl_2$. To this solution, 3-chloroperoxybenzoic acid (2.09 g, 12.11 mmol) was added slowly. The mixture was stirred for 72 h at room temperature and then concentrated via

rotary evaporator. The crude product was dissolved in a minimal amount of THF (5 mL) and dropped into a round-bottomed flask containing 1L diethyl ether. The solution was kept overnight at 0 °C and a white solid was obtained. The solution was decanted off and the solid was dried *in vacuo* to obtain poly(vl-evl), **AB** (1.95 g, 71%). $^{1}$H NMR (300 MHz, $CDCl_3$/$Me_4Si$): δ 4.09 (m,-C*H*$_2$-O-), 3.65 (m, $CH_3CH_2O$-), 2.96 (m, -C*H*(O)$CH_2$-), 2.75 (m, -CH(O)C*H*$_2$-), 2.47 (m, -CH(O)C*H*$_2$-), 2.35 (m, vl -$CH_2CH_2C(O)O$-, evl -$CHCH_2CH$-, -$CHCH_2CH$-), 1.68 (m, evl & vl -$CHCH_2CH_2$-), 1.25 (t, $CH_3CH_2O$-). $^{13}$C NMR (400 MHz, $CDCl_3$): 174.6, 173.1, 62.8, 51.7, 48.0, 43.3, 35.9, 33.1, 27.5, 25.9, 23.6, 20.9.

**Nanoparticle formation using epoxide-amine crosslinking.** To a 100 mL three-necked round bottom flask equipped with stir bar, condenser and septa, 2,2'-(ethylenedioxy)bis(ethylamine) (34.1 μL, 2.32 x$10^{-4}$ mol), and 28.5 mL $CH_2Cl_2$ were added. A solution of poly(vl-evl), **AB**, (0.14 g, $M_w$= 3550 Da, PDI = 1.17) in 0.2 mL $CH_2Cl_2$ was added dropwise via a peristaltic pump at 13 mL/min with vigorous stirring. The mixture was heated at 44 °C for 12 h. Residual diamine was removed by dialyzing with SnakeSkin® Pleated Dialysis Tubing (MWCO = 10,000) against dichloromethane to yield particles (0.13 g). DLS: $D_H$ = 255.7 ± 22.5 nm. $^{1}$H NMR (300 MHz, $CDCl_3$/$Me_4Si$): The significant change is the reduction of the epoxide protons at 2.94, 2.75 and 2.47 ppm and the appearance of signals at 3.64 and 2.97 ppm corresponding to the protons neighboring the secondary amine of the PEG linker after cross-linking. All other aspects of the spectrum are similar to that of **AB**.

**Nonaqueous titration of $AB_1$ nanoparticles.** A weighed amount of nanoparticles was dissolved in 10 mL chloroform. A solution of salicylaldehyde in chloroform (0.1 mL of $1.87x10^{-2}$ M) and 6 drops 0.5 % bromocresol green (in methanol) were added to the dissolved nanoparticles and the solution stirred for 10 min at room temperature. The stirred sample was titrated with $1.175x10^{-3}$ M perchloric acid (standardized with potassium hydrogen phthalate primary standard) in glacial acetic acid until the appearance of a light yellow color. The titrant volume at the end point was recorded and 10 drops 0.1 % congo red (in methanol) were added. The solution was then titrated with the perchloric acid solution till the appearance of a pure green color. The final value was the average of three replicate runs.

**Nanoparticle formation from two polymers using epoxide-amine cross-linking.** In a 100 mL three-necked round bottom flask equipped with stir bar, condenser and septa, a solution of 2,2'-(ethylenedioxy)bis(ethylamine) (28.2 μL, $1.95x10^{-4}$ mol) in 29.8 mL $CH_2Cl_2$ was heated at 44 °C. In a vial, **ABD** (0.030 g, $M_w$ = 3190 Da, PDI = 1.27) and **ABC** (0.070 g, $M_w$= 3371 Da, PDI = 1.25) were dissolved in $CH_2Cl_2$ (0.2 mL) and added dropwise to the three-necked round bottom flask via a peristaltic pump at 13 mL/min with vigorous stirring. The reaction mixture was heated at 45 °C for 12 h. Residual diamine was removed by dialyzing with SnakeSkin® Pleated Dialysis Tubing (MWCO = 10,000) against dichloromethane to yield particles (96.8 mg). DLS: $D_H$ = 43.5 ± 3.5 nm. $^1$H NMR (300 MHz, $CDCl_3/Me_4Si$): The two polymers are incorporated into the nanoparticles as evidenced by the protons at 2.01 and 4.34 ppm characteristic of poly(vl-evl-pvl), **ABC**, and poly(vl-evl-opd), **ABD**, respectively. In addition, there is the

reduction of the epoxide protons at 2.96, 2.75 and 2.47 ppm and the appearance of signals at 3.62 and 2.99 ppm corresponding to the protons neighboring the secondary amine of the PEG linker after cross-linking. All other aspects of the spectrum are similar to that of **ABC** and **ABD**.

**One pot synthesis of nanoparticles using epoxide-amine cross-linking.** In a 100 mL three-necked round bottom flask equipped with stir bar, condenser and septa, 2,2'-(ethylenedioxy)bis(ethylamine) (34.1 μL, 2.32 x$10^{-4}$ mol), 28.5 mL $CH_2Cl_2$ and a solution of poly(vl-evl), **AB**, (0.14 g, $M_w$= 3550 Da, PDI = 1.17) in 0.2 mL $CH_2Cl_2$ were added. The mixture was heated at 44 ºC for 12 h. Residual diamine was removed by dialyzing with SnakeSkin® Pleated Dialysis Tubing (MWCO = 10,000) against dichloromethane to yield particles (0.13 g). DLS: $D_H$ = 272.3 ± 23.3 nm. $^1$H NMR (300 MHz; $CDCl_3$/$Me_4Si$): δ The significant change is the reduction of the epoxide protons at 2.94, 2.75 and 2.47 ppm and the appearance of signals at 3.64 and 2.97 ppm corresponding to the protons neighboring the secondary amine of the PEG linker after cross-linking. All other aspects of the spectrum are similar to that of **AB**.

References

1. Alexis, F.; Rhee, J. W.; Richie, J. P.; Radovic-Moreno, A. F.; Langer, R.; Farokhzad, O. C., New frontiers in nanotechnology for cancer treatment. *Urologic Oncology-Seminars and Original Investigations* **2008,** *26* (1), 74-85.

2. Uhrich, K. E.; Cannizzaro, S. M.; Langer, R. S.; Shakesheff, K. M., Polymeric systems for controlled drug release. *Chemical Reviews* **1999,** *99* (11), 3181-3198.

3. Shuai, X. T.; Ai, H.; Nasongkla, N.; Kim, S.; Gao, J. M., Micellar carriers based on block copolymers of poly(e-caprolactone) and poly(ethylene glycol) for doxorubicin delivery. *Journal of Controlled Release* **2004,** *98* (3), 415-426.

4. Langer, R., Biomaterials in drug delivery and tissue engineering: One laboratory's experience. *Accounts of Chemical Research* **2000,** *33* (2), 94-101.

5. Kohane, D. S.; Tse, J. Y.; Yeo, Y.; Padera, R.; Shubina, M.; Langer, R., Biodegradable polymeric microspheres and nanospheres for drug delivery in the peritoneum. *Journal of Biomedical Materials Research Part A* **2006,** *77A* (2), 351-361.

6. Cheng, J.; Teply, B. A.; Sherifi, I.; Sung, J.; Luther, G.; Gu, F. X.; Levy-Nissenbaum, E.; Radovic-Moreno, A. F.; Langer, R.; Farokhzad, O. C., Formulation of functionalized PLGA-PEG nanoparticles for in vivo targeted drug delivery. *Biomaterials* **2007,** *28* (5), 869-876.

7. Agrawal, C. M.; Haas, K. F.; Leopold, D. A.; Clark, H. G., Evaluation of Poly(L-Lactic Acid) as a Material for Intravascular Polymeric Stents. *Biomaterials* **1992,** *13* (3), 176-182.

8. Nuutinen, J.-P.; Valimaa, T.; Clerc, C.; Tormala, P., Mechanical properties and in vitro degradation of bioresorbable knitted stents. *Journal of Biomaterials Science, Polymer Edition* **2002,** *13* (12), 1313-1323.

9. Valimaa, T.; Laaksovirta, S.; Tammela, T. L. J.; Laippala, P.; Talja, M.; Isotalo, T.; Petas, A.; Tarri, K.; Tormala, P., Viscoelastic memory and self-expansion of self-reinforced bioabsorbable stents. *Biomaterials* **2002,** *23* (17), 3575-3582.

10. Tomita, M.; Lavik, E.; Klassen, H.; Zahir, T.; Langer, R.; Young, M. J., Biodegradable polymer composite grafts promote the survival and differentiation of retinal progenitor cells. *Stem Cells* **2005,** *23* (10), 1579-1588.

11. Wuisman, P. I. J. M.; Smit, T. H., Bioresorbable polymers: heading for a new generation of spinal cages. *European Spine Journal* **2006,** *15* (2), 133-148.

12. Yang, J.; Webb, A. R.; Ameer, G. A., Novel citric acid-based biodegradable elastomers for tissue engineering. *Advanced Materials* **2004,** *16* (6), 511-+.

13. Nasongkla, N.; Bey, E.; Ren, J. M.; Ai, H.; Khemtong, C.; Guthi, J. S.; Chin, S. F.; Sherry, A. D.; Boothman, D. A.; Gao, J. M., Multifunctional polymeric micelles as cancer-targeted, MRI-ultrasensitive drug delivery systems. *Nano Letters* **2006,** *6* (11), 2427-2430.

14. Mouffouk, F.; Chishti, Y.; Jin, Q. L.; Rosa, M. E.; Rivera, M.; Dasa, S.; Chen, L. H., Polymeric micelle-based bioassay with femtomolar sensitivity. *Analytical Biochemistry* **2008,** *372* (2), 140-147.

15. Park, Y. J.; Lee, J. Y.; Chang, Y. S.; Jeong, J. M.; Chung, J. K.; Lee, M. C.; Park, K. B.; Lee, S. J., Radioisotope carrying polyethylene oxide-polycaprolactone copolymer micelles for targetable bone imaging. *Biomaterials* **2001,** *23* (3), 873-879.

16. Zhang, Z.; Feng, S.-S., Nanoparticles of poly(lactide)/vitamin E TPGS copolymer for cancer chemotherapy: synthesis, formulation, characterization and in vitro drug release. *Biomaterials* **2006,** *27* (2), 262-70.

17. Olson, D. A.; Gratton, S. E. A.; DeSimone, J. M.; Sheares, V. V., Amorphous linear aliphatic polyesters for the facile preparation of tunable rapidly degrading elastomeric devices and delivery vectors. *Journal of the American Chemical Society* **2006,** *128* (41), 13625-13633.

18. Olson, D. A.; Sheares, V. V., Preparation of unsaturated linear aliphatic polyesters using condensation polymerization. *Macromolecules* **2006,** *39* (8), 2808-2814.

19. Delie, F., Evaluation of nano- and microparticle uptake by the gastrointestinal tract. *Advanced Drug Delivery Reviews* **1998,** *34* (2-3), 221-233.

20. Maassen, S.; Fattal, E.; Mueller, R. H.; Couvreur, P., Cell cultures for the assessment of toxicity and uptake of polymeric particulate drug carriers. *S.T.P. Pharma Sciences* **1993,** *3* (1), 11-22.

21. Dong, Y. C.; Feng, S. S., Poly(D,L-lactide-co-glycolide)/montmorillonite nanoparticles for oral delivery of anticancer drugs. *Biomaterials* **2005,** *26* (30), 6068-6076.

22. Durrer, C.; Irache, J. M.; Duchene, D.; Ponchel, G., Study of the interactions between nanoparticles and intestinal mucosa. *Progress in Colloid & Polymer Science* **1994,** *97*, 275-80.

23. Jani, P.; Halbert, G. W.; Langridge, J.; Florence, A. T., Nanoparticle uptake by the rat gastrointestinal mucosa: quantitation and particle size dependency. *The Journal of pharmacy and pharmacology* **1990,** *42* (12), 821-6.

24. Kumar, M. N. V. R.; Bakowsky, U.; Lehr, C. M., Preparation and characterization of cationic PLGA nanospheres as DNA carriers. *Biomaterials* **2004,** *25* (10), 1771-1777.

25. Zweers, M. L. T.; Grijpma, D. W.; Engbers, G. H. M.; Feijen, J., The preparation of monodisperse biodegradable polyester nanoparticles with a controlled size. *Journal of Biomedical Materials Research Part B-Applied Biomaterials* **2003,** *66B* (2), 559-566.

26. Oster, C. G.; Wittmar, M.; Bakowsky, U.; Kissel, T., DNA nano-carriers from biodegradable cationic branched polyesters are formed by a modified solvent displacement method. *Journal of Controlled Release* **2006,** *111* (3), 371-381.

27. Muller, K.; Klapper, M.; Mullen, K., Polyester nanoparticles by non-aqueous emulsion polycondensation. *Journal of Polymer Science Part a-Polymer Chemistry* **2007,** *45* (6), 1101-1108.

28. Gaumet, M.; Gurny, R.; Delie, F., Fluorescent biodegradable PLGA particles with narrow size distributions: Preparation by means of selective centrifugation. *International Journal of Pharmaceutics* **2007,** *342* (1-2), 222-230.

29. Amsden, B. G.; Misra, G.; Gu, F.; Younes, H. M., Synthesis and characterization of a photo-cross-linked biodegradable elastomer. *Biomacromolecules* **2004,** *5* (6), 2479-2486.

30. Brown, A. H.; Sheares, V. V., Amorphous unsaturated aliphatic polyesters derived from dicarboxylic monomers synthesized by Diels-Alder chemistry. *Macromolecules* **2007,** *40* (14), 4848-4853.

31. Cordova, A.; Hult, A.; Hult, K.; Ihre, H.; Iversen, T.; Malmstroem, E., Synthesis of a Poly(Îµ-caprolactone) Monosubstituted First Generation Dendrimer by Lipase Catalysis. *Journal of the American Chemical Society* **1998,** *120* (51), 13521-13522.

32. Kricheldorf, H. R.; Lee, S. R.; Bush, S., Polylactones .36. Macrocyclic polymerization of lactides with cyclic Bu(2)Sn initiators derived from 1,2-ethanediol, 2-mercaptoethanol, and 1,2-dimercaptoethane. *Macromolecules* **1996,** *29* (5), 1375-1381.

33. Pang, X.; Chen, X.; Zhuang, X.; Jing, X., Crown-like macrocycle zinc complex derived from Î²-diketone ligand for the polymerization of rac-lactide. *Journal of Polymer Science, Part A Polymer Chemistry* **2007,** *46* (2), 643-649.

34. Cobb, A. J. A.; Marson, C. M., Asymmetric synthesis using catalysts containing multiple stereogenic centres and a trans-1,2-diaminocyclohexane core; reversal of predominant enantioselectivity upon N-alkylation. *Tetrahedron* **2005,** *61* (5), 1269-1279.

35. Coulembier, O.; Delcourt, C.; Dubois, P., Bulk polymerization of (L,L)-lactide using non-organometallic triazolium carbene: limited advantages. *Open Macromolecules Journal* **2007,** *1*, 1-5.

36. Douglas, A. F.; Patrick, B. O.; Mehrkhodavandi, P., A highly active chiral indium catalyst for living lactide polymerization. *Angewandte Chemie, International Edition* **2008,** *47* (12), 2290-2293.

37. Kowalski, A.; Duda, A.; Penczek, S., Mechanism of cyclic ester polymerization initiated with tin(II) octoate. 2. Macromolecules fitted with tin(II) alkoxide species observed directly in MALDI-TOF spectra. *Macromolecules* **2000,** *33* (3), 689-695.

38. Kowalski, A.; Libiszowski, J.; Biela, T.; Cypryk, M.; Duda, A.; Penczek, S., Kinetics and mechanism of cyclic esters polymerization initiated with tin(II) octoate. Polymerization of epsilon-caprolactone and L,L-lactide co-initiated with primary amines. *Macromolecules* **2005,** *38* (20), 8170-8176.

39. Van Horn, B. A.; Iha, R. K.; Wooley, K. L., Sequential and single-step, one-pot strategies for the transformation of hydrolytically degradable polyesters into multifunctional systems. *Macromolecules* **2008,** *41* (5), 1618-1626.

40. Parrish, B.; Emrick, T., Aliphatic polyesters with pendant cyclopentene groups: Controlled synthesis and conversion to polyester-graft-PEG copolymers. *Macromolecules* **2004,** *37* (16), 5863-5865.

41. Sasatsu, M.; Onishi, H.; Machida, Y., In vitro and in vivo characterization of nanoparticles made of MeO-PEG amine/PLA block copolymer and PLA. *International Journal of Pharmaceutics* **2006,** *317* (2), 167-174.

42. Mohamed, F.; van der Walle, C. F., Engineering biodegradable polyester particles with specific drug targeting and drug release properties. *Journal of Pharmaceutical Sciences* **2008,** *97* (1), 71-87.

43. Riva, R.; Lenoir, S.; Jerome, R.; Lecomte, P., Functionalization of poly(epsilon-caprolactone) by pendant hydroxyl, carboxylic acid and epoxide groups by atom transfer radical addition. *Polymer* **2005,** *46* (19), 8511-8518.

44. Parrish, B.; Breitenkamp, R. B.; Emrick, T., PEG- and peptide-grafted aliphatic polyesters by click chemistry. *Journal of the American Chemical Society* **2005,** *127* (20), 7404-7410.

45. Galindo-Rodriguez, S.; Allemann, E.; Fessi, H.; Doelker, E., Physicochemical parameters associated with nanoparticle formation in the salting-out, emulsification-diffusion, and nanoprecipitation methods. *Pharmaceutical Research* **2004,** *21* (8), 1428-1439.

46. Zweers, M. L. T.; Engbers, G. H. M.; Grijpma, D. W.; Feijen, J., Release of anti-restenosis drugs from poly(ethylene oxide)-poly (DL-lactic-co-glycolic acid) nanoparticles. *Journal of Controlled Release* **2006,** *114* (3), 317-324.

47. Renard, E.; Ternat, C.; Langlois, V.; Guerin, P., Synthesis of graft bacterial polyesters for nanoparticles preparation. *Macromolecular Bioscience* **2003,** *3* (5), 248-252.

48. Taden, A.; Antonietti, M.; Landfester, K., Enzymatic polymerization towards biodegradable polyester nanoparticles. *Macromolecular Rapid Communications* **2003,** *24* (8), 512-516.

49. Kallinteri, P.; Higgins, S.; Hutcheon, G. A.; St Pourcain, C. B.; Garnett, M. C., Novel functionalized biodegradable polymers for nanoparticle drug delivery systems. *Biomacromolecules* **2005,** *6* (4), 1885-1894.

50. Burke, S. K.; Slatopolsky, E. A.; Goldberg, D. I., RenaGel(R), a novel calcium- and aluminium-free phosphate binder, inhibits phosphate absorption in normal volunteers. *Nephrology Dialysis Transplantation* **1997,** *12* (8), 1640-1644.

51. Kioussis, D. R.; Smith, D. F.; Kofinas, P., Ammonium perchlorate-binding poly(allylamine hydrochloride) hydrogels for wastewater remediation. *Journal of Applied Polymer Science* **2001,** *80* (11), 2073-2083.

52. Parrish, B.; Quansah, J. K.; Emrick, T., Functional polyesters prepared by polymerization of alpha-allyl(valerolactone) and its copolymerization with epsilon-caprolactone and delta-valerolactone. *Journal of Polymer Science Part a-Polymer Chemistry* **2002,** *40* (12), 1983-1990.

53. Mecerreyes, D.; Miller, R. D.; Hedrick, J. L.; Detrembleur, C.; Jerome, R., Ring-opening polymerization of 6-hydroxynon-8-enoic acid lactone: Novel biodegradable copolymers containing allyl pendent groups. *Journal of Polymer Science Part a-Polymer Chemistry* **2000,** *38* (5), 870-875.

54. Latere, J. P.; Lecomte, P.; Dubois, P.; Jerome, R., 2-oxepane-1,5-dione: A precursor of a novel class of versatile semicrystalline biodegradable (Co)polyesters. *Macromolecules* **2002,** *35* (21), 7857-7859.

55. Huang, K.; Voss, B.; Kumar, D.; Hamm, H. E.; Harth, E., Dendritic molecular transporters provide control of delivery to intracellular compartments. *Bioconjugate Chemistry* **2007,** *18* (2), 403-409.

56. Harth, E.; Van Horn, B.; Lee, V. Y.; Germack, D. S.; Gonzales, C. P.; Miller, R. D.; Hawker, C. J., A facile approach to architecturally defined nanoparticles via intramolecular chain collapse. *Journal of the American Chemical Society* **2002,** *124* (29), 8653-8660.

57. Thurmond, K. B.; Kowalewski, T.; Wooley, K. L., Water-soluble knedel-like structures: The preparation of shell-cross-linked small particles. *Journal of the American Chemical Society* **1996,** *118* (30), 7239-7240.

58. Win, K. Y.; Feng, S. S., Effects of particle size and surface coating on cellular uptake of polymeric nanoparticles for oral delivery of anticancer drugs. *Biomaterials* **2005,** *26* (15), 2713-2722.

59. Critchfield, F. E.; Johnson, J. B., Determination of Aliphatic Primary and Secondary Plus Tertiary Amines. *Analytical Chemistry* **1957,** *29* (6), 957-959.

60. van der Ende, A. E.; Kravitz, E. J.; Harth, E., Approach to formation of multifunctional polyester particles in controlled nanoscopic dimensions. *Journal of the American Chemical Society* **2008,** *130* (27), 8706-8713.

# CHAPTER III

# CLICK REACTIONS: NOVEL CHEMISTRIES FOR FORMING WELL-DEFINED POLYESTER PARTICLES

## Introduction

Cu(I)-catalyzed 1,3-dipolar cycloaddition of azides and alkynes named click chemistry has emerged as an attractive and promising tool to construct novel polymers with well-defined architectures.[1] The introduction and development of the alkyne-azide click approach has had a transformational impact on applications extending to the preparation of dendrimers,[2-4] synthesis of functional block copolymers,[5, 6] synthesis of uniformly structured hydrogels,[7-9] the preparation of enzyme inhibitors *in situ*,[10] and many others.[6, 11, 12] The great success of this process relies on its simplicity, efficiency and selectivity, wide scope applicability regardless of the reagents' molecular complexity, and ability to occur under aerobic conditions.[10] Click chemistry, however, also encompasses other well-known reactions, such as the hetero-Diels-Alder reaction[11, 12] and the carbonyl transformation into oxime ethers.[13, 14]

Another reaction that has recently emerged as an attractive click process is the addition of thiols to alkenes, which is called thiol-ene coupling or thiol-ene click reaction.[15] Thiol-ene chemistry has many of the attributes of alkyne-azide click chemistry, such as tolerance to many different reaction conditions, facile synthetic strategies and clearly defined reaction pathways. Therefore, the thiol-ene click reaction has been utilized for a range of applications, including cross-linked polymeric matrices, such as hydrogels,[16, 17] polymer and nanoparticle functionalization,[21, 22] dendrimer synthesis,[18] and nanoprinting and patterning.[19, 20]

While both the alkyne-azide and thiol-ene click chemistries have been extensively used for a large number of applications, ranging from optical components[21] and biomaterials,[27, 28] these chemistries have not been thoroughly investigated for the controlled assembly of supramolecular structures in the form of 3-D degradable nanoparticles. Traditional mechanisms for forming polyester materials, such as solvent displacement[22] and salting-out methods[23] do not allow for the controlled implementation of network architectures and, therefore, the tailoring of release profiles and degradation of such materials has been challenging, which is an indirect result of the self-assembly of the linear polyester. It was found that the formation of degradable nanoparticles via intermolecular chain cross-linking reactions shows a tremendous versatility regarding nanoscopic size control, degradation and linear release kinetics.[24] These factors will be become increasingly critical to facilitate delivery systems to respond to the demands of different types of cancers in single and combination therapy, as we have recently investigated in preliminary tumor growth delay studies,[25] and for the optimum treatment for a broad range of diseases requiring targeted and non-targeted sustained delivery systems. As the importance of this methodology for nanoparticle formation continued to be recognized, other chemistries that are capable of facilitating the nanoparticle formation with the same efficiency as the reported epoxide-amine cross-linking reaction were investigated.[24] Similar to the epoxide amine reaction, reactions were selected that did not require the addition of any other reagents, were considered high yielding, and were carried out under mild reaction conditions, such as alkyne-azide and thiol-ene click chemistries. This work reports the successful systematic preparation of degradable nanoparticles in a variety of distinct nanoscopic size dimensions using the traditional

alkyne-azide click chemistry and the more recently developed thiol-ene click reaction by covalently cross-linking alkyne or allyl functionalized linear polyesters with bisazides or dithiols respectively. The intermolecular chain cross-linking reaction for nanoparticle formation has been shown to be driven by the efficiency of the cross-linking reaction and, therefore, procedures, such as the click reactions, which are highly adaptable, and novel processes for this technique, provide another avenue to these valuable biomaterials.

## Results and Discussion

### Nanoparticle Formation using Alkyne-Azide Click Cross-linking

Particle formation using the traditional alkyne-azide click chemistry started with the synthesis of a low molecular weight linear polyester with pendant alkyne groups, poly(valerolactone-propargylvalerolactone) (poly(vl-pvl)), and was synthesized by copolymerizing α-propargyl-δ-valerolactone with commercially available δ-valerolactone through ring-opening polymerization (ROP) with ethanol and tin(II) 2-ethylhexanoate, as

**Table III-1.** Multifunctional Linear Polyester Precursors **Ab** and **AC**.

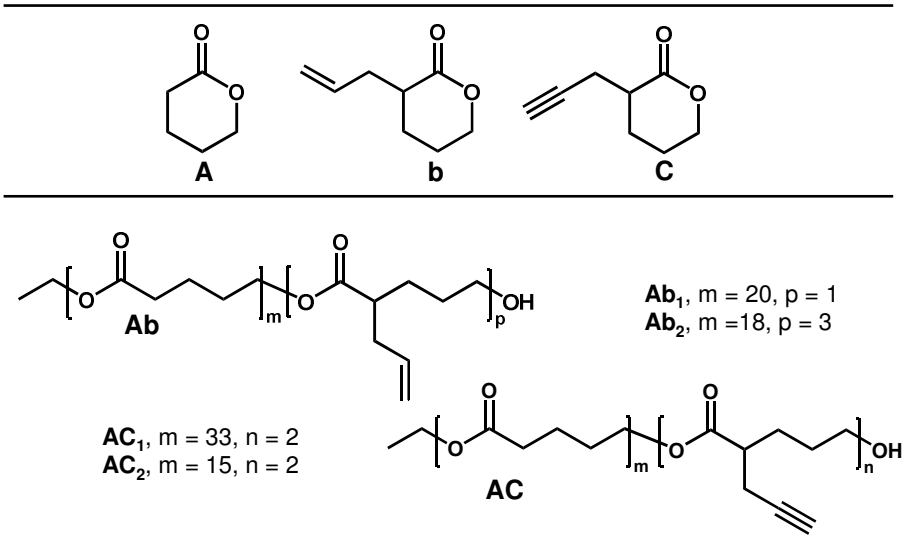

the intiator and catalyst respectively, to result in a linear polymer with 5 % alkyne functionality, $\mathbf{AC_1}$ (Table III-1).

Upon copolymerization, the alkyne functionalized polymer precursors were cross-linked with a bisazide, 1,8-diazide-3,6- dioxaoctane, to test the ability to prepare nanoparticles and control particle formation. A series of experiments were completed in which $\mathbf{AC_1}$, dissolved in dimethylformamide (DMF), was reacted with copper(I) bromide and either 2, 4, or 8 equivalents of azide per pendant alkyne in the polymer in a one-pot reaction (Scheme III-1), equivalent to the previously published one-pot intermolecular cross-linking technique.[26] The reactions were carried out at 45 °C for 24 h and

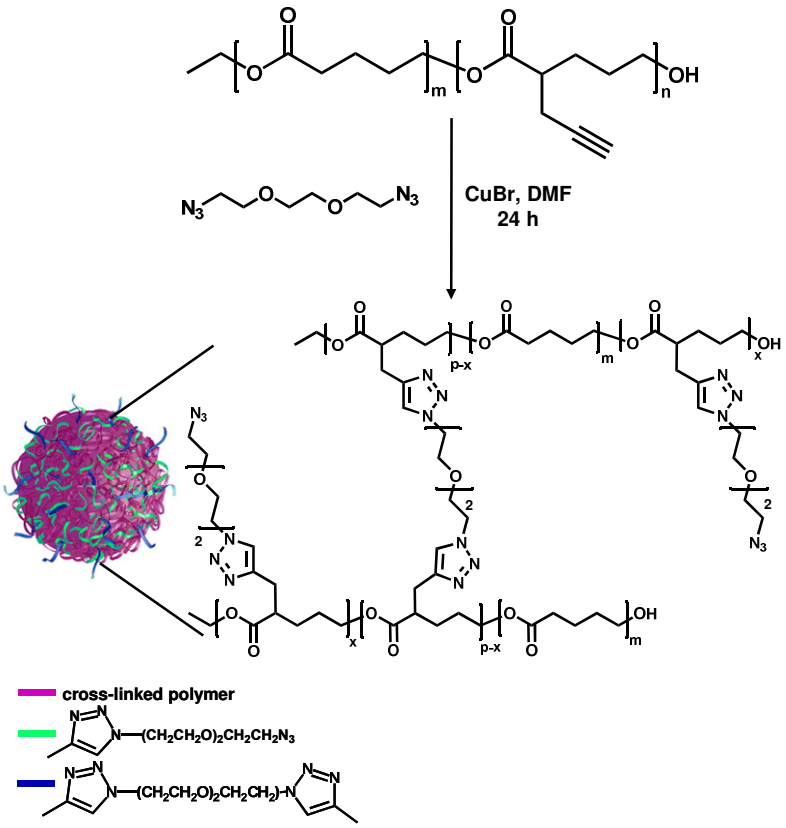


**Scheme III-1.** Nanoparticle formation using alkyne-azide click cross-linking.

subsequently dialyzed to remove unreacted starting materials. As evidenced by dynamic light scattering (DLS), each of the experiments was successful in forming well-defined monodispersed nanoparticles (Figure III-1). With 2 equivalents of azide per alkyne group, a particle of 39.8 ± 3.9 nm was obtained, whereas 4 equivalents of azide per alkyne moiety resulted in an 87.5 ± 5.3 nm particle. In addition to DLS, the spherical

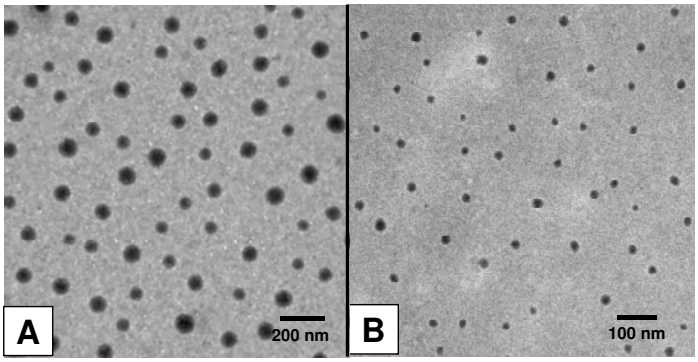


| Azide/ 1 Alkyne | Diameter (nm) $AC_1$ particles 45 °C | Diameter (nm) $AC_2$ particles 45 °C | Diameter (nm) $AC_1$ particles room temp. | Diameter (nm) $AC_2$ particles room temp. |
|---|---|---|---|---|
| 2 | 39.8 ± 3.9 | 84.1 ± 6.3 | 21.2 ± 1.7 | 45.9 ± 3.6 |
| 4 | 87.5± 5.3 | 177.5 ± 16.7 | 37.1 ± 2.9 | 75.6 ± 6.8 |
| 8 | 183.4 ± 14.4 | 367.1 ± 26.6 | 77.7 ± 4.7 | 178.8 ± 12.9 |

**Figure III-1. Top:** TEM images of $\mathbf{AC_1}$ and $\mathbf{AC_2}$ particles **(A)** $\mathbf{AC_1}$ particles prepared at 45°C with 4 equivalents azide and **(B)** $\mathbf{AC_2}$ particles prepared at room temperature with 2 equivalents azide. **Bottom:** Nanoparticle sizes, determined by DLS, of $\mathbf{AC_1}$ and $\mathbf{AC_2}$ particles formed at 45 °C or room temperature.

morphology of the particles was observed by transmission electron microscopy (TEM), as shown in Figure III-1. Both DLS and TEM underline the versatility of the alkyne-azide click approach to prepare well-defined nanoparticles in narrow nanoscopic size dimensions, controlled by the equivalents of bisazide. Analogous to the cross-linking reaction using the epoxide-amine chemistry, the nanoparticles are completely soluble in

organic solvents and inherit the solubility of the linear polymer precursor, an advantage for particle characterization and modification.

Using $^{1}$H NMR, nanoparticle formation was further confirmed, as evidenced by a reduction of the signal at 2.03 ppm due to the alkyne proton and the appearance of the peak at 7.49 ppm due to the proton from triazole formation as a result of cross-linking (Figure III-2). $^{1}$H NMR was also able to indicate an increase in particle size, since the

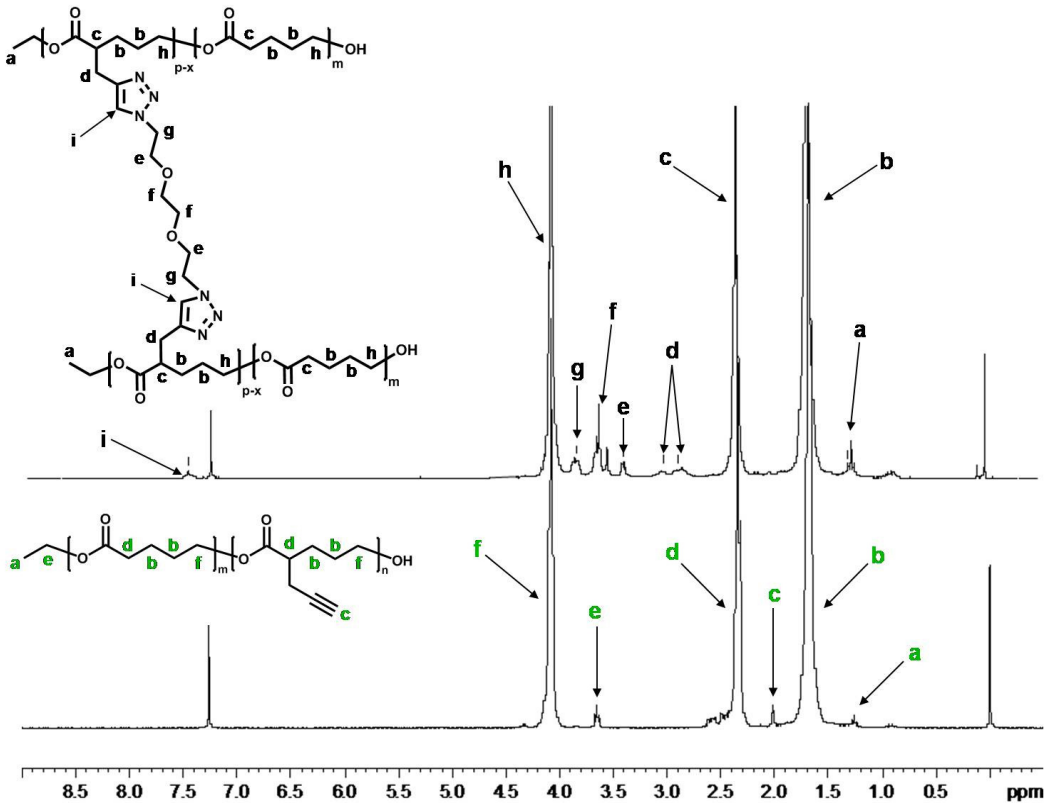


**Figure III-2.** (Top) $^{1}$H NMR spectra of **AC$_1$** particles, 87.5 nm and linear **AC$_1$** linear polymer precursor (Bottom).

signal at 3.40, 3.66 and 3.83 ppm characteristic of the methylene protons of the bisazide linker and the peak at 7.49 ppm corresponding to the triazole protons intensified as the particles became larger in size with the consecutive increase of the azide cross-linker and

is in agreement to the intermolecular cross-linking process demonstrated for the epoxide-amine cross-linking reaction as previously reported.[24]

The ability to control the size of the nanoparticles was examined in further detail by performing a second set of experiments in which the effect of increasing the amount of alkyne incorporated in the linear polymer from 5% to 12% was investigated. For these reactions, the equivalencies of the bisazide were varied from 2 to 8 azides per alkyne group in the polymer, $\mathbf{AC_2}$, containing 12% of the alkyne cross-linking unit, and were found to result in well-defined larger particles as compared to those formed from $\mathbf{AC_1}$. For example, 84 nm particles were obtained with 2 azides per alkyne moiety from $\mathbf{AC_2}$, whereas for $\mathbf{AC_1}$, 4 azides per alkyne group needed to be used in order to achieve 87 nm particles. It can be concluded that with the alkyne-azide cross-linking chemistry, nanoparticle size can be both regulated by the equivalencies of the azide cross-linker and the percentage of the incorporated alkyne entities in the linear polymer, in the same fashion as was observed for the epoxide-amine cross-linking reaction.[24] With this, another suitable reaction has been found to perform the intermolecular cross-linking in a controlled manner.

In addition to its simplicity and efficiency, the alkyne-azide cycloaddition has been shown to proceed with ease under mild conditions, such as room temperature.[27] Therefore, the capability of preparing particles at ambient temperature was explored for the possible future encapsulation of sensitive bioactive cargo, such as peptides and proteins, during particle formation. To achieve this goal, a series of reactions were completed at room temperature in which $\mathbf{AC_1}$ was coupled for 24 h in DMF with either 2, 4, or 8 equivalents of azide per alkyne in the presence of copper bromide. Analysis by

DLS demonstrated that the reduction in temperature was efficient in producing well-defined though slightly smaller particles (Figure III-1) as compared to those prepared at 45 °C.

By increasing the percent of incorporated alkyne groups in the linear polymer, the size of the particles can be systematically increased as was seen with the case of polymer **$AC_2$**, with 12% alkyne groups incorporated. Using 2 equivalents of azide per alkyne group, 45 nm particles can be prepared, whereas 4 equivalents of azide per alkyne unit were required to obtain 37 nm particles from polymer **$AC_1$** (Figure III-1). Although the ambient reaction temperature resulted in marginally smaller particles, it is evident that there remains excellent control over the formation of well-defined particles with varied distinct nanoscopic size dimensions.

Differential scanning calorimetry (DSC) was used to determine the thermal properties of two sets of **$AC_2$** nanoparticles prepared from cross-linking polymer **$AC_2$** with 2 equivalents of azide per alkyne either at room temperature or at 45 °C. From the DSC results, it was evident that both sets of particles were amorphous at the intended temperature of use, at 37 °C, with glass transition temperatures reaching from –1.7 to -2.5 °C (Figure III-3). The increase in $T_g$, in comparison to the glass transition temperatures, –25.4 to -33.2 °C, of the epoxide-amine cross-linked particles can be explained by the presence of rigid triazole rings formed by the alkyne-azide click reactions, which increase the energy required for the onset of molecular motion.[28] The crystallinity of these particles ranged from 19.3% to 19.9% with the highest value corresponding to the smallest particle, 45.9 ± 3.6 nm. As the crystallinity decreased with increasing diameter of the nanoparticle, a shift of the melting temperature from 42.0 °C to 41.8 °C was

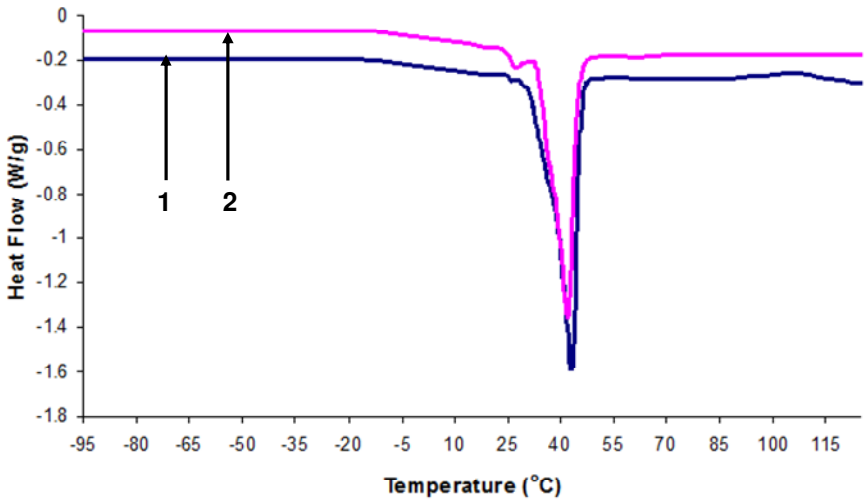


| Entry | Nanoparticle | Diameter (nm) | Reaction temp (°C) | $T_g$ (°C)[a] | $T_m$ (°C)[a] | $\Delta H_m$ (J/g)[a] | Crystallinity (%)[b] |
|---|---|---|---|---|---|---|---|
| 1 | $AC_2$ | 45.9 ± 3.6 | rt[c] | -2.5 | 42.0 | 57.73 | 19.9 |
| 2 | $AC_2$ | 84.1 ± 6.3 | 45 | -1.7 | 41.8 | 55.86 | 19.3 |

**Figure III-3.** DSC trace overlay of 45.9 ± 3.6 nm $AC_2$ nanoparticles, **1**, and 84.1 ± 6.3 nm $AC_2$ nanoparticles, **2**. [a] determined by DSC. [b] determined by taking the ratios of $\Delta H_m$ of the samples to the $\Delta H_m$ of a 100% crystalline polyester. [c] room temperature.

observed. Therefore, by varying the alkyne-azide cross-linking reaction temperature, not only can the size of the nanoparticle be tailored, but also the thermal properties of the particles can be modified.

## Nanoparticle Formation using Thiol-Ene Click Cross-linking

In addition to the alkyne-azide chemistry, there has been significant development with click reactions that do not require any metal catalyst while exhibiting all of the beneficial properties of the copper catalyzed alkyne-azide click reaction, such as the thiol-ene click reaction. Therefore, the thiol-ene reaction was an attractive approach for

the formation of nanoparticles since this chemistry can be utilized with no catalysts or other toxic reagents and is known to be highly efficient.[29, 30]

Assembly of the nanoparticles using thiol-ene click coupling begins in a very similar manner to that of the particles formed by the alkyne-azide reaction, with the synthesis of a low molecular weight linear copolymer, however, with pendant allyl groups instead of alkyne units. Integration of the allyl moieties, the critical functionality for cross-linking, was accomplished by copolymerizing α-allyl-δ-valerolactone (b) with δ-valerolactone (A) via ROP as previously reported[24] to afford poly(valerolactone-allylvalerolactone) (poly(vl-avl)), **Ab$_1$**, with 5% allyl groups incorporated (Table III-1) .

Subsequent to copolymerization, the allyl functionalized linear polyester was primed for covalent cross-linking with dithiol in order to form nanoparticles (Scheme III-2). In comparison to the epoxide-amine cross-linking technique, the allyl functionalized linear polymer, poly(valerolactone-allylvalerolactone) (poly(vl-avl)), still required oxidation to provide the epoxide functionality for cross-linking with diamine (2,2'-(ethylenedioxy)bis(ethylamine)). However, with the current approach, the oxidation reaction has been eliminated and particle formation has been simplified.

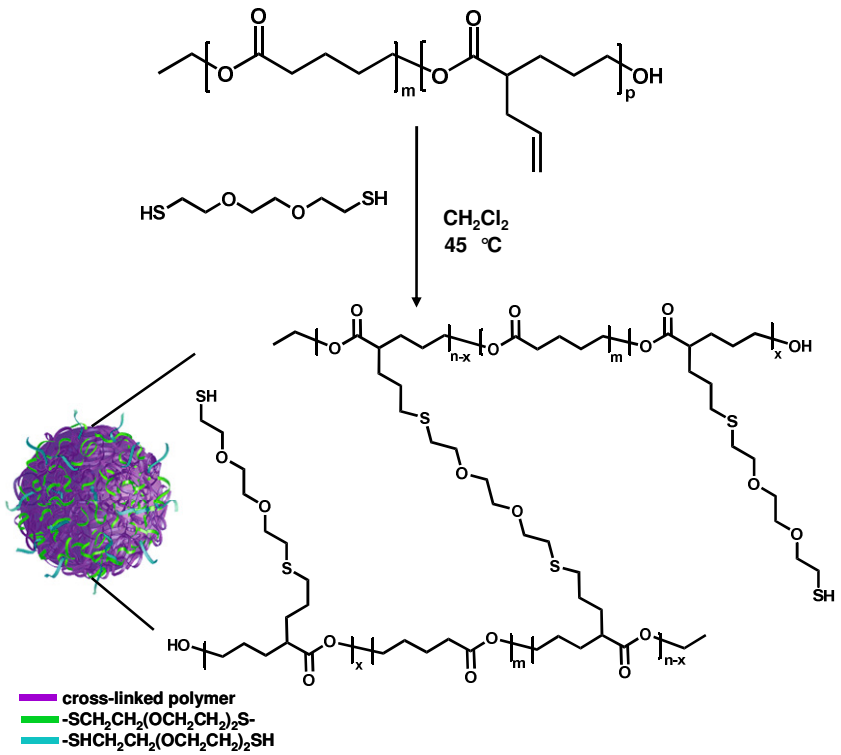


**Scheme III-2.** Nanoparticle formation using thiol-ene click cross-linking.

To form the nanoparticles, the linear polymer **Ab** was dissolved in $CH_2Cl_2$, added to a solution of 3,6-dioxa-1,8-octanedithiol in $CH_2Cl_2$, and then heated at 45 °C for 24 h (Scheme III-2), a straightforward one-pot technique for forming well-defined particles.[26] The cross-linker 3,6-dioxa-1,8-octanedithiol, the dithiol version of 1,8-diazide-3,6-dioxaoctane used in the aforementioned approach, was specifically chosen to compare the particles prepared from the two click cross-linking processes. In addition, it was previously shown that the thiol-ene click chemistry, in the absence of catalyst or initiator, proceeded with the greatest efficiency with slightly elevated temperatures[26] and, therefore, particle formation was carried out at 45 °C.

As a starting point for achieving monodisperse particles with controlled nanoscopic size dimensions, the effect of varying the amount of dithiol available for

cross-linking with the linear polymer was first investigated. Equivalents of dithiol cross-linker were increased from 1 to 8 thiols per allyl group in **$Ab_1$**. As a result of varying the equivalents of thiol, the size of the particle can be precisely controlled as seen by DLS analysis (Figure III-4). By relating the size of the particle to the equivalents of dithiol used, it is apparent that there is a polynomial increase in nanoscopic diameter. The morphology of the particles was investigated by TEM and shown in Figure III-4. From both DLS and TEM, it can be concluded that this thiol-ene cross-linking method affords particles with well-defined size and shape.

Since the nanoparticles inherit their linear polyester precursors' solubility, the

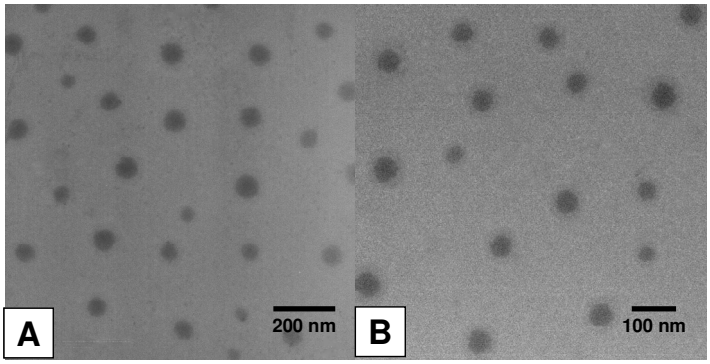


| Thiol/ 1 Allyl | Diameter (nm) $Ab_1$ particles 12 h | Diameter (nm) $Ab_1$ particles 24 h | Diameter (nm) $Ab_2$ particles 12 h | Diameter (nm) $Ab_2$ particles 24 h |
|---|---|---|---|---|
| 1 | 20.5 ± 1.5 | 29.1 ± 2.1 | 56.9 ± 2.2 | 185.5 ± 8.5 |
| 2 | 49.6 ± 2.6 | 68.4 ± 2.7 | 109.4 ± 9.0 | 256.7 ± 14.4 |
| 3 | 72.6 ± 2.8 | 89.0 ± 3.8 | 142.5 ± 11.0 | 301.1 ± 16.2 |
| 4 | 109.4 ± 7.4 | 123.1 ± 7.8 | 189.1 ± 15.9 | 349.8 ± 20.9 |
| 6 | 253.3 ± 11.2 | 299.5 ± 13.4 | 343.6 ± 22.7 | 500.7 ± 35.0 |
| 8 | 397.2 ± 18.0 | 429.3 ± 20.1 | 692.4 ± 46.9 | 884.1 ± 78.2 |

**Figure III-4.** (Top) TEM images of **$Ab_1$** and **$Ab_2$** particles **(A) $Ab_1$** particles prepared from a 12 h reaction with 3 equivalents thiol and **(B) $Ab_2$** particles formed from a 12 reaction with 1 equivalent of thiol. (Bottom) Nanoparticle sizes, determined by DLS, of **$Ab_1$** and **$Ab_2$** particles obtained from 12 or 24 h reactions at 45 °C.

particles were also characterized by $^{1}$H NMR. With $^{1}$H NMR, nanoparticle formation was confirmed by the resonance shift from 2.73 to 2.69 ppm due to the dithiol's methylene protons adjacent to the thiol functionalities (Figure III-5). In addition, the

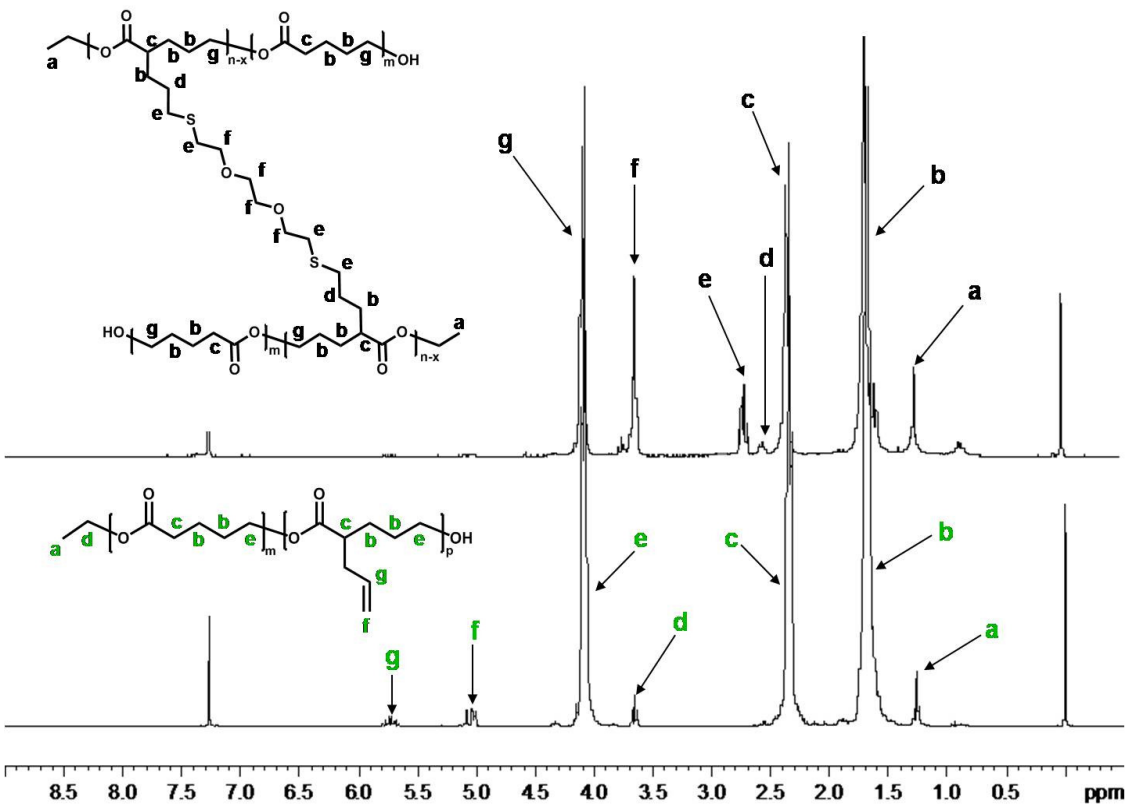


**Figure III-5.** (Top) $^{1}$H NMR spectra of **Ab$_1$** particles, 123.1 nm (24 h) and linear **Ab$_1$** linear polymer precursor (Bottom).

signals characteristic of the dithiol's methylene protons neighboring the oxygens experience a shift in resonance from 3.70 to 3.64 ppm. Both of these resonance shifts along with the reduction in the allyl protons verify successful cross-linking of the dithiol with the linear polymer.

In conjunction with examining the effect of dithiol equivalents for nanoparticle formation, the result of altering the quantity of allyl groups incorporated in the linear

polymer precursor was also studied. For this investigation, another polymer, **$Ab_2$**, with 12 % allyl groups was synthesized. With this linear polymer, a series of experiments were completed in which the equivalents of thiol were increased from 1 to 8. In accordance with the alkyne-azide cross-linking approach, the nanoparticle size dimension systematically increased with the higher percentage of allyl groups in the linear polymer precursors and with the increase in equivalents of thiol, as was seen by DLS (Figure III-4).

Important information regarding the morphology of the thiol-ene cross-linked nanoparticles was inferred from their thermal properties gathered through DSC. The thermal properties of several **$Ab_2$** nanoparticle samples, formed from cross-linking

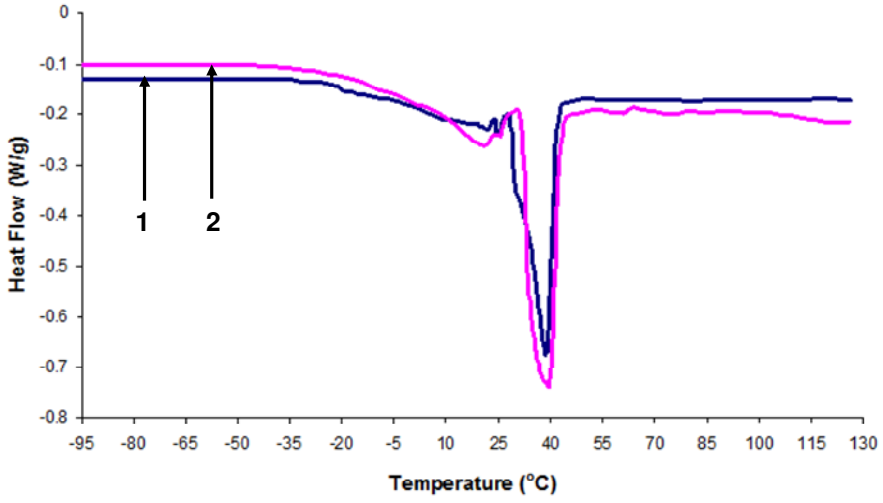


| Entry | Nanoparticle | Diameter (nm) | Reaction time (h) | $T_g$ (°C)[a] | $T_m$ (°C)[a] | $\Delta H_m$ (J/g)[a] | Crystallinity (%)[b] |
|---|---|---|---|---|---|---|---|
| 1 | **$Ab_2$** | 56.9 ± 2.2 | 12 | -20 | 38.7 | 29.56 | 10.2 |
| 2 | **$Ab_2$** | 185.5 ± 8.5 | 24 | -20 | 39.1 | 28.65 | 9.9 |

**Figure III-6.** DSC trace overlay of 56.9 ± 2.2 nm **$Ab_2$** nanoparticles, **1**, and 185.5 ± 8.5 nm **$Ab_2$** nanoparticles, **2**. [a] determined by DSC. [b] determined by taking the ratios of $\Delta H_m$ of the samples to the $\Delta H_m$ of a 100% crystalline polyester.

polymer **$Ab_2$** with 1 equivalent of thiol per allyl for either 12 or 24 h, were investigated. From the DSC results, it was evident that the **$Ab_2$** particles were amorphous at the intended temperature of use and have more predominant lower glass transition temperatures (Figure III-6), -19.6 °C to -20.2°C, in comparison to the **$AC_2$** particle samples. The decrease in $T_g$ can be explained by the increased particle flexibility due to the absence of triazole rings, which were prevalent in the alkyne-azide cross-linking reaction. Additionally, for these sets of particles, the crystallinities were significantly lower, 9.9% and 10.2%, than that of the alkyne-azide particles, which again can be explained by the lack of triazole rings, and can be tuned by varying the reaction time. Increasing the duration of the cross-linking reaction from 12 to 24 h, not only increased the size of the particle, but also decreased the crystallinity of the particle. The capacity to modify the particle's crystallinity will have a great impact on the ability to tailor the particle for different drug delivery applications.

**Comparison of Alkyne-Azide and Thiol-Ene Cross-linking**

Comparing the particle formation at 45 °C using the thiol-ene and alkyne-azide click chemistries, it is evident that the thiol-ene coupling resulted in reasonably larger particles than the alkyne-azide reaction. For example, for thiol-ene cross-linking, 4 equivalents of thiol per allyl group in **$Ab_1$** resulted in 123 nm particles, whereas for the alkyne-azide reaction, 87 nm particles were obtained with 4 equivalents of azide per alkyne unit in **$AC_1$**. As a further assessment of the thiol-ene cross-linking efficiency, a series of reactions was carried out at 45 °C for only 12 h, which remains a sufficient amount of time to form discrete particles, with equivalences of cross-linker varied from 1

to 8 thiols per allyl group. While reducing the reaction time from 24 to 12 h decreased the sizes of the particles, the sizes were, however, still slightly larger than those prepared by the alkyne-azide coupling with similar equivalencies of cross-linker (Figure III-1 and Figure III-4). From these results, it was established that the thiol-ene click reaction, which did not require the use of a catalyst or initiator, was very effective in forming well-defined nanoparticles as compared to the alkyne-azide click cross-linking.

The copper-catalyzed click reaction between azides and alkynes is ideal for many applications, however it has been reported that the copper(I) has the undesirable side effect of being cytotoxic if not removed thoroughly from the product.[16, 31] For the removal of the catalyst, the nanoparticles needed to be dialyzed for several days until the solution became free of copper. To evaluate the cellular cytotoxicity of the purified nanoparticles, the cellular viability was evaluated by utilizing an MTT assay (Figure III-7A). The cellular toxicity was determined by incubating HeLa cells for 24 h with varying concentrations of particles in triplicate ranging from 5 mg $mL^{-1}$ to 0.001 mg $mL^{-1}$. As seen in Figure III-7A, the nanoparticles did not cause significant cytotoxicity against the HeLa cell line as compared to other polyester materials reported in the literature.[32] The experimental $TC_{50}$ value for the particles was found to be approximately 0.88 mg $mL^{-1}$.

The biocompatibility of the particles formed from thiol-ene cross-linking was evaluated utilizing an MTT assay (Figure III-7B). Cytotoxicity against HeLa cells was determined as a function of nanoparticle concentration (ranging from 0.001 mg $mL^{-1}$ to 5 mg $mL^{-1}$), and untreated cells were used as the negative control. After 24 h exposure to the particles, cellular viability was measured and the particle concentration causing a 50% cytotoxic effect was found to be approximately 1.5 mg $mL^{-1}$. In contrast with the alkyne-azide cross-linked particles, which had a $TC_{50}$ of 0.88 mg $mL^{-1}$, the thiol-ene cross-linked particles exhibited a lower cytotoxicity which could be due to the absence of residual copper catalyst.

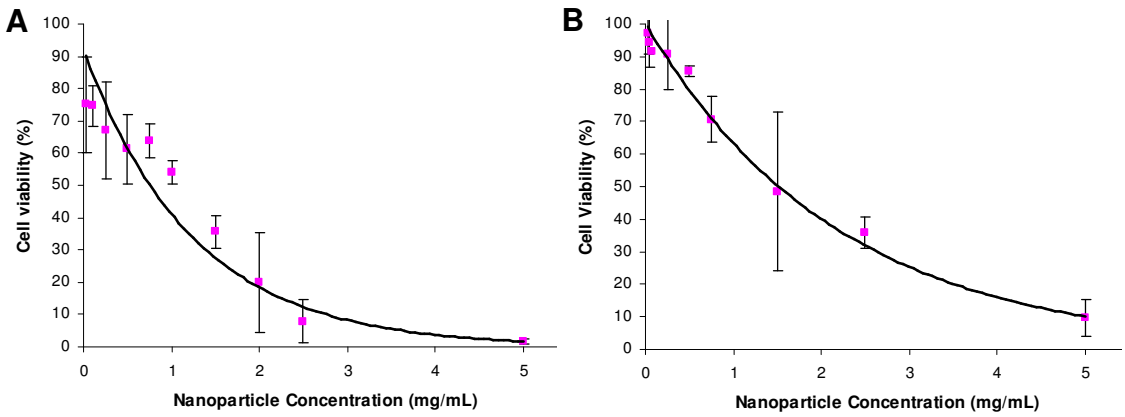


**Figure III-7.** Cytotoxicity of particles on HeLa cells using the MTT assay. Fitted curves show HeLa cell viability incubated for 24 h with **(A)** alkyne-azide cross-linked particles and **(B)** thiol-ene cross-linked particles.

## Conclusion

In summary, this work has demonstrated that 'click' chemistries, such as the alkyne-azide reaction and the thiol-ene coupling, are effective cross-linking reactions to form well-defined polyester particles via intermolecular chain collapse in selected nanoscopic size dimensions. Linear polyester precursors were effectively transformed

into particles of selected size dimensions by reacting the polymers' pendant alkyne groups with 1,8-diazide-3,6-dioxaoctane in the presence of copper(I) bromide and varying both the equivalencies of azide and the amount of alkyne groups incorporated in the linear polymer. The fact that the alkyne-azide cross-linking reaction can be successfully carried out at room will be an important asset for the further development of this technique for the encapsulation of sensitive cargo. In comparison to the alkyne- azide chemistry, the thiol-ene click reaction, performed without the use of any catalyst or initiator, was equally efficient in the performance of a controlled intermolecular cross-linking reaction. For particle formation, the pendant allyl moieties of linear poly(vl-avl) were coupled with 3,6-dioxa-1,8-octanedithiol to give distinct spherical nanoparticles in controlled size dimensions. Once more, it was found that particle size can be effectively directed by the quantity of incorporated allyl units in the polymer and the equivalencies of thiol cross-linking partner. Additionally, by reducing the duration of the thiol-ene cross-linking reaction from 24 h to 12 h, the ability to form discrete nanoparticles efficiently in half the amount of time was demonstrated in contrast to the alkyne-azide cross-linking reaction at 45 °C. Both the alkyne-azide and thiol-ene click chemistries have led to the development of two additional novel intermolecular chain cross-linking reactions for the successful preparation of well-defined spherical particles, which is further evidence for the synthetic utility of click chemistry in materials science.

## Experimental

**Characterization.** $^{1}H$ NMR spectra were obtained from a Bruker AC300 Fourier Transform Spectrometer, with $CDCl_3$/TMS as the solvent. $^{13}C$ NMR spectra were

obtained from a Bruker AC400 Fourier Transform Spectrometer with $CDCl_3$ as the solvent. Gel-permeation chromatography (GPC) was carried out with a Waters chromatograph system equipped with a Waters 2414 refractive index detector, a Waters 2481 dual λ absorbance detector, a Waters 1525 binary HPLC pump, and four 5 mm Waters columns (300 mm x 7.7 mm), connected in series with increasing pore size (100, 1000, 100,000 and 1,000,000 Å respectively). All runs were performed with tetrahydrofuran (THF) as the eluent at a flow rate of 1 mL/min. For dynamic light scattering (DLS), a Malvern Nano ZS system by Malvern Instruments (Malvern Zetasizer Nanoseries, Malvern, UK) was employed at a fixed angle of 90º at 25 ºC, taking the average of three measurements. The particles were diluted with toluene to a concentration which gave the desired number of counts in order to obtain a good signal-to-noise ratio. Samples for transmission electron microscopy (TEM) imaging were prepared by dissolving 0.5 mg nanoparticles in 1 mL isopropanol, and 0.4 mL acetonitrile. The samples were sonicated for 5 min and were stained with 5 drops of 3% phosphotungstic acid. The carbon grids were prepared by slowly dipping an Ultrathin Carbon Type-A 400 Mesh Copper Grid (Ted Pella, Inc., Redding, CA) into the particle solutions three times and drying the grid at ambient temperature. A Philips CM20T transmission electron microscope operating at 200 kV in bright-field mode was used to obtain TEM micrographs of the polymeric nanoparticles. Differential scanning calorimetry (DSC) was performed under nitrogen atmosphere using 40 μL aluminum pans on a TA Instruments 2920 MDSC with a heating rate of 10 °C/min from -100 ºC to 125 ºC and a cooling rate of 10 °C/min. Three complete cycles were recorded. Glass transitions were determined at the inflection point of the endotherm, and melting points were determined at the peak of

the endotherm. The degree of crystallinity was determined by quantifying the enthalpy associated with the melting temperature of the nanoparticles. The enthalpies were used to calculate the % crystallinity by ratioing against the heat of fusion for a 100% crystalline sample (290 J/g).

**Materials.** Reagent chemicals were purchased from Aldrich (St. Louis, MO), and Acros (Morris Plains, NJ) and used as received, unless otherwise stated. Spectra/Por® Dialysis membrane and SnakeSkin® Pleated Dialysis Tubing, regenerated cellulose, were purchased from Spectrum Laboratories Inc. and Pierce Biotechnology, respectively. Analytical TLC was performed on commercial Merck plates coated with silica gel 60 $F_{254}$. Silica gel for column chromatography was Sorbent Technologies 60 Å (40-63 μm, technical grade). Monomers α-allyl-δ-valerolactone and α-propargyl-δ-valerolactone and poly(vl-avl), **Ab**, were synthesized as previously reported.[24]

**Synthesis of copolymer poly(vl-pvl) (AC).** A 25 mL 3-necked round bottom flask, equipped with stir bar, was sealed with two septa and a gas inlet. The flask was evacuated and refilled with argon three times. Stock solutions of 1.7 M ethanol (EtOH) in THF and $3.7x10^{-2}$ M tin(II) 2-ethylhexanoate ($Sn(Oct)_2$) in THF were made in sealed $Ar_{(g)}$ purged flasks. Solutions of EtOH (0.13 mL, 0.22 mmol) and $Sn(Oct)_2$ (0.12 mL, $4.3x10^{-3}$ mmol) were combined in the $Ar_{(g)}$ purged 3-necked round bottom flask. After stirring the mixture for 20 min, α-propargyl-δ-valerolactone (pvl, 0.35 g, 2.5 mmol) and δ-valerolactone (vl, 1.1 g, 10.0 mmol) were added. The reaction vessel stirred at 105 °C for

48 h. Residual monomer and catalyst were removed by precipitating the polymer into cold diethyl ether to give a golden brown polymer (1.18 g, 81.4 %). $M_w$ = 3000 Da, PDI = 1.18. $^1$H NMR (300 MHz, $CDCl_3$/$Me_4Si$): δ 4.10 (m,-C*H*$_2$-O-), 3.64 (m, $CH_3$C*H*$_2$O-), 2.59 (m, pvl, HC≡CC*H*$_2$CH-), 2.35 (m, vl, -$CH_2$C*H*$_2$C(O)O-, pvl, HC≡C$CH_2$C*H*-, HC≡CC*H*$_2$CH-), 2.03 (m, *H*C≡C-), 1.68 (m, pvl & vl, -CHC*H*$_2$C*H*$_2$-), 1.25 (t, C*H*$_3$$CH_2$O-); $^{13}$C NMR (400 MHz, $CDCl_3$): δ 174.7 (avl, -*C*(O)-), 172.7 (pvl, -*C*(O)-), 134.6 ($H_2$C=*C*H-), 116.4 ($H_2$*C*=CH-), 82.0, 70.7, 68.9, 38.7, 35.9, 27.5, 23.9, 23.6, 21.3, 20.9.

**Nanoparticle formation using alkyne-azide click cross-linking with 1,8-diazide-3,5-dioxaoctane.** Poly(vl-pvl), **AC$_1$**, (43.5 mg, $M_w$= 3000 Da, PDI = 1.18) was added to a vial, which was then sealed and purged with argon. To the vial, 1,8-diazide-3,5-dioxaoctane (10.4 mg, 5.2x10$^{-5}$ mmol) dissolved in anhydrous dimethylformamide (0.8 mL) and copper (I) bromide (52 μL, 7.0x10$^{-2}$ M solution in DMF) were added. The reaction mixture stirred for 24 h at room temperature. Residual azide and copper bromide were removed by dialyzing with SnakeSkin® Pleated Dialysis Tubing (MWCO = 25,000) against 50/50 dichloromethane/methanol to yield particles (43.4 mg). DLS: $D_H$ = 87.5 ± 5.3 nm. $^1$H NMR (300 MHz, $CDCl_3$/$Me_4Si$): δ The significant change is the reduction of the alkyne proton at 2.03 ppm and the appearance of signals at 3.83, 3.66 and 3.40 ppm corresponding to the protons of the PEG linker and the signal at 7.49 ppm due to the protons from triazole formation as a result of cross-linking. All other aspects of the spectrum are similar to that of **AC$_1$**.

**Nanoparticle formation using thiol-ene cross-linking with 3,6-dioxa-1,8-octanedithiol.** A solution of poly(vl-avl), **Ab**, (0.14 g, $M_w$= 3042 Da, PDI = 1.18) dissolved in $CH_2Cl_2$ (0.2 mL) was added to a solution of 3,6-dioxa-1,8-octanedithiol (19.6 µL, 0.12 mmol) in $CH_2Cl_2$ (24.4 mL). The reaction mixture was heated for 12 h at 44 °C. Residual dithiol was removed by dialyzing with SnakeSkin® Pleated Dialysis Tubing (MWCO = 10,000) against $CH_2Cl_2$ to yield particles (0.13 g). DLS: $D_H$ = 72.6 ± 2.8 nm. $^1$H NMR (300 MHz, $CDCl_3$/$Me_4Si$) δ: The significant change is the reduction of the allyl protons at 5.06 and 5.77 ppm and the appearance of signals at 3.65 and 2.69 ppm corresponding to the protons neighboring the thiols of the PEG linker after cross-linking. All other aspects of the spectrum are similar to that of **Ab**.

**General procedure for *in vitro* cytotoxicity of nanoparticles (MTT assay).** The cytotoxicity of the nanoparticles was evaluated using an MTT assay. HeLa cells were cultured in Eagle's Minimum Essential Medium supplemented with 10% heat inactivated fetal bovine serum, L-glutamine, penicillin streptomycin sulfate antibiotic-antimycotic mixture and gentamicin. Cells were maintained at 37 ºC with 5% $CO_2$ in a 95% humidity incubator. The cells were seeded in a 96-well plate in 100 µL media per well at a density of 10,000 cells/well and incubated for 24 h. The media was then replaced with 100 µL of phenol red free medium-containing nanoparticles at different concentrations in triplicate and incubated for 24 h. After incubation, the nanoparticle containing media was removed, the cells were rinsed three times with PBS, to avoid interference in the assays, and 100 µL of fresh phenol red free media was added, followed by 10 µL MTT solution (5 mg/mL). The cells were incubated for 4 h, after which time the medium was carefully

removed. To the resulting purple crystals, 100 μL DMSO was added to lyse the cells and was incubated for 10 min at 37ºC. The MTT absorbance was measured at 540 nm using a Synergy HT Multi-mode microplate reader (Bio Tek Instruments, Winooski, VT). Optical densities measured for wells containing cells that received no nanoparticles were considered to represent 100% viability. Results are expressed as the mean±S.D. of viable cells.

## References


1. Zhang, W.; Mueller, A. H. E., A "Click Chemistry" Approach to Linear and Star-Shaped Telechelic POSS-Containing Hybrid Polymers. *Macromolecules* **2010,** *43* (7), 3148-3152.

2. Malkoch, M.; Schleicher, K.; Drockenmuller, E.; Hawker, C. J.; Russell, T. P.; Wu, P.; Fokin, V. V., Structurally diverse dendritic libraries: A highly efficient functionalization approach using Click chemistry. *Macromolecules* **2005,** *38* (9), 3663-3678.

3. Ornelas, C.; Aranzaes, J. R.; Cloutet, E.; Alves, S.; Astruc, D., Click assembly of 1,2,3-triazole-linked dendrimers, including ferrocenyl dendrimers, which sense both oxo anions and metal cations. *Angewandte Chemie-International Edition* **2007,** *46* (6), 872-877.

4. Lee, J. W.; Kim, J. H.; Kim, H. J.; Han, S. C.; Kim, J. H.; Shin, W. S.; Jin, S. H., Synthesis of symmetrical and unsymmetrical PAMAM dendrimers by fusion between azide- and alkyne-functionalized PAMAM dendrons. *Bioconjugate Chemistry* **2007,** *18* (2), 579-584.

5. Tsarevsky, N. V.; Bernaerts, K. V.; Dufour, B.; Du Prez, F. E.; Matyjaszewski, K., Well-Defined (Co)polymers with 5-Vinyltetrazole Units via Combination of Atom Transfer Radical (Co)polymerization of Acrylonitrile and "Click Chemistry"-Type Postpolymerization Modification. *Macromolecules* **2004,** *37* (25), 9308-9313.

6. Lundberg, P.; Hawker, C. J.; Hult, A.; Malkoch, M., Click assisted one-pot multi-step reactions in polymer science: Accelerated synthetic Protocols. *Macromolecular Rapid Communications* **2008,** *29* (12-13), 998-1015.

7. Diaz, D. D.; Punna, S.; Holzer, P.; McPherson, A. K.; Sharpless, K. B.; Fokin, V. V.; Finn, M. G., Click chemistry in materials synthesis. 1. Adhesive polymers from copper-catalyzed azide-alkyne cycloaddition. *Journal of Polymer Science Part a-Polymer Chemistry* **2004,** *42* (17), 4392-4403.

8. Ossipov, D. A.; Hilborn, J., Poly(vinyl alcohol)-based hydrogels formed by "click chemistry". *Macromolecules* **2006,** *39* (5), 1709-1718.

9. Johnson, J. A.; Lewis, D. R.; Diaz, D. D.; Finn, M. G.; Koberstein, J. T.; Turro, N. J., Synthesis of degradable model networks via ATRP and click chemistry. *Journal of the American Chemical Society* **2006,** *128* (20), 6564-6565.

10. Dondoni, A., The Emergence of Thiol-Ene Coupling as a Click Process for Materials and Bioorganic Chemistry. *Angewandte Chemie-International Edition* **2008,** *47* (47), 8995-8997.

11. Wiessler, M.; Waldeck, W.; Kliem, C.; Pipkorn, R.; Braun, K., The Diels-Alder-Reaction with inverse-Electron-Demand, a very efficient versatile Click-Reaction Concept for proper Ligation of variable molecular Partners. *International Journal of Medical Sciences* **2010,** *7* (1), 19-28.

12. Tonga, M.; Cengiz, N.; Kose, M. M.; Dede, T.; Sanyal, A., Dendronized Polymers via Diels-Alder "Click" Reaction. *Journal of Polymer Science Part a-Polymer Chemistry* **2010,** *48* (2), 410-416.

13. Kolb, H. C.; Finn, M. G.; Sharpless, K. B., Click chemistry: Diverse chemical function from a few good reactions. *Angewandte Chemie-International Edition* **2001,** *40* (11), 2004-2021.

14. Kolb, H. C.; Sharpless, K. B., The growing impact of click chemistry on drug discovery. *Drug Discovery Today* **2003,** *8* (24), 1128-1137.

15. Gu, W. F.; Chen, G. J.; Stenzel, M. H., Synthesis of Glyco-Microspheres via a Thiol-Ene Coupling Reaction. *Journal of Polymer Science Part a-Polymer Chemistry* **2009,** *47* (20), 5550-5556.

16. DeForest, C. A.; Polizzotti, B. D.; Anseth, K. S., Sequential click reactions for synthesizing and patterning three-dimensional cell microenvironments. *Nature Materials* **2009,** *8* (8), 659-664.

17. Salinas, C. N.; Anseth, K. S., Mixed mode thiol-acrylate photopolymerizations for the synthesis of PEG-peptide hydrogels. *Macromolecules* **2008,** *41* (16), 6019-6026.

18. Killops, K. L.; Campos, L. M.; Hawker, C. J., Robust, efficient, and orthogonal synthesis of dendrimers via thiol-ene "Click" chemistry. *Journal of the American Chemical Society* **2008,** *130* (15), 5062-5064.

19. Jonkheijm, P.; Weinrich, D.; Koehn, M.; Engelkamp, H.; Christianen, P. C. M.; Kuhlmann, J.; Maan, J. C.; Nuesse, D.; Schroeder, H.; Wacker, R.; Breinbauer, R.; Niemeyer, C. M.; Waldmann, H., Photochemical surface patterning by the thiol-ene reaction. *Angewandte Chemie-International Edition* **2008,** *47* (23), 4421-4424.

20. Campos, L. M.; Meinel, I.; Guino, R. G.; Schierhorn, M.; Gupta, N.; Stucky, G. D.; Hawker, C. J., Highly versatile and robust materials for soft imprint lithography based on thiol-ene click chemistry. *Advanced Materials* **2008,** *20* (19), 3728-3733.

21. Luo, J. D.; Zhou, X. H.; Jen, A. K. Y., Rational molecular design and supramolecular assembly of highly efficient organic electro-optic materials. *Journal of Materials Chemistry* **2009,** *19* (40), 7410-7424.

22. Oster, C. G.; Wittmar, M.; Bakowsky, U.; Kissel, T., DNA nano-carriers from biodegradable cationic branched polyesters are formed by a modified solvent displacement method. *Journal of Controlled Release* **2006,** *111* (3), 371-381.

23. Zweers, M. L. T.; Engbers, G. H. M.; Grijpma, D. W.; Feijen, J., Release of anti-restenosis drugs from poly(ethylene oxide)-poly (DL-lactic-co-glycolic acid) nanoparticles. *Journal of Controlled Release* **2006,** *114* (3), 317-324.

24. van der Ende, A. E.; Kravitz, E. J.; Harth, E., Approach to formation of multifunctional polyester particles in controlled nanoscopic dimensions. *Journal of the American Chemical Society* **2008,** *130* (27), 8706-8713.

25. Passarella, R. J.; Spratt, D. E.; van der Ende, A. E.; Phillips, J. G.; Wu, H.; Sathiyakumar, V.; Zhuo, L.; Hallahan, D. E.; Harth, E.; Diaz, R., *Cancer Research* **2010,** *In press*.

26. van der Ende, A.; Croce, T.; Hamilton, S.; Sathiyakumar, V.; Harth, E., Tailored polyester nanoparticles: post-modification with dendritic transporter and targeting units via reductive amination and thiol-ene chemistry. *Soft Matter* **2009,** *5* (7), 1417-1425.

27. Nwe, K.; Brechbiel, M. W., Growing Applications of "Click Chemistry" for Bioconjugation in Contemporary Biomedical Research. *Cancer Biotherapy and Radiopharmaceuticals* **2009,** *24* (3), 289-302.

28. Sperling, L. H., *Introduction to Physical Polymer Science*. 3rd ed.; Wiley-Interscience: Bethlehem, 2001.

29. Jones, M. W.; Mantovani, G.; Ryan, S. M.; Wang, X. X.; Brayden, D. J.; Haddleton, D. M., Phosphine-mediated one-pot thiol-ene "click" approach to polymer-protein conjugates. *Chemical Communications* **2009,** (35), 5272-5274.

30. Lowe, A. B., Thiol-ene "click" reactions and recent applications in polymer and materials synthesis. *Polymer Chemistry* **2010,** *1* (1), 17-36.

31. Jewett, J. C.; Sletten, E. M.; Bertozzi, C. R., Rapid Cu-Free Click Chemistry with Readily Synthesized Biarylazacyclooctynones. *Journal of the American Chemical Society* **2010,** *132* (11), 3688-3690.

32. van der Ende, A. E.; Sathiyakumar, V.; Diaz, R.; Hallahan, D. E.; Harth, E., Linear release nanoparticle devices for advanced targeted cancer therapies with increased efficacy. *Polymer Chemistry* **2010,** *1* (1), 93-96.

# CHAPTER IV

# TAILORED POLYESTER NANOPARTICLES: POST-MODIFICATION WITH DENDRITIC TRANSPORTER AND TARGETING UNITS VIA REDUCTIVE AMINATION AND THIOL-ENE CHEMISTRY

## Introduction

The rapid development of polyester materials towards specified biomedical applications is partially determined by the access to functionalities that allow the performance of reactions in sequential and orthogonal reaction pathways to integrate bioactive materials under mild conditions. Recent reports of functional linear polyester materials have demonstrated the versatility of ring-opening polymerization procedures[1] and polycondensation reactions[2, 3] to create materials[4-7] that can be tuned in their crystallinity, mechanical and biological function.[8-10] In general, functionalities integrated into linear polyester backbones are preferentially selected to undergo reactions that are highly efficient, compatible with biological materials, and lack the removal of agents in elaborate work-up procedures. In addition, conditions that inhibit the formation of active bioconjugate materials, such as elevated temperatures or catalysts that provoke uncontrolled side reactions, have to be avoided. Recently, however, synthetic procedures have been revitalized that comply with these challenges and have found widespread applications due to the presence of amine units and implemented carbonyl functionalities in biological systems, such as reductive amination, amine-oxy reactions and oxidative coupling strategies.[11-16] Not only amine groups, but also the presence of thiol groups in biological systems have stimulated the interest in thiol-ene chemistries to conjugate bioactive materials to scaffolds and

surfaces. Examples of the broad utility and commercial interest have been soft lithography,[17] photocurable materials,[18, 19] hydrogels[20-22] as well as the synthesis of macromolecular architectures.[23, 24] These types of reactions can be used in orthogonal functionalization approaches and are prone to enrich the availability of multifunctional bioconjugate materials through their synthetic ease and high yielding reactions.

While functionalized linear polyester polymers have been the subject of several post-modification strategies, the translation to 3-D functionalized polyester structures that are pertinent in the delivery and controlled release of drug molecules is only beginning to be exploited. Many potent drug molecules do not reach their cellular targets and transport across biological barriers remains challenging for therapeutics that are not allowed rapid entry due to their polarity, size and charge. Therefore, delivery strategies that target, but are also designed for rapid entry of infected tissues, are highly desirable. The lack of suitable functionalities limits the investigation of more efficient and orthogonal modification strategies that would enable the attachment of targeting and molecular building blocks to support the transport into cells and across other biological barriers in concert with the selected size and surface properties of the particles. Traditional bioconjugation chemistries of peptides with polyester particles include amide reactions, mostly EDC promoted, that require a high excess of targeting peptide units and yield often mixed products due to unselective reactions with the C terminus of the peptide sequences.

Peptidic cell penetrating peptides have been subject of intense investigations and are well documented as transport vectors.[25-29] Non-peptidic analogs, such as dendritic

molecular transporters[30-32] have just recently attracted interest caused by their macrosynthetic approach and, thereby, variability in preparation accompanied by a higher metabolic stability. For this reason, polyester materials with properties that are tunable in their physico-chemical parameters, size and morphology and allow the introduction of valuable functionalities to achieve controlled and high yielding bioactive materials will have greater impact to increase efficacies of current therapeutics and treatments.

This chapter reports the formation of polyester nanoparticles containing amine, keto, and allyl groups that can be tailored towards the conjugation of bioactive building blocks, such as a dendritic molecular transporter to facilitate cellular uptake, or peptides and dyes to accomplish targeting and imaging, respectively. In several examples of bioconjugate synthesis, the versatility of the particles is demonstrated through orthogonal attachment strategies involving high yielding thiol-ene reactions under mild conditions and reductive amination reactions, circumventing multi-step post-modification pathways.

## Results and Discussion

The potential of the prepared polyester materials for biomedical applications will be mainly determined by the synthetic ease of the sequential post-modification reactions with bioactive entities together with the physicochemical properties of the polyester particle, which can be controlled through the presented cross-linking method. Therefore, the primary goal was to develop strategies that allow orthogonal and mild modification approaches in which the cross-linked, but soluble, polyester

nanoparticle represents a multifunctional macromolecular reaction partner to provide a platform for materials that treat a broad array of diseases, directed by selected, conjugated bioactive units.

**Preparation of ABD Nanoparticle Peptide Conjugates**

Recent developments in cancer biology suggest that active targeting towards cancer provides an enhanced efficacy in drug delivery and is associated with limited side effects for the patient. These targeting units have a vast diversity in chemical nature, for example carbohydrates,[33, 34] folate,[35-38] and peptides[39-41] have been reported. Cell targeting peptides show high specificity and strong affinity for a given targeted cell line upon interactions with a receptor that is exclusively over-expressed by these cells. This work, therefore, has focused on the use of peptide targeting units, such as c-RGD that has been recognized to bind to integrin $\alpha_v\beta_3$ that is significantly up-regulated in endothelial cells of the angiogenic neovasculature within tumors, and the linear peptide GCGGGNHVGGSSV, which is known to bind x-ray treated tumors.[39, 42-44]

As an alternative to the reported strategies that form amide bonds using EDC activation, which are typically not very high yielding and require a high excess of expensive peptides, the use of reductive amination was investigated, in which the *N*-terminus of the targeting unit would be reacted with the keto group integrated in the polymer backbone of the developed polyester particle. In a model reaction, it was shown that *N*-boc-ethylenediamine (NBED) can be successfully coupled to the keto groups of the particle using reductive amination.[45] Applying these reaction conditions, the targeting

**Table IV-1.** Multifunctional linear polyester precursors with epoxide cross-linking moieties and allyl and keto groups for post modifications.

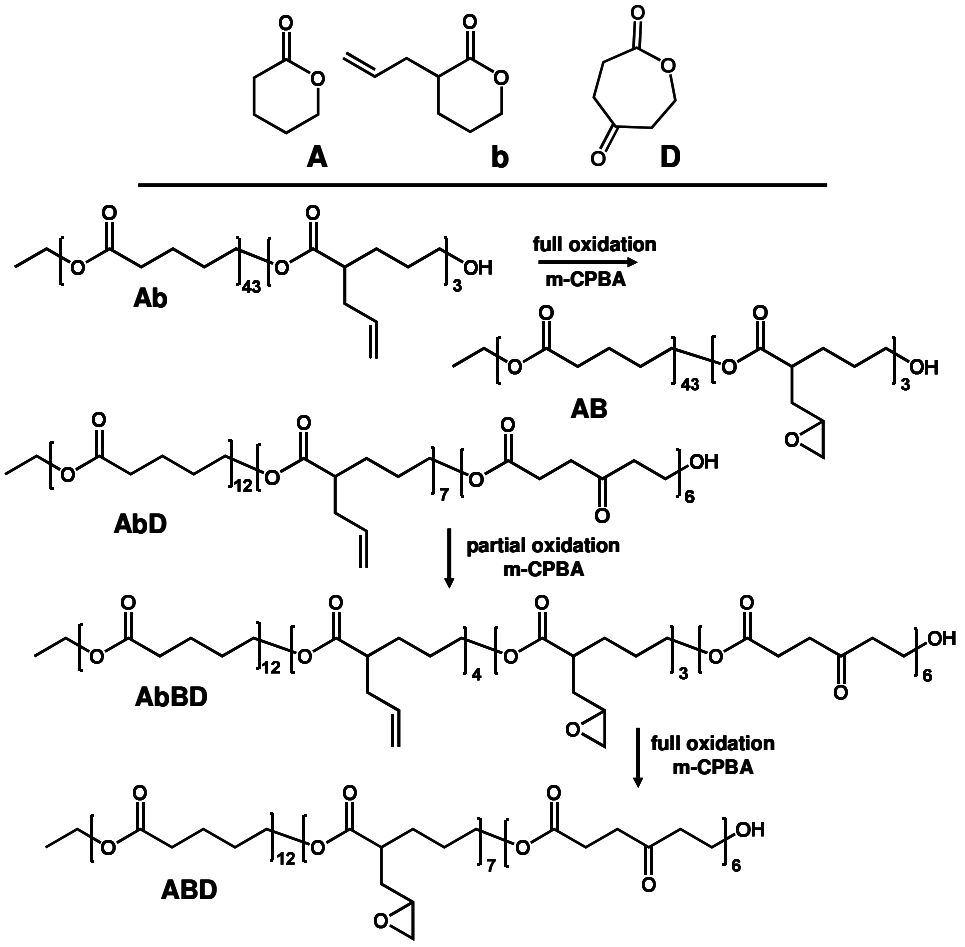

peptide sequence GCGGGNHVGGSSV,[39] was chosen for the reaction with a 118 nm **ABD** nanoparticle, which was prepared from the **ABD** linear precursor polymer (Table IV-1) with 1.5 equivalents of 2,2'-(ethylenedioxy)bis(ethylamine) cross-linking units per epoxide. After first capping the amine groups of the nanoparticle with *N*-acetoxysuccinimide, the modified particle and the peptide were solubilized in

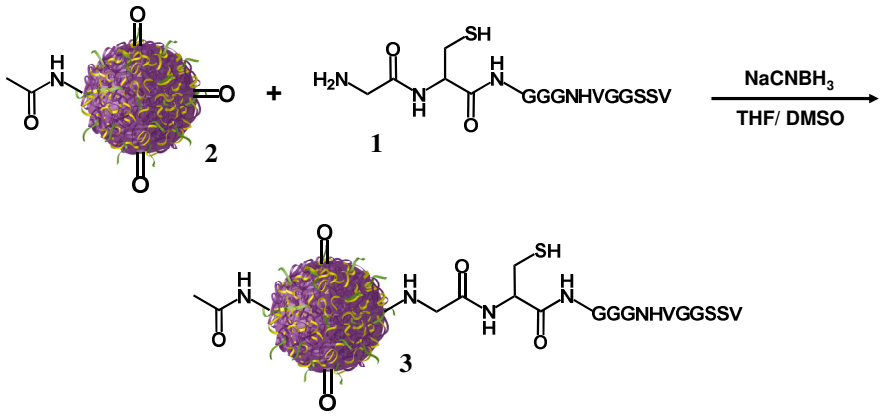


**Scheme IV-1.** Synthesis of **ABD** nanoparticle-peptide conjugate via reductive amination, ABD-NP-HVGGSSV (**3**).

tetrahydrofuran with $NaCNBH_3$ as the reducing reagent (Scheme IV-1). After purification through dialysis the peptide conjugated particles, **3**, were characterized with $^1$H NMR (Figure IV-2, at end of this Chapter) and DLS. The increase in hydrodynamic diameter from 118 ± 10 nm to 120 ± 10 nm indicated that the reductive amination conditions do not provoke significant degradation of the nanoparticle and that the reaction conditions are favorable for particle post-modification. Further investigations with $^1$H NMR showed the conjugation of peptides with the characteristic resonance peaks at 4.39 and 7.42 ppm. With additional analysis through static light scattering (SLS), the amount of peptide attached to the nanoparticle was determined and estimated to be 36 of the intended attachment of 40 peptides per particle. These results confirmed the

efficiency of the reductive amination reactions with the *N*-terminus of the selected peptidic units. Targeting units, however, that contain more than one amine group give mixed conjugation products and an alternative strategy has to be developed. For this reason, the use of thiol-ene type reactions was explored, which would be performed between cysteine units, integrated into the peptide sequence close to the *N*-terminus, and double bonds that are found in maleimides, vinylsulfones or allyl groups.

To integrate the reaction partner for the thiol/cysteine containing entities, such as peptides or oligonucleotides, onto the nanoparticles a suitable linker, which would be attached to the prepared particle, was synthesized. Therefore, a heterobifunctional linker containing a vinylsulfone and a free amine was synthesized by reacting the previously reported succinimidyl 2-(vinylsulfonyl)-ethyl carbonate (SVEC)[46] with N-boc-

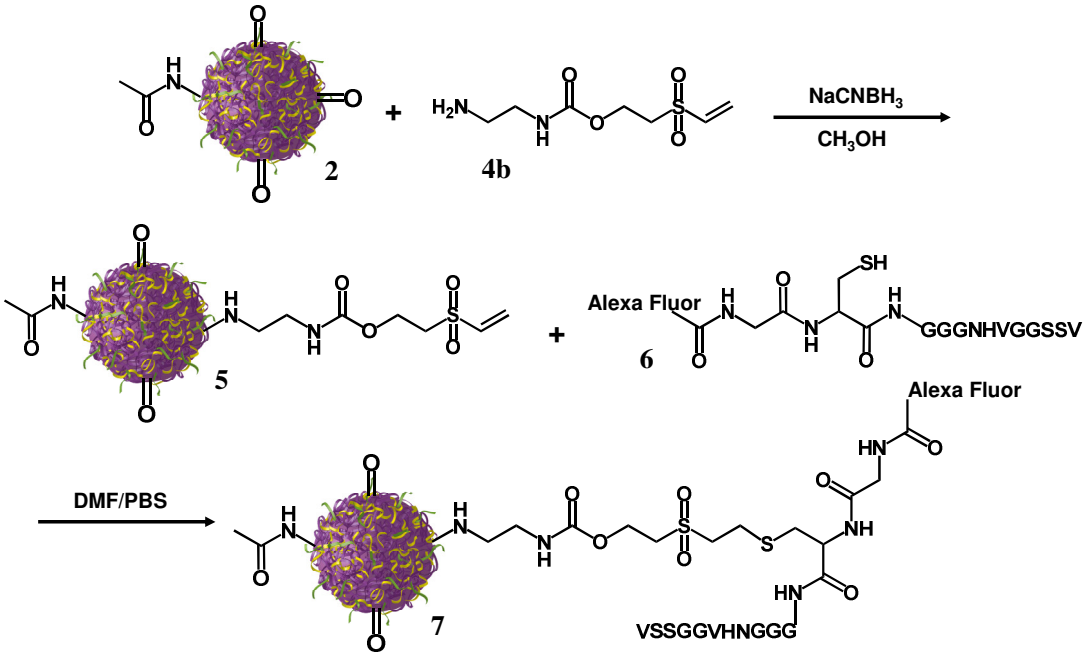


**Scheme IV-2.** Synthesis of **ABD** nanoparticle-peptide-dye conjugate via reductive amination and Michael addition, ABD-NP-Linker-HVGGSSV-dye (**7**).

ethylenediamine and deprotecting the tert-butyloxycarbonyl (boc) group to form 2-(vinylsulfonyl)ethyl 2-(amino)ethylcarbamate, **4b**. To incorporate the linker, the amine groups of the **ABD** nanoparticle were first capped with *N*-acetoxysuccinimide and then, using reductive amination, the linker was conjugated to the particle's ketone groups (Scheme IV-2).

Upon attachment of the linker, the system, **5**, was poised for conjugation to the peptidic targeting moiety GCGGGNHVGGSSV, engineered with a cysteine near the N-terminus specifically for nanoparticle modification. Prior to attachment, *N*-hydroxysuccinimidyl (NHS) Alexa Fluor® 750 dye was reacted to the N-terminus of the peptide to incorporate a fluorophore for imaging purposes. Immediately following the dye reaction, the Alexa Fluor® modified peptide was introduced to the linker-particle system by coupling the peptide's sulfhydryl group to the linker's vinylsulfone unit through a Michael-type addition, creating a targeted nanoparticle with *in vivo* imaging capabilities. While the incorporation of the 2-(vinylsulfonyl)ethyl 2-(amino)ethylcarbamate linker onto the particle allowed for the conjugation of targeting peptide, the linker's vinylsulfone unit, under certain conditions, cross-linked to form a gel product, which is not conducive for further modification. Therefore, other methods for integrating thiol containing cargo onto the nanoparticles were sought after.

**Formation of AbBD Nanoparticles**

To circumvent the conjugation of a linker molecule to facilitate the attachment of thiol containing entities, the integration of allyl groups in the polyester backbone as pendant functional units was investigated, which would be present in the linear polyester precursor before nanoparticle formation. So far in the presented work, all of the available allyl groups of the linear polyester precursors that stem from the α-allyl-δ-valerolactone have been completely oxidized to epoxide moieties to provide the critical units for cross-linking with the diamine (Table IV-1). However, with partial oxidation of the allyl groups, linear polyester precursors containing epoxide units and remaining allyl groups could be prepared. As the next step, a linear polyester **AbD**

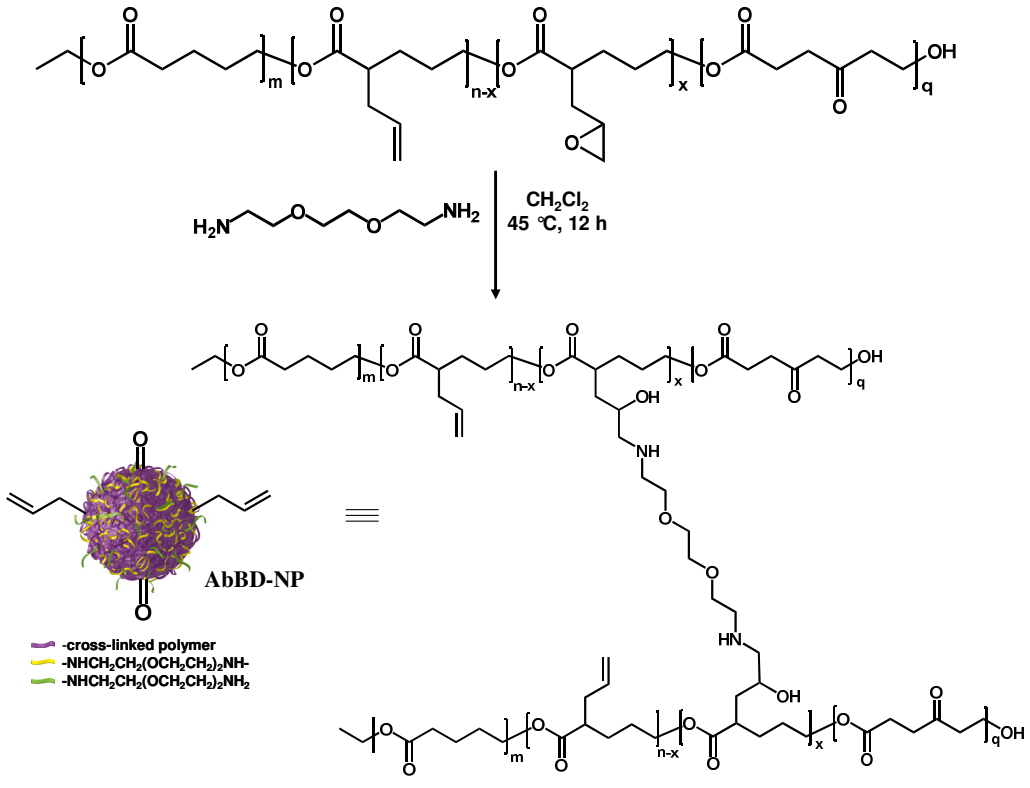


**Scheme IV-3.** Nanoparticle formation from linear polyester precursor **AbBD**.

that was partially oxidized to give **AbBD,** which was comprised of 16% allyl units and 11% epoxide units, was cross-linked with 3 equivalents of amine per epoxide, using the novel one-pot reaction procedure to examine the compatibility of the allyl groups to the conditions of nanoparticle formation (Scheme IV-3). As a comparison, the nanoparticle synthesis was carried out both with and without polyesters containing allyl functionalities and comparable epoxide percentages and very similar size distributions were obtained. The allyl resonance peaks were still present in the $^{1}$H NMR spectra of the particles and were found to be analogous to the resonances of the allyl functionalities in the linear precursor. These studies verified that the allyl moieties do not inhibit or complicate the production of well-defined nanoparticles.

**Optimization of Thiol-Ene Reaction Conditions**

After the successful synthesis of allyl functionalized polyester particles, reaction conditions to guarantee a high yielding and mild thiol-ene reaction between the polyester particle and a biological unit were investigated. In particular, it was of great interest to determine several conditions that did not necessitate the addition of organic or photochemical radical starters to form the free-radical induced (FRI) product. For these studies, benzylthiol was chosen as a model compound since this thiol would give rise to $^{1}$H NMR resonance peaks that could be conveniently detected apart from the ones of the polyester backbone. Intially, the thiol-ene reactions were conducted at ambient temperature without the addition of any organic initiators or catalysts. The first set of trials were carried out at 25 °C, with 2.8 molar equivalents of thiol units to allyl groups, and the conversion was monitored during a time frame

of 24, 48 and 72 hours by $^{1}$H NMR spectroscopy. After 72 hours, 26% of the allyl

**Table IV-2**. Thiol-ene chemistry model reactions with **AbBD** particles and benzylthiol.

| Trial | Solvent | [HS]/[Allyl] | T (°C) | $t_{reac}$ (h) | Conv.[a] (%) |
|---|---|---|---|---|---|
| I | toluene | 2.8 | 25 | 24 | — |
| II | toluene | 2.8 | 25 | 48 | 10 |
| III | toluene | 2.8 | 25 | 72 | 26 |
| IV | toluene | 2.8 | 30 | 24 | 10 |
| V | toluene | 2.8 | 30 | 48 | 20 |
| VI | toluene | 2.8 | 30 | 72 | 46 |
| VII | toluene | 2.8 | 35 | 24 | 54 |
| VIII | toluene | 2.8 | 35 | 48 | 65 |
| VIV | toluene | 2.8 | 35 | 72 | 76 |
| X | toluene | 1.5 | 30 | 24 | 37 |
| XI | toluene | 1.5 | 30 | 48 | 58 |
| XII | toluene | 1.5 | 30 | 72 | 71 |
| XIII | toluene | 1.5 | 35 | 24 | 40 |
| XIV | toluene | 1.5 | 35 | 48 | 64 |
| XV | toluene | 1.5 | 35 | 72 | 74 |
| XVI | methanol | 1.5 | 35 | 72 | 75 |
| XVII | DMSO | 1.5 | 33 | 72 | 62 |

[a]Conversion to product

groups had disappeared and an anti-Markovnikov product resulted from the thiol addition as it is also reported with comparable reactions of oligoisobutenes.[47] An increase of 5 °C to 30 °C improved the conversion to 46% of addition product and yet another raise of 5 °C could confirm the stepwise 30% increase of conversion to 76% (Table IV-2). The influence of the molar equivalencies of thiol was further investigated to determine the most beneficial ratios of these two components. From the studies, it was found that the equivalencies had a major effect on the efficiency of the reaction since 1.5 equivalents gave higher conversions compared to twice the amount of benzylthiol. Surprisingly, higher equivalents showed a negative effect on

the conversion at 30 °C that could be contributed to a faster formation of disulfide products than the addition product with the allyl group. These experiments demonstrated that the thiol-ene reactions could be performed at low temperatures, and are not restricted to highly elevated temperatures, and gives the opportunity for the addition of temperature-sensitive materials, such as peptides and oligonucleotides, in a conserving and efficient manner.

**Preparation of AbBD Nanoparticle Molecular Transporter Conjugate**

With the goal to find practical methods to integrate a variety of biological functions to the polyester particles, the optimized conditions of the thiol-ene reaction were first applied to the conjugation of functionalized dendritic transporter molecules. These macromolecular transporters were inspired from cell penetrating peptides which initiated the design of compact Newkome-type dendritic structures with differentiated peripheral guanidine units to transport cargo across cellular barriers into defined subcellular locations. The detailed synthesis and investigation of cellular uptake and subcellular localization of these molecules have been previously reported.[30] It is of particular interest to conjugate this building block to particles of different sizes as it would allow for cellular uptake through the ability of the attached transporter, independent of the particles' nanoscopic sizes or zeta potentials.

The focal point of the dendritic molecular transporter can be functionalized with 3-(2-pyridinyldithio)propanoic acid which is recognized as a valuable unit in thiol exchange reactions and is easily cleavable by reducing reagents, such as dithiothreitol (DTT). To have an efficient tool available to conduct uptake and transport of particles

through biological barriers of particles in a variety of nanoscopic dimensions, dye labeled conjugation products were synthesized. The conjugation strategy began with coupling NHS Alexa Fluor® 594 to the free amine groups on the particles, which are present as the result of the diamine cross-linking. After the attachment of approximately 20 dye molecules to the 126 nm **AbBD** nanoparticles, the material was

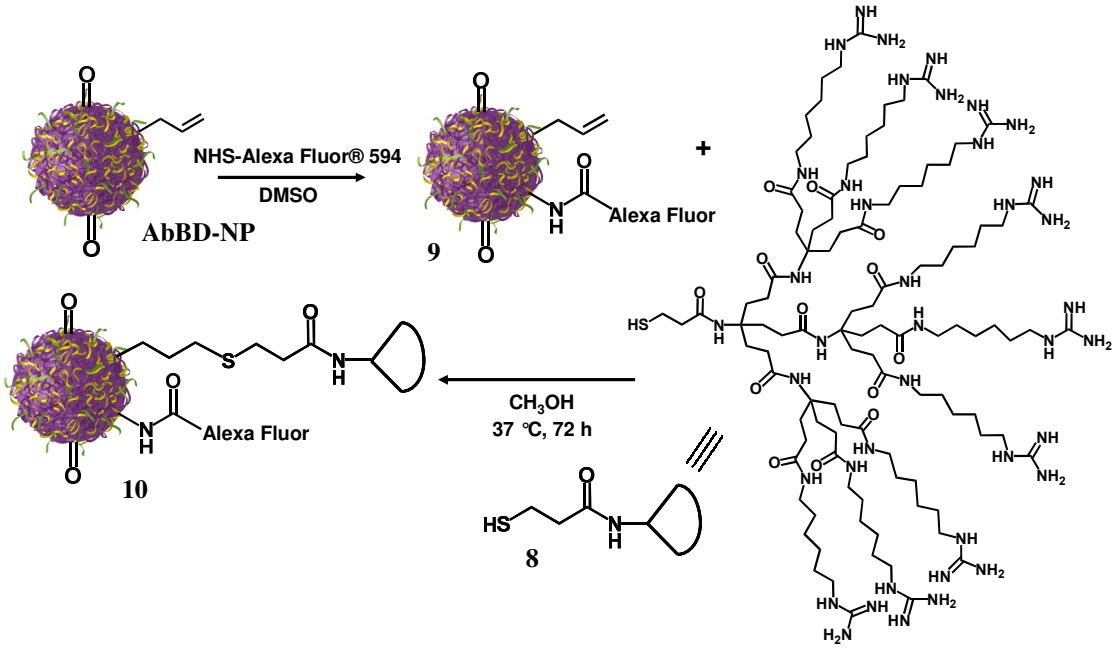


**Scheme IV-4.** Synthesis of dendritic molecular transporter-Alexa Fluor® 594 polyester nanoparticle conjugate, NP-MT-dye, AbBD-NP-594-MT (**10**).

dialyzed and the thiol-ene reaction was employed in which the free thiol of the dendritic transporter was coupled to the polyester particles' allyl units (Scheme IV-4). To prepare the dendritic transporter for the thiol-ene reaction, the disulfide bond was cleaved using DTT and the product was purified through size exclusion chromatography using a Sephadex column. While the nanoparticle was soluble in toluene, the solvent that was selected for the optimization trials, the thiol functionalized dendritic transporter is not. As a result solubility studies were

conducted and it was found that methanol was well suited to solubilize both reaction partners. Prior to the reaction with the transporter unit, a model reaction with benzylthiol was conducted to evaluate the conversion and progress of the reaction with the change of the solvent. After 72 hours a 75% conversion of the reaction in $CH_3OH$ could be achieved and, therefore, these reaction conditions were applied for the thiol-ene reaction of the transporter with the nanoparticle (Table IV-2, Scheme IV-4). Analysis with $^1H$ NMR, after thorough dialysis purification to remove any non-conjugated materials, showed the characteristic dendritic resonance peaks at 2.20, 1.98, 1.57 and 1.39 ppm. The integration of the protons and the quantification of the decrease of the allyl protons, which are conveniently detected apart from the ones of the polyester backbone, confirmed the attachment of 35 dendritic transporter units per particle. DLS showed that the nanoparticles do not exhibit any signs of degradation, as judged by the particle size distributions before and after the thiol-ene coupling. These results underline the versatility of the thiol-ene reaction which proved to be independent of the selected solvent. Investigation of the ability of this conjugate to cross biological barriers is in progress and will be reported elsewhere.

**Preparation of AbBD Nanoparticle Peptide Dye Conjugates**

In addition to conjugating the molecular transporter to the nanoparticles, the efficient thiol-ene reaction was used for the attachment of peptides to prepare other important biologically active compounds with the aforementioned targeting units toward cancer malignants. Here, two peptide targeting units were selected, one with a linear backbone, GCGGGNHVGGSSV and a HVGGSSV recognition unit containing a cysteine

unit near the *N*-terminus, and a novel cyclic peptide, designed and prepared in our laboratory, with an RGD recognition sequence. In contrast to other known cyclic RGD peptides, this novel RGD peptide was cyclized on-bead in high yields and incorporates a free amine and thiol group into the sequence to serve as functional moieties for labeling and further post-modifications. The designed novel RGD targeting peptide has the sequence (RGDEKf)-SH and provides an amine, though the integrated lysine (K), and a thiol, from the incorporated cysteine unit that is attached to the glutamic acid (E).

In view of further investigations to evaluate the targeting properties of each bioconjugate *in vitro*, the particle was labeled exclusively with Alexa Fluor® 594. Therefore, the *N*-terminus of the HVGGSSV peptide was first capped with *N*-acetoxysuccinimide and then a thiol-ene reaction was performed in dimethylsulfoxide (DMSO) to attach the peptide to a 126 nm **AbBD** nanoparticle. Finally the amine groups

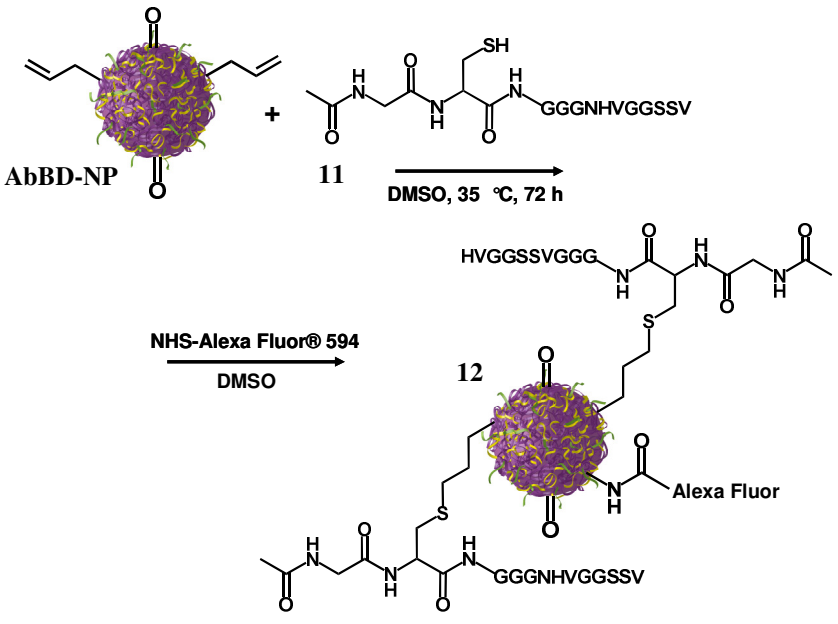


**Scheme IV-5.** Synthesis of NP-P-dye conjugate, AbBD-NP-cHVGGSSV-594 (**12**), utilizing thiol-ene chemistry.

of the peptide modified particle were labeled with NHS Alexa Fluor® 594 (Scheme IV-5).

Since the conjugated targeting unit HVGGSSV has only been recently discovered,[39] other comparative bioconjugates carrying more traditional targeting units, such as the c-RGD peptide, were also prepared for future studies comparing the binding capabilities of the conjugates. Therefore, the designed c-RGD includes a cysteine amino acid to perform the reactions as described for the linear HVGGSSV peptide. For possible future *in vitro* studies, Alexa Fluor® 594 dye, which had been previously proven to be stable towards the thiol-ene conditions, was used to label the particle. Therefore, the free amines of the **AbBD** nanoparticle were first modified with the NHS Alexa Fluor® and,

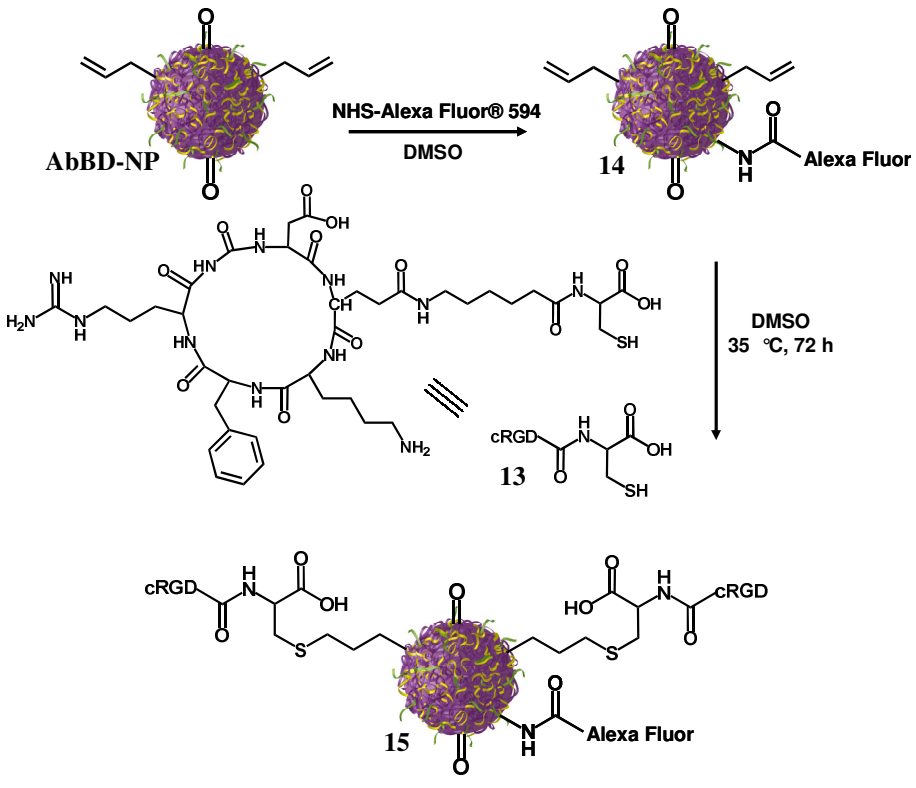


**Scheme IV-6.** Synthesis of NP-P-dye conjugate, AbBD-NP-594-cRGD (**15**), using thiol-ene chemistry.

after dialysis, the thiol-ene reaction with the c-RGD was conducted in DMSO as described above and purified against $CH_3OH$ to remove any remaining unreacted c-RGD.

Both of the conjugation products, AbBD-NP-cHVGGSSV-594, **12** (Scheme IV-5) and AbBD-NP-594-cRGD, **15**, (Scheme IV-6) were analyzed via $^1H$ NMR and the typical resonances of the peptides and the polyester backbone were observed. The decreased integration of allyl resonance peaks along with DLS and SLS analysis gave the ability to confirm and quantify the conjugation of peptidic units to the polyester backbone. So far the conjugation of one type of bioactive unit, either peptide or dendritic transporter, has been demonstrated through the reductive amination or thiol-ene reaction achieved with optimized, high yielding conditions.

**Preparation of AbBD Nanoparticle Peptide Molecular Transporter Dye Conjugates**

As the next step, the complementary biological functions of the targeting unit and the molecular transporter unit were combined in the same nanoparticle scaffold. While targeted delivery systems increase the efficacy of therapeutics significantly, the access to intracellular sites or penetration of tissue barriers of solid tumors and other challenging tissues represents a major problem. As a result, two strategies for the attachment of both of the biological units, the dendritic transporter and the targeting unit were developed. In one strategy, peptide and transporter units were exclusively added to the allyl functionality, and in a second strategy, an orthogonal conjugation approach was employed, utilizing the keto group for a reductive amination reaction and the allyl group for the described thiol-ene chemistry. Along with the transporter

molecules and targeting peptides, imaging units were the third important function to be incorporated, which are critical to monitor the efficiency in the delivery of the designed scaffold to specific tissues and intracellular locations.

For the first approach, the free amines of the linear peptide GCGGGNHVGGSSV were capped with *N*-acetoxysuccinimide. Following the protection of the amines, peptides were conjugated to the allyl functionality of a 126 nm **AbBD** nanoparticle through the thiol of the cysteine unit as discussed above (Scheme IV-5). After conjugating the peptides, the imaging reagent NHS Alexa Fluor® 594 was introduced to label approximately 20 of the incorporated amine units on the nanoparticle. In a sequential thiol-ene reaction, the conjugation of 30 dendritic transporter molecules was achieved (Scheme IV-7), as confirmed via $^{1}$H NMR

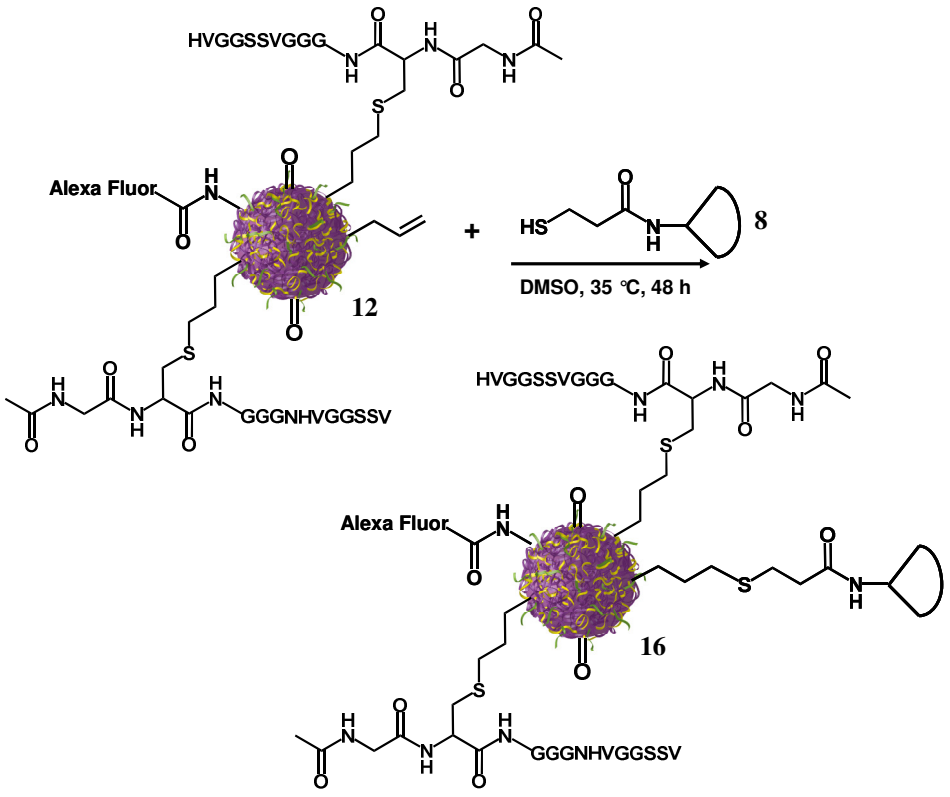


**Scheme IV-7.** Synthesis of NP-P-MT-dye conjugate, AbBD-NP-cHVGGSSV-594-MT (**16**).

spectroscopy. The sequential conjugation of the bioactive compounds can be followed with an overlay of the $^{1}$H NMR spectra that shows the addition of first the peptide and the remaining allyl groups of the nanoparticle and the characteristic peaks of the molecular transporter molecule at 2.0 and 3.2 ppm (Figure IV-2).

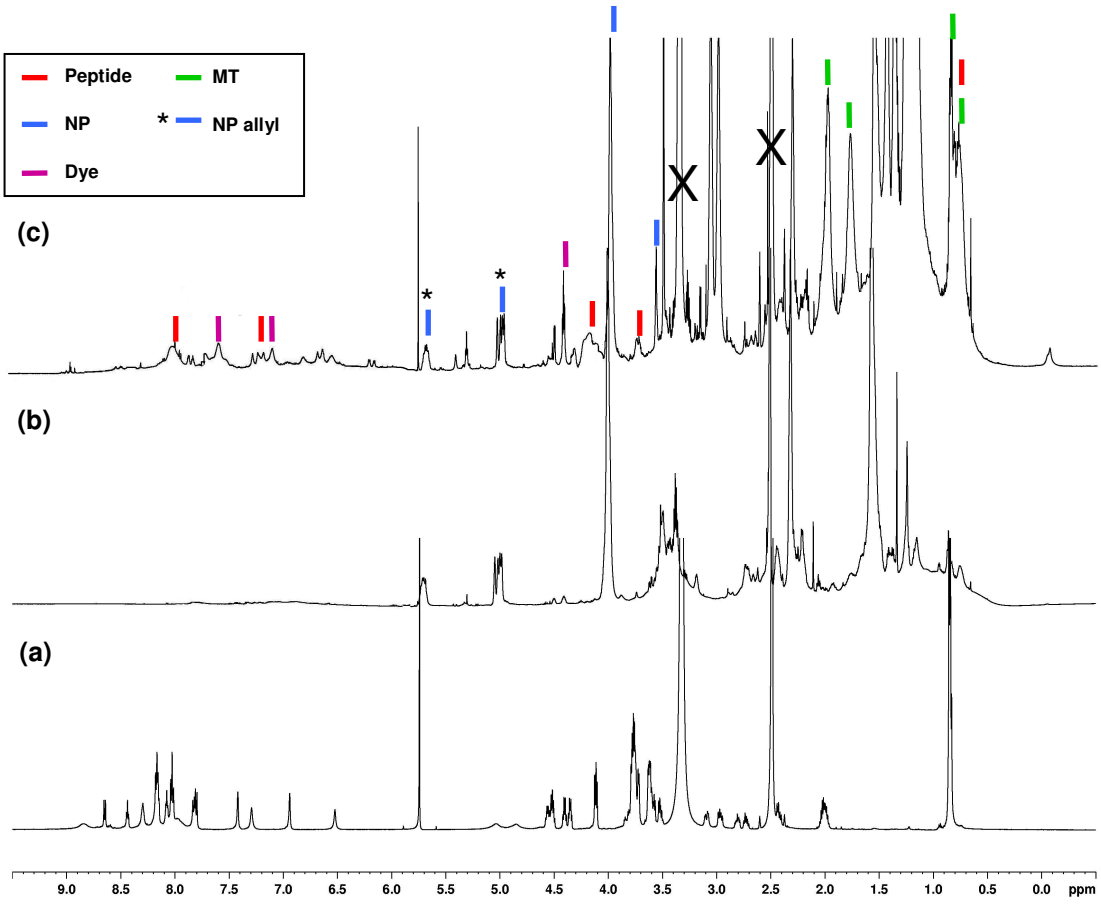


**Figure IV-1.** $^{1}$H NMR spectra overlay **(a)** GCGGGNHVGGSSV; **(b)** AbBD-NP; **(c)** AbBD-NP-cHVGGSSV-594-MT **(16)** in DMSO-d6.

The reaction sequence was changed to obtain a similar bioconjugate product that was only differentiated by the peptidic targeting unit. The amine groups of the c-RGD unit were not capped to avoid inactivation of the arginine recognition unit. Therefore, the conjugation strategy first involved the labeling of the particle's amine groups with

the NHS Alexa Fluor® 594 dye followed by the thiol-ene reaction with the targeting unit as shown in Scheme IV-7. In the last step, same as in the previous reaction, the dendritic transporter units were added in a sequential thiol-ene reaction (Scheme IV-8) to yield conjugate **17** (Scheme IV-8, and Figure IV-3 at the end of this Chapter).

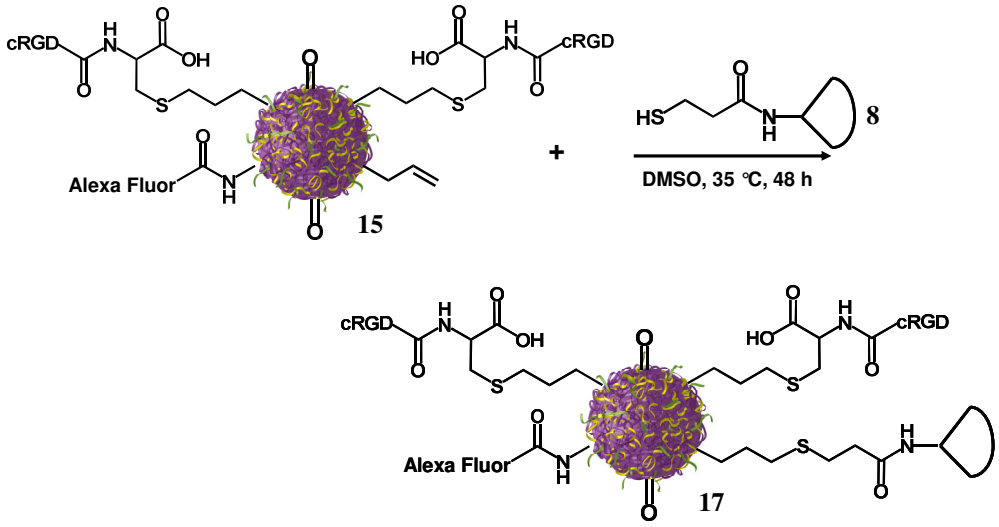


**Scheme IV-8.** Synthesis of NP-P-MT-dye conjugate, AbBD-NP-594-cRGD-MT (**17**).

In a third and final reaction sequence, the versatility the nanoparticle's functional groups was demonstrated by carrying out an orthogonal conjugation. For this approach, the free amine groups of the nanoparticle were capped with *N*-acetoxysuccinimide to prevent interference with the following reductive amination reaction between the keto group of the polyester backbone and the *N*-terminus of the unmodified targeting HVGGSSV peptides. After the reductive amination reaction was completed in the same fashion as described for compound **3** and analyzed by $^{1}$H NMR (Figure IV-4 seen at the end of this Chapter), a thiol-ene reaction between the allyl groups of the nanoparticle and the thiol group of the molecular transporter (Scheme

IV-9) achieved the attachment of 30 units according to $^{1}H$ NMR spectroscopy analysis. With the additional final characterization of the modified particles using SLS, the number of conjugated peptides was determined to be 37 peptides per particle. As the last step, the NHS Alexa Fluor® 594 dye was modified with thiolethylamine to label exclusively the particle through a thiol-ene reaction for *in vitro* imaging. The Alexa Fluor® 594 dye proved to be stable under the conditions and another example of the chemical versatility of the system was given.

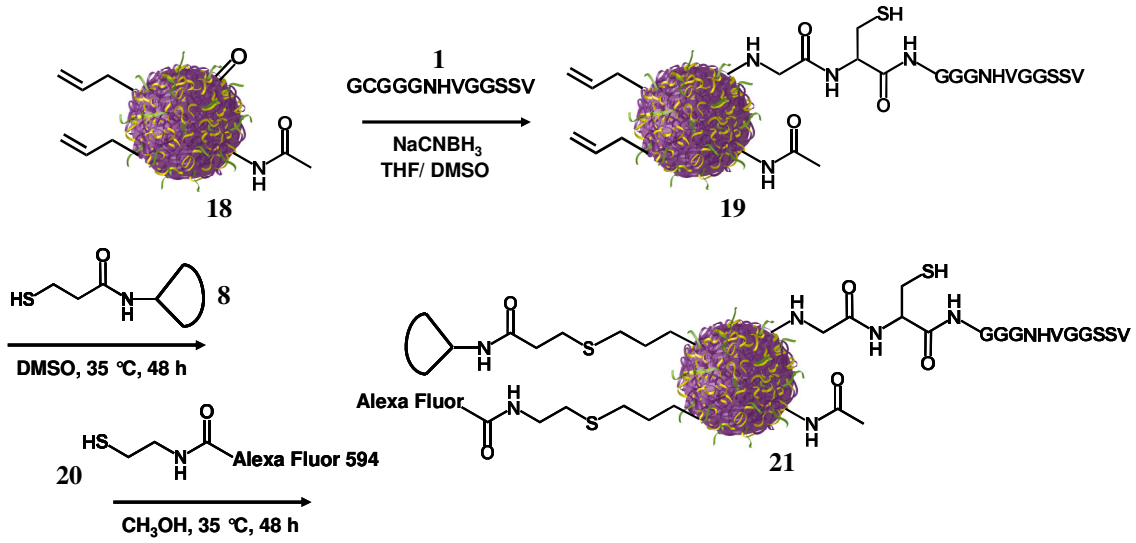


**Scheme IV-9.** Synthesis of NP-P-MT-dye conjugate, AbBD-NP-HVGGSSV-594-MT (**21**), utilizing reductive amination and thiol-ene chemistry.

## Conclusion

Functionalized polyester particles have been successfully prepared using an optimized one-pot synthesis approach which has demonstrated the control over the individual nanoscale dimensions. The partial oxidation of allyl groups provided access to linear precursors which feature epoxide groups for cross-linking, but also provided access to remaining allyl groups for post modification. From nanoparticle

formation, it was evident that the number or reactivity of the pendant allyl groups did not diminish and were available as additional valuable functionalities together with amine and keto groups for post-modification strategies. Investigations through model reactions to find mild conditions to employ thiol-ene reactions with biological compounds provided the basis of the successful attachment of thiol functionalized dendritic molecular transporter and targeting peptides to the nanoparticle backbone.

**Table IV-3.** Summary of nanoparticle conjugates.

| Particle Type[a] | Targeting Peptide[b] | Alexa Fluor® Dye | Molecular Transporter[c] | Compound Name[d] | Compound Class |
|---|---|---|---|---|---|
| **ABD** | HVGGSSV | — | — | ABD-NP-HVGGSSV (**3**) | NP-P |
| **ABD** | HVGGSSV | 750 | — | ABD-NP-L-HVGGSSV-750 (**7**) | NP-L-P-Dye |
| **AbBD** | — | 594 | MT | AbBD-NP-594-MT (**10**) | NP-MT-Dye |
| **AbBD** | cHVGGSSV | 594 | — | AbBD-NP-cHVGGSSV-594 (**12**) | NP-P-Dye |
| **AbBD** | cRGD | 594 | — | AbBD-NP-594-cRGD (**15)** | NP-P-Dye |
| **AbBD** | cHVGGSSV | 594 | MT | AbBD-NP-cHVGGSSV-594-MT (**16**) | NP-P-MT-Dye |
| **AbBD** | cRGD | 594 | MT | AbBD-NP-594-cRGD-MT (**17**) | NP-P-MT-Dye |
| **AbBD** | HVGGSSV | — | — | AbBD-NP-HVGGSSV (**19**) | NP-P |
| **AbBD** | HVGGSSV | 594 | MT | AbBD-NP-HVGGSSV-MT-594 (**21**) | NP-P-MT-Dye |

Summary of nanoparticle conjugates with definition of particle type depending on linear polymer precursor[a] and connected targeting peptide[b]: 'c' for capped N-terminus of peptide with HVGGSSV recognition unit via N-acetoxysuccinimide and 'c' for cyclic RGD with the sequence (RGDEKf)-SH. [c]Dendritic molecular transporter is abbreviated as MT, and the compound name[d] is given in the order of attachment

Several conjugation strategies were employed that included the utilization of the keto functionality in reductive amination reactions along with thiol-ene chemistry to prepare four classes of conjugate materials composed of nanoparticle-peptide-dye conjugates (NP-P-dye/NP-P), nanoparticle-dendritic molecular transporter-dye (NP-MT-dye) and nanoparticle-peptide-molecular transporter-dye conjugates (NP-P-MT-dye) (Table IV-3). The bioconjugates contained peptides developed to target radiated and non-radiated tumor vasculature, HVGGSSV and a novel c-RGD and will be

further investigated in their interaction with biological tissues and membranes towards the development of specialized biomedical materials.

## Experimental

**Characterization.** $^{1}$H nuclear magnetic resonance spectra were obtained from a Bruker AC300 or a Bruker AV-II603 spectrometer. Chemical shifts are reported in ppm and referenced to the corresponding residual nuclei in deuterated solvents. Gel-permeation chromatography (GPC) was carried out with a Waters chromatograph system equipped with a Waters 2414 refractive index detector, a Waters 2481 dual λ absorbance detector, a Waters 1525 binary HPLC pump, and four 5 mm Waters columns (300 mm x 7.7 mm), connected in series with increasing pore size (100, 1000, 100,000 and 1,000,000 Å respectively). All runs were performed with tetrahydrofuran (THF) as the eluent at a flow rate of 1 mL/min. For dynamic light scattering (DLS), a Malvern Nano ZS system by Malvern Instruments (Malvern Zetasizer Nanoseries, Malvern, UK) was employed at a fixed angle of 90º at 25 ºC, taking the average of three measurements. The particles were diluted with toluene to a concentration, which gave the desired number of counts in order to obtain a good signal-to-noise ratio. Static light scattering was also performed on the Malvern Nano ZS to obtain the absolute weight average molecular weights of the nanoparticles. Different sample concentrations (0.25-0.67 mg/mL) were prepared by dilution of a high concentration stock solution in toluene (1 mg/mL) to obtain the weight average molecular weight. Reverse-phase high-performance liquid chromatography (RP-HPLC) was carried out with a Waters HPLC using two Delta-Pak$^{TM}$ PrepLC$^{TM}$ 25 mm Columns (Waters, C18, 300Å, 25 x 100 mm each) with a PrepLC$^{TM}$ 25 mm Radial

Compression Module. The products were eluted using a solvent gradient (solvent A = 0.05% trifluoroacetic acid (TFA)/ $H_2O$; solvent B = 0.05% TFA/ $CH_3CN$). Accurate molecular mass and purity of the peptides were determined by MALDI-MS, with α-cyano-4-hydroxycinnamic acid as the matrix, on a Perspective Biosystems Voyager-DE STR (Framingham, MA) equipped with delayed extraction technology operating in reflector mode.

**Materials.** Reagent chemicals were purchased from Aldrich and Acros, and used as received, unless otherwise stated. Spectra/Por® Dialysis membrane and SnakeSkin® Pleated Dialysis Tubing, regenerated cellulose, were purchased from Spectrum Laboratories Inc. and Pierce Biotechnology, respectively. Size exclusion chromatography was performed with Sephadex LH-20 from GE Healthcare Life Sciences. Fmoc protected amino acids were obtained from Advanced ChemTech (Louisville, KY). Monomers α-allyl-δ-valerolactone, and 2-oxepane-1,5-dione were synthesized as previously described in Chapter 2. The molecular transporter dendrimer was synthesized according to published procedures.[30]

**Synthesis of copolymer poly(vl-avl-opd) (AbD).** To a 25 mL 3-necked round bottom flask, equipped with stir bar, gas inlet and 2 rubber septa, 2-oxepane-1,5-dione (0.70 g, 5.46 mmol) was added. The round bottom flask was purged with argon for 10 min and then dry toluene (4 mL) was added. The mixture stirred in an oil bath at 80 °C to dissolve the monomer. Upon dissolving, $Sn(Oct)_2$ (11.1 mg, 27.3 μmol) in 0.5 mL dry toluene,

absolute ethanol (20.5 mg, 440 μmol), α-allyl-δ-valerolactone (1.15 g, 8.19 mmol) and δ-valerolactone (1.37 g, 13.7 mmol) were then added to the reactor and the mixture was heated for 48 h at 105 °C. Residual monomer and catalyst were removed by dialyzing with Spectra/Por® dialysis membrane (MWCO = 1000) against $CH_2Cl_2$ to give a golden brown polymer, **AbD** (2.70 g, 85%). $M_w$ = 3287 Da, PDI = 1.17. $^1$H NMR (300 MHz, $CDCl_3$/$Me_4Si$): δ 5.72 (m, $H_2C$=C*H*-), 5.06 (m, *H*$_2$C=CH-), 4.34 (m, -$CH_2CH_2C(O)CH_2CH_2O$-), 4.08 (m, -C*H*$_2$O-), 3.67 (m, -OC*H*$_2$$CH_3$), 2.78 (m, opd -$OC(O)CH_2CH_2C(O)CH_2$-), 2.58 (m, opd -$OC(O)CH_2CH_2C(O)CH_2$-), 2.34 (m, vl -$CH_2CH_2C(O)O$-, avl $H_2C$=$CHCH_2CH$-, $H_2C$=$CHCH_2CH$-), 1.66 (m, avl & vl -$CHCH_2CH_2$-), 1.25 (t, -$CH_2CH_3$); $^{13}$C NMR (400 MHz, $CDCl_3$): δ 204.9, 175.2, 173.7, 173.2, 135.0, 117.0, 63.9, 44.8, 36.4, 33.6, 28.0, 26.3, 21.3.

**Synthesis of poly(vl-evl-opd) (ABD).** To a solution of **AbD** (2.70 g, 4.67 mmol) in $CH_2Cl_2$ (37 mL), 3-chloroperoxybenzoic acid (1.46 g, 8.48 mmol) was added. The mixture stirred for 72 h at room temperature and then concentrated via rotary evaporator. The crude product was dissolved in a minimal amount of tetrahydrofuran (THF) (5 mL) and dropped into a round bottom flask containing 1L diethyl ether. The solution was kept overnight at 0 °C and a white solid was obtained. The solution was decanted off and the solid was dried *in vacuo* to obtain poly(vl-evl-opd), **ABD** (1.95 g, 72%). $M_w$ = 3392 Da, PDI = 1.19. $^1$H NMR (300 MHz, $CDCl_3$/$Me_4Si$): δ 4.34 (m, -$CH_2CH_2C(O)CH_2CH_2O$-), 4.08 (m, -C*H*$_2$O-), 3.67 (m, -OC*H*$_2$$CH_3$), 2.96 (m, -C*H*(O)$CH_2$-), 2.78 (m, -CH(O)C*H*$_2$-, opd -$OC(O)CH_2CH_2C(O)CH_2$-), 2.58 (m, opd -$OC(O)CH_2CH_2C(O)CH_2$-), 2.47 (m, -CH(O)C*H*$_2$-), 2.34 (m, vl -$CH_2CH_2C(O)O$-, evl -$CHCH_2CH$-, -$CHCH_2CH$-), 1.66 (m, evl

& vl, -CHC$H_2$C$H_2$-), 1.25 (t, -$CH_2$C$H_3$); $^{13}$C NMR (400 MHz, $CDCl_3$): δ 204.8, 175.7, 173.7, 173.2, 63.9, 51.5, 47.9, 44.8, 36.4, 32.6, 28.0, 26.3, 21.3.

**Nanoparticle formation from ABD using epoxide-amine crosslinking (ABD-NP).** A solution of **ABD** (0.11 g, $M_w$= 3392 Da, PDI = 1.19) dissolved in $CH_2Cl_2$ (0.26 mL) was added to a solution of 2,2'-(ethylenedioxy)diethylamine (76.4 μL, 0.52 μmol) in $CH_2Cl_2$ (40.3 mL). The mixture was heated for 12 h at 44 °C with vigorous stirring. Residual diamine was removed by dialyzing with SnakeSkin® Pleated Dialysis Tubing (MWCO = 10,000) against dichloromethane to yield nanoparticles (0.17 g). DLS: $D_H$ = 118.3 ± 9.6 nm. SLS: $M_w$ = 323,000. $^1$H NMR (300 MHz, $CDCl_3$\$Me_4$Si): δ The significant change is the disappearance of the epoxide protons at 2.94, 2.75 and 2.47 ppm and the appearance of signals at 3.54 and 2.97 ppm corresponding to the protons neighboring the secondary amine of the PEG linker after cross-linking. All other aspects of the spectrum are similar to that of **ABD**.

**N-Boc-ethylenediamine (NBED) conjugated ABD nanoparticles.** To a solution of **ABD** nanoparticles (20 mg, 0.06 μmol) in tetrahydrofuran (THF) (2 mL), N-acetoxysuccinimide (0.02 g, 0.13 mmol) was added. The reaction mixture stirred for 3 h. Residual N-acetoxysuccinimide was removed by dialyzing with SnakeSkin® Pleated Dialysis Tubing (MWCO = 10,000) against THF. Once the product was concentrated and dried, the nanoparticles (18 mg, 0.05 μmol) were dissolved in a mixture of $CH_2Cl_2$ and $CH_3OH$ (1:1, v/v, 2 mL). To this solution, N-Boc-ethylenediamine (4.6 μL of 1.59 M

NBED in $CH_3OH$) and $NaCNBH_3$ (21.8 μL of 1.0 M $NaCNBH_3$ in THF) were added. The reaction mixture stirred for 12 h at room temperature and then was purified by dialyzing with SnakeSkin® Pleated Dialysis Tubing (MWCO = 10,000) against 1:1 $CH_2Cl_2/CH_3OH$ to yield NBED conjugated nanoparticles (18 mg, 88%). DLS: $D_H$ = 119.5 ± 10.3 nm; original particle $D_H$ = 118.3 ± 9.6 nm. $^1H$ NMR (300MHz, $CDCl_3\backslash Me_4Si$): δ The significant change is the appearance of the peak at 1.43 ppm due to the Boc protecting group. All other aspects of the spectrum are similar to that of the **ABD** nanoparticles.

**Synthesis of GCGGGNHVGGSSV (HVGGSSV) peptide (1).** The HVGGSSV peptide was synthesized by solid-phase peptide synthesis using standard Fmoc chemistry on a Model 90 Peptide Synthesizer (Advanced ChemTech).

*Attachment of N-Fmoc amino acids to resin*. After swelling with dichloromethane (20 mL) for 20 min, H-val-2-Cl-Trt resin (0.20 g, 1.03 mmol/g, 0.21 mmol surface amino acids) was treated with a solution of Fmoc-protected amino acids (4.4 equiv, 0.9 mmol) in dimethylformamide (DMF) (9 mL). The amino acids were attached to the resin using double coupling with a solution (9 mL) consisting of *N*-hydroxybenzotriazole monohydrate (HOBt) (0.9 mmol, 0.14 g) *o*-(benzotriazole-*N,N,N′,N′*-tetramethyluronium hexafluorophosphate (HBTU) (0.9 mmol, 0.34 g), *N,N'*-diisopropylethylamine (DIPEA) (1.8 mmol, 0.31 mL) in 9 mL DMF. The reaction mixture was shaken for 60 min and washed with DMF (4 x 10 mL), methanol (4 x 10 mL) and DMF (4 x 10 mL). The end of the coupling was controlled by the Ninhydrin test. A 20% (v/v) piperidine in DMF solution was used to deprotect the Fmoc groups. The amino acids were attached to the

resin in the following sequence: Ser, Ser, Gly, Gly, Val, His, Asn, Gly, Gly, Gly, Cys, and Gly.

*Cleavage of peptide from resin*. The resin was treated with Reagent R, a solution of trifluoroacetic acid (TFA), thioanisole, anisole, and ethanedithiol (90:5:3:2, 6 mL), for 4 h. After removal of the resin by filtration, the filtrate was concentrated to precipitate the peptide with cold diethyl ether. Crude peptides were purified by RP-HPLC and lyophilized. Peptide identity was confirmed by MS. *m/z* (MALDI) 1088.1 ($M^+$, 98%).

**HVGGSSV peptide conjugated ABD nanoparticles (3).** To a solution of **ABD** nanoparticles (20.0 mg, 0.06 μmol) in THF (2 mL), N-acetoxysuccinimide (3 mg, 18.1 μmol) was added. The reaction mixture stirred for 3 h. Residual N-acetoxysuccinimide was removed by dialyzing with SnakeSkin® Pleated Dialysis Tubing (MWCO = 10,000) against 1:1 THF/$CH_3OH$ to give amine capped **ABD** nanoparticles, **2**. To a solution of **2** (0.0174 g, 0.05 μmol, in 3 mL THF), **1** (3.5 mg, 3.18 μmol) dissolved in DMSO (2 mL) and $NaCNBH_3$ (6.36 μL 1.0 M $NaCNBH_3$ in THF) were added. The reaction mixture stirred for 12 h at room temperature. The reaction mixture was purified by dialyzing with SnakeSkin® Pleated Dialysis Tubing (MWCO = 10,000) against 1:1 THF/$CH_3CN$ to yield **3** (19 mg, 88%). DLS: $D_H$ = 120.5 ± 10.2 nm; original particle $D_H$ = 118.3 ± 9.6 nm. SLS: $M_w$ = 362,000; original particle $M_w$ = 323,000. $^1$H NMR (600 MHz, $(CD_3)_2SO$): δ The significant change is the appearance of the following peaks: 8.26-7.87, 7.42, 6.90, 4.39, 4.25, and 3.71 ppm due to the attachment of the peptide. All other aspects of the spectrum are similar to that of the **ABD** nanoparticles.

**Synthesis of 2-vinylsulfanylethanol.** A 3-necked 250 mL round bottom flask, equipped with stir bar, was sealed with septa and purged with nitrogen. To the flask, sodium ethoxide solution (23.7 mL, 21 wt% in ethanol, 63.6 mmol) and 2-mercaptoethanol (3.56 mL, 50.8 mmol) were added at room temperature. At 0°C, vinyl bromide solution (80 mL, 1 M in THF, 55 mmol) was added slowly and then transferred to a stainless steel reactor, where it was heated to 110 °C for 6 h. After removing the solvent via rotary evaporator, water (30 mL) was added to the crude product and the solution was extracted with 6 x 30 mL diethyl ether. The organic layer was dried with $MgSO_4$ and then concentrated *in vacuo*. Column chromatography with 50% ethyl acetate in hexanes as the eluent gave a brown oil (4.42 g, 83.5%). $^1$H NMR (300 MHz, $CDCl_3$\$Me_4Si$): δ 6.34 (dd, J = 16.9 Hz, J = 10.1 Hz, 1H, $H_2C$=C*H*-), 5.25 (d, J = 9.5 Hz, 1H, *H*$_2$C=CH-), 5.23 (d, J = 9.5 Hz, 1H, *H*$_2$C=CH-), 3.78 (m, 2H, -C*H*$_2$OH), 3.05 (s, 1H, -OH), 2.89 (t, 2H, -SC*H*$_2$-); $^{13}$C NMR (300 MHz, $CDCl_3$): δ 130.9, 111.7, 60.2, 33.9.

**Synthesis of succinimidyl 2-vinylsulfanylethyl carbonate.** To a stirring solution of 2-vinylsulfanylethanol (2.05 g, 19.7 mmol) in dry acetonirile (80 mL) in a $N_2$ purged round bottom flask, N,N'-disuccinimidylcarbonate (7.36 g, 28.7 mmol) was added at room temperature. To the cloudy reaction mixture, triethylamine (5.98 g, 59.1 mmol) was added and after a couple of minutes the reaction became clear. After removing the solvent *in vacuo*, the residue was dissolved in $CH_2Cl_2$ (100 mL) and washed with saturated $NaHCO_3$ (3 x 50 mL). The organic phase was then washed with 60 mL brine, dried with $MgSO_4$, and concentrated *in vacuo*. The crude product was purified via flash chromatography with $CH_2Cl_2$ as the solvent to yield succinimidyl 2-vinylsulfanylethyl

carbonate (3.31 g, 68.5%). $^{1}$H NMR (300 MHz, $CDCl_3$\$Me_4Si$): δ 6.30 (dd, J = 16.9 Hz, J = 10.1 Hz, 1H, $H_2C$=C*H*-), 5.28 (d, J = 9.5 Hz, 1H, *$H_2$*C=CH-), 5.25 (d, J = 9.5 Hz, 1H, *$H_2$*C=CH-), 4.45 (t, J = 7.0 Hz, 2H, $H_2C$=CHS$CH_2C$*$H_2$*- ), 3.04 (t, J = 7.2 Hz, 2H, $H_2C$=CHSC*$H_2$*$CH_2$- ), 2.84 (s, 4H, -C(O)C*$H_2$*C*$H_2$*C(O)-); $^{13}$C NMR (300 MHz, $CDCl_3$): δ 168.6, 151.3, 130.3, 113.0, 68.9, 29.0, 25.4.

**Synthesis of succinimidyl 2-vinylsulfonylethyl carbonate (SVEC).** To a stirring solution of succinimidyl 2-vinylsulfanylethyl carbonate (2.3 g, 9.4 mmol) in glacial acetic acid (5 mL), peracetic acid (3.96 mL, 32 wt% in acetic acid, 18.8 mmol) was added dropwise at 0 °C. After 30 min the ice/water bath was removed and the reaction stirred for an additional 2 h. The solvent was removed *in vacuo* and the residue was dissolved in water (55 mL). The product was extracted with $CH_2Cl_2$ (3 x 60 mL) and concentrated via rotary evaporator to yield the crystalline product (2.3 g, 88.5%). $^{1}$H NMR (300 MHz, $CD_3CN$): δ 6.79 (dd, J = 16.6 Hz, J = 9.4 Hz, 1H, $H_2C$=C*H*-), 6.33 (d, J = 16.5 Hz, 1H, *$H_2$*C=CH-), 6.22 (d, J = 16.5 Hz, 1H, *$H_2$*C=CH-), 4.65 (t, J = 5.6 Hz, 2H, $H_2C$=CHSCH-$_2C$*$H_2$*- ), 3.49 (t, J = 5.7 Hz, 2H, $H_2C$=CHSC*$H_2$*$CH_2$- ), 2.76 (s, 4H, -C(O)C*$H_2$*C*$H_2$*C(O)-); $^{13}$C NMR (300 MHz, $CDCl_3$): δ 170.5, 152.3, 137.5, 131.7, 65.2, 53.2, 26.4.

**Attachment of NBED to succinimidyl 2-vinylsulfonylethyl carbonate (4a).** To a stirring solution of SVEC (0.6 g, 2.2 mmol) in acetonitrile (30 mL), N-Boc-ethylenediamine (0.38 g, 2.4 mmol), water (30 mL), and sodium bicarbonate (0.2 g, 2.4 mmol) were added. After stirring for 4 h at room temperature, the acetonitrile was

removed *in vacuo* and the remaining solution was diluted with brine (30 mL). The product was extracted with $CH_2Cl_2$ (4 x 60 mL), dried with $MgSO_4$ and concentrated. The crude product was purified by flash column chromatography with ethylacetate as the eluent to yield a white crystalline product **4a** (0.65 g, 93.3 %). $^1$H NMR (300 MHz, $CD_3Cl_3$): δ 6.68 (dd, J = 16.3 Hz, J = 9.2 Hz, 1H, $H_2C$=C*H*-), 6.48 (d, J = 16.4 Hz, 1H, *H*$_2$C=CH-), 6.21 (d, J = 16.4 Hz, 1H, *H*$_2$C=CH-), 5.33 (s, 1H, -OC(O)N*H*-), 4.91 (s, 1H, -OC(O)NHCH$_2$CH$_2$N*H*-), 4.46 (t, J = 5.5 Hz, 2H, -CH$_2$C*H*$_2$O-), 3.33 (m, 6H, -C*H*$_2$CH$_2$OC(O)NHC*H*$_2$C*H*$_2$-), 1.44 (s, 9H, -C(O)OC(C*H*$_3$)$_3$); $^{13}$C NMR (300 MHz, $CDCl_3$): δ 157.8, 137.9, 130.5, 58.9, 54.0, 40.4, 39.0, 26.4.

**Deprotection of 2-(vinylsulfonyl)ethyl 2-(boc-amino)ethylcarbamate (4b).** To a stirring solution of **1a** (0.15 g, 0.45 mmol) in dioxane (2 mL), hydrochloric acid in dioxane (2 mL, 4 M) was added slowly at 0 °C. After 30 min the ice/water bath was removed and the reaction stirred for an additional 3 h. To remove remaining acid, toluene was added to the product and evaporated off as an azeotropic mixture to yield the crystalline product (99.4 mg, 95.6%). $^1$H NMR (300 MHz, $CD_3OD$): δ 6.75 (dd, J = 16.3 Hz, J = 9.2 Hz, 1H, $H_2C$=C*H*-), 6.08 (d, J = 16.4 Hz, 1H, *H*$_2$C=CH-), 6.07 (d, J = 16.4 Hz, 1H, *H*$_2$C=CH-), 4.21 (m, 2H, -CH$_2$C*H*$_2$O-), 2.71-3.12 (m, 6H, -C*H*$_2$CH$_2$OC(O)NHC*H*$_2$C*H*$_2$-); $^{13}$C NMR (300 MHz, $CDCl_3$): δ 157.8, 137.9, 130.5, 58.9, 54.0, 40.4, 39.0.

**Attachment of 2-(vinylsulfonyl)ethyl 2-aminoethylcarbamate to ABD nanoparticles (5).** To a solution of **ABD** nanoparticles (100 mg, 0.3 μmol) in THF (10 mL), N-acetoxysuccinimide (15 mg, 90.5 μmol) was added. The reaction mixture stirred for 3 h. Residual N-acetoxysuccinimide was removed by dialyzing with SnakeSkin® Pleated Dialysis Tubing (MWCO = 10,000) against 1:1 THF/$CH_3OH$ to give amine capped **ABD** nanoparticles, **2**. To a solution of **2** (84.5 mg, 0.25 μmol) in $CH_2Cl_2$ (12.5 mL), 2-(vinylsulfonyl)ethyl 2-aminoethylcarbamate, **4b**, (69 μL, 0.85 M in $CH_3OH$) and $NaCNBH_3$ (11.1 mg**,** 17.6 mmol) in $CH_3OH$ (12.5 mL) were added. The pH was adjusted to 6-7 with 1N NaOH and the reaction stirred for 24 h at room temperature and then was purified by dialyzing with SnakeSkin® Pleated Dialysis Tubing (MWCO = 10,000) against 1:1 $CH_2Cl_2/CH_3OH$ to yield vinyl sulfone linker conjugated nanoparticles **(3)** (89.8 mg). $^1H$ NMR (300 MHz, $CDCl_3\backslash Me_4Si$): δ The significant change is the appearance of the peaks at 6.3-6.7 ppm due to the vinyl protons of the linker. Also the peak at 4.42 ppm further confirms the attachment of the vinylsulfone unit, otherwise all other aspects of the spectrum are similar to that of the **ABD** nanoparticles.

**Alexa Fluor® 750 conjugated GCGGGNHGVSSGV peptide (AF750-GCGGGDHGVSSGV) (6).** To a solution of peptide (2.0 mg, 1.8 μmol) in dry dimethylsulfoxide (0.1 mL), NHS Alexa Fluor® 750 (1.6 mg, 15.4 μM solution in DMF) was added. The reaction mixture stirred for 24 h at room temperature in the dark. The Alexa Fluor® 750-peptide conjugate was used without further purification.

**Attachment of Alexa Fluor® 750-peptide to linker conjugated nanoparticles (7).** The linker modified nanoparticles (29.9 mg) in 1:5 DMF: DPBS buffer solution (0.7 mL) were added to the Alexa Fluor® 750-peptide (0.56 mg, 0.41 μmol) followed by an additional 2.1 mg of unmodified HVGGSSV peptide in 150 μL PBS buffer. This was allowed to stir for 24 h. The reaction was diluted with $H_2O$ and was transferred to 10 000 MWCO concentrator tubes. The samples were centrifuged at 3000xg for 12 min a total of 17 times until no dye was seen in the filtrate. The solution, which remained in the upper portion of the concentrator tube, was blue in color. $^1$H NMR (300 MHz, $D_2O$): δ The significant change is the appearance of broad peaks at: 8.38, 7.14, 3.29, 2.95, and 0.83 ppm due to the peptide.

**Synthesis of poly(vl-evl-avl-opd) (AbBD).** To a solution of **AbD** (1.70 g, 1.56 mmol) in $CH_2Cl_2$ (30 mL), 3-chloroperoxybenzoic acid (0.22 g, 1.28 mmol) was added. The mixture stirred for 72 h at room temperature and then was concentrated via rotary evaporator. The crude product was dissolved in a minimal amount of THF (5 mL) and poured into a round bottom flask containing 1L diethyl ether. The solution was kept overnight at 0 °C and a white solid was obtained. The solution was decanted off and the solid was dried *in vacuo* to obtain **AbBD** (1.2 g, 71%). $M_w$ = 3356 Da, PDI = 1.18. $^1$H NMR (300 MHz, $CDCl_3$/$Me_4Si$): δ 5.72 (m, $H_2C$=C*H*-), 5.06 (m, *H*$_2$C=CH-), 4.34 (m, -$CH_2CH_2C(O)CH_2CH_2O$-), 4.08 (m, -C*H*$_2$O-), 3.67 (m, -OC*H*$_2$$CH_3$), 2.96 (m, -C*H*(O)$CH_2$-), 2.78 (m, -CH(O)C*H*$_2$-, opd -OC(O)$CH_2$C*H*$_2$C(O)$CH_2$-), 2.58 (m, opd -OC(O)$CH_2CH_2C(O)CH_2$-), 2.47 (m, -CH(O)C*H*$_2$-), 2.34 (m, vl -$CH_2$C*H*$_2$C(O)O-, avl $H_2C$=CHC$H_2$C*H*-, $H_2C$=CHC*H*$_2$CH-), 1.66 (m, avl & vl -CHC*H*$_2$C*H*$_2$-), 1.25 (t,

-$CH_2CH_3$); $^{13}C$ NMR (400 MHz, $CDCl_3$): δ 205.1, 175.2, 173.7, 173.2, 135.7, 115.7, 63.9, 52.0, 48.0, 44.8, 36.4, 33.6, 28.0, 26.6, 21.2.

**Nanoparticle formation from AbBD using epoxide-amine crosslinking (AbBD-NP).** To a solution of 2,2'-(ethylenedioxy)diethylamine (26.2 μL, 0.18 mmol) in $CH_2Cl_2$ (34.6 mL), a solution of **AbBD** (0.13 g, $M_w$= 3356 Da, PDI = 1.18) in $CH_2Cl_2$ (0.24 mL) was added. The mixture was heated at 45 °C for 12 h. Residual diamine was removed by dialyzing with SnakeSkin® Pleated Dialysis Tubing (MWCO = 10,000) against $CH_2Cl_2$ to obtain nanoparticles (0.15 g, 94%). DLS: $D_H$ = 126.6 ± 9.3 nm. SLS: $M_w$ = 350,000. $^1H$ NMR (300 MHz, $CDCl_3$/$Me_4Si$): δ The significant change is the disappearance of the epoxide protons at 2.94, 2.75 and 2.47 ppm and the appearance of signals at 3.54 and 2.97 ppm corresponding to the protons neighboring the secondary amine of the PEG linker after cross-linking. All other aspects of the spectrum are similar to that of **AbBD**.

**General procedure for the attachment of benzyl mercaptan to AbBD nanoparticles.** To a solution of **AbBD** nanoparticles (15 mg, 0.04 μmol) in toluene (0.5 mL), benzyl mercaptan (3.5 μL, 29 μmol) was added. The reaction mixture was heated for 72 h at 35 °C. The remaining toluene was removed *in vacuo* and residual benzyl mercaptan was removed by dialyzing with SnakeSkin® Pleated Dialysis Tubing (MWCO = 10,000) against $CH_2Cl_2$. $^1H$ NMR (300 MHz, $CDCl_3$/$Me_4Si$): δ The significant change is the reduction of the allyl protons at 5.72 and 5.06 ppm and the appearance of signals at 3.73 and 7.30 ppm corresponding to the methylene and benzene protons respectively of the

attached benzyl mercaptan. All other aspects of the spectrum are similar to that of **AbBD** nanoparticles.

**Deprotection of molecular transporter (MT) (8).** To a solution of LL-MT (15 mg, 4.56 μmol) in $CH_3OH$ (0.4 mL), a solution of *D,L*-dithiothreitol in $CH_3OH$ (0.2 mL) was added. The reaction mixture stirred for 3 h at room temperature. Residual dithiothreitol was removed by purification with Sephadex LH-20. The product was immediately attached to **AbBD** nanoparticles.

**Model reaction of attachment of MT to AbBD nanoparticles.** To a solution of **AbBD** nanoparticles (15 mg) in $CH_3OH$ (0.2 mL), **8** (3.9 mg, 1.2 μmol) in $CH_3OH$ (0.4 mL) was added. The reaction mixture was heated for 72 h at 37 °C. Residual **8** was removed by dialyzing with SnakeSkin® Pleated Dialysis Tubing (MWCO = 10,000) against methanol to obtain MT conjugated nanoparticles (18.3 mg). DLS: $D_H$ = 128.9 ± 10.2 nm; original particle $D_H$ = 126.6 ± 9.3 nm. $^1$H NMR (300 MHz, $CD_3OD$): δ The significant change is the reduction of the allyl protons at 5.72 and 5.06 ppm and the appearance of signals at 2.20-1.98 (m, $CH_2$), 1.57 (m, $CH_2$) and 1.39 (m, $CH_2$) ppm due to the dendritic backbone of the MT. All other aspects of the spectrum are similar to that of **AbBD** nanoparticles.

**Alexa Fluor® 594 conjugated AbBD nanoparticles (9).** To a solution of **AbBD** nanoparticles (0.021 g) in dry THF (0.5 mL), NHS Alexa Fluor® 594 (0.14 mL of 10

mg/mL NHS Alexa Fluor® 594 in DMF, 1.7 μmol) was added. The reaction mixture stirred for 24 h at room temperature. Residual NHS Alexa Fluor® 594 was removed by dialyzing with SnakeSkin® Pleated Dialysis Tubing (MWCO = 10,000) against $CH_3OH$ to obtain **9** (15.2 mg). $^1H$ NMR (300 MHz, $CD_3OD$): δ The significant change is the appearance of the following peaks due to Alexa Fluor® 594: 7.14-7.20, 6.78, 5.48, 4.48, 3.62, 3.43, and 1.24 ppm. $^1H$ NMR (600 MHz, $(CD_3)_2SO$): δ The significant change is the appearance of the following peaks due to Alexa Fluor® 594: 7.52, 7.47, 7.08, 5.32, 4.44, 4.35, 3.58, 3.16, 2.03, and 1.25 ppm. All other aspects of the spectrum are similar to that of **AbBD** nanoparticles.

**Attachment of MT to Alexa Fluor® 594 conjugated AbBD nanoparticles, NP-594-MT (10).** To a solution of **9** (8 mg) in $CH_3OH$ (0.2 mL), **8** (2 mg, 0.88 μmol) in $CH_3OH$ (0.4 mL) was added. The reaction mixture was heated for 72 h at 37 °C. Residual **8** was removed by dialyzing with SnakeSkin® Pleated Dialysis Tubing (MWCO = 10,000) against $CH_3OH$ to yield **10** (9 mg). DLS: $D_H$ = 129.4 ± 9.8 nm; original particle $D_H$ = 126.6 ± 9.3 nm. SLS: $M_w$ = 445,000; original particle $M_w$ = 350,000. $^1H$ NMR (300 MHz, $CD_3OD$): δ The significant change is the reduction of the allyl protons at 5.72 and 5.06 ppm and the appearance of signals at 2.20-1.98 (m, $CH_2$), 1.57 (m, $CH_2$) and 1.39 (m, $CH_2$) ppm due to the dendritic backbone of the MT. All other aspects of the spectrum are similar to that of **9**.

**N-acetoxysuccinimide conjugated HVGGSSV peptide, cHVGGSSV (11).** To a solution of **1** (29.4 mg, $2.7x10^{-5}$ mol) dissolved in $CH_3CN$ (3 mL), N-acetoxysuccinimide (0.42 g, $2.7x10^{-3}$ mol) was added. The reaction mixture stirred for 3 h at room temperature. After removal of the solvent under reduced pressure, the crude product was purified by RP-HPLC. *m/z* (MALDI) 1175 ($M^+$, 97%).

**cHVGGSSV conjugated Alexa Fluor® 594-AbBD nanoparticles, NP-cHVGGSSV-594 (12).** To a solution of **AbBD** nanoparticles (0.021 g) in dimethylsulfoxide (0.7 mL), **11** (2.9 mg, 2.46 μmol) was added. The reaction mixture was heated for 72 h at 35 °C. To this solution, NHS Alexa Fluor® 594 (0.14 mL of 10 mg/mL NHS Alexa Fluor® 594 in DMF, 1.7 μmol) was added. Residual NHS Alexa Fluor® 594 and peptide were removed by dialyzing with SnakeSkin® Pleated Dialysis Tubing (MWCO = 10,000) against 1:1 $CH_3OH/CH_3CN$ to obtain **12** (20.1 mg). DLS: $D_H$ =128.9 ± 10.9 nm; original particle $D_H$ = 126.6 ± 9.3 nm. SLS: $M_w$ = 404,000; original particle $M_w$ = 350,000. $^1H$ NMR (600 MHz, $(CD_3)_2SO$): δ The significant change is the reduction of the allyl protons at 5.72 and 4.97 ppm and the appearance of the following sets of significant signals: 8.21, 7.83, 4.55, 3.73 and 0.80 ppm due to the peptide, and 7.25, 7.16, 6.53, 5.32, 4.44, 4.37, and 1.25 ppm due to the Alexa Fluor® 594. All other aspects of the spectrum are similar to that of **AbBD** nanoparticles.

**Attachment of MT to cHVGGSSV conjugated Alexa Fluor® 594-AbBD nanoparticles, NP-cHVGGSSV-594-MT (16).** To a solution of **12** (6 mg) in DMSO

(0.1 mL), **8** (1.4 mg, 0.59 μmol) in $CH_3OH$ (0.3 mL) was added. The reaction mixture was heated for 48 h at 35°C. Residual **8** was removed by dialyzing with SnakeSkin® Pleated Dialysis Tubing (MWCO = 10,000) against 1:1 $CH_3OH/CH_3CN$ to yield **11** (7.4 mg). DLS: $D_H$ = 130.7 ± 9.4 nm; original particle $D_H$ = 126.6 ± 9.3 nm. SLS: $M_w$ = 473,000; original particle $M_w$ = 350,000. $^1H$ NMR (600 MHz, $(CD_3)_2SO$): δ The significant change is the reduction of the allyl protons at 5.72 and 4.97 ppm and the appearance of signals at 3.06 (m, $CH_2$), 2.96 (m, $CH_2$), 1.97 (m, $CH_2$), 1.77 (m, $CH_2$), 1.41 (m, $CH_2$) and 1.35 (m, $CH_2$) ppm due to the dendritic backbone of the MT. All other aspects of the spectrum are similar to that of **12**.

**Synthesis of cyclic RGD, cRGD (13).** The RGD peptide was synthesized by solid-phase peptide synthesis using standard Fmoc chemistry on a Model 90 Peptide Synthesizer (Advanced ChemTech).

*Synthesis of Linear RGD.* After swelling with dichloromethane (20 mL), Fmoc-Cys-2-Cl-Trt resin (0.20 g, 0.9 mmol/g, 0.18 mmol surface amino acids) was deprotected with a 20% (v/v) piperidine in DMF solution and treated with a solution of Fmoc-protected amino acid (4.4 equiv, 0.9 mmol) in dimethylformamide (DMF) (9 mL). The amino acids were attached to the resin using double coupling with a solution (9 mL) consisting of *N*-hydroxybenzotriazole monohydrate (HOBt) (0.9 mmol, 0.14 g) *o*-(benzotriazole-*N,N,N',N'*-tetramethyluronium hexafluorophosphate (HBTU) (0.9 mmol, 0.34 g), *N,N'*-diisopropylethylamine (1.8 mmol, 0.31 mL) in 9 mL DMF. The reaction mixture was shaken for 60 min and washed with DMF (4 x 10 mL), methanol (4 x 10 mL) and DMF

(4 x 10 mL). A 20% (v/v) piperidine in DMF solution was used to deprotect the Fmoc groups. An amino-hexyl spacer was coupled to the cystine on the resin, followed by glutamic acid, aspartic acid, glycine, arginine, phenylalanine, and finally lysine.

*Cyclization of RGD.* The peptide was cyclized by utilizing an ODmab group, which allows for the selective deprotection carboxylic acid side chain of the glutamic acid, which can then be coupled to the N-terminus. The ODmab was deprotected using 2% v/v hydrazine monohydrate/DMF added to the resin and shaken for 7 min. Next it was washed with 20 mL of DMF followed by 10 mL of a 5% v/v DIPEA/DMF solution which was allowed to shake for 10 min. Carboxyl activation was achieved through the use of N,N'-dicyclohexylcarboimide (DCC) (44.6 mg, 0.22 mmol) and HOBt (29.2 mg, 0.22 mmol) which was added to 10 mL of DMF and then added to the resin and allowed to shake for 18 h.

*Cleavage of peptide from resin*. The resin was treated with Reagent R, a solution of trifluoroacetic acid (TFA), thioanisole, anisole, and ethanedithiol (90:5:3:2, 6 mL), for 3 h. After removal of the resin by filtration, the filtrate was concentrated to precipitate the peptide with cold diethyl ether. The crude peptide was collected by centrifugation, purified by RP-HPLC and lyophilized. Peptide identity was confirmed by MALDI-MS *m/z* 946.7 ($M^+$, 98%).

**Attachment of cRGD to Alexa Fluor® 594 conjugated AbBD nanoparticles, NP-594-cRGD (15).** To a solution of **AbBD** nanoparticles (23.0 mg) in THF (2.3 mL), Alexa Fluor® 594 (0.15 mL of 10 mg/mL Alexa Fluor® 594 in DMF, 1.83 μmol) was added. After stirring the reaction mixture for 24 h at room temperature, the solvent was removed

via rotary evaporator. To the Alexa Fluor® 594 conjugated nanoparticles, **14**, methanol (0.35 mL) and **13** (2.4 mg, 2.5 μmol), dissolved in DMSO (0.35 mL), were added. The reaction mixture was heated for 72 h at 35 °C. Residual Alexa Fluor® 594 and peptide were removed by dialyzing with SnakeSkin® Pleated Dialysis Tubing (MWCO = 10,000) against 1:1 $CH_3OH/CH_3CN$ to obtain **15** (22.0 mg). DLS: $D_H$ = 129.8± 9.6 nm; original particle $D_H$ = 126.6 ± 9.3 nm. SLS: $M_w$ = 394,000; original particle $M_w$ = 350,000. $^1H$ NMR (600 MHz, $(CD_3)_2SO$): δ The significant change is the reduction of the allyl protons at 5.72 and 4.97 ppm and the appearance of the following sets of significant signals: 7.37, 4.79, 2.23 and 1.66 ppm due to cRGD, and 7.25, 6.55, 5.31, 4.44, and 1.23 ppm due to the Alexa Fluor® 594. All other aspects of the spectrum are similar to that of **AbBD** nanoparticles.

**Attachment of MT to cRGD conjugated Alexa Fluor® 594-AbBD nanoparticles, NP-594-cRGD-MT (17).** To a solution of **15** (7.8 mg) in DMSO (0.1 mL), **8** (1.8 mg, 0.79 μmol) in $CH_3OH$ (0.3 mL) was added. The reaction mixture was heated for 48 h at 35 °C. Residual **8** was removed by dialyzing with SnakeSkin® Pleated Dialysis Tubing (MWCO = 10,000) against 1:1 $CH_3OH/CH_3CN$ to yield **12** (7.6 mg). DLS: $D_H$ = 131.9 ± 10.6 nm; original particle $D_H$ = 126.6 ± 9.3 nm. SLS: $M_w$ = 461,000; original particle $M_w$ = 350,000. $^1H$ NMR (600 MHz, $(CD_3)_2SO$): δ The significant change is the reduction of the allyl protons at 5.72 and 4.97 ppm and the appearance of signals at 3.04 (m, $CH_2$), 2.98 (m, $CH_2$), 1.98 (m, $CH_2$), 1.75 (m, $CH_2$), 1.41 (m, $CH_2$), and 1.35 (m, $CH_2$) ppm due to the dendritic backbone of the MT. All other aspects of the spectrum are similar to that of **15**.

**HVGGSSV conjugated AbBD nanoparticles, NP-HVGGSSV (19).** To a solution of **AbBD** nanoparticles (50.0 mg) in THF (2 mL), N-acetoxysuccinimide (7 mg, 44.5 μmol) was added. The reaction mixture stirred for 3 h. Residual N-acetoxysuccinimide was removed by dialyzing with SnakeSkin® Pleated Dialysis Tubing (MWCO = 10,000) against 1:1 THF/$CH_3OH$ to give amine capped **AbBD** nanoparticles, **18**. To a solution of **18** (50.0 mg in 3 mL THF), **1** (9.3 mg, 8.57 μmol) dissolved in DMSO (2 mL) and $NaCNBH_3$ (17.1 μL 1.0 M $NaCNBH_3$ in THF) were added. The reaction mixture was stirred for 12 h at room temperature. The reaction mixture was purified by dialyzing with SnakeSkin® Pleated Dialysis Tubing (MWCO = 10,000) against 1:1 THF/$CH_3CN$ to obtain **19** (43.2 mg). DLS: $D_H$ = 129.7 ± 9.5 nm; original particle $D_H$ = 126.6 ± 9.3 nm. SLS: $M_w$ = 391,000; original particle $M_w$ = 350,000. $^1H$ NMR (600 MHz, $(CD_3)_2SO$): δ The significant change is the appearance of the following peaks: 8.21, 7.85, 4.55, 3.73 and 0.80 ppm due to the peptide. All other aspects of the spectrum are similar to that of **AbBD** nanoparticles.

**Thiolated Alexa Fluor® 594 (20).** To a solution of NHS Alexa Fluor® 594 (0.2 mL of 10 mg/mL NHS Alexa Fluor® 594 in DMF, 2.4 μmol), cystemaine (68.4 μL of 2.5 mg/mL cysteamine in DMSO, 2.2 μmol) was added. The reaction mixture stirred for 3 h at room temperature. The product was immediately attached to **19**.

**Attachment of MT to HVGGSSV conjugated Alexa Fluor® 594-AbBD nanoparticles, NP-HVGGSSV-594-MT (21).** To a solution of **19** (16 mg) in DMSO

(0.2 mL), **20** (1 mg, 1.23 μmol) in DMSO (0.2 mL) and **8** (3.2 mg, 1.4 μmol) in $CH_3OH$ (0.4 mL) were added. The reaction mixture was heated for 48 h at 35 °C. Residual **8** and **20** were removed by dialyzing with SnakeSkin® Pleated Dialysis Tubing (MWCO = 10,000) against $CH_3OH$ to yield **21** (18.5 mg). DLS: $D_H$ = 132.1 ± 9.3 nm; original particle $D_H$ = 126.6 ± 9.3 nm. SLS: $M_w$ = 475,000; original particle $M_w$ = 350,000. $^1H$ NMR (600 MHz; $(CD_3)_2SO$): δ The significant change is the reduction of the allyl protons at 5.72 and 4.97 ppm and the appearance of the following sets of significant signals: 3.08, 2.99, 1.97, 1.79, 1.43 and 1.34 ppm due to the dendritic backbone of the MT, and 7.27, 7.07, 6.53, 5.32, 4.46, 4.37, and 1.24 ppm due to the Alexa Fluor® 594. All other aspects of the spectrum are similar to that of **19**.

**$^{1}$H NMR Characterization of Nanoparticle Conjugates:**

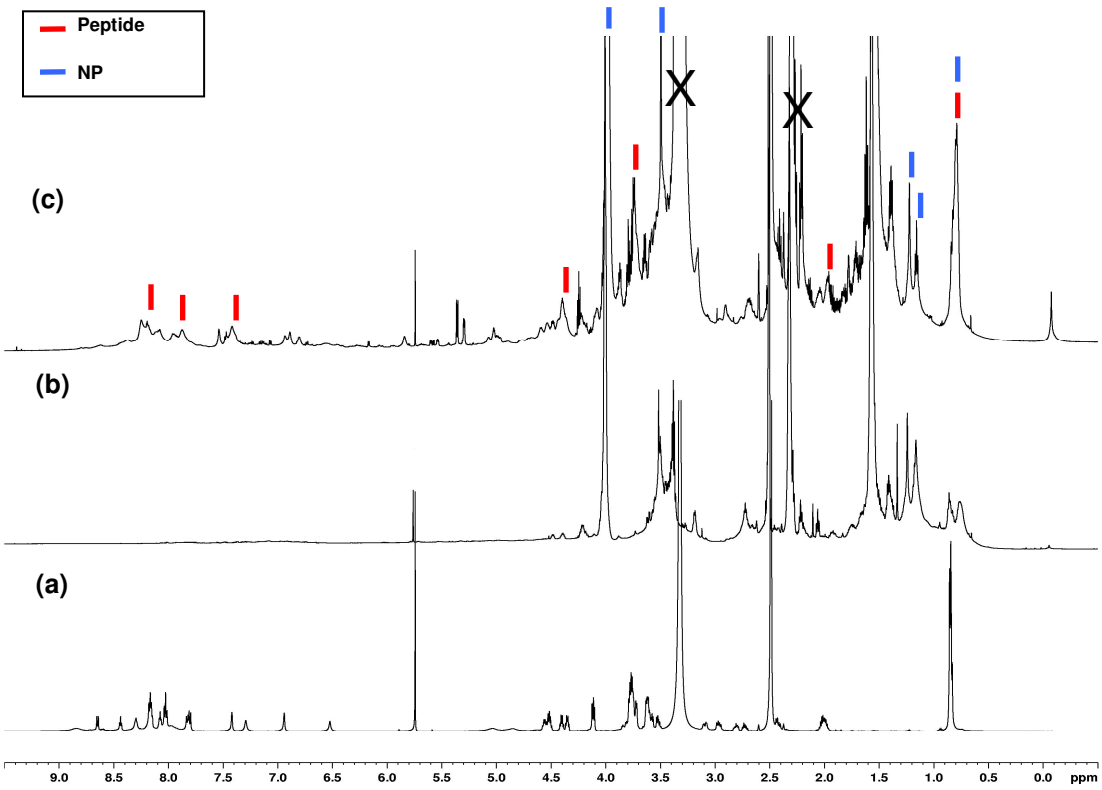


**Figure IV-2.** $^{1}$H NMR (600 MHz) spectra overlay: **(a)** GCGGGNHVGGSSV; **(b)** ABD-NP; **(c)** ABD-NP-HVGGSSV **(3)**.

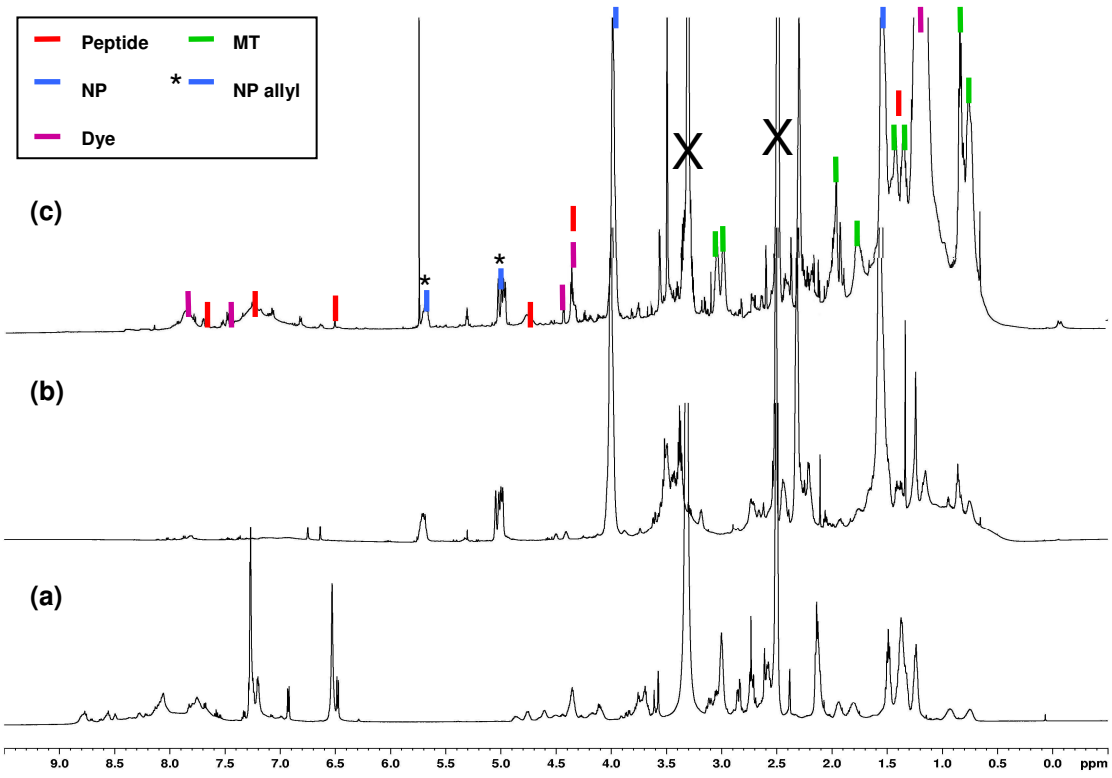


**Figure IV-3.** $^{1}$H NMR (600 MHz) spectra overlay: **(a)** cRGD; **(b)** AbBD-NP; **(c)** AbBD-NP-594-cRGD-MT (**17**) in DMSO-d6.

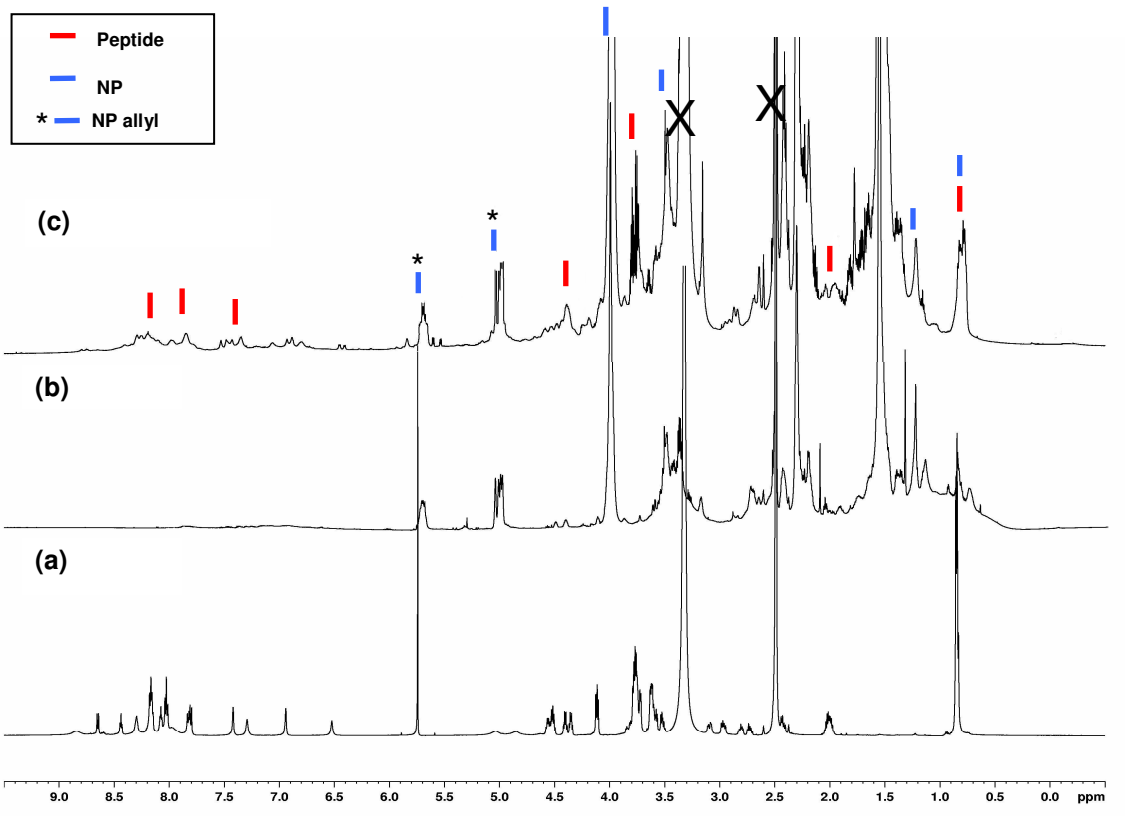


**Figure IV-4.** $^{1}$H NMR (600 MHz) spectra overlay: **(a)** GCGGGNHVGGSSV; **(b)** AbBD-NP; **(c)** AbBD-NP-HVGGSSV (**19**).

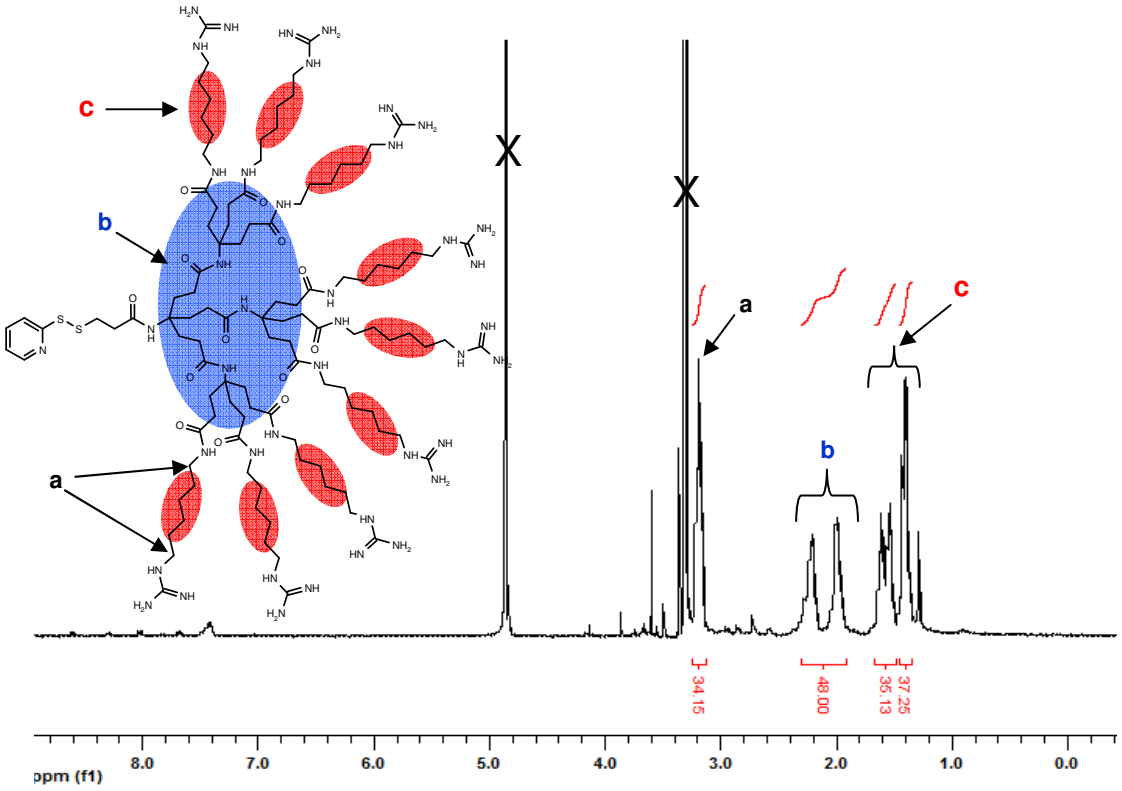


**Figure IV-5.** $^{1}$H NMR spectra of deprotected MT in MeOH-d4 (insoluble in DMSO-d6).

References

1. Parrish, B.; Quansah, J. K.; Emrick, T., Functional polyesters prepared by polymerization of alpha-allyl(valerolactone) and its copolymerization with epsilon-caprolactone and delta-valerolactone. *Journal of Polymer Science Part a-Polymer Chemistry* **2002,** *40* (12), 1983-1990.

2. Olson, D. A.; Gratton, S. E. A.; DeSimone, J. M.; Sheares, V. V., Amorphous linear aliphatic polyesters for the facile preparation of tunable rapidly degrading elastomeric devices and delivery vectors. *Journal of the American Chemical Society* **2006,** *128* (41), 13625-13633.

3. Olson, D. A.; Sheares, V. V., Preparation of unsaturated linear aliphatic polyesters using condensation polymerization. *Macromolecules* **2006,** *39* (8), 2808-2814.

4. Parrish, B.; Emrick, T., Aliphatic polyesters with pendant cyclopentene groups: Controlled synthesis and conversion to polyester-graft-PEG copolymers. *Macromolecules* **2004,** *37* (16), 5863-5865.

5. Parrish, B.; Breitenkamp, R. B.; Emrick, T., PEG- and peptide-grafted aliphatic polyesters by click chemistry. *Journal of the American Chemical Society* **2005,** *127* (20), 7404-7410.

6. Van Horn, B. A.; Iha, R. K.; Wooley, K. L., Sequential and single-step, one-pot strategies for the transformation of hydrolytically degradable polyesters into multifunctional systems. *Macromolecules* **2008,** *41* (5), 1618-1626.

7. Schappacher, M.; Soum, A.; Guillaume, S. M., Synthesis of polyester-polypeptide diblock and triblock copolymers using amino poly(epsilon-caprolactone) macroinitiators. *Biomacromolecules* **2006,** *7* (4), 1373-1379.

8. Van Horn, B. A.; Wooley, K. L., Toward cross-linked degradable polyester materials: Investigations into the compatibility and use of reductive amination chemistry for cross-linking. *Macromolecules* **2007,** *40* (5), 1480-1488.

9. Brown, A. H.; Sheares, V. V., Amorphous unsaturated aliphatic polyesters derived from dicarboxylic monomers synthesized by Diels-Alder chemistry. *Macromolecules* **2007,** *40* (14), 4848-4853.

10. Zhang, Z.; Feng, S.-S., Nanoparticles of poly(lactide)/vitamin E TPGS copolymer for cancer chemotherapy: synthesis, formulation, characterization and in vitro drug release. *Biomaterials* **2006,** *27* (2), 262-70.

11. Heredia, K. L.; Maynard, H. D., Synthesis of protein-polymer conjugates. *Organic & Biomolecular Chemistry* **2007,** *5* (1), 45-53.

12. Heredia, K. L.; Tolstyka, Z. P.; Maynard, H. D., Aminooxy end-functionalized polymers synthesized by ATRP for chemoselective conjugation to proteins. *Macromolecules* **2007,** *40* (14), 4772-4779.

13. Kopping, J. T.; Tolstyka, Z. P.; Maynard, H. D., Telechelic aminooxy polystyrene synthesized by ATRP and ATR coupling. *Macromolecules* **2007,** *40* (24), 8593-8599.

14. Esser-Kahn, A. P.; Francis, M. B., Protein-cross-linked polymeric materials through site-selective bioconjugation. *Angewandte Chemie-International Edition* **2008,** *47* (20), 3751-3754.

15. Douglas, E. S.; Chandra, R. A.; Bertozzi, C. R.; Mathies, R. A.; Francis, M. B., Self-assembled cellular microarrays patterned using DNA barcodes. *Lab on a Chip* **2007,** *7* (11), 1442-1448.

16. Hooker, J. M.; Esser-Kahn, A. P.; Francis, M. B., Modification of aniline containing proteins using an oxidative coupling strategy. *Journal of the American Chemical Society* **2006,** *128* (49), 15558-15559.

17. Jhaveri, S. B.; Beinhoff, M.; Hawker, C. J.; Carter, K. R.; Sogah, D. Y., Chain-end functionalized nanopatterned polymer brushes grown via in situ nitroxide free radical exchange. *Acs Nano* **2008,** *2* (4), 719-727.

18. Cook, W. D.; Chausson, S.; Chen, F.; Le Pluart, L.; Bowman, C. N.; Scott, T. F., Photopolymerization kinetics, photorheology and photoplasticity of thiol-ene-allylic sulfide networks. *Polymer International* **2008,** *57* (3), 469-478.

19. Reddy, S. K.; Okay, O.; Bowman, C. N., Network development in mixed step-chain growth thiol-vinyl photopolymerizations. *Macromolecules* **2006,** *39* (25), 8832-8843.

20. Lee, T. Y.; Carioscia, J.; Smith, Z.; Bowman, C. N., Thiol-allyl ether-methacrylate ternary systems. Evolution mechanism of polymerization-induced shrinkage stress and mechanical properties. *Macromolecules* **2007,** *40* (5), 1473-1479.

21. Rydholm, A. E.; Reddy, S. K.; Anseth, K. S.; Bowman, C. N., Development and characterization of degradable thiol-allyl ether photopolymers. *Polymer* **2007,** *48* (15), 4589-4600.

22. Salinas, C. N.; Cole, B. B.; Kasko, A. M.; Anseth, K. S., Chondrogenic differentiation potential of human mesenchymal stem cells photoencapsulated within poly(ethylene glycol)-arginine-glycine-aspartic acid-serine thiol-methacrylate mixed-mode networks. *Tissue Engineering* **2007,** *13* (5), 1025-1034.

23. Nilsson, C.; Simpson, N.; Malkoch, M.; Johansson, M.; Malmstrom, E., Synthesis and thiol-ene photopolymerization of allyl-ether functionalized dendrimers. *Journal of Polymer Science Part a-Polymer Chemistry* **2008,** *46* (4), 1339-1348.

24. Killops, K. L.; Campos, L. M.; Hawker, C. J., Robust, efficient, and orthogonal synthesis of dendrimers via thiol-ene "Click" chemistry. *Journal of the American Chemical Society* **2008,** *130* (15), 5062-+.

25. Torchilin, V. P., Tat peptide-mediated intracellular delivery of pharmaceutical nanocarriers. *Advanced Drug Delivery Reviews* **2008,** *60* (4-5), 548-558.

26. Kale, A. A.; Torchilin, V. P., "Smart" drug carriers: PEGylated TATp-Modified pH-Sensitive Liposomes. *Journal of Liposome Research* **2007,** *17* (3-4), 197-203.

27. Foerg, C.; Merkle, H. P., On the biomedical promise of cell penetrating peptides: Limits versus prospects. *Journal of Pharmaceutical Sciences* **2008,** *97* (1), 144-162.

28. Foerg, C.; Ziegler, U.; Fernandez-Carneado, J.; Giralt, E.; Merkle, H. P., Differentiation restricted endocytosis of cell penetrating peptides in MDCK cells corresponds with activities of Rho-GTPases. *Pharmaceutical Research* **2007,** *24* (4), 628-642.

29. Wender, P. A.; Kreider, E.; Pelkey, E. T.; Rothbard, J.; VanDeusen, C. L., Dendrimeric molecular transporters: Synthesis and evaluation of tunable polyguanidino dendrimers that facilitate cellular uptake. *Organic Letters* **2005,** *7* (22), 4815-4818.

30. Huang, K.; Voss, B.; Kumar, D.; Hamm, H. E.; Harth, E., Dendritic molecular transporters provide control of delivery to intracellular compartments. *Bioconjugate Chemistry* **2007,** *18* (2), 403-409.

31. Goun, E. A.; Pillow, T. H.; Jones, L. R.; Rothbard, J. B.; Wender, P. A., Molecular transporters: Synthesis of oligoguanidinium transporters and their application to drug delivery and real-time imaging. *Chembiochem* **2006,** *7* (10), 1497-1515.

32. Maiti, K. K.; Lee, W. S.; Takeuchi, T.; Watkins, C.; Fretz, M.; Kim, D. C.; Futaki, S.; Jones, A.; Kim, K. T.; Chung, S. K., Guanidine-containing molecular transporters: Sorbitol-based transporters show high intracellular selectivity toward mitochondria. *Angewandte Chemie-International Edition* **2007,** *46* (31), 5880-5884.

33. Barthel, S. R.; Gavino, J. D.; Descheny, L.; Dimitroff, C. J., Targeting selectins and selectin ligands in inflammation and cancer. *Expert Opinion on Therapeutic Targets* **2007,** *11* (11), 1473-1491.

34. Lee, C. C.; MacKay, J. A.; Frechet, J. M. J.; Szoka, F. C., Designing dendrimers for biological applications. *Nature Biotechnology* **2005,** *23* (12), 1517-1526.

35. Zhao, H. Z.; Yue, L.; Yung, L., Selectivity of folate conjugated polymer micelles against different tumor cells. *International Journal of Pharmaceutics* **2008,** *349* (1-2), 256-268.

36. Pasut, G.; Canal, F.; Via, L. D.; Arpicco, S.; Veronese, F. A.; Schiavon, O., Antitumoral activity of PEG-gemcitabine prodrugs targeted by folic acid. *Journal of Controlled Release* **2008,** *127* (3), 239-248.

37. Patri, A. K.; Kukowska-Latallo, J. F.; Baker, J. R., Targeted drug delivery with dendrimers: Comparison of the release kinetics of covalently conjugated drug and non-covalent drug inclusion complex. *Advanced Drug Delivery Reviews* **2005,** *57* (15), 2203-2214.

38. Pan, D.; Turner, J. L.; Wooley, K. L., Folic acid-conjugated nanostructured materials designed for cancer cell targeting. *Chemical Communications* **2003,** (19), 2400-2401.

39. Han, Z.; Fu, A.; Wang, H.; Diaz, R.; Geng, L.; Onishko, H.; Hallahan, D. E., Noninvasive assessment of cancer response to therapy. *Nature Medicine* **2008,** *14* (3), 343-349.

40. Hariri, G.; Croce, T.; Harth, E.; Han, Z.; Tantawy, N.; Peterson, T.; Baldwin, R.; Hallahan, D., Radiation guided peptide targeting to tumor microvasculature using nanoparticle carriers. *International Journal of Radiation Oncology Biology Physics* **2007,** *69* (3), S151-S152.

41. Fu, A.; Han, Z.; Hallahan, D. E., Recombinant peptides that rapidly assess cancer susceptibility to tyrosine kinase inhibitors combined with radiation. *International Journal of Radiation Oncology Biology Physics* **2006,** *66* (3), S548.

42. Murphy, E. A.; Majeti, B. K.; Barnes, L. A.; Makale, M.; Weis, S. M.; Lutu-Fuga, K.; Wrasidlo, W.; Cheresh, D. A., Nanoparticle-mediated drug delivery to tumor vasculature suppresses metastasis. *Proceedings of the National Academy of Sciences of the United States of America* **2008,** *105* (27), 9343-9348.

43. Xie, J.; Shen, Z.; Li, K. C. P.; Danthi, N., Tumor angiogenic endothelial cell targeting by a novel integrin-targeted nanoparticle. *International Journal of Nanomedicine* **2007,** *2* (3), 479-485.

44. Montet, X.; Montet-Abou, K.; Reynolds, F.; Weissleder, R.; Josephson, L., Nanoparticle imaging of integrins on tumor cells. *Neoplasia* **2006,** *8* (3), 214-222.

45. van der Ende, A. E.; Kravitz, E. J.; Harth, E., Approach to formation of multifunctional polyester particles in controlled nanoscopic dimensions. *Journal of the American Chemical Society* **2008,** *130* (27), 8706-8713.

46. Hojfeldt, J. W.; Blakskjaer, P.; Gothelf, K. V., A cleavable amino-thiol linker for reversible linking of amines to DNA. *Journal of Organic Chemistry* **2006,** *71* (25), 9556-9559.

47. Boileau, S.; Mazeaud-Henri, B.; Blackborow, R., Reaction of functionalised thiols with oligoisobutenes via free-radical addition. Some new routes to thermoplastic crosslinkable polymers. *European Polymer Journal* **2003,** *39* (7), 1395-1404.

# CHAPTER V

# THERAPEUTIC NANOSPONGES FOR THE TREATMENT OF A BROAD RANGE OF DISEASES

## Introduction

The major challenge of drug delivery is the liberation of therapeutic at the correct time in a safe and reproducible manner to a specific target site.[1] Conventional drug administration, such as intravenous injections, only offer limited control over the rate of drug release into the body, which predominately results in the immediate release of the therapeutic.[2] Consequently, to achieve therapeutic levels that extend over time, the initial concentration of the drug in the body must be high, causing peaks that gradually diminish to ineffective levels. This peak and valley delivery is known to cause toxicity in certain cases, for example chemotherapeutics. For some of the more potent drugs, the therapeutic window is often narrow and toxicity is observed for concentration spikes which render the traditional methods of drug delivery ineffective. Systemically administering bolus doses of potent therapeutics often results in severe side effects due to the action of the drugs on sites other than the intended target. Due to this nonspecific drug action, the concentration of drug available at the site of action is potentially below the minimal effective concentration, which creates a dilemma between administering a near-toxic effective dose and a safe ineffective dose.[3]

In addition to these obstacles, more than half of active substances identified through combinatorial screening programs are difficult to formulate for administration due to their significant insolubility in water.[4, 5] The classical approach to deal with this

issue is to generate various salts of a poorly water-soluble molecule so as to improve its solubility while retaining biological activity.[6] However, these approaches are not frequently successful and the product is launched with suboptimal properties including poor bioavailability, lack of optimal dosing, presence of extra excipients such as Cremophor® EL that pose limitations with respect to dose escalation, and, ultimately poor patient compliance.[6] To alleviate these challenges of conventional drug delivery, significant interest has been focused on the development of delivery systems that can enhance therapeutic solubility, release the drug in a sustained manner, preferentially localize the therapeutic to the site of action, and overall enhance therapeutic efficacy.

Nanoparticle drug delivery, using biodegradable polymers, provides a more efficient and less adverse solution to overcome the aforementioned challenges of drug delivery. The use of polymeric nanoparticle drug delivery systems exhibits their greatest advantage as methods of continuous administration of drugs to maintain extended plasma drug levels.[7] Particles can encapsulate the therapeutic, shielding the drug during circulation and protecting it from degradation or loss of biological activity, thereby increasing drug efficacy, specificity, tolerability and therapeutic index.[8] With such therapeutic enhancement, there can be a reduction in dosage, patient expenses, and risks of toxicity. In addition, nanoparticles are opening new therapeutic opportunities for drugs that cannot be used effectively as conventional formulations due to poor availability or drug instability.[9]

Traditional polyester nanoparticle delivery systems are typically self-assembled from linear polyesters chains driven by the polarity of the solvent, emulsion composition, and addition techniques.[10-12] These procedures, however, predetermine the drug loading

during nanoparticle formation and limit post-modification chemistries in organic and aqueous solutions.[13] Furthermore, the result of this self-assembly process is mirrored in the morphology and degradation properties of the release systems. It has been recognized that the degradation behavior of the nanoparticles and release profiles of the entrapped drug molecules are the key factors in establishing predictable pharmacokinetic profiles[14, 15] in effective multidrug cancer therapies. So far, release kinetics is challenged by a rapid release of the drug molecules in the first 24–48 h followed by a slower release, referred to as a 'burst-effect'.[11, 16] These release profiles prevent the establishment of reliable dosages and contribute to developing multidrug resistance (MDR),[17] oftentimes the result of non-optimized drug concentrations. Therefore, there still remains a need for the development of delivery systems which allow for the controlled linear release of therapeutics and overcome the additional challenges of conventional drug delivery.

This chapter presents the synthesis and evaluation of novel drug delivery systems, with and without active targeting, based on the developed chemistries reported in the previous chapters. The innovation in the presented approaches illustrates the versatile nature of the aforementioned nanoparticle platform which can be tailored to meet the needs of a specific biomedical application. By means of this technology, particles, based on the epoxide-amine chemistry, have been shown to be unique in their capability to entrap high concentrations of hydrophobic therapeutics, such as Taxol, and maintain a linear release profile which can be tuned to the demands of a disease as a result of the adjustable supramolecular architecture accomplished through the intermolecular cross-linking technique. With the established conjugations chemistries, as seen in Chapter IV,

these particles have been modified with targeting units to increase the site-specific localization of the particles and their payload as has been seen with *in vivo* studies.

In addition to the encapsulation and delivery of small molecules, the alkyne-azide click cross-linking has been shown to be efficient for the formation of particles that encapsulate sensitive bioactive cargo, such as peptides, to afford peptide-loaded particles. Along with the alkyne-azide cross-linking, the thiol-ene click chemistry has been utilized to form particles in water using a novel water soluble polymer for the future encapsulation of siRNA. The ability to incorporate all of these properties into a single nanoparticle carrier system demonstrates that, with increasingly advanced iterations, the particles have been efficiently optimized for numerous therapeutic applications, such as the treatment of cancer and glaucoma, and the encapsulation of macromolecular therapeutics.

## Results and Discussion

### Nanoparticle Degradation and Cellular Uptake

To determine if the amorphous properties of poly(valerolactone-epoxyvalerolactone), poly(vl-evl), **AB**,[18] particles have a positive effect on the degradation behavior, a series of degradation studies[19] in phosphate buffered saline (PBS) was completed at pH 7.4 at 37 °C with continuous stirring,[20] investigating particles from a completed series of linear precursors and increasing amounts of difunctionalized cross-linkers with controlled nanoscopic dimensions (Figure V-1). Samples were removed every 48 h over a time period of 240 hours (10 days). The degradation of the particles

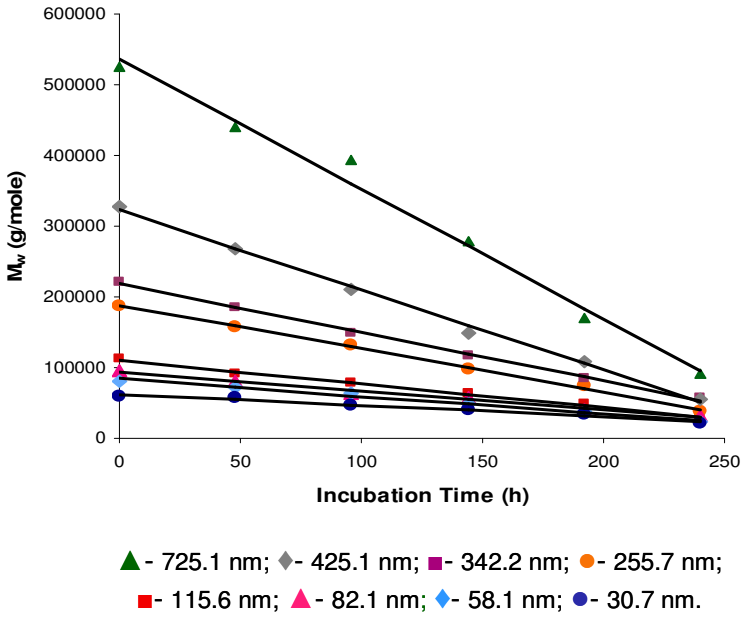


**Figure V-1.** Hydrolytic degradation studies of (▲) 725.1 ± 94.3 nm **$AB_1$** nanoparticles to (●) 30.71 ± 2.21 nm **$AB_1$** nanoparticles.

was monitored by the change of the absolute molecular weight[21] as determined through static light scattering illustrated in Figure V-1. A linear degradation profile was observed for all investigated sizes as a result of the low crystallinity of the samples. The largest particle of 725.1 ± 94.3 nm experienced the highest loss of molecular weight with 17.5% of total molecular mass remaining after 10 days. Smaller particles with a slightly higher degree of crystallinity of 20.6% were degraded to 26% of their original molecular weight. An even smaller particle of 30.7 ± 2.2 nm experienced an anticipated lower molecular weight loss, with 35% of remaining molecular mass of the particle. The observed linear degradation kinetics is a critical parameter that will determine the quality of the developed particles towards applications as controlled release systems. Future studies will include the investigation of particles with lower and even higher degrees of cross-

linking densities and particles with longer pegylated diamine cross-linkers to further extend the degradation profile to longer or shorter time frames if needed.

In an effort to determine the biological effect of the epoxide-amine cross-linked particles, preliminary *in vitro* uptake studies were conducted with a 50 nm Alexa Fluor® 594 modified **$AB_1$** nanoparticle in a human lung carcinoma cell line, NIH-H460. The conjugate was allowed to incubate with the cells for 30 min, 45 min, 1 h, and 1.5 h

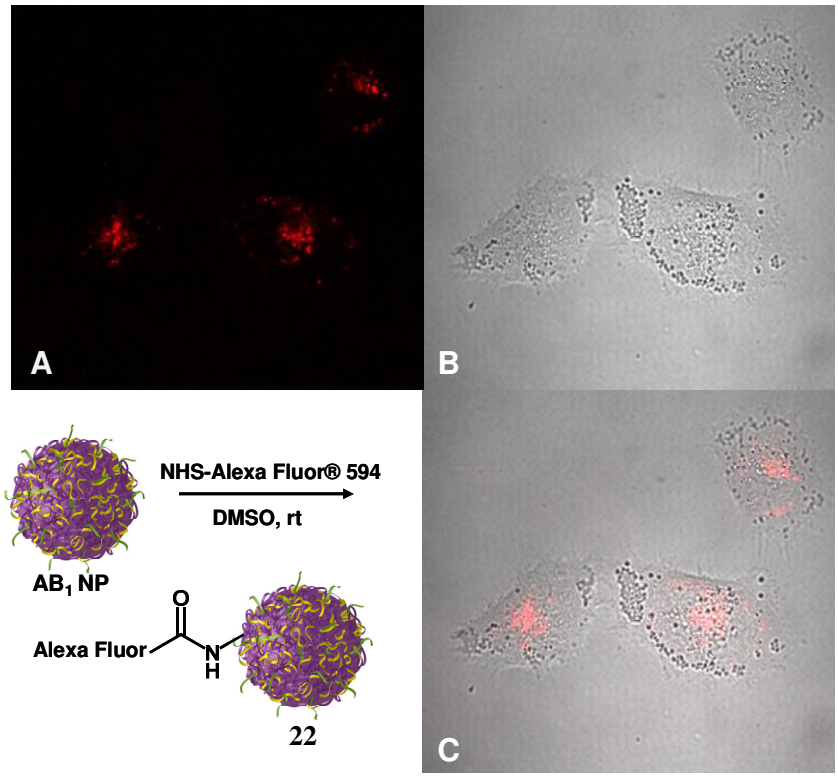


**Figure V-2.** Confocal images of Alexa Fluor®594 modified **$AB_1$** nanoparticles, **22**, in H460 cells using filters **(A)** QDot 585 (555-655 nm); **(B)** DIC; and **(C)** overlay of images **A**, and **B** at 100x magnification. The cells were incubated for 1.5 h with a 40 µM solution.

followed by removal of the conjugate and subsequently washed to remove residual compound and imaged using confocal microscopy. These data revealed that while uptake

did take place within 45 min of nanoparticle treatment, greater contrast was apparent within longer time periods with the brightest contrast taking place at the 1.5 h time point (Figure V-2). From the confocal images, the Alexa Fluor® modified nanoparticles were dispersed within the cell and did not localize in any particular compartment, suggesting that endocytosis may be the method of uptake. Further studies will be completed with these particles to investigate particle size dependency for cellular uptake and localization.

**Encapsulation of Small Hydrophobic Drugs: Paclitaxel**

As a next step, it was necessary to investigate the capacity to encapsulate small molecule drugs, such as paclitaxel (Taxol) which exhibits short circulation half-life and poor aqueous solubility.[22] Traditional polyester particles, produced with salting-out or nanoprecipitation methods, typically do not exceed a drug loading over 5% that is facilitated during nanoparticle formation. However, the developed nanoparticles consist of cross-linked supramolecular structures that are readily soluble in organic solvents without affecting the 3-D architecture. This property gives the opportunity to load the particles after formation by dissolving the particles in dimethyl sulfoxide (DMSO)

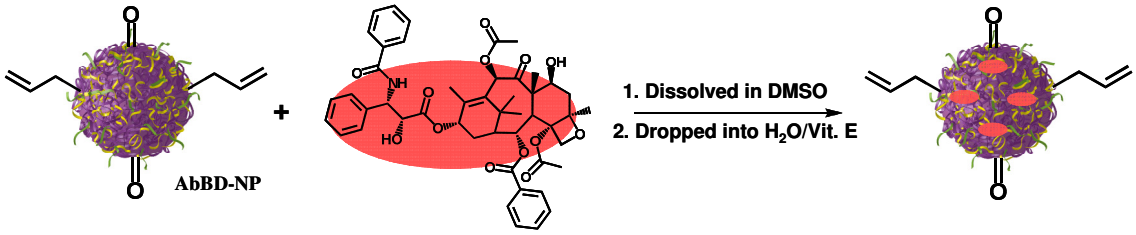


**Figure V-3.** Encapsulation of paclitaxel using a novel formulation technique, in which the AbBD-NP and paclitaxel were dissolved together in dimethyl sulfoxide (DMSO), dropped into a rapidly stirring solution of $_{D}$-α-tocopherol polyethylene glycol 1000 succinate (vit E.) and collected using centrifugation.

together with cancer therapeutics, such as paclitaxel, and precipitating into a rapidly stirring solution of water with $_{D}$-α-tocopherol polyethylene glycol 1000 succinate (vitamin E TPGS) (Figure V-3), leading to a higher drug payload. The previously discussed experiments to determine the drug loading capacity were performed with particles of 53 nm in diameter from linear precursors poly(vl-avl-evl-opd), **AbBD**,[18] containing 11% epoxide and cross-linked with 2 equivalents of diamines per epoxide. In view of future *in vivo* experiments, the encapsulation method was optimized to increase the homogeneity of the particle dispersion in water for a practical administration of the drug loaded particles by injection. Here, an emulsification process was utilized with vitamin E TPGS,[23] that achieved a homogenous dispersion of the loaded or un-loaded particles in water or buffer. The resulting particles were analyzed by UV-Vis with a NanoDrop™ Spectrophotometer at 254 nm, and along with a calibration curve, the drug loading with paclitaxel was found to be 15.7 wt% for an aimed 20 wt% drug load and 11.3 wt% for a 15 wt% drug load, respectively. It can be concluded that with this process, it is not only possible to load therapeutic drug molecules to a higher degree into prepared nanoparticles, but also a method has been found for the solubilization of hydrophobic cancer therapeutics in aqueous solutions. As a result, it can be anticipated that side effects known to be caused by adjuvant agents, such as Cremophor® EL (50:50 ethanol–polyoxyethylated castor oil),[24-26] which are used to solubilize hydrophobic drug molecules for intravenous injections, can be avoided.[27]

To ensure that no cellular toxicity is caused by the vitamin E TPGS formulated particles prior to drug loading, the cellular viability was assessed by utilizing a MTT assay[11] (Figure V-4). The cellular toxicity was determined by incubating HeLa cells with varying concentrations of particles in triplicate ranging from 5 mg $mL^{-1}$ to 0.001 mg $mL^{-1}$. Following 24 h of incubation with particles, cell viability was assessed. As seen in Figure V-4, the nanoparticles did not cause significant cytotoxicity against the HeLa cell line. The experimental $TC_{50}$ value for the formulated particles was found to be 1.0 mg $mL^{-1}$, which was within the range of the $TC_{50}$ values, 0.88 mg $mL^{-1}$ and 1.5 mg $mL^{-1}$, as determined for the previously reported particles from the alkyne-azide and thiol-ene cross-linking reactions, respectively.

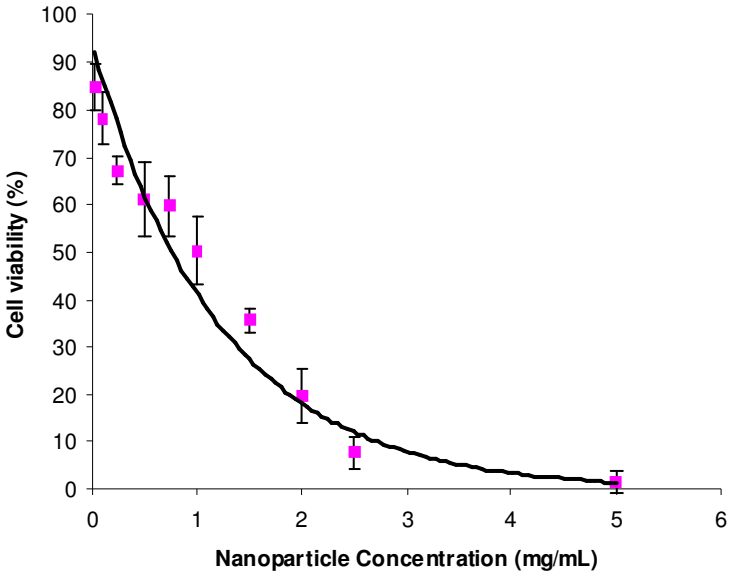


**Figure V-4.** Cytotoxicity of vitamin E TPGS formulated nanoparticles on HeLa cells after 24 h incubation using the MTT assay. Fitted curve shows cellular viability of the HeLa cell line.

Moreover, it was found that the emulsification had a profound effect on the degradation profile and correlated with the *in vitro* release studies. Over the period of 16 days, the particles experienced a low controlled degradation, as seen by the linear degradation, finishing with 70% of its original molecular weight remaining (Figure V-5). The slower degradation rate can be attributed to the well-defined structure of the nanoparticle and the vitamin E TPGS that might remain present at the surface to stabilize the particles. Consequently, this gradual constant degradation profile of the particles is a

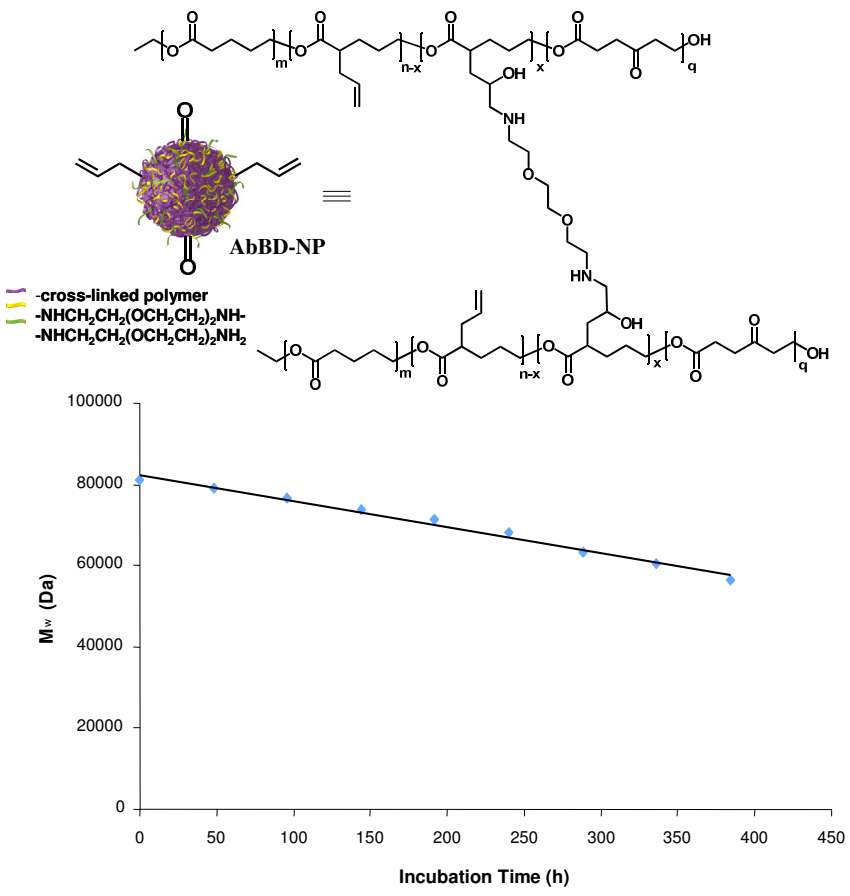


**Figure V-5.** *In vitro* degradation profile of vitamin E TPGS formulated **AbBD** nanoparticles of 53 nm in PBS at pH 7.4 and 37 ºC over a period of 384 h (16 days).

desirable feature since it could translate into the controlled and sustained release of therapeutics.

**Nanoparticle Drug Release Profiles**

After establishing procedures for the loading and solubilization of drug molecules in the particles, the next step was to evaluate the particles' drug release profile *in vitro*. The paclitaxel release kinetics from the vitamin E TPGS formulated nanoparticles was assessed by monitoring the cumulative release of Taxol at 37 °C in PBS at pH 7.4. At particular time intervals, the samples were centrifuged and the supernatant was collected

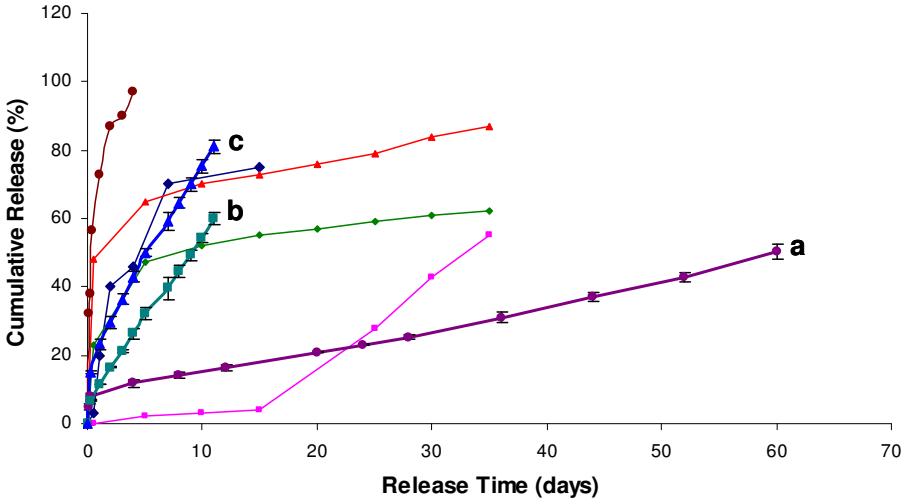


**Figure V-6.** *In vitro* release profiles of paclitaxel from particles loaded with Taxol prepared by the emulsification method (**a**) 53 nm particle with 7% cross-linking and 12 % drug loading; (**b**) 50 nm particle with 2% cross-linking with 13% drug loading; (**c**) 52 nm particle, prepared from linear precursor with 7% cross-linking density coupled with a longer diamine linker, with 11% drug loading. As a comparison, the other graphs show release of paclitaxel from PLGA based nanoparticles, as found in the literature.[11, 16, 28, 29]

for the quantification of paclitaxel by NanoDrop$^{TM}$ spectrophotometry (254 nm). Figure V-6 depicts the cumulative release of paclitaxel from the particles. Profile **a** shows a collective release of 4.4% and 7.4% Taxol in the first 2 and 6 h respectively, followed by a slow and sustained release over 60 days, which again confirmed the efficient encapsulation of paclitaxel within the cross-linked nanoparticles. The initial instant release of paclitaxel in the first several hours may be due to the dissolution or diffusion of the drug that was absorbed onto the nanoparticle surface, while the linear, slow, continuous release may be attributed to the diffusion of the drug encapsulated in the nanoparticle during degradation. Traditional poly(lactic-co-glycolic acid) (PLGA) nanoparticles, however, experience an erratic nonlinear drug release, that includes a 'burst-effect' in which about 40% of Taxol is released in the first day, followed by a fast release of about 10–30% in the next 2–5 days and then finally a slow release until no paxlitaxel remains.[28] Therefore, the release properties of these reported particles are superior to the traditional PLGA polyester particles[11, 16, 28, 29] (as seen in Figure V-6) as they provide a preferred controlled linear release without a 'burst-effect', which is critical in optimizing therapy for a specific disease, such as cancer.

For the further development and optimization of the nanoparticles for clinical use, it was found that the drug release kinetics can be controlled. The linear release kinetics are adjustable by decreasing the density of the cross-linker in linear polymer and increasing the length of the diamine linker to release therapeutic at a faster rate from particles of comparable sizes. By decreasing the cross-linking density from 7% to 2%, the paclitaxel was released from a 50 nm particle at a faster rate, with 50% released in 10 days (Figure V-6, Profile **b**). To afford an even faster release of the drug, a longer diamine linker,

Jeffamine® ED-2003 with a molecular weight of 2000 Da, was coupled with a linear polymer with 7% evl cross-linker to design a 52 nm particle with a wider network architecture for a more rapid release of therapeutic, in which 50% of the drug is released in 5 days (Figure V-6, Profile **c**). Further studies will be necessary to investigate particles with lower and even higher degrees of cross-linking densities and particles with longer pegylated diamine cross-linkers for the optimization of drug delivery for particular biomedical applications.

In view of future *in vivo* studies in which the particle sizes play an important role in the interaction with the tumor vasculature, the influence of formulation and encapsulation of small molecule drugs on the diameter of the nanoparticles was

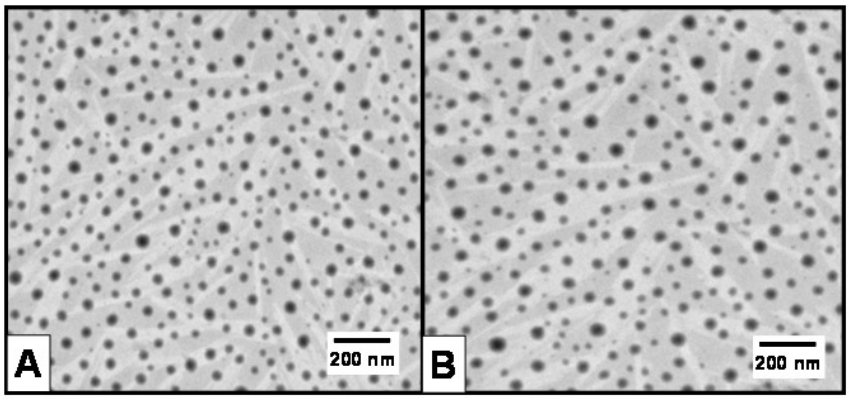


**Figure V-7.** Transmission electron microscopy (TEM) images of **(A)** nanoparticles without paclitaxel with a size of 53 nm and **(B)** nanoparticles encapsulated with 11.3% Taxol with a size dimension of 57 nm.

evaluated. Interestingly, it was found that based on the 3-D cross-linked network structure, the size dimension slightly changes from 53 nm to 57 nm, which indicates the conformity of the 3-D network structure upon encapsulation, as seen by transmission electron microscopy (TEM), (Figure V-7), with 2–8 times more drug incorporated compared to traditional polyester nanoparticle systems.[22, 28, 30]

Encouraged by the linear release kinetic profiles and structural integrity of the investigated particles, these controlled release systems were advanced to targeted nanoparticles for future evaluation of these properties *in vivo*. As previously reported, the developed nanoparticle synthesis pathway allows for the introduction of functional groups, such as alkyne, allyl or keto functionalities, that are not affected by the cross-linking reactions and nanoparticle formation.[18] Using the previously reported thiol-ene click reactions, targeting peptides with integrated cysteines, added to the sequence near the N-terminus, could be conjugated to the particle under mild reaction conditions without the addition of radical starters.[31]

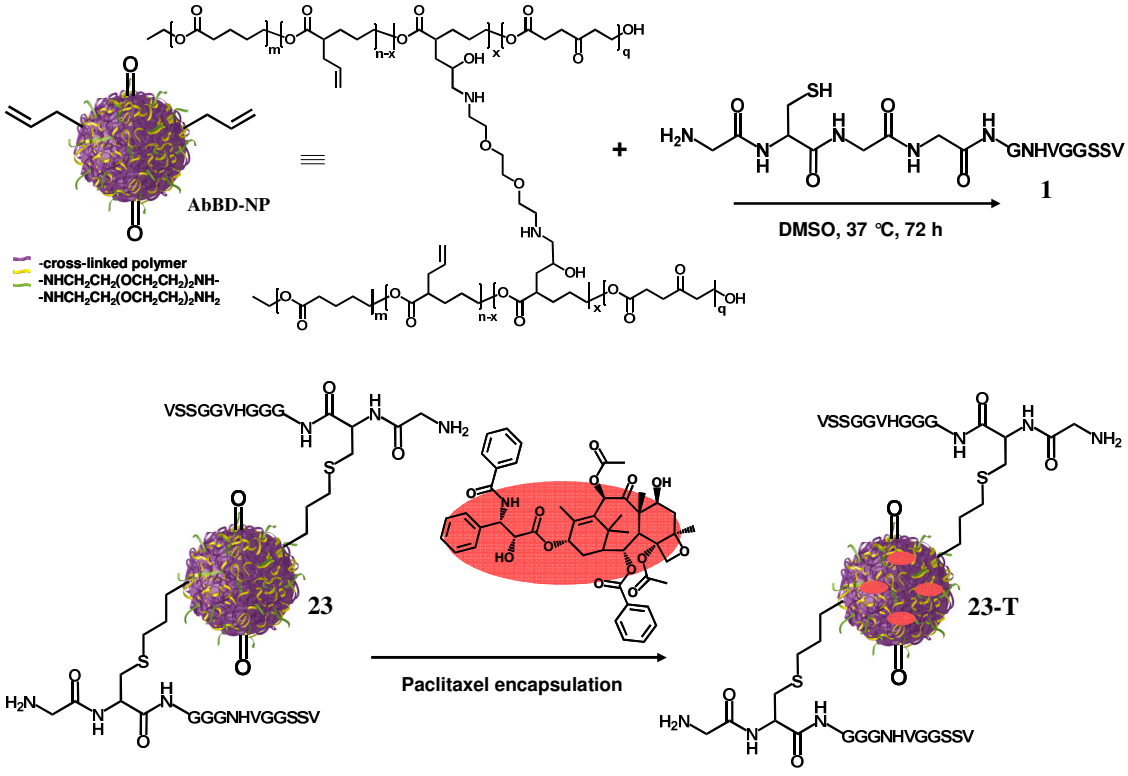


**Scheme V-1.** Synthesis of paclitaxel loaded AbBD-NP-HVGGSSV system. The targeting HVGGSSV peptide was conjugated to the particle using thiol-ene 'click' chemistry. Paclitaxel was then incorporated into the cavities of the particles by the vitamin E TPGS formulation technique which resulted in the paclitaxel loaded HVGGSSV-nanoparticle, **23-T**.

To synthesize the drug delivery system, the linear poly(vl-avl-evl-opd), **AbBD**, precursor was first synthesized with 7% evl incorporated in the polymer backbone, which was then cross-linked with 1 equivalent of diamine per epoxide to form a 53 nm nanoparticle.[31] The remaining allyl groups were then functionalized with peptides, **23**, (Scheme V-1), such as the reported peptide with the recognition unit HVGGSSV,[32] to target irradiated[32, 33] tumor vasculature. The bioconjugate was analyzed via NMR, DLS and SLS and was then loaded with paclitaxel and formulated with vitamin E TPGS. Using NanoDrop™ UV-Vis, the loading capacity was found to be 11 wt%, when aiming for a 15 wt% drug load. The *in vivo* investigation of this targeted drug delivery system, **23-T**, in tumor suppression studies will be carried out in the near future.

**GIRLRG-AbBD Nanoparticle Drug Delivery System for Cancer Therapy**

The efficacy of current cancer therapeutics, such as paclitaxel, is limited by the non-optimized delivery of therapeutics to the tumor and their toxic effects to non-tumor tissues. Therefore, as mentioned previously, the obstacle in cancer treatment is to design a vector that enables specific targeting to the tumor site and allows for the controlled, linear release of therapeutic. To address this challenge, a novel nanoparticle drug delivery system (DDS) has been developed in which the particle has been labeled with a targeting peptide, KKCGGGGIRLRG, with the recognition unit GIRLRG, discovered by the Hallahan and Diaz lab at Vanderbilt University, and loaded with Taxol.[34]

The GIRLRG sequence, which has been identified through the use of screening phage-display libraries,[32, 35-37] has been proven to target the neovasculature following a clinically relevant dosage of radiation. Preliminary targeting studies were conducted by

the Hallahan and Diaz lab to ensure the GIRLRG peptide was the functional motif for binding to x-ray treated (XRT) tumors *in vivo*. This was accomplished by using a streptavidin-biotinylated KKGGGGIRLRG conjugate, which was used to mimic a targeted particle system, with an Alexa Fluor® 750 label on the N-terminus of the peptide conjugate. Near infrared (NIR) imaging, with a Xenogen IVIS imaging system, was used to follow the biodistribution of the peptide within glioma (GL261) tumor-bearing mice, which demonstrated the selectivity of the GIRLRG targeting unit to localize at the XRT tumor versus the non-irradiated tumor (Figure V-8). [34]

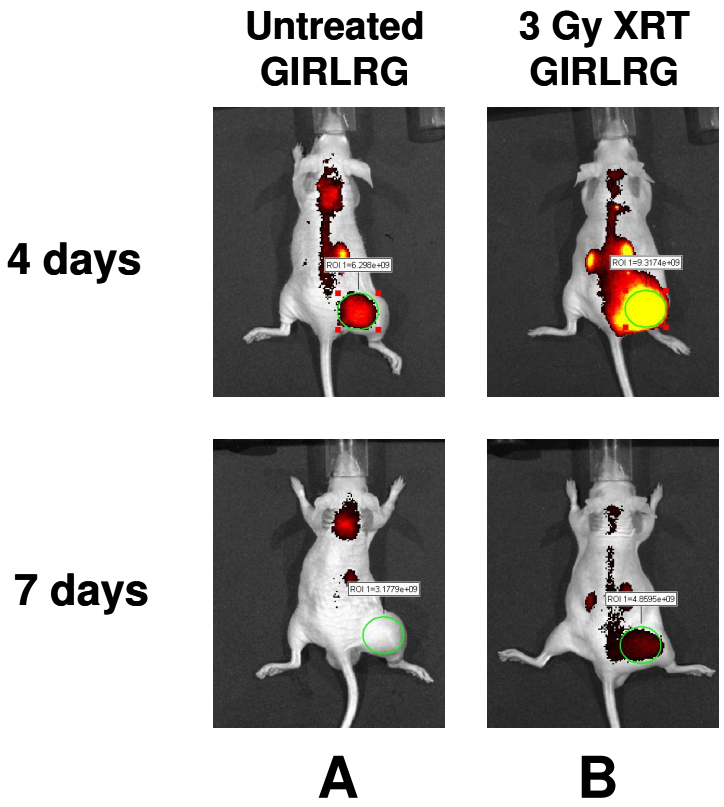


**Figure V-8.** Biotinylated-KKGGGGIRLRG peptide, with fluorescent label, preferentially binds to radiation treated tumors (3 Gy XRT) in GL261 xenografts **(B)** compared to untreated tumors **(A)** in nude mice as determined by the Hallahan lab.[34]

To incorporate the GIRLRG targeting moiety onto the nanoparticle, the peptide was first modified and synthesized, by solid-phase peptide synthesis, to contain a cysteine near the N-terminus, the vital sulfhydryl group, for integration onto the particle using the novel thiol-ene click chemistry. Following the preparation of a 53 nm **AbBD** nanoparticle,[31] the GIRLRG peptide was conjugated to the particle using the high yielding thiol-ene reaction,[38] reacting the free thiol of the cysteine near the N-terminus of the KKCGGGGIRLRG peptide with the allyl functionalities on the nanoparticle to form **25** (Scheme V-2). Analysis with $^{1}$H NMR, after thorough dialysis purification to remove

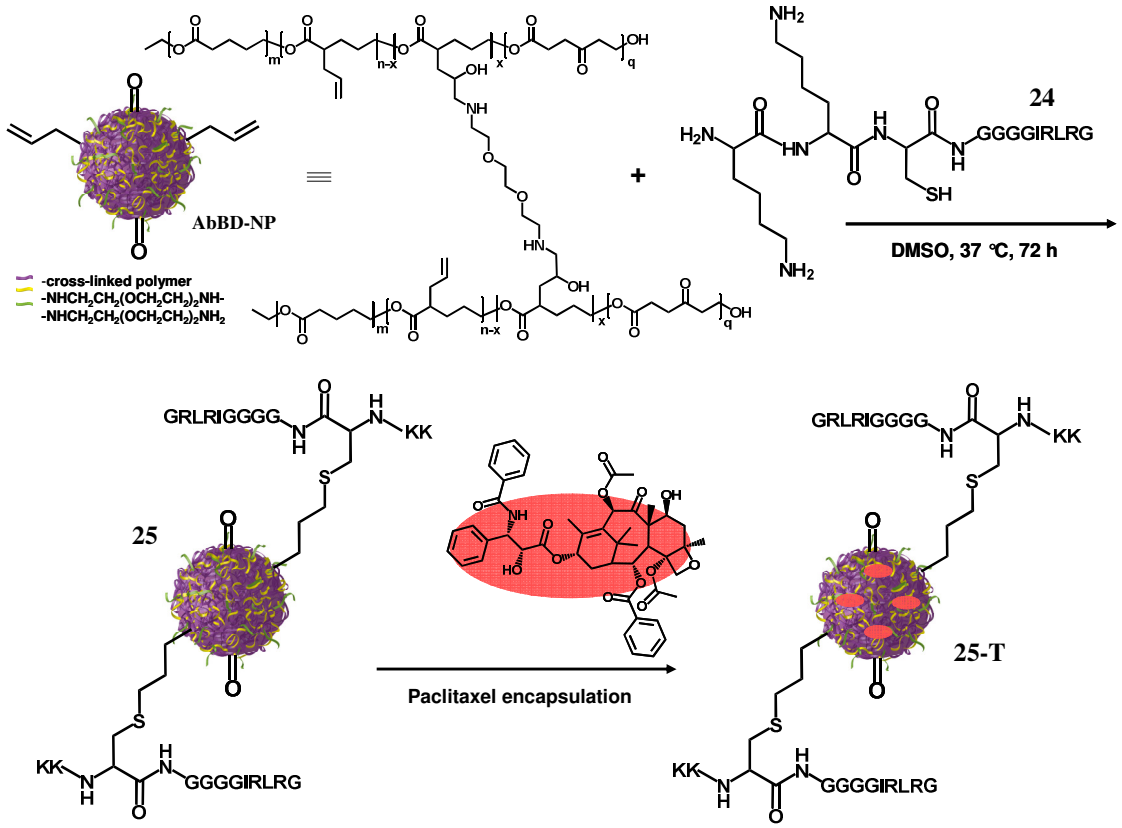


**Scheme V-2.** Synthesis of GIRLRG-targeted **AbBD** nanoparticle drug delivery system, **25-T**. The targeting GIRLRG peptide, **24**, was conjugated to the **AbBD** particle through thiol-ene chemistry via the free allyl moieties on the particle and the free cysteine at the N-terminus of the peptide, **25**. Paclitaxel was then encapsulated into the particle, **25-T**, *via* the developed vitamin E TPGS emulsification.

any non-conjugated materials, showed the characteristic peptide resonance peaks at 4.40, 3.07, 1.39 and 0.80 ppm. The integration of the protons and the quantification of the decrease of the allyl protons, which are conveniently detected apart from the ones of the polyester backbone, confirmed the attachment of 37 peptide units per particle. As the final step, paclitaxel was incorporated into the GIRLRG-particle conjugate using the aforementioned vitamin E TPGS emulsification process, resulting in an 11.2 wt% Taxol loading in the GIRLRG-nanoparticle conjugate, **25-T**, which dispersed well in a Cremophor-free solution. The biocompatibity of the peptide targeted particles, **25**, in concentrations applied for *in vivo* studies was confirmed by MTT assays (Figure V-9). The cellular toxicity of the peptide-nanoparticle conjugate was determined by incubating HeLa cells with varying concentrations of particles in triplicate ranging from 5 mg/mL to 0.01 mg/mL. Following 24 h of incubation with particles, cellular viability was assessed

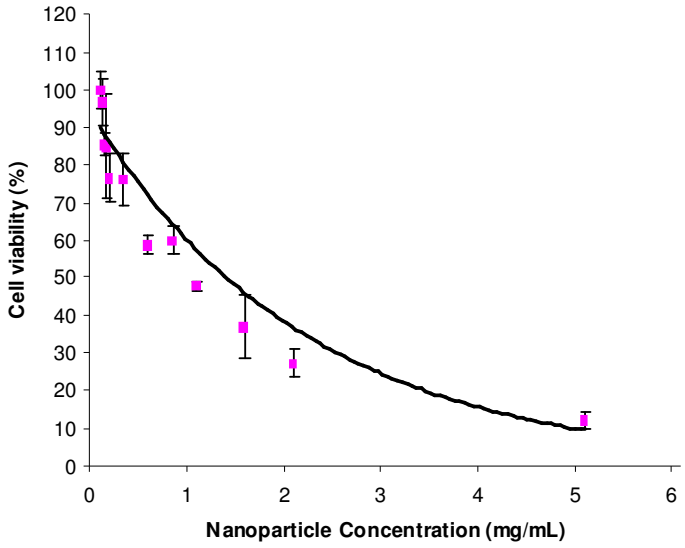


**Figure V-9.** Cytotoxicity of vitamin E TPGS formulated GIRLRG peptide targeted nanoparticles on HeLa cells after 24 h incubation using the MTT assay. Fitted curve shows cell viability of HeLa cell line with concentrations of particles from 5 mg/mL to 0.01 mg/mL.

by using the MTT assay. As seen in Figure V-9, the nanoparticles did not cause significant cytotoxicity against the HeLa cell line. The experimental $TC_{50}$ value for the formulated particles was found to be 0.97 mg/mL.

In collaboration with the Hallahan and Diaz lab, the effects of the GIRLRG-targeted **AbBD** nanoparticle DDS, **25-T**, on paclitaxel concentration and apoptosis in tumors were investigated. MDA-MB-231 breast carcinomas were implanted in the hind limbs of nude mice and treated with 3 Gy of XRT daily for three days, and systemic paclitaxel, GIRLRG-targeted **AbBD** nanoparticle DDS or random peptide nanoparticle DDS on the second day once the tumors had reached a volume of 450 $mm^3$. Tumors were harvested at one and three weeks post-treatment and the levels of paclitaxel (Figure V-10A) and apoptosis (Figure V-10B) were quantified with the respective cell staining assay. Paclitaxel was found in significantly greater concentrations in the targeted

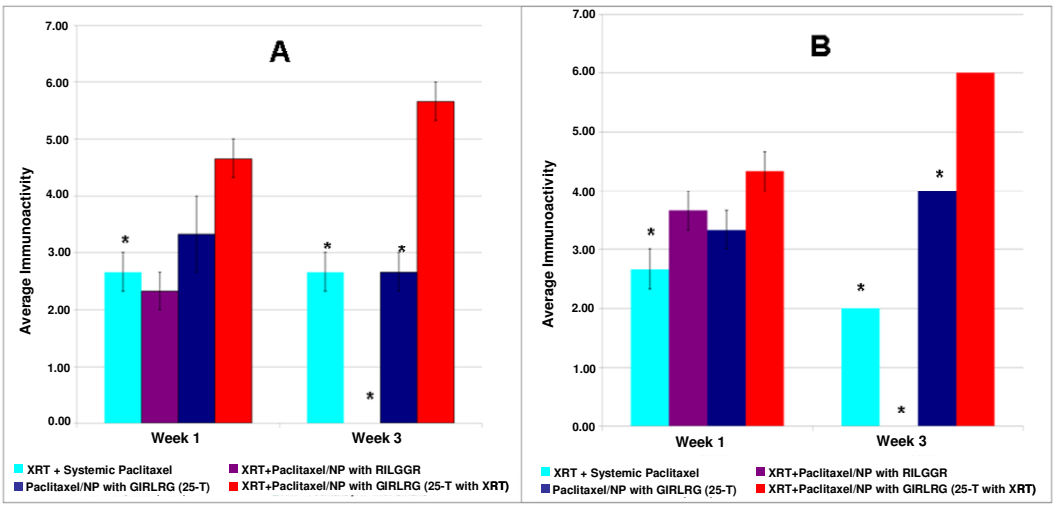


**Figure V-10.** Paclitaxel loaded AbBD-NP-GIRLRG, **25-T**, increases paclitaxel concentration and apoptosis in irradiated tumors. **(A)** Analysis of paclitaxel levels shows that the GIRLRG-targeted nanoparticle DDS increases paclitaxel concentration in irradiated breast cancers; **(B)** Relative levels of apoptosis in tumor sections removed at one week and three weeks post-treatment as determined by the Hallahan lab.[34]

nanoparticle group, **25-T**, with the use of irradiation over all other treatment groups at one and three weeks (Figure V-10A). Similarly, terminal deoxynucleotidyl transferase dUTP nick end labeling (TUNEL) staining of these tumor sections showed that at one and three weeks the **25-T** with XRT was superior to radiation and systemic paclitaxel treatment in maintaining persistent cytotoxicity, as evidenced by cell death (Figure V-10B). Staining for paclitaxel and apoptosis notably persisted for three weeks after only a single administration of **25-T** (with XRT) over the other control groups, indicating that **25-T** provides a prolonged and sustained release of paclitaxel to the XRT tumor. Additionally, TUNEL staining for apoptosis at both one and three weeks were greatly increased, which indicates that **25-T** with XRT was superior to radiation and systemic paclitaxel in maintaining persistent cytotoxicity (Figure V-10B). From this data, it can be

concluded that the taxol loaded AbBD-NP-GIRLRG system is effective in delivering a significant payload of paclitaxel to the irradiated tumor in a sustained manner.

The overall efficacy of the paclitaxel loaded GIRLRG-NP system, **25-T**, was assessed by determining the tumor volume tripling time in both human tumor cell lines and in syngeneic mouse tumors, which was performed in collaboration with the Hallahan and Diaz group. To carry out the experiments, MDA-MB-231 breast carcinomas were implanted in nude mice and GL261 gliomas in C57/B16 mice and a tumor growth delay study was performed after treating the mice as shown in Figure V-11 and Figure V-12. The results of the study showed that MDA-MB-231 tumor tripling time was prominently delayed for 55 days with the combination therapy of **25-T** and XRT, compared to 11-14 days observed from the three other XRT-treatment groups (Figure V-11). Control animals

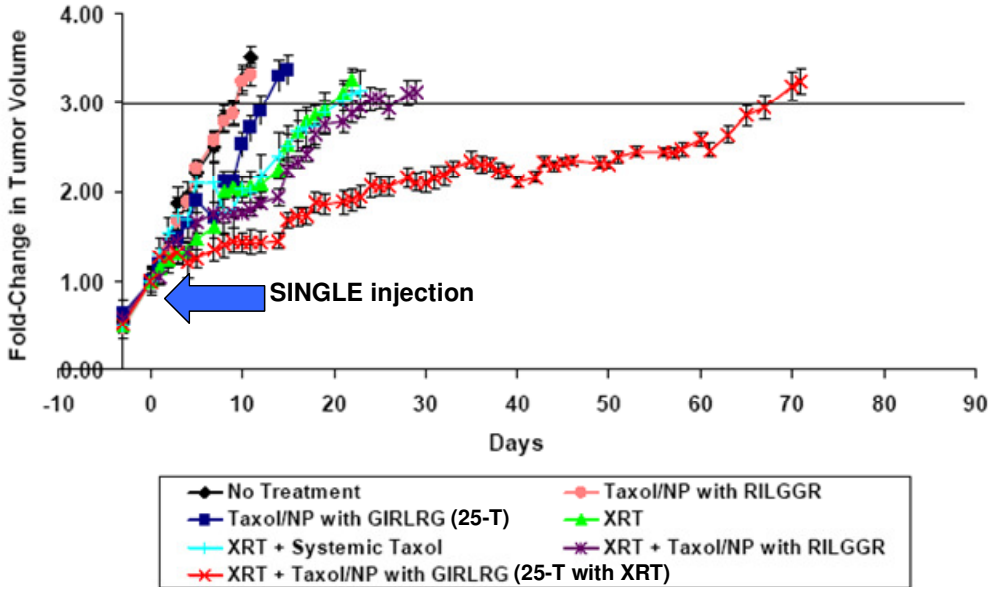


**Figure V-11.** GIRLRG-targeted nanoparticle DDS, **25-T**, causes significant tumor growth delay *in vivo* for MDA-MB-231 tumor model after only a single injection (10 mg paclitaxel/kg mouse).

that were not irradiated and received drug-loaded particles did not exhibit significant tumor growth delay when compared to the untreated control. Likewise, the administration of radiation with systemic paclitaxel or with untargeted nanoparticle (nanoparticle-RILGGR) provided no significant tumor growth delay when compared to radiation alone (Figure V-11). Similarly, in the GL261 group, tumor tripling time was significantly delayed by 12 days with **25-T** and XRT-treatment; however, all other treatment groups failed to significantly delay tumor tripling time compared to untreated controls (Figure V-12). Thus a single administration of **25-T** achieved tumor growth delay in irradiated tumors, which was significantly greater than conventional systemic chemotherapy and radiation. Undoubtedly, this novel nanoparticle drug delivery system promises future

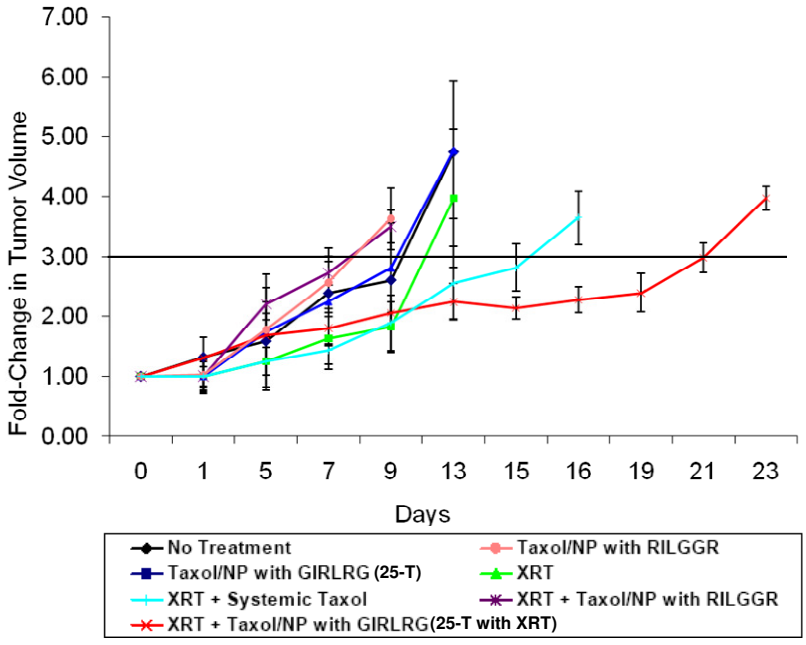


**Figure V-12.** Tumor growth delay study *in vivo* for the GL261 tumor model after a single injection (20 mg paclitaxel/kg mouse).

applications in the clinic as it encompasses the latest discovery in advanced developments in nanoparticle design with targeting to guarantee a high drug load and adjustable pharmacokinetic profiles.

**Nanoparticle Systems for the Treatment of Glaucoma**

The development of effective drug delivery systems that can transport and deliver a drug precisely and safely to its site of action is also becoming a highly important research area for ophthalmology. Recently, increased attention has been focused on improving ocular dosage forms and delivery systems for the treatment of glaucoma, a progressive optic neuropathy characterized by elevated intraocular pressure (IOP), which has become the second leading cause of irreversible blindness.[39] Conventional treatments of glaucoma have shown that the effectiveness of the therapy depends strongly on the delivery of therapeutic drug concentrations to the retina. However, currently existing therapies, such as topical eye drops and systemic therapy, achieve only low drug levels to the retina and the potential for systemic drug absorption and side effects are substantial.[40, 41] Clearly then, a new and promising ophthalmic drug delivery system for this anterior segmental disease is urgently needed. Therefore, several different delivery systems based on the **AB** nanoparticle that has the capability to incorporate ophthalmic therapeutics, such as brimonidine and bimatoprost, have been developed to provide a sustained release of drug to the retina for the treatment of glaucoma.

To gain insight into the extent of localization of the **AB** nanoparticles in the eye, dye was encapsulated within the particles to model and image the distribution of small drug molecules. Neuro-DiO, a hydrophobic green dye, was incorporated into 53 nm $\mathbf{AB_1}$

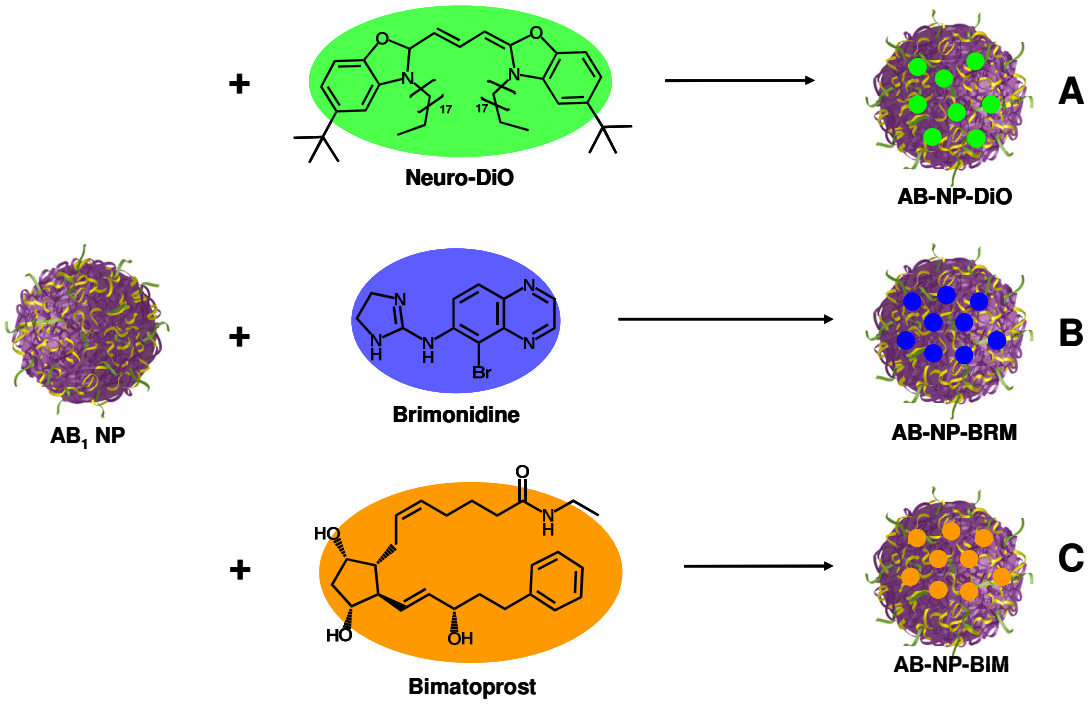


**Figure V-13.** Encapsulation of small hydrophobic molecules into $\mathbf{AB_1}$ nanoparticles for glaucoma therapy: **(A)** Neuro-DiO loaded $\mathbf{AB_1}$ nanoparticles, AB-NP-DiO, for localization studies; **(B)** Brimonidine loaded $\mathbf{AB_1}$ nanoparticles, AB-NP-BRM, for IOP lowering and neuroprotection; and **(C)** Bimatoprost loaded $\mathbf{AB_1}$ nanoparticles, AB-NP-BIM, for IOP lowering.

particles (Figure V-13) using the developed vitamin E TPGS formulation encapsulation method as established for the incorporation of small molecule drugs. By this methodology, it was possible to prepare Neuro-DiO loaded nanoparticles, AB-NP-DiO, with 10.6 wt% dye, when aiming for a 15 wt% loading. The distribution of AB-NP-DiO was investigated in collaboration with Dr. David Calkins' lab from the Vanderbilt Eye Institute at three different time points after posterior chamber injections (Figure V-14 and Figure V-15) (3, 7, and 14 days post injection) of the Neuro-DiO loaded nanoparticles in phosphate buffered saline (PBS) into the eyes of C57BL/6 mice. Once the injections were completed, the eyes were removed and dissected to study the distribution of the

therapeutic. A large amount of nanoparticles was evident in the vitreous humor of all eyes at all time points. The retinas were immunostained for retinal ganglion cells (RGC) using the marker estrogen related receptor beta (ERRβ) (red) to determine the

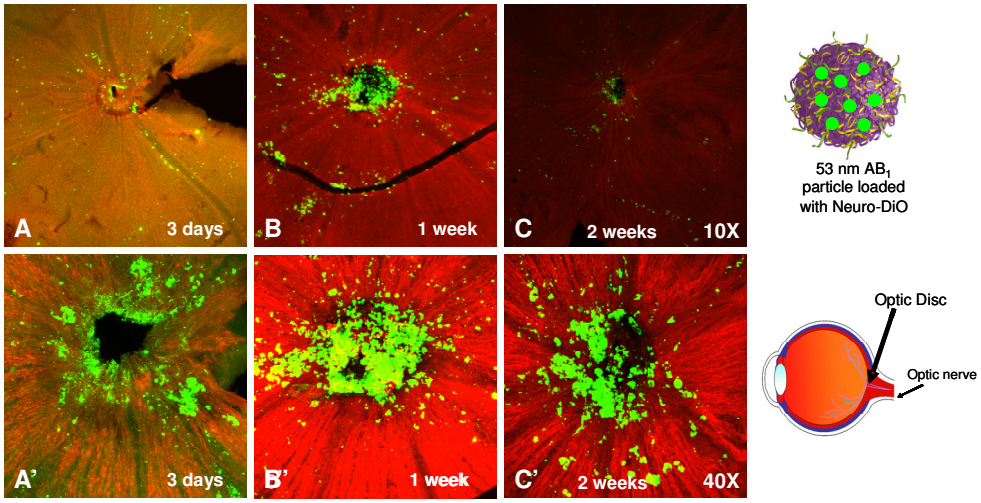


**Figure V-14.** *In vivo* studies: 1.5 µm confocal slices of Neuro-DiO loaded **$AB_1$** nanoparticles, AB-NP-DiO, delivered to the optic disc via intravitreal injection, imaged for Neuro-DiO (green) and ERRβ (red). **A**, **B**, and **C** show images at magnifications of 10X and **A'**, **B'**, and **C'** show the same images at higher magnification, 40X.

localization, as well as to rule out any toxic effects, of the nanoparticles. Examination of the optic disc under a confocal microscope showed high concentration of the nanoparticle at the time points of 3, 7, and 14 days (Figure V-14) at two different magnifications, 40X and 120X. Further investigations of flat-mounted retinas by confocal microscopy showed a fairly uniform distribution of the nanoparticles across the entire retina at all time points. Higher magnification exhibited that the RGC layer and optic fiber layer appeared normal with no obvious changes in density of cell bodies or axons (Figure V-14), indicating that the particles were not cytotoxic and did not bring about any retinal defects. After 3 days,

nanoparticles were evident from the surface of the inner retina, the interface between the retina and vitreous humor, to the outer retina. However, most of the nanoparticles in the retina were localized in the nerve fiber layer and RGC layer (Figure V-15). This

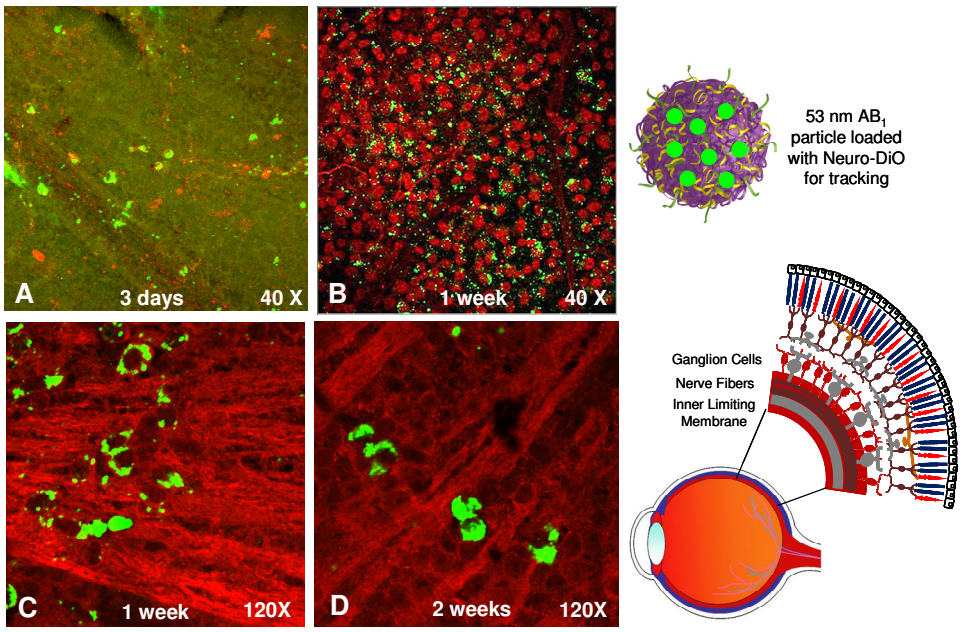


**Figure V-15.** *In vivo* studies: 1.5 µm confocal slices of Neuro-DiO loaded **$AB_1$** nanoparticles delivered to the retinal ganglion cells (RGCs), imaged for Neuro-DiO (green) and ERRβ (red) (images **A**, **B**, **C**, **D**). Images **C** and **D** show the uptake of the AB-NP-DiO into RGCs.

distribution indicates that the nanoparticles have successfully passed the inner limiting membrane, a barrier to many potential therapeutic compounds. The ability of the nanoparticles to pass through this membrane and to still be present after a period of weeks makes them a promising vehicle for drug delivery to the retina.

In conjunction with the localization studies of the Neuro DiO loaded particles, the Calkins' lab examined the area of the retina covered by DiO released nanoparticle as a function of time after the injection. Deposition of DiO was defined very conservatively, as the portion of the retina that contained DiO signal intensity of 100% contrast relative

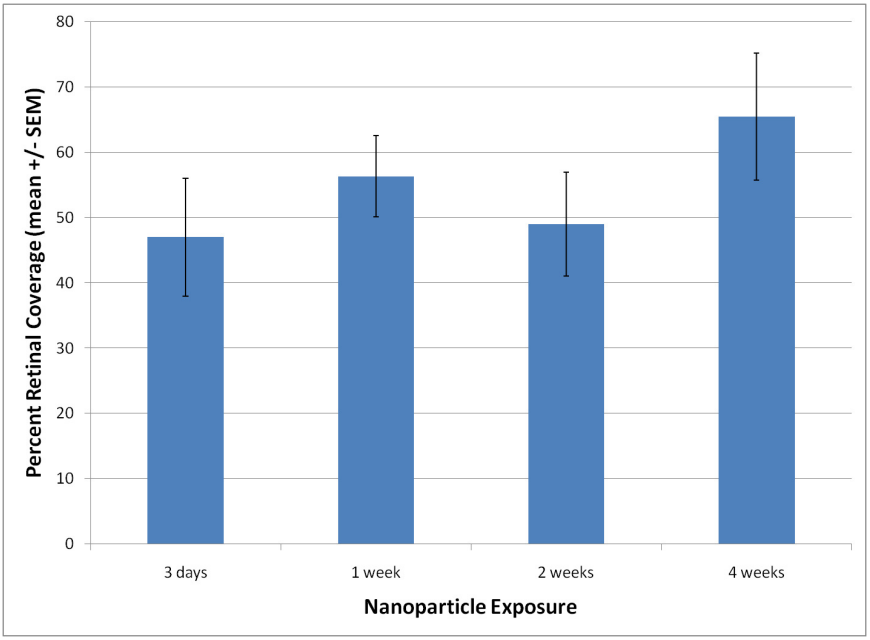


**Figure V-16.** Deposition of DiO on the retinal surface over time after a single injection of AB-NP-DiO.

to background. The area of the retina represented by DiO label was compared to the total surface area of the retina. Retinas were examined at 3 days, 1 week, 2 weeks, and 4 weeks post-nanoparticle injection. It was found that over a 4 week period, DiO deposition appeared to increase on the retinal surface by about 15% compared to the initial measurement. During this period, deposition was statistically constant in contrast to the initial measurement as well (Figure V-16). This implies that retinal uptake of the DiO is fairly consistent and matches its slow release from the nanoparticle complex. Therefore, it can be concluded that retinal exposure to a released drug would be constant in between nanoparticle injections.

Following the successful distribution and circulation studies, the next step was to initiate the investigation of the delivery of ocular therapeutics, more specifically brimonidine, encapsulated within the nanoparticle to test its efficacy on decreasing IOP in

Dr. Calkins' C57BL/6 mice model of glaucoma. Therefore, brimonidine, an $\alpha_2$-adrenoreceptor agonist that lowers intraocular pressure by reducing aqueous humor production and by increasing aqueous uveoscleral outflows,[42] was incorporated into 53 nm **$AB_1$** particles using the aforementioned vitamin E TPGS formulation encapsulation method (Figure V-13). Using this formulation technique, it was possible to prepare brimonidine loaded nanoparticles, AB-NP-BRM, with 3.3 wt% of brimonidine, when aiming for a 15 wt% loading, as determined by NanoDrop™ UV-Vis at 389 nm. To study the efficacy of AB-NP-BRM *in vivo*, IOP measurement experiments were performed in collaboration with Dr. Calkins' lab using C57BL/6 mice. Both eyes of two C57BL/6 mice had elevated IOP via the Microbead Occlusion Model, which was developed in the Calkins lab.[43] The IOP of all eyes was measured using a portable tonometer prior to IOP elevation to determine baseline IOP, and prior to particle injection treatment to

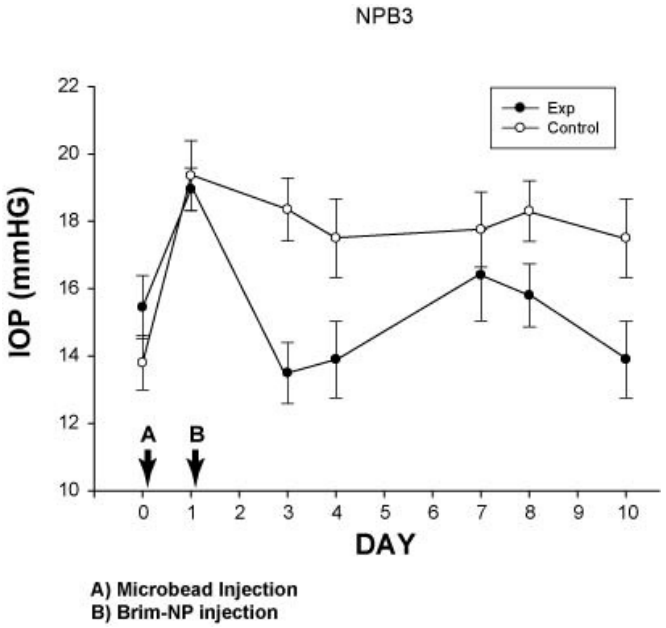


**Figure V-17.** Treatment with AB-NP-BRM delivered via intravitreal injection lowered IOP to normal levels 1 day later. IOP remained at or below baseline levels for 6 days before slowly returning to elevated levels.

demonstrate elevated IOP. Following IOP elevation, the mice were treated with a single intravitreal injection of brimonidine loaded particles into one eye and PBS in the other, to serve as a control.

A reduction of IOP to baseline levels was apparent the following day for the particle treated eye whereas the control eye still remained elevated. Over the course of 10 days, the IOP of the nanoparticle treated eyes remained significantly lower near or at baseline levels. From these results (Figure V-17), it was evident that AB-NP-BRM can successfully reduce and maintain IOP. Therefore, it can be concluded that the particles provide a controlled release of brimonidine to lower the intraocular pressure over the duration of the *in vivo* study.

With intravitreal injections, it was shown that the AB-NP-BRM provided a short duration of IOP lowering which can be due to the fact that the particles are capable of moving towards the optic disc out the optic nerve, as was seen with the AB-NP-DiO distribution studies. Therefore, administering the drug loaded nanoparticles intravitreally does not fully capitalize on the particles' slow sustained release of the therapeutic, which was previously shown through the drug release studies using a particle of comparable cross-linking density and size (Figure V-6a). The administration of nanoparticles,[44] microparticles[39, 45] and liposomes[46] by the subconjunctival route, which has been thoroughly investigated, however, has been shown to provide a more effective therapy by sustaining retinal drug delivery[45] and prolonging the lifetime of the delivery system within the eye.[39, 46] Therefore, to enhance the **AB** particle's lifetime and retention within the eye, subconjunctival injections will be investigated in the near future.

In addition to encapsulating brimonidine, bimatoprost, a hydrophobic prostaglandin analog that lowers IOP by increasing the outflow of aqueous fluid from the eyes, was loaded into 53 nm **$AB_1$** particles using the vitamin E TPGS formulation technique (Figure V-13). With the formulation method, bimatoprost was encapsulated into the nano-network of the particles to incorporate 16.4 wt% bimatoprost, while striving for a 30 wt% drug load, as determined by NanoDrop$^{TM}$ UV-Vis at 262 nm. By achieving a higher drug loading, owing to the increased hydophobicity of the therapeutic, it is postulated that the AB-NP-BIM will have a more prolonged lowering of the IOP. To study the efficacy of AB-NP-BIM, *in vivo* IOP measurement experiments will be performed in collaboration with Dr. Calkins' lab. Further experiments will also be conducted to enhance the encapsulation and release of therapeutic by tailoring the particle's size and cross-linking density to optimize the therapeutic dosage for the effective treatment of glaucoma.

**Encapsulation of Peptides**

Significant challenges also remain in the delivery of biological therapeutics. In many instances, peptides and proteins in circulation are rapidly cleared enzymatically by specific recognition or through renal filtration and, therefore, necessitates frequent administration by injection.[47, 48] Nanoparticle and microparticle formulations, however, have attracted considerable interest for the development of optimal vectors for improving the stability of peptides against degradation, and thereby reducing dosing frequency and increasing patient compliance.[49] Entrapment of peptides has been achieved by adsorbing them onto preformed nanoparticles.[50] However, surface adsorbed peptides are not

physically protected from proteolytic enzymes and, hence, are more likely to be degraded than encapsulated peptides.[51] While there have been various advances in this technology, there are only a few products that have received regulatory approval and, therefore, there still remains a need for efficient systems.[48] As a result, two methods for the preparation of peptide loaded particles have been developed, which entail either peptide encapsulation after particle formation using the epoxide-amine cross-linked particles and the vitamin E TPGS formulation technique or peptide encapsulation during particle

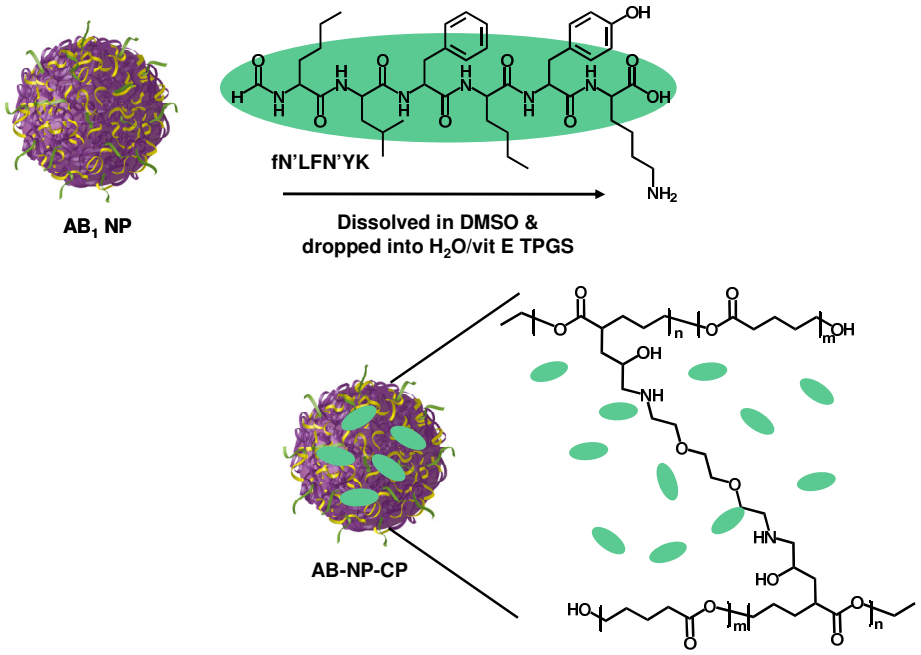


**Scheme V-3.** Encapsulation of fN'LFN'YK chemoattractant peptide (CP) into $\mathbf{AB_1}$ nanoparticles using the vitamin E TPGS formulation technique to give peptide loaded nanoparticles, AB-NP-CP

formation employing the ambient alkyne-azide cross-linking.

The ability to efficiently encapsulate hydrophobic peptides into the nanoparticles has been achieved using the aforementioned vitamin E TPGS formulation technique with epoxide-amine cross-linked $\mathbf{AB_1}$ particles. To conduct the encapsulation, a model

peptide, fN'LFN'YK, a chemotactic agent that is known to induce dendritic cell migration for vaccine therapy,[52] was chosen due to its hydrophobicity and low molecular weight. Subsequent to forming a 50 nm $\mathbf{AB_1}$ nanoparticle, the peptide was effectively encapsulated into the particles' nano-network using the formulation process (Scheme V-3) to achieve a loading of 16.3 wt%, when aiming for a 20 wt% payload, as determined by NanoDrop™ UV-Vis at 280 nm. Future investigations with these peptide loaded particles, AB-NP-CP, will include release studies and *in vitro* experiments for potential application as a sustained release system in vaccine therapy.

While the method for peptide encapsulation after particle formation was found to

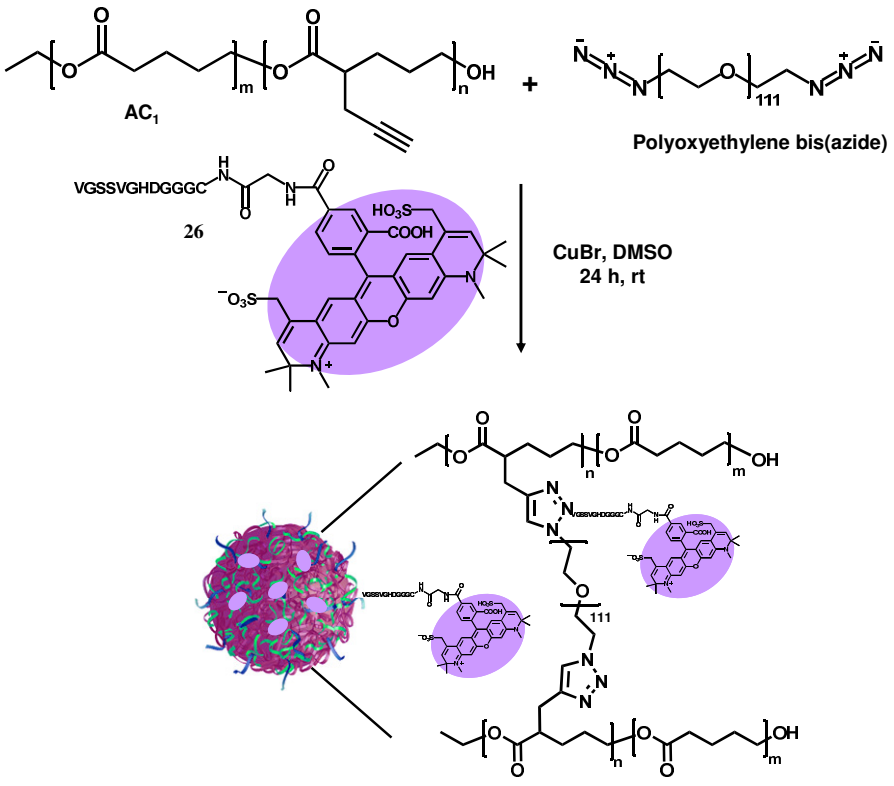


**Scheme V-4.** Encapsulation of Alexa Fluor® labeled GCGGDHGVSSGV, AF-GCGGDHGVSSGV, during particle formation using alkyne-azide cross-linking with linear polymer $\mathbf{AC_1}$ and polyoxyethylene bis(azide).

be advantageous for small hydrophobic peptides, an alternative technique was required for the incorporation of hydrophilic peptides as there was a risk for peptide loss into the aqueous phase during the vitamine E TPGS formulation process. Therefore, for the encapsulation of larger hydrophilic peptides, the alkyne-azide cross-linking was employed using the ambient reaction conditions as previously described in Chapter III, so that the peptides are encapsulated during particle formation. Prior to encapsulation, the N-terminus of a model hydrophilic peptide, GCGGGDHGVSSGV, was labeled with Alexa Fluor® 594 NHS ester to allow for quantification after incorporation. Upon purification of the Alexa Fluor® labeled peptide, AF-GCGGDHGVSSGV, the alkyne-azide cross-linking was conducted at room temperature by coupling linear polymer $\mathbf{AC_2}$, which had 12% alkyne incorporated in the polymer backbone, with 1.5 equivalencies of polyoxyethylene bis(azide), with a molecular weight of 5000 Da, in the presence of the dye labeled peptide in DMSO with copper(I) bromide as the catalyst (Scheme V-4). Polyoxyethylene bis(azide) was specifically chosen as the cross-linker for the encapsulation in order to obtain larger particles with wider network architecture for the loading of higher molecular weight therapeutics. Following encapsulation, the peptide loaded particles were thoroughly purified by dialysis to remove any free peptide, polymer, and bisazide. Using NanoDrop$^{TM}$ UV-Vis at 601 nm, it was found that the ambient cross-linking conditions allowed for the incorporation of 1 wt%, 5 wt% and 8 wt% of peptide into the particles, when striving for a 5 wt%, 10 wt% and 15 wt% peptide loading respectively.

The influence of peptide encapsulation during nanoparticle formation on the shape and size of the particles was investigated using TEM and dynamic light scattering

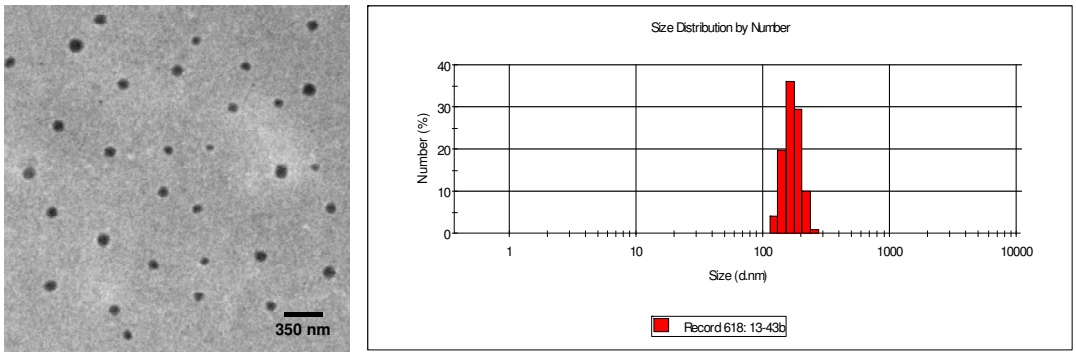


**Figure V-18.** TEM and DLS analysis of $\mathbf{AC_2}$ nanoparticles with 8 wt% AF-GCGGDHGVSSGV encapsulated during particle formation.

(DLS). From both TEM and DLS analysis, it was evident that the encapsulation was successful in forming well-defined monodispersed particles with a diameter of 160 nm (Figure V-18). While further studies will be required to determine the maximum peptide loading and the release profile of the peptide from the particle, these preliminary results show that the mild conditions of the alkyne-azide cross-linking, in the presence of hydrophilic peptide, can be successfully employed to encapsulate the peptide to afford spherical well-defined peptide-loaded particles.

**Nanovector for the Encapsulation of siRNA**

In addition to peptidic therapeutics, there is currently enormous interest in the use of small interfering ribonucleic acids (siRNA) as therapeutic agents. By introducing siRNA, specific genes can be silenced, resulting in either decreased translational product of the silenced gene, or increased protein levels of a gene that is downregulated by the silenced sequence, which has emerged as a promising approach for the treatment of diseases, such as cancer[53, 54] and age-related macular degeneration (AMD).[55, 56] However,

the successful *in vivo* delivery of siRNA has been a challenge due to the instability of siRNA in blood, its poor cellular uptake, and its insufficient tissue bioavailability. As a result of these limitations, the native delivery of siRNA is not effective.[57, 58] To overcome these challenges, the siRNA can be chemically modified. However, these modifications can cause decreased messenger RNA (mRNA) hybridization, higher cytotoxicity, and increased unspecific effects.[59] Systemic administration of gene silencing therapy has been so far limited by the inexistence of adequate carrier systems. Therefore, with the presented novel nanoparticle technology, a completely water soluble system has been developed for the future encapsulation and delivery of siRNA.

The progression of loading siRNA into the nanoparticles began with preparing $\mathbf{AB_1}$ particles formed by coupling linear polymer $\mathbf{AB_1}$ with Jeffamine® D-4000. By using 0.25 equivalents of amine per epoxide in the linear polymer, 240.8 nm particles were obtained with wider cross-links, due to the long pegylated Jeffamine®, specifically for the encapsulation of the siRNA. As a model system, a siRNA known to silence green fluorescent protein (GFP), GFP siRNA was employed, as part of a collaboration with Dr. Andries Zijlstra in the Department of Pathology and Cancer Biology at Vanderbilt University. Using the vitamin E TPGS formulation technique that was established for the encapsulation of small drug molecules, the GFP siRNA was incorporated into the nanoparticles. However, with this method a low siRNA loading was achieved, 1.7 wt% as determined by NanoDrop™, and the siRNA could only be partially enveloped within the particle due its large size. In addition to these disadvantages, the encapsulation product was not thoroughly washed with water, as had been completed with the small drug and peptide encapsulations, since this would have led to the possible release of the siRNA

from the nanoparticle. While the formulation methodology has been shown to be efficient in encapsulating hydrophobic therapeutics, it was apparent that a different technique was required for the efficient encapsulation of the hydrophilic siRNA into the particles to achieve a high therapeutic loading.

Due to the hydrophilic nature of siRNA and its sensitivity to organic solvents, it was determined that the siRNA should be incorporated during particle formation using mild aqueous conditions, which would be compatible for the siRNA. For the encapsulation during particle formation, the thiol-ene click cross-linking would be utilized at a slightly elevated temperature, as it has been shown in the literature to proceed efficiently in water.[60] To be able to conduct the cross-linking with aqueous conditions, a linear polymer precursor modified to be water soluble was required since the previously synthesized polyesters were completely water insoluble. Therefore, poly(vl-avl), **Ab**, the polymer employed for thiol-ene cross-linking, would be made water soluble by incorporating a water-soluble ligand. One such important ligand that is known to be biologically safe and has been used for drug delivery is poly(ethylene glycol) (PEG). To enhance the water solubility of **Ab**, PEG would be grafted onto the linear polymer using a thiol-functionalized PEG which would be coupled to the free allyl groups on the polymer using thiol-ene chemistry.

In order to attach the thiol-PEG, polymer **Ab**, with a high content of allyl groups, 40%, was synthesized to provide an adequate number of allyl groups for PEG conjugation and for cross-linking after achieving water solubilization. Upon polymerization of **Ab**, the polymer was primed for PEG conjugation. The PEG ligands chosen initially for attachment were 2-(2-methoxyethoxy)ethanethiol ($PEG_2$) and O-(2-mercaptoethyl)-O'-methyl-hexa(ethyleneglycol) ($PEG_6$). Attachment strategies were aimed at coupling a 50/50 mixture of $PEG_2$ and $PEG_6$ with approximately 25% of the allyl groups on **Ab** using thiol-ene click chemistry in dimethylformamide at 40 °C for 72 h. However, these experiments were unsuccessful in grafting on the desired amount of PEG. According to $^1$H NMR, only 8% of the allyl groups had been efficiently conjugated with $PEG_2$ and $PEG_6$ as determined by quantifying the reduction of the polymer's allyl protons. Therefore, to improve the efficiency of the PEG attachment,

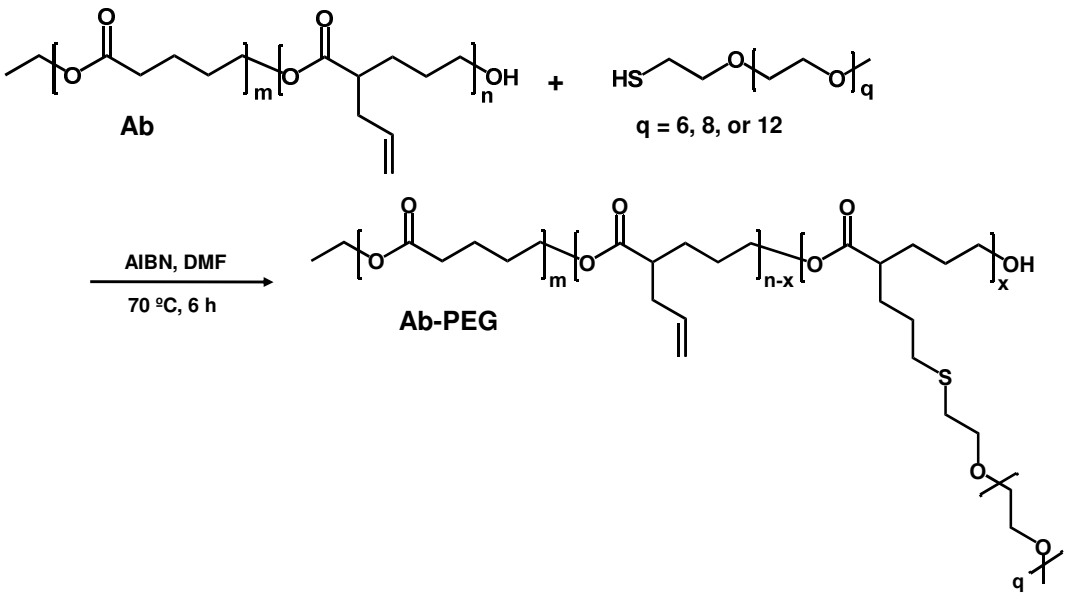


**Scheme V-5.** Attachment of thiol-functionalized polyethylene glycol (PEG) to linear polymer **Ab** using thiol-ene chemistry with azobisisobutyronitrile (AIBN).

azobisisobutyronitrile (AIBN), a known thermal radical initiator used for thiol-ene chemistry,[61] and an elevated temperature of 70 °C were employed (Scheme V-5). By introducing a small amount of AIBN and increasing the temperature of the reaction, the grafting of $PEG_2$ and $PEG_6$ onto the linear polymer increased to 20% and the duration of the reaction was decreased from 72 h to 6 h. While these conditions were effective in providing the increased attachment of PEG, they were not sufficient in imparting the desired polymer water solubility. Consequently, instead of attaching 50/50 $PEG_2$ and $PEG_6$, the next step was to only couple $PEG_6$ to the polymer, thus eliminating the use of $PEG_2$ since it was found that $PEG_2$ could not attribute to the polymer's water solubility. However, coupling $PEG_6$ alone to the linear polymer in varying amounts, from 15 to 30%, was still not adequate in providing a water soluble polymer.

Increasing the length of the PEG from 6 ethylene glycol units ($PEG_6$) to 8 or 12 ethylene glycol units, $PEG_8$ or $PEG_{12}$ respectively, for conjugation was the next strategy employed to enhance the polymer's water solubility. Using the optimized conditions with AIBN at 70°C, $PEG_8$ and $PEG_{12}$ were grafted individually onto **Ab** with 57% allyl groups incorporated into the polymer backbone. However, despite the increased percent of allyl groups in the polymer, only a 9% attachment of $PEG_8$ was achieved when aiming for 40% conjugation and the water solubility of the polymer showed no enhancement. Employing $PEG_{12}$ also showed similar results. An attachment of only 11% of $PEG_{12}$ was obtained when striving for 40% and once more there was no improvement in the polymer's solubility. From these experiments, it was evident that as the length of the PEG increased, the amount of attached PEG decreased due to steric hinderance, thereby inhibiting the improvement of the polymer's water solubility.

As an alternative approach to grafting PEG onto the polymer precursor, the water soluble monomer, glycidol, was incorporated into the polymer during polymerization to impart water solubility and to enhance the degradation of the system for future siRNA delivery. With traditional polyester nanoparticle systems, the rate of siRNA release and subsequent gene knockdown are often too slow and not tuned to generate an optimal response.[62] By incorporating glycidol, the degradation rate of the polymer can be tuned as has been shown in the literature.[63] Glycidol's polar hydroxyl groups result in the favorable adsorption and penetration of water which accelerate the degradation of the polymer,[64] and then would release the siRNA more quickly.

To integrate glycidol into the polyesters, a model ring-opening polymerization was conducted first with 10% δ-valerolactone and 90% glycidol in the presence of tin 2-ethylhexanoate ($Sn(Oct)_2$), the catalyst, and ethanol, the initiator, to ensure successful polymerization. According to $^1H$ NMR, the polymerization effectively resulted in the incorporation of 8% δ-valerolactone and 92% glycidol to form poly(vl-gl), **AG**. Moreover, this ratio of δ-valerolactone to glycidol led to the formation of a completely

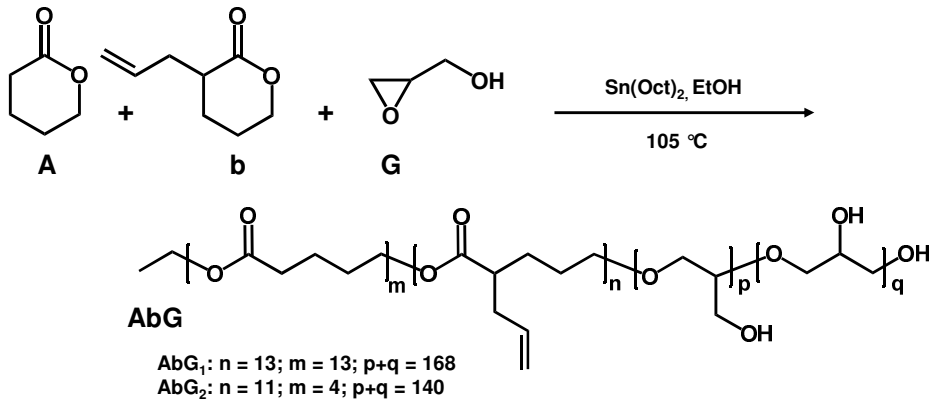


**Scheme V-6.** Ring-opening polymerization of δ-valerolactone (A) with α-allyl-δ-valerolactone (b) and glycidol (G) to form poly(vl-avl-gl), **AbG**.

water soluble polymer. Based on these results, subsequent polymerizations were carried out using similar reaction conditions to polymerize glycidol (G) with not only δ-valerolactone (A), but also with α-allyl-δ-valerolactone (b) (Scheme V-6), in order to incorporate allyl functionalities for future particle formation and siRNA encapsulation using the thiol-ene cross-linking. **AbG** copolymers with 10/10/80 vl/avl/gl (**$AbG_1$**) and 3/7/90 vl/avl/gl (**$AbG_2$**) were synthesized and found to be water soluble. Decreasing the amount of glycidol below 80%, however, lowers the water solubility of the polymer. Detailed characterization of the glycidol copolymers by $^1$H NMR showed that each of the monomers was successfully incorporated at the desired ratios. Analysis by $^{13}$C NMR not only confirmed the integration of the monomers, but also revealed the production of both linear and branched architectures as evidenced by the peaks at 80.1 and 81.5 ppm due to the branched and linear analogs respectively, as has been demonstrated in the literature.[65-67] However, the product only includes approximately 30% branched polymer as determined by $^{13}$C NMR with inverse gated decoupling.

As the next step toward particle formation, model reactions were carried out with polymer **$AbG_1$** and thioglycolic acid to investigate the reactivity of the thiol-ene coupling in water. A set of four experiments was conducted in which thiolglycolic acid was reacted with **$AbG_1$** in water for 0, 3, 6, or 12 h at 37 °C. Using $^1$H NMR, each of the crude products was analyzed to determine the extent of thioglycolic acid attachment through the reduction of the allyl protons of the polymer at 5.77 and 5.02 ppm. As the reaction time progressed from 0 to 12 h, there was a significant reduction in the intensity of the polymer's allyl protons (Figure V-19). After 12 h, approximately 70% of the allyl groups were conjugated with thioglycolic acid. From these results, it can be concluded

that the thiol-ene coupling reaction can be effectively performed under mild aqueous conditions.

With the successful attachment of thioglycolic acid to the linear polymer, the allyl functionalized polymer **AbG$_1$** precursors were then cross-linked with a dithiol, 3,6-dioxa-1,8-octanedithiol, to test the ability to prepare nanoparticles in mild aqueous conditions. For the cross-linking reaction, **AbG$_1$**, dissolved in $H_2O$, was treated with 2 equivalents of thiol per pendant allyl in the polymer in a one-pot reaction (Figure V-20) at 37 °C for 12 h and subsequently dialyzed in $H_2O/CH_3OH$ to remove unreacted starting materials.

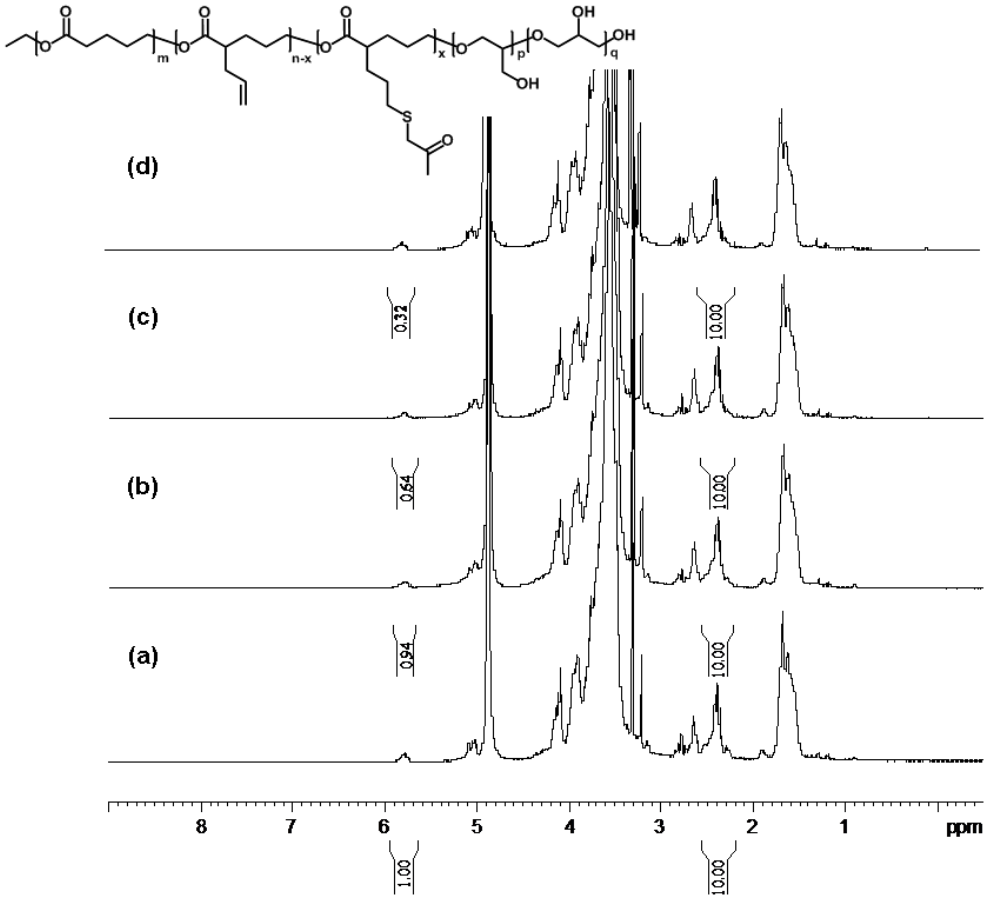


**Figure V-19.** $^1$H NMR spectra overlay for the thiol-ene coupling reaction between polymer **AbG$_1$** with thioglycolic acid: **(a)** 0 h, **(b)** 3 h, **(c)** 6 h, and **(d)** 12 h time point.

During the course of the experiment, the reaction mixture became cloudy, which may be evident of particle formation.

As observed by TEM, the thiol-ene cross-linking reaction was successful in forming small quantities of well-defined spherical nanoparticles (Figure V-20) with a size of 105.3 ± 10.2 nm. Further characterization by $^{1}$H NMR confirmed the formation of particles as evidenced by the significant reduction of the allyl peaks at 5.06 and 5.77 ppm. From these preliminary results, it can be concluded that the thiol-ene cross-linking occurred under mild aqueous conditions to form distinct particles, which was not inhibited by the presence of branched polymer. Further research will be conducted with the **AbG** polymers to optimize the conditions for thiol-ene cross-linking in water to

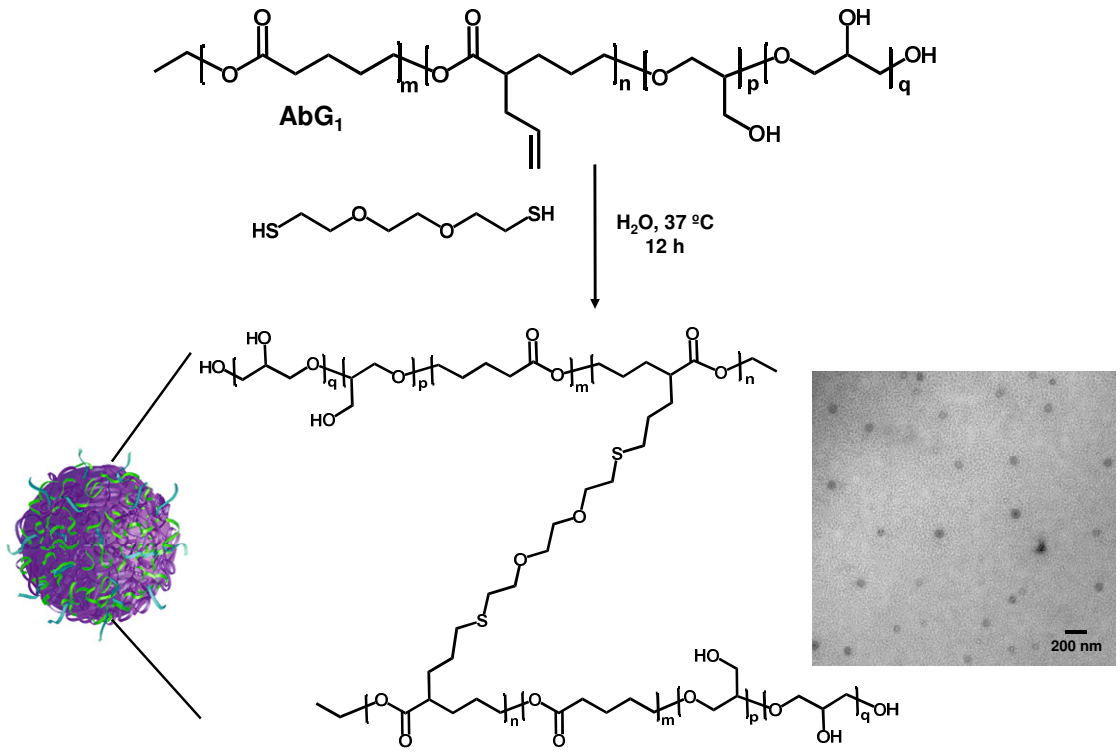


**Figure V-20.** Nanoparticle formation using thiol-ene click cross-linking in water with **AbG$_1$** and 3,6-dioxa-1,8-octanedithiol. TEM image of **AbG$_1$** particles, 105 nm, prepared with 2 equivalents of thiol.

increase the nanoparticle yield and prepare well-defined particles of different sizes for the future incorporation of siRNA.

## Conclusion

In summary, it has been demonstrated that the previously described intermolecular cross-linking technique leading to supramolecular 3D nano-networks provided the basis for the preparation of targeted and sustained delivery systems. It was found that small drug molecules can be incorporated after nanoparticle formation, with and without targeting units attached, and a higher efficacy in drug loading was achieved than reported for traditional polyester particle systems. Furthermore, an applied emulsification approach during drug loading could prolong the linear degradation rate and resulted in the water-dispersion of the final targeted drug delivery systems with paclitaxel incorporated. The particle sizes did not change significantly upon drug loading, which can contribute to the stable, cross-linked supramolecular structure of the 3-D nano-networks. Based on the versatility of nanoparticle formation and adjustment of cross-linking density in achieving different degradation profiles, the technique provides a means to adjust the linear release profiles of the drug delivery systems to the physiological demands *in vivo*. The observed linear release kinetics of paclitaxel without a 'burst-effect' is another indication that the developed techniques for nanoparticle formation, encapsulation and post-modification will provide effective targeted delivery systems with predictable pharmacokinetic profiles.

With the aforementioned conjugation chemistries, described in Chapter IV, and established drug encapsulation technique, a novel nanoparticle drug delivery system

(DDS) has been developed to enable specific targeting to the tumor site and allow for the controlled, linear release of therapeutic. After conjugating the controllable, sustained drug release of the **AB** nanoparticles with a GIRLRG targeting peptide, the paclitaxel loaded particles specifically targeted chemotherapeutics directly to x-ray treated tumors causing significant tumor growth delay. The targeted nanoparticle DDS has shown a significant increase in the efficacy of cancer treatment over current clinical models and, with further investigation, we anticipate to implement this system into clinical trials.

With a growing ageing population, the development of effective drug delivery systems for the treatment of glaucoma has also received increasing attention. Therefore, several different delivery systems based on the **AB** nanoparticle that incorporate ophthalmic therapeutics, such as brimonidine and bimatoprost, have been developed to provide a sustained release of drug to the retina for the treatment of glaucoma. From *in vivo* distribution studies, it was concluded that the nanoparticles, loaded with Neuro-DiO, successfully reached the retina and could pass through the inner limiting membrane to the nerve fiber and RGC layer, which are sites of treatment for several retinal diseases, such as glaucoma. Preliminary studies have shown the success of the brimonidine loaded nanoparticles to reduce and maintain IOP. With these results, further experiments will be conducted to investigate posterior and subconjunctival injections of the particle drug delivery system with different therapeutics and drug loadings to determine the most effective and least invasive treatment.

In addition to the delivery of small molecules, significant attention has been focused on the delivery of macromolecular therapeutics, such as peptides and siRNA. For the encapsulation of peptides, several systems have been successfully developed which

entail either peptide encapsulation after particle formation using the epoxide-amine cross-linked particles and the vitamin E TPGS formulation technique or peptide encapsulation during particle formation employing the ambient alkyne-azide cross-linking. To incorporate siRNA into the nanoparticles, a water soluble polymer was developed which incorporated glycidol with α-allyl-δ-valerolactone and δ-valerolactone. With the polymer's pendant allyl groups, thiol-ene cross-linking was preformed, with 3,6-dioxa-1,8-octanedithiol as the cross-linker, under mild aqueous conditions to form well-defined spherical particles. The ability to form nanoparticles using aqueous reaction conditions will greatly aid in the future incorporation and delivery of siRNA.

## Experimental

**Characterization.** $^1$H NMR spectra were obtained from a Bruker DPX-300 or a Bruker AV-II 600 MHz Fourier Transform Spectrometer, with $CDCl_3$/TMS or DMSO-$d_6$ as the NMR solvent. Reverse-phase high-performance liquid chromatography (RP-HPLC) was carried out with a Waters HPLC using two Delta-Pak™ PrepLC™ 25 mm Columns (Waters, C18, 300 Å , 25 x 100 mm each) with a PrepLC™ 25 mm Radial Compression Module. The products were eluted using a solvent gradient (solvent A = 0.05% trifluoroacetic acid (TFA)/ $H_2O$; solvent B = 0.05% TFA/ $CH_3CN$). Accurate molecular mass and purity of the peptides were determined by MALDI-MS, with α-cyano-4-hydroxycinnamic acid as the matrix, on a Perspective Biosystems Voyager-DE STR (Framingham, MA) equipped with delayed extraction technology operating in reflector mode. For dynamic light scattering (DLS), a Malvern Nano ZS system by Malvern Instruments (Malvern Zetasizer Nanoseries, Malvern, UK) was employed at a fixed angle

of 90º at 25 ºC, taking the average of three measurements. The particles were diluted with toluene to a concentration which gave the desired number of counts in order to obtain a good signal-to-noise ratio. Static light scattering was also performed on the Malvern Nano ZS to obtain the absolute weight average molecular weights of the nanoparticles. Different sample concentrations (0.5-1.2 mg/mL) were prepared by dilution of a high concentration stock solution in toluene (3 mg/mL) to obtain the weight average molecular weight. Samples for transmission electron microscopy (TEM) imaging were prepared by dispersing 0.5 mg nanoparticles in 1 mL Lonza cell culture water. The samples were sonicated for 5 min and were stained with 6 drops of 3% phosphotungstic acid. The carbon grids were prepared by slowly dipping an Ultrathin Carbon Type-A 400 Mesh Copper Grid (Ted Pella, Inc., Redding, CA) into the particle solutions three times and drying the grid at ambient temperature. A Philips CM20 transmission electron microscope operating at 200 kV in bright-field mode was used to obtain TEM micrographs of the polymeric nanoparticles. Samples were centrifuged at 8000 rpm on a GS-15 Centrifuge from Beckman (Brea, CA). UV-Vis measurements were made via a Thermo Scientific NanoDrop$^{TM}$ 1000 spectrophotometer (Wilmington, DE).

**Materials.** All reagents and solvents were purchased from commercial sources and used as received, unless otherwise stated. Spectra/Por® Dialysis membrane and SnakeSkin® Pleated Dialysis Tubing, regenerated cellulose, were obtained from Spectrum Laboratories Inc. (Rancho Dominguez, CA) and Pierce Biotechnology (Thermo Fisher Scientific, Rockford, IL), respectively. Fmoc protected amino acids were obtained from Advanced ChemTech (Louisville, KY). Analytical TLC was performed on commercial

Merck plates coated with silica gel 60 $F_{254}$. Silica gel for column chromatography was Sorben Technologies 60 Å (40-63 μm, technical grade). GCGGGNHVGGSSV (HVGGSSV) peptide was synthesized as previously described in Chapter II. Monomers α-allyl-δ-valerolactone, and 2-oxepane-1,5-dione, and linear polymer **AbBD** were also synthesized as reported in Chapter II. **AbBD** nanoparticles were prepared as described in Chapter IV.

***In vitro* $AB_1$ nanoparticle degradation studies.** $AB_1$ nanoparticles (10 mg) were suspended in 2 mL Phosphate Buffered Saline (PBS) (pH 7.4) in 1 dram vials equipped with stir bars. The vials were sealed to avoid evaporation and the samples were maintained at 37 °C under continuous stirring. At 48 h intervals, samples were removed and dichloromethane was added (3 x 4 mL) to extract remaining nanoparticles. The extraction solutions were concentrated via rotary evaporator and dried *in vacuo*. The degradation of the nanoparticles was monitored by the change in molecular weight, as determined by SLS, with incubation time.

**Alexa Fluor® 594 conjugated $AB_1$ nanoparticles (22).** To a solution of $AB_1$ nanoparticles (0.030 g) in anhydrous dimethylsulfoxide (0.5 mL), NHS Alexa Fluor® 594 (0.25 mL of 10 mg/mL NHS Alexa Fluor® 594 in DMF, 3.0 μmol) was added. The reaction mixture stirred for 24 h at room temperature. Residual NHS Alexa Fluor® 594 was removed by dialyzing with SnakeSkin® Pleated Dialysis Tubing (MWCO = 10,000) against $CH_3OH$ to obtain **22** (15.2 mg). $^1H$ NMR (300 MHz, $CD_3OD$): δ The significant

change is the appearance of the following peaks due to Alexa Fluor® 594: 7.14-7.20, 6.78, 5.48, 4.48, 3.62, 3.43, and 1.24 ppm.

**Cell Culture and Alexa Fluor 594®-$AB_1$ Cell Uptake by Confocal Microscopy.** NIH H460 human lung cancer cells (ATCC HTB-177, American Type Culture Collection) were grown in Roswell Park Memorial Institute 1640 media (RPMI-1640, GIBCO) supplemented with 10% fetal bovine serum (ATCC) and 1% antibiotic-antimytotic (Invitrogen, 15240) at 37 °C with 5% $CO_2$ in a 95% humidity incubator. Confocal microscopy was performed using an Olympus FV-1000 inverted confocal microscope equipped with an argon laser, a 543 nm HeNe laser, a SPlan-UApo 20x/0.80, a Plan-Neofluor 40x/1.3 oil lens, and a SPlan-UApo 100x /1.40 oil lens. Samples were analyzed using two channel confocal laser scanning microscopy to obtain a DIC image and an Alexa Fluor® 594 image. The H460 cells were plated on uncoated, 14 mm diameter Microwell, No. 1.5 MatTek dishes at a density of 2.5 x $10^6$ cells per well in medium. On the day of experiments, cells were washed with pre-warmed Hank's buffered saline solution (HBSS) with $Ca^{2+}$ and $Mg^{2+}$ supplemented with 5 mM glucose and incubated with HBSS for 1 h before adding functionalized star polymers. Cells were treated with 100 µL of 40 µM Alexa Fluor® 594 modified **$AB_1$** nanoparticles for 30 min – 1.5 h, washed twice with HBSS without $Ca^{2+}$ and $Mg^{2+}$, and fed with HBSS with $Ca^{2+}$ and $Mg^{2+}$ supplemented with 5 mM glucose for visualization by confocal microscopy.

**Formulation of AbBD nanoparticles with vitamin E-TPGS.** To a 150 mL beaker containing $_{D}$-α-tocopheryl polyethylene glycol 1000 succinate (vitamin E TPGS) (0.28 g) dissolved in Lonza cell culture water (55 mL), nanoparticles (0.0977g) dissolved in dimethyl sulfoxide (DMSO) (0.50 mL) were added slowly with vigorous stirring. The solution was split equally into two 50 mL centrifuge tubes. The nanoparticles were rinsed by applying three cycles of centrifugation (8000 rpm for 30 min) and reconstituted with cell culture water. The nanoparticle suspension was then lyophilized.

***In vitro*** **AbBD nanoparticle degradation studies.** TPGS formulated **AbBD** nanoparticles (10 mg) were suspended in 2 mL of Phosphate Buffered Saline (PBS) (pH 7.4) in 2 dram vials equipped with stir bars. The vials were sealed to avoid evaporation and the samples were maintained at 37 °C under continuous stirring. At 48 h intervals, samples were removed and dichloromethane was added (3 x 4 mL) to extract remaining nanoparticles and degradation products. The extraction solutions were concentrated via rotary evaporator and dried *in vacuo*. The degradation of the nanoparticles was monitored by the change in molecular weight, as determined by static light scattering, with incubation time.

***In vitro*** **cytotoxicity of formulated AbBD nanoparticles (MTT assay).** The cytotoxicity of TPGS formulated nanoparticles was evaluated using an MTT assay. HeLa cells were cultured in Eagle's Minimum Essential Medium supplemented with 10% heat inactivated fetal bovine serum, L-glutamine, penicillin streptomycin sulfate antibiotic-

antimycotic mixture and gentamicin. Cells were maintained at 37 °C with 5% $CO_2$ in a 95% humidity incubator. The cells were seeded in a 96-well plate in 100 μL media per well at a density of 10,000 cells/well and incubated for 24 h. The media was then replaced with 100 μL of phenol red free medium-containing nanoparticles at different concentrations in triplicate and incubated for 24 h. After incubation, the nanoparticle containing media were removed, the cells were rinsed three times with PBS to avoid interference in the assays and 100 μL of fresh phenol red free media was added, followed by 10 μL MTT solution (5 mg/mL). The cells were incubated for 4 h, after which time the medium was carefully removed. To the resulting purple crystals, 100 μL DMSO was added to lyse the cells and the cells were incubated for 10 min at 37 °C. The absorbance was measured at 540 nm using a Synergy HT Multi-mode microplate reader (Bio Tek Instruments, Winooski, VT). Optical densities measured for wells containing cells that received no nanoparticle were considered to represent 100% viability. Results are expressed as the mean±S.D. of viable cells.

***In vitro*** **release of paclitaxel from AbBD nanoparticles.** To a 150 mL beaker containing $_D$-α-tocopherol polyethylene glycol 1000 succinate (0.34 g) dissolved in Lonza cell culture water (68 mL), **AbBD** nanoparticles (56.5 mg) and paclitaxel (8.5 mg) dissolved in dimethyl sulfoxide (0.50 mL) were added slowly with vigorous stirring. The solution was split equally into two 50 mL centrifuge tubes. The paclitaxel loaded nanoparticles were purified by applying three cycles of centrifugation (8000 rpm for 30 min) and reconstituted with cell culture water. The nanoparticle suspension was then lyophilized. The concentration of encapsulated paclitaxel was determined by

NanoDrop™ UV-Vis at a wavelength of 254 nm. Paclitaxel standards (0.398-2.39 mg/mL) were measured by UV-Vis and a calibration curve was rendered. With the calibration curve, the amount of encapsulated paclitaxel in the particles was determined by measuring its absorbency at 254 nm and the loading was found to be 11.3 weight (wt)%. The release of paclitaxel from the nanoparticles was measured in PBS (pH 7.4) at 37 °C. The paclitaxel-loaded nanoparticles (20 mg) were suspended in PBS (20 mL). At particular time intervals, the nanoparticle dispersion was centrifuged, the supernatant was removed and the released paclitaxel was extracted from the supernatant with $CH_2Cl_2$. The concentration of released paclitaxel was determined by NanoDrop™ UV-Vis at a wavelength of 254 nm as mentioned above.

**Attachment of HVGGSSV peptide to AbBD nanoparticles (23).** To a solution of **AbBD** nanoparticles (70 mg) in DMSO ( mL), HVGGSSV peptide (20.7 mg, 19.0 μmol) in DMSO (2 mL) was added. The reaction mixture was heated for 72 h at 37 °C. Residual peptide was removed by dialyzing with SnakeSkin® Pleated Dialysis Tubing (MWCO = 10,000) against 50/50 THF/$CH_3CN$ to yield peptide conjugated nanoparticles (87 mg). DLS: $D_H$ = 55.3 ± 3.6 nm; original particle $D_H$ = 52.9 ± 3.3 nm. SLS: $M_w$ = 185,000 Da; original particle $M_w$ = 147,000 Da. $^1$H NMR (600 MHz, DMSO-$d_6$): δ The significant change is the reduction of the allyl protons at 5.69 and 5.00 ppm and the appearance of signals at 0.80, 1.39, 1.65, 2.74, 3.07, 3.75, 4.40 and 7.11-8.32 ppm due to the peptide. All other aspects of the spectrum are similar to that of the **AbBD** nanoparticles.

**Encapsulation of paclitaxel in HVGGSSV conjugated AbBD nanoparticles (23-T).** To a 150 mL beaker containing $_{D}$-α-tocopherol polyethylene glycol 1000 succinate (0.30 g) dissolved in Lonza cell culture water (60 mL), HVGGSSV-nanoparticles (0.070 g) and paclitaxel (10.5 mg) dissolved in dimethyl sulfoxide (0.50 mL) were added slowly with vigorous stirring. The solution was split into two 50 mL centrifuge tubes. The paclitaxel loaded nanoparticles were purified by applying two cycles of centrifugation (8000 rpm for 30 min) and reconstituted with cell culture water. The nanoparticle suspension was then lyophilized. The loading ratio of paclitaxel for the encapsulation was determined by NanoDrop™ UV-Vis at 254 nm as mentioned above and was found to be 11 wt%.

**Synthesis of KKCGGGGIRLRG (GIRLRG) peptide (24).** The GIRLRG peptide was synthesized by solid-phase peptide synthesis using standard Fmoc chemistry on a Model 90 Peptide Synthesizer (Advanced ChemTech).

*Attachment of N-Fmoc amino acids to resin*. After swelling with dichloromethane (20 mL) for 20 min, Fmoc-Gly-2-Cl-Trt resin (0.20 g, 0.7 mmol/g, 0.14 mmol surface amino acids) was treated with a solution of Fmoc-protected amino acids (4 equiv, 0.6 mmol) in dimethylformamide (DMF) (6 mL). The amino acids were attached to the resin using double coupling with a solution (6 mL) consisting of *N*-hydroxybenzotriazole monohydrate (HOBt) (0.6 mmol, 91.8 mg) *o*-(benzotriazole-*N,N,N′,N′*-tetramethyluronium hexafluorophosphate (HBTU) (0.6 mmol, 0.23 g), *N,N'*-diisopropylethylamine (DIPEA) (1.2 mmol, 0.21 mL) in 6 mL DMF. The reaction mixture was shaken for 60 min and washed with DMF (4 x 10 mL), methanol (4 x 10 mL) and DMF (4 x 10 mL). A 20% (v/v) piperidine in DMF solution was used to

deprotect the Fmoc groups. The amino acids were attached to the resin in the following sequence: Arg, Leu, Arg, Ile, Gly, Gly, Gly, Gly, Cys, Lys, and Lys.

*Cleavage of peptide from resin*. The resin was treated with Reagent R, which is a solution of TFA, thioanisole, anisole, and ethanedithiol (90:5:3:2, 6 mL), for 4 h. After removal of the resin by filtration, the filtrate was concentrated to precipitate the peptide with cold diethyl ether. Crude peptides were purified by RP-HPLC and lyophilized. Peptide identity was confirmed by MALDI-MS (*m/z*: 1201.5).

**Attachment of GIRLRG peptide to AbBD nanoparticles (25).** To a solution of nanoparticles (105 mg) in DMSO (3 mL), GIRLRG peptide (34.3 mg, 28.6 μmol) in DMSO (2 mL) was added. The reaction mixture was heated for 72 h at 37 °C. Residual peptide was removed by dialyzing with SnakeSkin® Pleated Dialysis Tubing (MWCO = 10,000) against 50/50 THF/$CH_3CN$ to yield peptide conjugated particles. $^1H$ NMR (600MHz, DMSO-$d_6$): δ The significant change is the reduction of the allyl protons at 5.69 and 5.00 ppm and the appearance of signals at 0.80, 1.39, 1.65, 2.74, 3.07, 3.75, 4.40 and 7.11-8.32 ppm due to the peptide. All other aspects of the spectrum are similar to that of the **AbBD** nanoparticles.

**Encapsulation of paclitaxel in GIRLRG conjugated nanoparticles (25-T).** To a 150 mL beaker containing $_D$-α-tocopherol polyethylene glycol 1000 succinate (0.30 g) dissolved in Lonza cell culture water (60 mL), GIRLRG-nanoparticles (0.0681 g) and paclitaxel (10.2 mg) dissolved in dimethyl sulfoxide (0.50 mL) were added slowly with

vigorous stirring. The solution was split into two 50 mL centrifuge tubes. The paclitaxel loaded nanoparticles were purified by applying two cycles of centrifugation (8000 rpm for 30 min) and reconstituted with cell culture water. The nanoparticle suspension was then lyophilized. The loading of paclitaxel in the particles was determined by NanoDrop$^{TM}$ UV-Vis at 254 nm as mentioned above and was found to be 11.2 wt%.

**Preparation for GIRLRG-Nanoparticle Drug Delivery Animal Studies.** All animal experiments were performed in compliance with Institutional Animal Care and Use Committee (IACUC) animal research guidelines. The mice, implanted with MDA-MB-231 or GL261 tumors, were randomized, coded by ear punching and weighed. The weights were recorded (by collaborator) and used to calculate for 10 mg paclitaxel/kg mouse for the MDA-MB-231 tumor model or 20 mg paclitaxel/kg mouse for the GL261 tumor model. Stock solutions of paclitaxel, GIRLRG-nanoparticle DDS, and RILGGR-nanoparticle DDS were prepared in PBS buffer. Aliquots were removed from the stock solutions and diluted to the proper concentration of 10 mg/kg or 20 mg/kg using PBS buffer for a total of 200 μL per aliquot. The solutions were given to the collaborator, who then performed the injections and the remainder of the studies.

**Encapsulation of Neuro-DiO in $AB_1$ nanoparticles (AB-NP-DiO).** To a 150 mL beaker containing $_D$-α-tocopherol polyethylene glycol 1000 succinate (0.14 g) dissolved in Lonza cell culture water (27 mL), nanoparticles (55.2 mg) and Neuro-DiO (5.5 mg) dissolved in dimethyl sulfoxide (0.46 mL) were added dropwise with vigorous stirring.

The solution was split equally into two 50 mL centrifuge tubes. The Neuro-DiO loaded nanoparticles were purified by applying three cycles of centrifugation (8000 rpm for 30 min) and reconstituted with cell culture water. The nanoparticle suspension was then lyophilized. The amount of encapsulated Neuro-DiO was determined by NanoDrop™ UV-Vis at a wavelength of 513 nm. Neuro-DiO standards (0.32-1.92 mg/mL) were measured by UV-Vis and a calibration curve was rendered. With the calibration curve, the concentration of encapsulated Neuro-DiO in the nanoparticle was determined from its absorbance at 513 nm, a 7.1 wt% loading.

**Encapsulation of brimonidine in $AB_1$ nanoparticles (AB-NP-BRM).** To a 150 mL beaker containing $_D$-α-tocopherol polyethylene glycol 1000 succinate (0.15 g) dissolved in Lonza cell culture water (30 mL), **AB** nanoparticles (60.5 mg) and brimonidine (6.1 mg) dissolved in dimethyl sulfoxide (0.50 mL) were added dropwise with vigorous stirring. The solution was split equally into two 50 mL centrifuge tubes. The brimonidine loaded nanoparticles were purified by applying three cycles of centrifugation (8000 rpm for 30 min) and reconstituted with cell culture water. The nanoparticle suspension was then lyophilized. The amount of encapsulated brimonidine was determined by NanoDrop™ UV-Vis at a wavelength of 389 nm. Brimonidine standards (0.32-1.92 mg/mL) were measured by UV-Vis and a calibration curve was rendered. With the calibration curve, the concentration of encapsulated brimonidine in the particles was determined by measuring its absorbence at 389 nm and the loading in the particles was found to be 3.3 wt%.

**Encapsulation of bimatoprost in $AB_1$ nanoparticles (AB-NP-BIM) (conducted with Julia Meyer).** To a vial containing $_D$-α-tocopherol polyethylene glycol 1000 succinate (33.3 mg) dissolved in Lonza cell culture water (6.7 mL), **AB** nanoparticles (13.2 mg) and bimatoprost (4 mg) dissolved in dimethyl sulfoxide (110 μL) were added dropwise with vigorous stirring. The solution was transferred into a 15 mL centrifuge tube. The bimatoprost loaded nanoparticles were purified by applying three cycles of centrifugation (8000 rpm for 30 min) and reconstituted with cell culture water. The nanoparticle suspension was then lyophilized. The amount of encapsulated bimatoprost was determined by NanoDrop™ UV-Vis at a wavelength of 262 nm. Bimatoprost standards (0.3-2 mg/mL) were measured by UV-Vis and a calibration curve was rendered. With the calibration curve, the concentration of encapsulated bimatoprost in the particles was determined by measuring its absorbence at 262 nm and the loading in the particles was found to be 16.4 wt%.

**General Preparation for Intraocular Pressure (IOP) Animal Studies.** All animal experiments were performed in compliance with Institutional Animal Care and Use Committee (IACUC) animal research guidelines. The Calkins lab elevated the IOP by the injection of polystyrene microbeads into the anterior chamber of C57BL/6 mice to occlude aqueous outflow. After monitoring IOP elevation for several days, the mice were treated with a single intravitreal injection of 1 μL AB-NP-BRM (16.96 mg/mL in PBS) into one eye and PBS in the other, to serve as a control. The IOP for each mouse was monitored using tonometry as performed by the collaborators.

**Encapsulation of formyl-N'LFN'YK peptide in $AB_1$ nanoparticles (AB-NP-CP) (conducted with Julia Meyer).** To a vial containing $_D$-α-tocopherol polyethylene glycol 1000 succinate (25 mg) dissolved in Lonza cell culture water (5 mL), **AB** nanoparticles (9.5 mg) and fN'LFN'YK (1.8 mg) dissolved in dimethyl sulfoxide (100 μL) were added dropwise with vigorous stirring. The solution was transferred into a 15 mL centrifuge tube. The peptide loaded nanoparticles were purified by applying three cycles of centrifugation (8000 rpm for 30 min) and reconstituted with cell culture water. The nanoparticle suspension was then lyophilized. The amount of encapsulated peptide was determined by NanoDrop™ UV-Vis at a wavelength of 280 nm. Peptide standards (0.3-2 mg/mL) were measured by UV-Vis and a calibration curve was rendered. With the calibration curve, the concentration of encapsulated peptide in the particles was determined by measuring its absorbency at 280 nm and the loading in the particles was found to be 16.3 wt%.

**Alexa Fluor® 594 conjugated GCGGGDHGVSSGV peptide (AF-GCGGGDHGVSSGV) (26).** To a solution of peptide (6.0 mg, 5.5 μmol) in dry dimethylsulfoxide (0.7 mL), Alexa Fluor® 594 (0.5 mL, 12.2 mM solution in DMF) was added. The reaction mixture stirred for 24 h at room temperature in the dark. Residual Alexa Fluor® 594 was removed by dialyzing with SnakeSkin® Pleated Dialysis Tubing (MWCO = 1,000) against deionized water to yield Alexa Fluor® conjugated peptide (7.3 mg, 73%). Successful dye conjugation was determined by NanoDrop™ UV-Vis at a wavelength of 601 nm. Alexa Fluor® 594 standards (0.02-0.08 mg/mL) were measured by UV-Vis and a calibration curve was rendered. With the calibration curve, conjugation

efficiency was determined by the absorbence of the dye attached to the nanoparticle at 601 nm and was found to be 100%.

**Encapsulation of Alexa Fluor® conjugated peptide (26) during particle formation using alkyne-azide crosslinking.** Poly(vl-pvl), **$AC_2$**, (0.7 mg, $M_w$= 3000 Da, PDI = 1.18) was added to a vial, which was then sealed and purged with argon. Copper (I) bromide (1.89 μL, $4.0x10^{-2}$ M solution in DMF), and polyoxyethylene bis(azide) (5.5 mg, 1.1 μmol) and AF-GCGGGDHGVSSGV, **26**, (0.92 mg), dissolved in anhydrous dimethylformamide (0.6 mL), were added. The reaction mixture stirred for 24 h at room temperature. Residual azide, copper bromide and peptide were removed by dialyzing with SnakeSkin® Pleated Dialysis Tubing (MWCO = 25,000) against methanol/acetonitrile/tetrahydrofuran. The concentration of encapsulated AF-peptide was determined by NanoDrop™ UV-Vis at a wavelength of 601 nm. AF-peptide standards (0.02-0.08 mg/mL) were measured by UV-Vis and a calibration curve was rendered. With the calibration curve, the amount of encapsulated peptide in the particles was determined by measuring the absorbency at 601 nm and for the above procedure the loading ratio was found to be 8 wt%.

**Attachment of O-(2-mercaptoethyl)-O'-methyl-hexa(ethyleneglycol) ($PEG_6$) to poly(vl-avl) (Ab).** To a solution of **Ab** (25 mg) in DMF (0.2 mL), $PEG_6$ (15.1 mg, 42.3 μmol) and azobisisobutyronitrile (3.5 mg, 21.1 μmol) were added. The reaction mixture was heated for 6 h at 70 °C. Residual $PEG_6$ and AIBN were removed by dialyzing with

SnakeSkin® Pleated Dialysis Tubing (MWCO = 1,000) against $CH_3OH/CH_2Cl_2$ to yield **Ab-PEG$_6$** (28 mg). $^1$H NMR (300 MHz, $CD_3Cl_3$): δ The significant change is the reduction of the allyl protons at 5.72 and 5.06 ppm and the appearance of signals at 3.65, and 2.54 ppm due to the PEG protons. All other aspects of the spectrum are similar to that of **Ab**.

**Synthesis of poly(valerolactone-allylvalerolactone-glycidol) (poly(vl-avl-gl)) (AbG).** A 25 mL 3-necked round bottom flask, equipped with stir bar, was sealed with two septa and a gas inlet. The flask was evacuated and refilled with $Ar_{(g)}$ three times. Stock solutions of 1.7 M ethanol in THF and $3.7x10^{-2}$ M $Sn(Oct)_2$ in THF were made in sealed $Ar_{(g)}$ purged flasks. Solutions of ethanol (0.36 mL, $6.16x10^{-1}$ mmol) and $Sn(Oct)_2$ (0.33 mL, $1.21x10^{-2}$ mmol) were combined in the $Ar_{(g)}$ purged 3-necked flask. After stirring the mixture for 30 min, α-allyl-δ-valerolactone (0.5 g, 3.6 mmol), δ-valerolactone (0.36 g, 3.6 mmol) and glycidol (2.1 g, 28.6 mmol) were added. The reaction vessel stirred at 105 °C for 28 h. Residual monomer and catalyst were removed by precipitating the polymer into diethyl ether to give a viscous polymer (1.39 g). $M_w$ = 15, 000 (as determined by $^1$H NMR). $^1$H NMR (300 MHz, $CD_3OD$): δ 5.80 (m, $H_2C$=C*H*-), 5.03 (m, *H*$_2$C=CH-), 4.09 (m, avl & vl, -C*H*$_2$O-), 3.55-3.90 (m, -OC*H*$_2$C*H*(OH)C*H*$_2$-, -OC*H*$_2$C*H*(C*H*$_2$OH)-), 2.37 (m, vl, -CH$_2$C*H*$_2$C(O)O-, avl, $H_2C$=CHCH$_2$C*H*-, $H_2C$=CHC*H*$_2$CH-), 1.55-1.67 (m, avl & vl, -CHC*H*$_2$C*H*$_2$-), 1.25 (m, C*H*$_3$CH$_2$O-); $^{13}$C NMR (400 MHz, $CDCl_3$): δ 177.9, 175.6, 136.9, 117.7, 81.5, 80.2, 74.3, 72.7, 70.8, 65.0, 62.6, 44.7, 38.3, 35.1, 33.0, 31.4, 29.3, 23.1.

**Attachment of thioglycolic acid to poly(vl-avl-gl) ($AbG_1$) (conducted with Jameson Harrell).** To a solution of **$AbG_1$** (27 mg) in $H_2O$ (5 mL), and thioglycolic acid (1.1 µL, 15 µmol) were added. The reaction mixture was heated for 0, 3, 6, or 12 h at 37 °C. The reaction mixture was frozen and then lyophilized to remove the water. $^1$H NMR (300 MHz, $CD_3OD$): δ The significant change is the reduction of the allyl protons at 5.72 and 5.06 ppm. All other aspects of the spectrum are similar to that of **$AbG_1$**.

**Nanoparticle formation using thiol-ene cross-linking with 3,6-dioxa-1,8-octanedithiol and AbG.** A solution of poly(vl-avl-gl), **AbG**, (0.11 g) dissolved in $H_2O$ (12 mL) was added to a solution of 3,6-dioxa-1,8-octanedithiol (10.3 µL, 63.2 µmol) in $H_2O$ (15 mL). The reaction mixture was heated for 12 h at 37 °C. Residual dithiol and polymer were removed by dialyzing with SnakeSkin® Pleated Dialysis Tubing (MWCO = 10,000) initially against 50/50 $H_2O/CH_3OH$ and then progressing to 100% $CH_3OH$ to yield particles. TEM: 105.3 ± 10.2 nm. $^1$H NMR (300 MHz, $CD_3OD$) δ: The significant change is the reduction of the allyl protons at 5.06 and 5.77 ppm. All other aspects of the spectrum are similar to that of **AbG**. $^{13}$C NMR (400MHz, $CDCl_3$): δ 176.9, 175.6, 136.8, 117.6, 81.6, 80.2, 74.2, 72.2, 70.9, 64.5, 62.7, 46.3, 38.1, 34.8, 32.9, 31.4, 29.2, 22.6.

References

1. Orive, G.; Hernandez, R. M.; Rodriguez Gascon, A.; Dominguez-Gil, A.; Pedraz, J. L., Drug delivery in biotechnology: present and future. *Current Opinion in Biotechnology* **2003,** *14* (6), 659-664.

2. Manmode, A. S.; Sakarkar, D. M.; Mahajan, N. M., Nanoparticles-tremendous therapeutic potential: a review. *International Journal of PharmTech Research* **2009,** *1* (4), 1020-1027.

3. van Vlerken, L. E.; Amiji, M. M., Multi-functional polymeric nanoparticles for tumour-targeted drug delivery. *Expert Opinion on Drug Delivery* **2006,** *3* (2), 205-216.

4. Kocbek, P.; Baumgartner, S.; Kristl, J., Preparation and evaluation of nanosuspensions for enhancing the dissolution of poorly soluble drugs. *International Journal of Pharmaceutics* **2006,** *312* (1-2), 179-186.

5. Merisko-Liversidge, E. M.; Liversidge, G. G., Drug nanoparticles: formulating poorly water-soluble compounds. *Toxicologic Pathology* **2008,** *36* (1), 43-48.

6. Lipinski, C. A., Drug-like properties and the causes of poor solubility and poor permeability. *Journal of Pharmacological and Toxicological Methods* **2001,** *44* (1), 235-249.

7. Jagur-Grodzinski, J., Polymers for targeted and/or sustained drug delivery. *Polymers for Advanced Technologies* **2009,** *20* (7), 595-606.

8. Kumari, A.; Yadav, S. K.; Yadav, S. C., Biodegradable polymeric nanoparticles based drug delivery systems. *Colloids and Surfaces, B Biointerfaces* **2010,** *75* (1), 1-18.

9. Nazarov, G. V.; Galan, S. E.; Nazarova, E. V.; Karkishchenko, N. N.; Muradov, M. M.; Stepanov, V. A., Nanosized forms of drugs (A Review). *Pharmaceutical Chemistry Journal* **2009,** *43* (3), 163-170.

10. Uhrich, K. E.; Cannizzaro, S. M.; Langer, R. S.; Shakesheff, K. M., Polymeric systems for controlled drug release. *Chemical Reviews* **1999,** *99* (11), 3181-3198.

11. Chan, J. M.; Zhang, L. F.; Yuet, K. P.; Liao, G.; Rhee, J. W.; Langer, R.; Farokhzad, O. C., PLGA-lecithin-PEG core-shell nanoparticles for controlled drug delivery. *Biomaterials* **2009,** *30* (8), 1627-1634.

12. Kumar, M. N. V. R.; Bakowsky, U.; Lehr, C. M., Preparation and characterization of cationic PLGA nanospheres as DNA carriers. *Biomaterials* **2004,** *25* (10), 1771-1777.

13. Cheng, J.; Teply, B. A.; Sherifi, I.; Sung, J.; Luther, G.; Gu, F. X.; Levy-Nissenbaum, E.; Radovic-Moreno, A. F.; Langer, R.; Farokhzad, O. C., Formulation of functionalized PLGA-PEG nanoparticles for in vivo targeted drug delivery. *Biomaterials* **2007,** *28* (5), 869-876.

14. Hasan, A. S.; Socha, M.; Lamprecht, A.; El Ghazouani, F.; Sapin, A.; Hoffman, A.; Maincent, P.; Ubrich, N., Effect of the microencapsulation of nanoparticles on the reduction of burst release. *International Journal of Pharmaceutics* **2007,** *344* (1-2), 53-61.

15. Hasan, A. S.; Sapin, A.; Lamprecht, A.; Emond, E.; El Ghazouani, F.; Mainchent, *European Journal of Pharmaceutics and Biopharmaceutics* **2009**.

16. Feng, S. S.; Zhao, L. Y.; Zhang, Z. P.; Bhakta, G.; Win, K. Y.; Dong, Y. C.; Chien, S., Chemotherapeutic engineering: Vitamin E TPGS-emulsified nanoparticles of biodegradable polymers realized sustainable paclitaxel chemotherapy for 168 h in vivo. *Chemical Engineering Science* **2007,** *62* (23), 6641-6648.

17. Harasym, T. O.; Liboiron, B. D.; Mayer, L. D., Drug ratio-dependent antagonism: a new category of multidrug resistance and strategies for its circumvention. *Methods in Molecular Biology* **2010,** *596*, 291-323.

18. van der Ende, A. E.; Kravitz, E. J.; Harth, E., Approach to formation of multifunctional polyester particles in controlled nanoscopic dimensions. *Journal of the American Chemical Society* **2008,** *130* (27), 8706-8713.

19. Tserki, V.; Matzinos, P.; Pavlidou, E.; Panayiotou, C., Biodegradable aliphatic polyesters. Part II. Synthesis and characterization of chain extended poly(butylene succinate-co-butylene adipate). *Polymer Degradation and Stability* **2005,** *91* (2), 377-384.

20. Giunchedi, P.; Conti, B.; Scalia, S.; Conte, U., In vitro degradation study of polyester microspheres by a new HPLC method for monomer release determination. *Journal of Controlled Release* **1998,** *56* (1-3), 53-62.

21. Umare, S. S.; Chandure, A. S.; Pandey, R. A., Synthesis, characterization and biodegradable studies of 1,3-propanediol based polyesters. *Polymer Degradation and Stability* **2007,** *92* (3), 464-479.

22. Yu, D. H.; Lu, Q.; Xie, J.; Fang, C.; Chen, H. Z., Peptide-conjugated biodegradable nanoparticles as a carrier to target paclitaxel to tumor neovasculature. *Biomaterials* **2010,** *31* (8), 2278-2292.

23. Mu, L.; Feng, S. S., Vitamin E TPGS used as emulsifier in the solvent evaporation/extraction technique for fabrication of polymeric nanospheres for controlled release of paclitaxel (Taxol (R)). *Journal of Controlled Release* **2002,** *80* (1-3), 129-144.

24. Gradishar, W. J.; Tjulandin, S.; Davidson, N.; Shaw, H.; Desai, N.; Bhar, P.; Hawkins, M.; O'Shaughnessy, J., Phase III trial of nanoparticle albumin-bound paclitaxel compared with polyethylated castor oil-based paclitaxel in women with breast cancer. *Journal of Clinical Oncology* **2005,** *23* (31), 7794-7803.

25. Henderson, I. C.; Bhatia, V., Nab-paclitaxel for breast cancer: a new formulation with an improved safety profile and greater efficacy. *Expert Review of Anticancer Therapy* **2007,** *7* (7), 919-943.

26. Morris, P. G.; Fornier, M. N., Novel anti-tubulin cytotoxic agents for breast cancer. *Expert Review of Anticancer Therapy* **2009,** *9* (2), 175-185.

27. Li, Y. P.; Pan, S. R.; Zhang, W.; Du, Z., Novel thermo-sensitive core-shell nanoparticles for targeted paclitaxel delivery. *Nanotechnology* **2009,** *20* (6), 1-11.

28. Vicari, L.; Musumeci, T.; Giannone, I.; Adamo, L.; Conticello, C.; De Maria, R.; Pignatello, R.; Puglisi, G.; Gulisano, M., Paclitaxel loading in PLGA nanospheres affected the in vitro drug cell accumulation and antiproliferative activity. *Bmc Cancer* **2008,** *8*, 212-222.

29. Chavanpatil, M. D.; Patil, Y.; Panyam, J., Susceptibility of nanoparticle-encapsulated paclitaxel to P-glycoprotein-mediated drug efflux. *International Journal of Pharmaceutics* **2006,** *320* (1-2), 150-156.

30. Debotton, N.; Parnes, M.; Kadouche, J.; Benita, S., Overcoming the formulation obstacles towards targeted chemotherapy: In vitro and in vivo evaluation of cytotoxic drug loaded immunonanoparticles. *Journal of Controlled Release* **2008,** *127* (3), 219-230.

31. van der Ende, A.; Croce, T.; Hamilton, S.; Sathiyakumar, V.; Harth, E., Tailored polyester nanoparticles: post-modification with dendritic transporter and targeting units via reductive amination and thiol-ene chemistry. *Soft Matter* **2009,** *5* (7), 1417-1425.

32. Han, Z.; Fu, A.; Wang, H.; Diaz, R.; Geng, L.; Onishko, H.; Hallahan, D. E., Noninvasive assessment of cancer response to therapy. *Nature Medicine* **2008,** *14* (3), 343-349.

33. Diaz, R.; Passarella, R. J.; Hallahan, D. E., Determining glioma response to radiation therapy using recombinant peptides. *Expert Review of Anticancer Therapy* **2008,** *8* (11), 1787-1796.

34. Passarella, R. J.; Spratt, D. E.; van der Ende, A. E.; Phillips, J. G.; Wu, H.; Sathiyakumar, V.; Zhou, L.; Hallahan, D. E.; Harth, E.; Diaz, R., Targeted Nanoparticles That Deliver a Sustained, Specific Release of Paclitaxel to Irradiated Tumors. *Cancer Research* **2010,** *70* (11), 4550-4559.

35. Ruoslahti, E., Vascular zip codes in angiogenesis and metastasis. *Biochemical Society Transactions* **2004,** *32*, 397-402.

36. Pasqualini, R.; Ruoslahti, E., Organ targeting in vivo using phage display peptide libraries. *Nature* **1996,** *380* (6572), 364-366.

37. Arap, W.; Kolonin, M. G.; Trepel, M.; Lahdenranta, J.; Cardo-Vila, M.; Giordano, R. J.; Mintz, P. J.; Ardelt, P. U.; Yao, V. J.; Vidal, C. I.; Chen, L.; Flamm, A.; Valtanen, H.; Weavind, L. M.; Hicks, M. E.; Pollock, R. E.; Botz, G. H.; Bucana, C. D.; Koivunen, E.; Cahill, D.; Troncoso, P.; Baggerly, K. A.; Pentz, R. D.; Do, K. A.; Logothetis, C. J.; Pasqualini, R., Steps toward mapping the human vasculature by phage display. *Nature Medicine* **2002,** *8* (2), 121-127.

38. van der Ende, A. E.; Sathiyakumar, V.; Diaz, R.; Hallahan, D. E.; Harth, E., Linear release nanoparticle devices for advanced targeted cancer therapies with increased efficacy. *Polymer Chemistry* **2010,** *1* (1), 93-96.

39. Bertram, J. P.; Saluja, S. S.; McKain, J.; Lavik, E. B., Sustained delivery of timolol maleate from poly(lactic-co-glycolic acid)/poly(lactic acid) microspheres for over 3 months. *Journal of Microencapsulation* **2009,** *26* (1), 18-26.

40. Hsiue, G. H.; Chang, R. W.; Wang, C. H.; Lee, S. H., Development of in situ thermosensitive drug vehicles for glaucoma therapy. *Biomaterials* **2003,** *24* (13), 2423-2430.

41. Seider, N.; Miller, B.; Beiran, I., Topical glaucoma therapy as a risk factor for nasolacrimal duct obstruction. *American Journal of Ophthalmology* **2008,** *145* (1), 120-123.

42. De, T. K.; Rodman, D. J.; Holm, B. A.; Prasad, P. N.; Bergey, E. J., Brimonidine formulation in polyacrylic acid nanoparticles for ophthalmic delivery. *Journal of Microencapsulation* **2003,** *20* (3), 361-374.

43. Sappington Rebecca, M.; Carlson Brian, J.; Crish Samuel, D.; Calkins David, J., The microbead occlusion model: a paradigm for induced ocular hypertension in rats and mice. *Investigative Ophthalmology & Visual Science 51* (1), 207-16.

44. Kang, S. J.; Durairaj, C.; Kompella, U. B.; O'Brien, J. M.; Grossniklaus, H. E., Subconjunctival Nanoparticle Carboplatin in the Treatment of Murine Retinoblastoma. *Archives of Ophthalmology* **2009,** *127* (8), 1043-1047.

45. Ayalasomayajula, S. P.; Kompella, U. B., Subconjunctivally administered celecoxib-PLGA microparticles sustain retinal drug levels and alleviate diabetes-induced oxidative stress in a rat model. *European Journal of Pharmacology* **2005,** *511* (2-3), 191-198.

46. Meisner, D.; Mezei, M., Liposome Ocular Delivery Systems. *Advanced Drug Delivery Reviews* **1995,** *16* (1), 75-93.

47. Kim, H.; Csaky, K. G., Nanoparticle-integrin antagonist C16Y peptide treatment of choroidal neovascularization in rats. *Journal of Controlled Release* **2010,** *142* (2), 286-293.

48. Kakizawa, Y.; Nishio, R.; Hirano, T.; Koshi, Y.; Nukiwa, M.; Koiwa, M.; Michizoe, J.; Ida, N., Controlled release of protein drugs from newly developed amphiphilic polymer-based microparticles composed of nanopcarticles. *Journal of Controlled Release* **2010,** *142* (1), 8-13.

49. Di Marco, M.; Shamsuddin, S.; Abdul Razak, K.; Abdul Aziz, A.; Devaux, C.; Borghi, E.; Levy, L.; Sadun, C., Overview of the main methods used to combine proteins with nanosystems: absorption, bioconjugation, and encapsulation. *International Journal of Nanomedicine 5*, 37-49.

50. Fresta, M.; Puglisi, G., Association of Netilmicin Sulfate to Poly(Alkylcyanoacrylate) Nanoparticles - Factors Influencing Particle Delivery Behavior. *Drug Development and Industrial Pharmacy* **1994,** *20* (14), 2227-2243.

51. Peula, J. M.; Hidalgo-Alvarez, R.; Nieves, F. J. D., Covalent binding of proteins to acetal-functionalized latexes. II. Colloidal stability and immunoreactivity. *Journal of Colloid and Interface Science* **1998,** *201* (2), 139-145.

52. Zhao, X. J.; Jain, S.; Larman, H. B.; Gonzalez, S.; Irvine, D. J., Directed cell migration via chemoattractants released from degradable microspheres. *Biomaterials* **2005,** *26* (24), 5048-5063.

53. Devi, G. R., siRNA-based approaches in cancer therapy. *Cancer Gene Therapy* **2006,** *13* (9), 819-829.

54. Takeshita, F.; Ochiya, T., Therapeutic potential of RNA interference against cancer. *Cancer Science* **2006,** *97* (8), 689-696.

55. Fattal, E.; Bochot, A., Ocular delivery of nucleic acids: Antisense oligonucleotides, aptamers and siRNA. *Advanced Drug Delivery Reviews* **2006,** *58* (11), 1203-1223.

56. Whitehead, K. A.; Langer, R.; Anderson, D. G., Knocking down barriers: advances in siRNA delivery. *Nature Reviews Drug Discovery* **2009,** *8* (2), 129-138.

57. Baigude, H.; Rana, T. M., Delivery of Therapeutic RNAi by Nanovehicles. *Chembiochem* **2009,** *10* (15), 2449-2454.

58. Nimesh, S.; Chandra, R., Polyethylenimine nanoparticles as an efficient in vitro siRNA delivery system. *European Journal of Pharmaceutics and Biopharmaceutics* **2009,** *73* (1), 43-49.

59. Weyermann, J.; Lochmann, D.; Georgens, C.; Zimmer, A., Albumin-protamine-oligonucleotide-nanoparticles as a new antisense delivery system. Part 2: cellular uptake and effect. *European Journal of Pharmaceutics and Biopharmaceutics* **2005,** *59* (3), 431-438.

60. Jones, M. W.; Mantovani, G.; Ryan, S. M.; Wang, X. X.; Brayden, D. J.; Haddleton, D. M., Phosphine-mediated one-pot thiol-ene "click" approach to polymer-protein conjugates. *Chemical Communications* **2009,** (35), 5272-5274.

61. Campos, L. M.; Killops, K. L.; Sakai, R.; Paulusse, J. M. J.; Damiron, D.; Drockenmuller, E.; Messmore, B. W.; Hawker, C. J., Development of thermal and photochemical strategies for thiol-ene click polymer functionalization. *Macromolecules (Washington, DC, United States)* **2008,** *41* (19), 7063-7070.

62. Wang, C.; Ge, Q.; Ting, D.; Nguyen, D.; Shen, H. R.; Chen, J. Z.; Eisen, H. N.; Heller, J.; Langer, R.; Putnam, D., Molecularly engineered poly(ortho ester)

microspheres for enhanced delivery of DNA vaccines. *Nature Materials* **2004,** *3* (3), 190-196.

63. Hans, M.; Keul, H.; Moeller, M., Poly(ether-ester) Conjugates with Enhanced Degradation. *Biomacromolecules* **2008,** *9* (10), 2954-2962.

64. Mao, J.; Gan, Z. H., The Influence of Pendant Hydroxyl Groups on Enzymatic Degradation and Drug Delivery of Amphiphilic Poly[glycidol-block-(epsilon-caprolactone)] Copolymers. *Macromolecular Bioscience* **2009,** *9* (11), 1080-1089.

65. Pitet, L. M.; Hait, S. B.; Lanyk, T. J.; Knauss, D. M., Linear and branched architectures from the polymerization of lactide with glycidol. *Macromolecules* **2007,** *40* (7), 2327-2334.

66. Wurm, F.; Nieberle, J.; Frey, H., Double-hydrophilic linear-hyperbranched block copolymers based on poly(ethylene oxide) and poly(glycerol). *Macromolecules* **2008,** *41* (4), 1184-1188.

67. Kainthan, R. K.; Muliawan, E. B.; Hatzikiriakos, S. G.; Brooks, D. E., Synthesis, characterization, and viscoelastic properties of high molecular weight hyperbranched polyglycerols. *Macromolecules* **2006,** *39* (22), 7708-7717.

# CHAPTER VI

## CONCLUSION AND FUTURE OUTLOOK

This work documents the development of a novel approach for the formation of multifunctional polyester nanoparticles with amorphous and semicrystalline morphologies in selected size dimensions via a controlled intermolecular chain cross-linking process. The technique involves the coupling of epoxide functionalized polyesters with diamine, which leads to the preparation of well-defined nanoparticles with narrow size distribution and selected nanoscopic sizes. Nanoparticle formation and the control over their sizes were found to be influenced by the degree of the epoxide entity implemented in the precursor polymers and the amount of diamine as the cross-linking reagent. Diverse functionalized polyesters, synthesized with pendant functionalities via ring-opening polymerization, were prepared as linear precursors which facilitated the formation of 3-D nanoparticles with functionalities, such as amines, keto groups, and alkynes for post modification reactions. In this way, a plethora of well-defined functionalized polyester nanoparticles could be prepared in different sizes and functionalities.

The synthesis of discrete polyester nanoparticles using the controlled intermolecular chain cross-linking process has also been successfully facilitated via click chemistry approaches, employing the Cu(I)-catalyzed 1,3-dipolar cycloaddition of azides and alkynes and the more recently developed thiol-ene reaction. Both click reactions have led to the formation of well-defined particles with narrow size distribution and selected

nanoscopic size dimensions. The controlled coupling involves the cross-linking of an alkyne functionalized polyester with a bisazide, and an allyl functionalized polyester with dithiol. It was found that the nanoparticle formation and the control over the nanoscopic dimension are primarily influenced by the degree of the alkyne or allyl entity implemented in the precursor polymer and the amount of bisazide and dithiol cross-linking reagents respectively. These results have underlined the versatility of the intermolecular chain cross-linking technique, which is not merely limited to the epoxide-amine chemistry, but can also be extended to click reactions to form controlled nanoparticles with comparable efficiencies.

Synthetic strategies that enable efficient chemistries to conjugate targeting units and dendritic molecular transporter entities to the functionalized polyester particles have been developed to form potent carrier systems for targeted drug delivery and transport across biological barriers. The formation of polyester nanoparticles containing amine, keto, and allyl groups has allowed for the tailoring of the particles towards the conjugation of bioactive building blocks, such as a dendritic molecular transporter and targeting peptides. Integrated keto functionalities were utilized with amines of the N-terminus of peptide targeting units in high yielding reductive amination reactions. Thiol-ene reaction conditions were developed and optimized to perform mild addition reactions with targeting units, such as a novel c-RGD, but also cell penetrating dendritic transporter structures. Using these mild conjugation chemistries, several efficient post-modification strategies have been established to form polyester bioconjugates with specific functionalities to serve as a platform for an array of therapeutic applications.

The intermolecular cross-linking technique leading to the formation of supramolecular 3D nano-networks has provided the basis for the preparation of targeted and sustained delivery systems. The cross-linked supramolecular structure of the nanoparticles has led to the increased and efficient encapsulation of hydrophobic small molecule drugs, such as paclitaxel, after particle formation and post-modification with targeting peptides. A prolonged linear release profile of the therapeutic without the typical 'burst effect' was observed in emulsified particles, which is critical for establishing controlled and predictable pharmacokinetics for the treatment of diseases, such as cancer.

Employing the nanoparticles' linear drug release, a novel nanoparticle drug delivery system has been developed for cancer therapy, which has enabled specific targeting to the tumor site and allowed for the controlled, linear release of therapeutic causing significant apoptosis and tumor growth delay. This particle system has shown considerable efficacy over current clinical models and with further investigation we expect to implement this system into clinical trials.

Significant advances have also been made in optimizing the delivery of drugs to target the retina for the treatment of glaucoma. Several different delivery systems based on the **AB** nanoparticle that incorporate ophthalmic therapeutics, such as brimonidine and bimatoprost, have been developed to provide a sustained release of therapeutic. Preliminary studies have shown the success of the nanoparticles to reach the retina, and reduce and maintain IOP. With these promising results, further experiments will be conducted to investigate other methods of administering the particle drug delivery system with different drug loadings to determine the most effective and least invasive treatment.

In addition to the delivery of small molecules, substantial attention has been focused on the delivery of macromolecular therapeutics, such as peptides and siRNA. For the encapsulation of peptides, several systems have been successfully developed involving encapsulation either after or during particle formation. Along with the encapsulation of peptide, a water soluble system has been cultivated for the encapsulation of siRNA. With the incorporation of glycidol into the linear polyester backbone, a completely water soluble has been prepared and cross-linked to form nanoparticles under aqueous reaction conditions, which will greatly aid in the future incorporation and delivery of siRNA.

The aforementioned developed technology affords the efficient formation of functionalized monodisperse particles with a variety of distinct size dimensions. The particles' adjustable architecture and amorphous properties has led to the sustained linear release of drug molecules and the encapsulation of diverse therapeutics. With these flexible properties, the particles' 3-D biodegradable nano-networks serve as the ideal delivery platform for the delivery of drug molecules, specifically for the treatment of cancer and glaucoma.